THE UNIVERSITY OF NOTTINGHAM

SCHOOL OF ELECTRICAL AND ELECTRONIC ENGINEERING

Direct Computation of Statistical Variations in Electromagnetic Problems

By

Ajibola Ajayi

Thesis submitted to the University of Nottingham for the Degree of Doctor of Philosophy, May 2008.

ACKNOWLEDGEMENTS

I would first like to thank God who gave me the grace and privilege to pursue this programme and successfully complete it in spite of many challenges faced. The journey has been quite remarkable and it is a unique stepping stone to many exploits ahead.

I would like to express my profound gratitude to my supervisors, Professor Christos Christopoulos and Professor Phillip Sewell for their visionary support and unwavering guidance throughout the course of this work. I also reserve special thanks to Prof. Leonardo de Menezes for his invaluable contribution to this work during his sabbatical leave from the University of Brasilia.

I would like to thank my colleagues at the George Green Institute of Electromagnetic Research. I am particularly grateful to Dr. Carl Styan for his help with algorithm development during the initial period of my programme. I am also thankful to Dr. Jim Wykes and Dr. John Paul for useful discussions especially on the subject of Transmission Line Modelling. I would like to thank Dr. Konrad Biwojno for his advice on how to cope with the different rigours associated with this project. I am also very thankful for all my many **friends**. When times were tough, you gave me the confidence and strength to keep pressing on to achieve all my goals. God bless you all.

Finally, I would like to dedicate this thesis to my family. The sacrifice you made throughout my years here are simply ineffable. The belief you have in me and the support you gave instilled the values and virtues that see me through on a daily basis. I thank my father for encouraging me to embark on the project and for being a stalwart at all times. I thank my mother for her tender, loving care and compassion. I thank my sisters for their kindness and warmth throughout the years.

ABSTRACT

This work described in this thesis develops a computationally efficient approach to performing electromagnetic simulations in the presence of statistically defined uncertainties caused by either material inhomogeneities, or fabrication and placement tolerances. Comparisons are made with results from Monte Carlo simulations and a sequence of higher order approximation extensions is considered.

There are two main techniques used to achieve the overall objective of this thesis namely: the Direct Solution Technique (DST) and the Unscented Transform (UT) method.

The DST based on Taylor series approximations is intended to explicitly provide rapid approximate solutions that obviate the need for extremely slowly converging and time consuming Monte Carlo analysis of multiple simulations. The DST approach is useful in problems where sensitivity of system responses with respect to stochastic variables can be mathematically defined.

The UT method is similar to the Monte Carlo method but makes use of a significantly smaller number of simulations. As the number of random variables considered increases, the UT procedure requires more simulations. The advantage of the UT method is that it is applicable to black-box models and can therefore be extended to different electromagnetic solvers.

The case studies used in this thesis are developed using the Transmission Line Modelling (TLM) method. Both the DST and UT method were found to enhance the modelling of uncertainty in electromagnetic problems. The scopes of both methods are explored and observations made upon both the degree of problem complexity and the extent of stochastic variation permitted.

LIST OF PUBLICATIONS

- A. Ajayi, C. Christopoulos and P. Sewell, "Direct Computations of Statistical Variations in Electromagnetic Problems, EMC Europe 2006 International Symposium on Electromagnetic Compatibility, Barcelona-Spain, Sep. 2006.

- L. R.A.X. de Menezes, A. Ajayi, C. Christopoulos, P. Sewell and G. A. Borges, "Efficient Extraction of Statistical Moments in Electromagnetic Problems Solved with the Method of Moments" IEEE Microwave and Optoelectronics Conference, 2007.

- L. R.A.X. de Menezes, A. Ajayi, C. Christopoulos, P. Sewell and G. A. Borges, "Extracting Statistical Moments of Output Quantities from a Small Number of Time-Domain Simulations," Proceedings on Computational Electromagnetics in Time-Domain, Perugia, Italy, 2007.

- L. R.A.X. de Menezes, A. Ajayi, C. Christopoulos, P. Sewell and G. A. Borges, "Recent Advances in the Combination of the Unscented Transform (UT) with the Transmission Line Modelling Method (TLM)," Proc. of the Symposium in Honour of Prof. Wolfgang J. R. Hoefer, Technical University of Munich, May 2007.

- C. Christopoulos, P. Sewell, K. Biwojno, J. Wykes, J. D. Paul, D. W. P. Thomas, A. Ajayi, L. de Menezes, "Multi-Scale Problems and Complexity in Computational Electromagnetics" Computational Electromagnetics Workshop, Aug. 2007.

- L. R.A.X de Menezes, A. Ajayi, C. Christopoulos, P. Sewell and G. A. Borges "Efficient Computation of Stochastic Electromagnetic Problems

using Unscented Transforms," IET Science, Measurement and Technology, vol. 2, pp. 88-95, Mar. 2008.

- A. Ajayi, P. Ingrey, C. Christopoulos and P. Sewell, "Direct Computations of Statistical Variations in Electromagnetic Problems," IEEE Transactions on Electromagnetic Compatibility, vol. 50, pp. 325 – 332, May 2008.

- L. R.A.X. de Menezes, D.W.P Thomas, C. Christopoulos, A. Ajayi and P. Sewell, "The use of Unscented Transforms for statistical analysis in EMC, EMC Europe 2008 International Symposium on Electromagnetic Compatibility, Hamburg-Germany, Sep. 2008.

- L. R.A.X. de Menezes, D.W.P Thomas, C. Christopoulos, A. Ajayi and P. Sewell, "Extracting Statistical Moments of Output Quantities from a Small Number of Time-Domain Simulations," International Journal of Numerical Modelling, 2008 (Accepted).

"So far as the laws of mathematics refer to reality, they are not certain. And so far as they are certain, they do not refer to reality." Albert Einstein

CONTENTS

Chapter 1   Introduction

1.1   Statistical Variations

A significant issue that currently confronts engineers undertaking electromagnetic simulations is uncertainty in the geometrical, material, and excitation parameters. Fabrication tolerances, surface roughness and material inhomogeneity, as well as the exact placement of features such as wires, all contribute to the discrepancies between simulated and experimental results. Therefore, it is becoming of paramount importance to be able to perform simulations that predict the expected variation in the results due to the complex interplay between the variations in the problem parameters.

The solution to electromagnetic problems often commences with a mathematical model that describes the original system under investigation. Although considerable effort might be required to incorporate statistical variations into the modelling process, it can provide very useful results to help in system design. The information available from existing models can be used for quantitative uncertainty analysis in three stages. First, the uncertainties of model inputs are identified and characterised. The stochastic inputs are fed into transfer functions to indicate propagation through the system. Finally, the uncertainties of model outputs are estimated from the input parameters. This is repeated many times to cover the parameter space.

1.2   Limitations of Statistical Analysis

Presently, the use of repeated simulations with different sets of input parameters is often used to make predictions. This approach is referred to as the Monte Carlo method. The length of each simulation depends on the complexity of model and the number of random input variables. The statistics of system

responses is obtained from numerous simulations of random input parameters. These variables are selected according a known distribution relevant to the model. Although this procedure is quite accurate, the convergence rate is very slow resulting in unrealistic computational demands for electromagnetic simulations. This involves thousands of simulations each lasting several hours for typical electromagnetic problems. Therefore, there is an emphasis on the development of computationally efficient paradigms for uncertainty estimation.

1.3   Objective of Thesis

The objective of this thesis is to develop computationally efficient techniques to quantify uncertainty without resorting to a substantial number of simulations associated with the Monte Carlo method. The main motivation is to develop these alternative techniques with the ultimate aim to incorporate them into the computational modelling process. For this to be achieved, the relationship between input and output parameters of the model of choice must be clearly defined. There must be a way to relate output parameters to input parameters of the original system being assessed. The model has to contain sufficient detail to capture the pertinent attributes of the system.

The computational requirements for alternative statistical methods, their applicability to a variety of problems and their ease of implementation are important issues that will be addressed. The additional effort required to deploy alternative techniques has to be worthwhile when compared with the potential to save costs. The methods proposed in this thesis either involve using model algorithms directly or by making modifications using sensitivity analysis. All these methods will be compared with the traditional Monte Carlo approach. In a simple sentence, the aim of this thesis is the direct computation of statistical variations in electromagnetic problems.

1.4   Outline of Thesis

This chapter presents a brief introduction into the limitations associated with traditional method for uncertainty measurement. The objective of the thesis is also presented followed by an outline of the subsequent chapters.

Chapter 2 presents a review of literature on uncertainty analysis. The motivation for pursing this endeavour is discussed and the types of uncertainty are mentioned. The available methods for representing uncertainty are also reviewed. The different approaches to sensitivity analysis are summarised and the pros and cons of each method are identified. Finally, the application of statistical techniques to electromagnetic compatibility (EMC) is described through a number of case studies.

Chapter 3 outlines the foundation of stochastic EMC problems from basic theory behind the probabilistic techniques through to the electromagnetic problems to which they are applied.

Chapter 4 illustrates the constraints associated with Monte Carlo analysis of one-dimensional (1-D) electromagnetic problems. The numerical solutions to these problems are derived from the 1-D Transmission Line Modelling (TLM) method. An alternative method based on Taylor series expansion is also presented. The difficulties involved in deriving approximate expressions for statistical behaviour of problems in time domain are also discussed.

Chapter 5 presents the Direct Solution Technique (DST) which is developed as a computationally efficient method for uncertainty analysis of electromagnetic problems. The DST method is based on matrix algebra which is useful to interface with modelling algorithms that involve discretisation of problems. The idea behind this technique, how it is implemented and applied are discussed in detail. As all the models used in this thesis are developed using TLM, the DST is tested on a simple circuit representing transmission line behaviour. The approximations obtained from DST are compared with the benchmark Monte

Carlo method. Although as yet the DST approach is restricted to the frequency domain and requires that the parameter variations are small, it enables good quality predictions to be obtained for the problems. The improvements to this method are obtained by using higher order approximations.

Chapter 6 presents the application of the DST to two-dimensional (2-D) electromagnetic problems. The nature of DST makes it interface properly with the 2-D TLM method which is discussed in detail. A variety of case studies are analysed using DST and comparisons made with the Monte Carlo method.

Chapter 7 demonstrates the application of DST to three-dimensional (3-D) electromagnetic problems. The Symmetrical Condensed Node (SCN) is introduced as the basic building block for developing 3-D TLM models. Due to computational constraints, the case studies here were restricted to 2-D cross section. Again, the DST approach is compared with the Monte Carlo method.

Chapter 8 presents the theory behind the Unscented Transform (UT) method. This is another alternative to the time consuming Monte Carlo approach. This technique commences with the standardisation of model inputs. The corresponding responses from these inputs are collated and expressions derived for their statistical moments. A set of deterministic (sigma) points designated with weights are used to sample the distribution of input variables. These are referred to as UT parameters. The relationship between the statistical moments of input parameters (in terms of sigma points and weights) is used to approximate the distribution of response parameters. The nature and number of the UT parameters depend on the number of input random variables and the type of distribution each possesses.

Chapter 9 presents the application of the UT technique to electromagnetic problems (in time and frequency domains) modelled using TLM. The statistical moments of measured responses are compared with the Monte Carlo method.

Chapter 10 presents the conclusions of the thesis and recommendations for future work.

Chapter 2   Review of Literature

The development of statistical tools to identify and quantify uncertainty has become an integral part of design methodology. The major reason for this is that conventional deterministic techniques, used to model underlying phenomena, are incapable of accounting for the random nature of system parameters. The consequence of this is a limitation upon investigation of the effects of stochastic characteristics of complex systems. The ultimate aim of this endeavour is to improve robustness, enhance independence and allows for flexibility in conceptual implementation of systems and computational modelling practice [2.1, 2.2]. A broad range of measures have been advocated in the literature to describe uncertainty. This chapter will give a distilled version of the available methods to date. A review will also be provided of the statistical techniques deployed in engineering applications unique to Electromagnetic Compatibility (EMC) problems.

2.1   Motivation

The shift in attitudes towards uncertainty as a phenomenon fundamental to scientific and engineering principles was detailed in [2.3]. A concise account is presented in this section.

The sources of information can be incomplete, imprecise, fragmentary, unreliable, vague, contradictory or deficient in some other way. This deficiency is the cause of uncertainty. Thus, it will be appropriate to point out that the amount of uncertainty is intimately connected to the amount of information. The effect uncertainty has on the perception of the real-world cannot be overstated. It is an interwoven component of measurement at an experimental level based upon the resolution limits of instruments and measurement errors. The perception of uncertainty has undergone a significant change during the past century from a

traditional viewpoint, where it is avoided, to a fundamental alternative where its evasion will be unfavourable.

The paradigm shift concerning uncertainty began in the late nineteenth century, when Newtonian mechanics was inapplicable in scenarios where the knowledge of the system investigated is incomplete. The development of relevant statistical methods initiated a radical approach in how this processes were examined. This lead to a new branch of study called *statistical mechanics*. Exact numbers from analytic methods based on calculus were substituted with statistical averages based on probability theory. The traditional perception of uncertainty was gradually suppressed and altered when statistical mechanics became an accepted scientific discipline in 1902. Analytical methods were predominantly implemented for case studies involving a modest amount of entities under observation while statistical methods were constantly adopted in the event of more variables with a higher stochastic content. The advent of computer technology in the second half of the nineteenth century was not sufficient to deal with random problems of very high complexity. The result of this was a motivation to devise new concepts and theories that can successfully navigate this type of obstacle. This is the primary interest of the research work presented in the later chapters of this thesis.

2.2   Types of Uncertainty

The conceptual and computational framework for complex analyses enables uncertainty classification into different sub-types. These are termed aleatory uncertainty and epistemic uncertainty [2.4 – 2.8]. The knowledge of uncertainty can aid in the direction of supplementary study or different measurement methods to reduce its effects.

2.2.1   Aleatory Uncertainty

This arises because of the inherent vagueness in the behaviour of the system under study. The cause of this emanates from situations where the choice between available alternatives is indeterminate. The perception of this type of uncertainty can be quantified using conventional statistical methods. This can be improved if better theories describing system behaviour become available. The sources of aleatory uncertainty can be distinguished from other forms by their depiction as randomly distributed quantities. These can take values in an established range with the actual one varying within. Other similar terminology for aleatory uncertainty include: stochastic, variability, irreducible, noncognitive and type A uncertainty [2.6 – 2.8].

2.2.2   Epistemic Uncertainty

This is associated ambiguity in accurate distinctions of parameters in the domain of interest. There are three types of ambiguity: nonspecificity, dissonance and confusion [2.5]. Nonspecificity is connected with the size of possible alternatives that govern the prospective behaviour of corresponding system entries. Dissonance deals with conflicting alternatives that give rise to contradictory entries. Confusion is when the possible alternatives do not overlap or only do so partially.

Unlike aleatory uncertainty which is down to capriciousness in system behaviour, this is a direct consequence of the lack of system information. The use of mathematical models and the choice of model assumptions can contribute to this effect. The resolution from the numerical grid cell size of a model offers an approximation to system behaviour which can be a source of epistemic uncertainty. The simplification of complex nonlinear systems using linear approximate models gives rise to this type of uncertainty. This becomes evident when these models are juxtaposed with more inclusive surrogate types. In addition, when making prediction via extrapolation, models ratified for a certain portion of the input space might be completely inconsistent for response

prognostication of other aspects of system entries. On that basis, the aftermath of disregarded phenomena becomes conspicuous as epistemic uncertainty. Other similar terminology for epistemic uncertainty include: subjective, state of knowledge, reducible, cognitive and type B uncertainty [2.7, 2.8].

2.3   Representations of Uncertainty

The appropriate representation of uncertainty is important due to the versatility of using the prescribed delineation across a variety of disciplines. The different manners of representing uncertainty presented here are highlighted in [2.3, 2.5, 2.8 - 2.15].

2.3.1   Classical Set Theory

Classical set theory is the conventional way to represent uncertainty [2.3, 2.10 – 2.12]. This is done using a collection of objections known as *elements* expressed by groups of alternatives in situations where only one scenario is feasible. This collection is commonly referred to as a crisp set [2.5], and is identified by the features of the comprising elements. The ideology behind this is the conformity to the rudimentary standard of precise reasoning. There is a characteristic function that discriminates between members and non-members of a set. The uncertainty expressed using this theory is due to the nonspecificity characteristic of each set. The size of a set is commensurate to the degree of specificity that accompanies its description. Complete specificity can only be achieved when only one alternative is possible [2.3].

2.3.2   Probability Theory

Probability theory is another classical approach to represent uncertainty in random experiments [2.3, 2.9, 2.10, 2.11]. The conventional way to define this

using set terminology is called a *probability space* [2.9, 2.11]. There are three facets that complete the characterisation of the probability space which are:

(i)   Universal Set – This contains the macrocosm of all possible outcomes of any event under examination. This is also known as the *universe of discourse* or the *sample space*. The uniquely classified members of a set are known as elementary events. It is important to note that there is a set that will give the most illumination on the outcomes of an analysis.

(ii)   Set of events – This is a restricted set of subsets, of possible outcomes, with an established consensus of membership. All subsets for the discrete sample space and only the measurable members in a continuous sample space correspond to events. A certain event is one that occurs in every trial.

(iii)   Probability – In non-specific experimentation, there is uncertainty affiliated with each possible event. The probability is the fundamental measure of likelihood for members of a subset. This can be defined as the ratio of the number of event occurrences to the size of the sample space. It is usually suitable to represent this as a number between zero and one. The probability of a sequence of disjoint sets from a given universe of discourse occurring either in isolation or in tandem is the sum of the probability ascribed to each event. The sum of the probability that an event exists and the probability that it does not must be unity. There is also the notion of dependency between two events. The probability that an event is conditional on another if this is equal to the ratio of the occurrence both events to that of the probability of the overriding event [2.7, 2.9 – 2.12].

In order to provide a pictorial description of information in the probability space, probability density functions (PDFs), cumulative distribution functions (CDFs) and complementary cumulative distribution functions (CCDFs) are deployed [2.9].

The CDF is a plot of points of the probability of a random variable assuming a value less than or equal to individual members of the universe of discourse. This is a monotonic function that increases from zero to one. Therefore, the first derivative of a CDF does not change sign from zero to one.

The PDF represents a probability as a function of a random variable so that that the total area under the curve translates to the sum of all probabilities of all events in the sample space and as such must be unity. The probability that a random variable exists between an interval of two different values is the area under the PDF graph bounded by the region of interest. Mathematically, the PDF of a continuous distribution is the derivative with respect to the random variable of the CDF [2.10 – 2.12].

The CCDF presents the probability of a random variable taking a value more than individual members of the sample space. Mathematically, this can be found by taking the difference between one and CDF. This makes the CCDF a monotonic function that decreases from one to zero [2.9].

The target of most probabilistic methods is on the use of functions. The uncertainty in the values of a function, defined using a probability space, can be characterised by the properties it has and the probability space of the independent random variable. In other words, the uncertainty in the range of a function can be adequately represented provided the domain of the function has a defined probability space [2.9, 2.11]. A Monte Carlo procedure is the most widely used technique to estimate the probability of the instance of a functional event from those of the independent random variable(s). The representation of uncertainty for stochastic problems in this thesis will be based solely on the axioms of probability theory. This is due mainly to this being the conventional approach for EMC problems upon which this thesis is founded.

2.3.3   Evidence Theory

The evidence theory allows for a more flexible concept of likelihood than is the case with a complete probabilistic specification. It can be viewed as a special application of probability theory. The probability space in the later case is replaced by an equivalent definition called the *evidence space* which has similar nomenclature for its members. [2.5, 2.9].

2.3.4   Possibility Theory

This is another variant to probability theory similar to evidence theory in expression of nonspecificity. The vagueness consistent with this type of representation is closely tied to fuzzy set theory where membership to a defined sample space is not an issue of affirmation or refusal but one of degree [2.3, 2.5, 2.7, 2.9].

2.3.5   Fuzzy Set Theory

The membership function defined for crisp sets allows for exclusivity of its elements to distinguish it from non-members. The representation of uncertainty using evidence theory or possibility theory is known as a *fuzzy measure* [2.3, 2.7]. In both cases, a graded value is assigned to crisp sets signifying the degree of membership to a universal set. The fuzzy measure is an outgrowth of the classical measure techniques that deals with ambiguity. It specifies the degree to which an arbitrary element of the universal set belongs to crisp subsets and aims to address the logical antinomies consistent with the classical theory. This provides a broader framework that has the capacity to handle the concept of partial truth and therefore allows for different formulations including and beyond the classical probability measures [2.5, 2.7].

2.3.6   Interval Analysis

This is based on using algebraic methods to propagate intervals from a domain of variables to the range of the function of these variables. This method is most suitable for problems where the sources of uncertainty are due to imprecise measurements and also because there are the available techniques to estimate model parameters are disparate in implementation and interpretation. The main advantage of using interval analysis is that it attends to problems where uncertainty cannot be assessed using probabilistic tools. This is especially the cases when the distributions of input parameters are unknown [2.13]. The range of a random function obtained using Monte Carlo techniques together with probability, evidence and possibility theory provide a reasonable approximation to the interval analysis solution given the *a priori* input probability structure. One drawback for using interval mathematics is that it ignores available information of stochastic inputs and thus will not be a recommended approach for problems of this nature. Another disadvantage is the lack of provision of adequate information on the uncertainty of system output as this is all confined into a single interval [2.7 - 2.9].

2.3.7   Rough Set Theory

This was proposed as a modified way to deal with imprecision in set boundaries [2.14, 2.15]. The philosophy behind this idea was based on the supposition that every object in a sample space has some information affiliated with it. The mathematical foundation of rough sets is an indiscernibility relation between the members. The implication of this is that rough sets have boundary line cases described by an ontological framework. This is contrary to crisp sets which can be classified in terms of the knowledge of their elements. The approach of using rough sets involves the replacement of vague boundaries by a lower and upper crisp set approximation. The lower approximation contains all objects that are surely members while the upper one has ambivalent members of the rough set.

2.4   Monte Carlo Analysis

Monte Carlo (MC) simulation techniques were introduced in the 1940s to deal with problems that comprise stochastic parameters from a system with probabilistic features. The implementation simply involves developing a mapping between model controlled and response variables using numerical integration [2.6].

The MC analysis is initiated by obtaining outputs from a sampled combination of inputs and completed by the statistical analysis of the outcomes. In order to ensure that the PDFs of output metrics are adequately described, analysis is carried out with sufficiently large samples. This is because as the number of samples increase without bound the MC procedure will converge towards the correct distribution function although the rate at which this happens depends on choice of sampling. This will always be the case, irrespective of the probability distribution type, provided the function to be sampled is continuous and every point in the sample space can be selected [2.9]. The probabilistic based procedure, used to generate samples, provides the basis to find the integral necessary to define distribution functions and their associated features. In all sampling based techniques, weights can be used in conjunction with the sample elements to calculate the expected value, variance and other entities. These statistical parameters are derived from the integration of the ensemble over entire universe of discourse.

Sampling based methods are widely used in the propagation of uncertainty in complex systems. The uncertainty in input parameters to the system is characterised using PDFs. This is then sampled and passed through the system equations to obtain the PDFs of the output parameters. Due to complexity, the performances of physical systems can be replaced by equivalent mathematical models. The input parameters to the model represent the physical characteristics, geometric properties or even boundary conditions for a differential equation describing the system [2.6]. For unique outcome of the analysis, the input variables must be unambiguously known and the purpose of sampling based

methods is to gain an insight into the behaviour of the model derived from the system under study. In addition, the variables with most significant contributions with respect to the uncertainty in analysis outcomes can be identified. Initial analysis can involve crude representations of variable uncertainty to decipher system behaviour; after which resources are channelled to improving uncertainty in important variables. Further iterations improve overall quality performance by providing repeated runs to validate the model under scrutiny and also the analysis implementation [2.16]. The system response can be assessed by a single representation of uncertainty; determined taking into account the aggregation of information from input variables. Some of the sampling based methods are more transparent than others depending on the ease of results. However, a common feature of this approach is that a large number of samples are required and the use of probability as the representation of uncertainty.

As shown in Fig. 2-1, the model derived can be used as a platform for any sampling based technique to propagate uncertainty as it is intrinsically a discretised version of the system it represents.
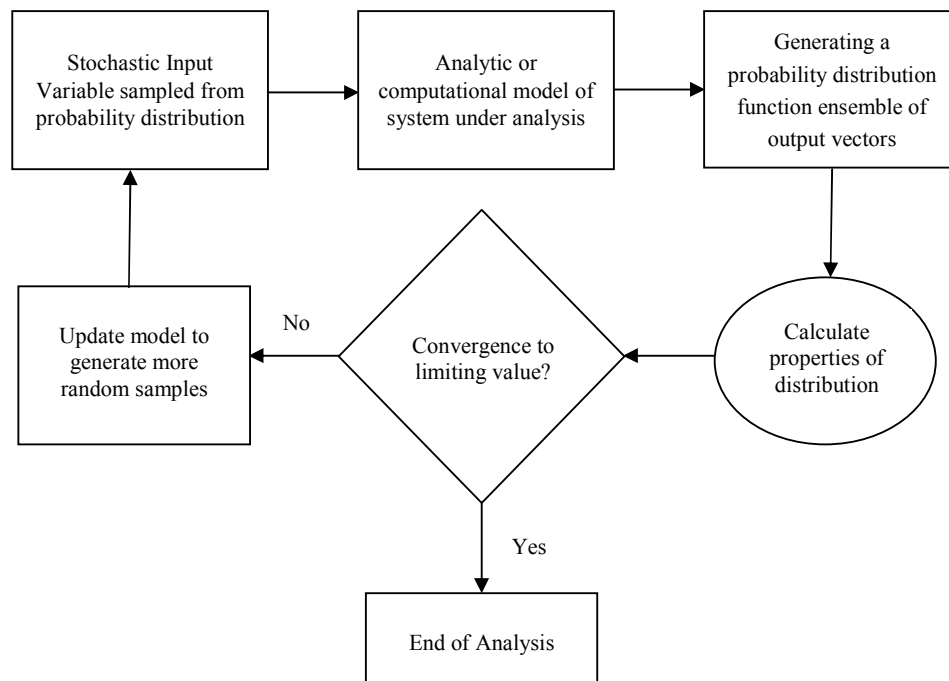
Fig. 2-1 Flow chart to express methodology behind uncertainty analysis using sampling based procedures

The total number of samples depends on the complexity of the problem and also the number of random variables described. For example, for nontrivial functions, there is a demand for extensive computation. A sequence of multiple simulations is executed until convergence of moments describing the distribution to a limiting value is attained [2.8]. It is also important than an appropriate resolution of model is used to ensure uncertainty exceeds the intrinsic error associated with measurement. This restricts analysis to stochastic system behaviour and not the numerical artefacts emanating from insufficient measurement resolution. An example of this is seen as numerical dispersion from discretisation and the introduction of stubs in Transmission Line Modelling (TLM) [2.17].

The application of the MC methods, ranging from environment monitoring or assessment to finance, is sometimes restricted to uncomplicated scenarios as it is prohibitive in terms of computational demands. The efficacy of this technique for diverse applications and the simplicity behind this approach is the main motivation for adopting it for some case studies in this thesis.

Some of the desirable features of the MC method include: the acquisition of results without the use of surrogate models, modifications to the original model are not required and as such it is easy to implement, the estimates of the distribution function can be known, the extensive sampling of stochastic variables leads to a full coverage of the range of uncertain variables and aids to identify fine features in distributions such as nonlinearities, thresholds and discontinuities. The overriding drawback is the computational cost for long running models which is a major stumbling block for complex non-deterministic problems [2.6].

Some of these sampling based methods include: *random sampling*, *Latin Hypercube sampling* and *stratified sampling*. Each method has a unique attribute that preserves its originality while maintaining the use of probabilistic weights to execute MC analysis. The similarity between them lies in the coverage of most of the specified regions or subsets of the sample space. The main distinguishing factor comes from the way the samples are stratified before selection in the generation of PDFs [2.6]. The random sampling is the preferred method in this

thesis due to its conceptual simplicity, ease of implementation and computational efficiency [2.18 – 2.20].

Random sampling is the simplest approach to MC analysis and is deployed in instances where sufficiently large samples arise to provide unbiased estimates of the moments of a probability distribution. Each element is generated from a particular subset at the same probability as that subset has for occurring. The use of evenly distributed bins in histogram generation illustrates this point. Each bin is considered the subset of the entire sample space. The elements that fall within the interval class so defined will have exactly the same probability formulating a uniform distribution. The envelope around the collection of bin sizes, each with a unique weight allocation, will correspond to the probability distribution of the random variable in question. The number of simulations is commensurate to the bins required to sample the distribution function. The sample elements are created using a reproducible algorithmic process rather than a purely random one and are thus called pseudorandom numbers. The pseudorandom number generators have an associated seed value that creates the same random sequence of samples.

2.5   Alternative Sampling Methods

This section describes sampling based methods that are available other than the MC technique.

2.5.1   Fourier Amplitude Sensitivity Test (FAST) Method

The FAST method was developed in 1973 [2.21] and is based on the Fourier series expansion of functional models using a dimension reduction, numerical integration scheme on nonlinear differential equations [2.22 – 2.24]. The beneficial traits of this method include: a complete exploration of the range of input variables, the direct estimation of expected value and variance and thus the avoidance of surrogate models, the contribution of each random variable to total

variance can be known, the effects of variable interactions can be determined and the modifications to the original model are not required. The mathematics to implement the FAST method is abstruse and this is the main reason why it not as ubiquitous as the MC method. There is also the computational demand involved in evaluating the required integrals. The method is also restricted to uncorrelated input variable types [2.6].

2.5.2   Reliability Based Method

The reliability based method has a history of about 70 to 80 years [2.25]. It provides estimates for measures of uncertainty using an iterative but comparatively less expensive approach than the MC method [2.26]. The computational efficiency of this method has seen it applied to design optimisation of engineering systems to evaluate probabilistic constraints of reliability analyses [2.27 – 2.31]. There are pros and cons associated with reliability based procedures like all the other sampling techniques. The expedient characteristics of the reliability based approach are the computational efficiency compared to MC methods and also the provision of each contribution of each random variable to the overall probability of failure. The hindrances to using the method is that the mapping procedure is more difficult to execute for black box models [2.32] and the calculation of probabilities of all random variables for multiple failure conditions will require considerable computational effort [2.7].

2.5.3   Response Surface Method

The response surface method was invented in 1951 [2.33] as another sampling based alternative to the MC procedure. The only difference between the two techniques is that the former executes sampling so that all stochastic variables are considered independently even if they are varied simultaneously. This approach to sampling methodology is known as *experimental design*. The uncertainty in the output of the system can be estimated by carrying out a MC simulation on the fitted response surface by using specific values and

interactions of crucial input parameters [2.6, 2.7, 2.34, 2.35].   Some advantages of using the response surface method include the ease to carry out sensitivity and uncertainty analyses from a fitted response surface in contrast to using the original model and the near accurate predictions it portrays for models involving linear or quadratic transfer functions. The drawbacks of using the method include the difficulty that can be involved in developing an experimental design, the need for a large number of design points for many input parameters, the difficulty on representing a detailed distribution function and the complication of finding the response surface that can approximate the model with minimal discrepancy [2.6].

2.5.4   Fast Probability Integration (FPI) Method

The FPI method was originated in 1956 [2.36] as a novel way to approximate analytically the integrals of multivariate functions depicting probability regions of interest [2.37, 2.38]. It is a precursor to the FAST method for circumventing the multidimensional numerical integration consistent with the MC method. The main desirable feature of FPI as a stand-alone method for uncertainty characterisation are the estimation of the tails or the more extreme output quantiles of a distribution at reduced computational expense in comparison to the conventional MC method. On the other hand, this method is deemed inadequate for instances where the calculation of a full distribution is required or where there are a lot of variates under consideration [2.6]. Other drawbacks to using FPI is the complicated nature of the mathematical procedure and also the computational demands surrounding the calculation of the partial derivatives required for its proper implementation [2.6].

2.6   Sensitivity Analysis

Sensitivity analysis is a branch of research that is closely related with the measurement of uncertainty. The sensitivity of any system involves the rate of change of the outcome variable with that of controlled model parameters and specifications. The information derived from the sensitivity of a system under consideration becomes desirable in the identification of the main contributors of uncertainty. The sensitivity analysis is vital for the evaluation of the usability of a model under analysis, determination of parameters required to have more accurate values and gain insight into the system characteristics. These features allow for parametric uncertainty to be directly incorporated into problem formulations.

Sensitivity measures can be generally classified into three broad divisions. Each classification employs a trade off between the accuracy in the estimates of the sensitivity measure and the extent of computation required. The first division is the *variation of parameters or model formulation*. This involves the execution of different combinations of the parameters of concern with a verified deterministic mathematical setup or by making improved modifications in the model structure such as enhancing the resolution of measurement. The second division is known as the *domain-wide sensitivity analysis*. This involves the study of the system behaviour over the whole range of parameter variation. The last division, the *local sensitivity analysis*, emphasises on the estimation of sensitivity by assessing the variation of parameters within close proximity of a sample point [2.7]. Several analytical methods based on sensitivity analysis have been proposed with widespread success across different subject areas.

2.6.1   Differential Analysis Method

This method is purely dependent on the premise that the model equations are known and can be differentiable with respect to a random parameter but are not explicitly determined. On the satisfaction of these conditions, there are two well known ways of implementing this technique [2.7]. The first is known as the

Neumann's expansion [2.39, 2.40]. This involves finding the inverse of the model operator from the equations that define it and then expressing it as a geometric series of the model solutions in the absence of randomness. The restriction here becomes apparent when the inverse of the operators are not readily tractable. The second is the perturbation method [2.39, 2.41] which is a renowned and widely adopted technique to compute sensitivity via the expansion of the stochastic parameter space in terms of the power series of small finite random disturbances or perturbations. This quantifies how much there is a deviation from an expected value of a precise solution to the problem defined. The impediment to adopting this particular scheme is in complex, nonlinear systems where perturbation terms are not small and hence require a greater number of series sensitivity coefficients to improve the order of the accuracy for the measured uncertainty approximation.

2.6.2   Green's Function Method

The Green's function is used in field theory to solve inhomogeneous ordinary differential equations with imposed boundary conditions compatible with the physics of the situation under observation [2.22, 2.42, 2.43]. This can be extended to stochastic problems by first making some mathematical alterations to system equations and then using Green's function to solve differential equations. The set of integrals obtained are easier to evaluate and better equipped to deal with higher order sensitivities [2.22, 2.44]. The robustness of the method is entrenched on the capacity to represent differential equations involving an arbitrary number of system parameters as a single set. The sensitivity coefficients of any order are expressed as an integral that is evaluated recursively. The calculation of well behaved integrals is simple in comparison to differential equations and hence is more economical when the number of system parameters is large [2.22].

2.6.3   Orthonormal Series Expansion Method

This method involves the definition of an arbitrary random process in terms of the Fourier series of orthonormal functions. The orthonormal functions have deterministic coefficients called the weights which represent the particular uncertainty distribution. The series expansion defined from this procedure is called the *polynomial chaos* expansion [2.30, 2.44 – 2.46] or the *Karhunen-Loeve* expansion [2.11, 2.46].

This polynomial chaos expansion establishes the foundation for the *Stochastic Response Surface Method* [2.7] and the *Deterministic Equivalent Modelling Method* [2.44, 2.45], both designed with the aim to alleviate the computational simulations required to sufficiently approximate uncertainty as demanded by the conventional approach. The input to the uncertain system undergoes a transformation via the series expansions and is used to project what the output behaviour is from a limited number of model simulations. The main advantage of this method is not only in its computational efficiency, but also the incentive created by using it on black-box or implicit type models or in scenarios where the sensitivities of random parameters cannot be explicitly determined. A natural and inevitable consequence of this is that modifications to the original model are not required to appreciate the potencies of the method. The unknown sensitivity coefficients that accompany the corresponding series expansion of model equations are not easily manipulated but can be estimated using a collocation method [2.45]. This imposes the condition that at a particular set of collocation points, the output metrics converge to a limiting value.

The Unscented Transform (UT) method [2.47] and the Moment Design Technique (MDT) [2.48] are other similar concepts of characterising uncertainty using series expansion. The idea behind this is to approximate a nonlinear mapping by a set of selected points called sigma points in UT and design points in MDT which are analogous to the collation points in polynomial chaos expansion. The output moments can be found through a weighted average of the sigma points determined by the moments of the input probability distribution

function. The UT approach will be included in this thesis as one of the proposed benchmark procedures of uncertainty propagation.

A major shortcoming with this stance of uncertainty estimation is the exponential increase in the number of test points required with the degrees of freedom.

2.6.4   Direct Method

The direct method simply involves finding the derivatives of the stochastic parameters of interest with respect to the input random variables. This is achieved by the differentiation of model equations that delineate system performance and finding the solution of the ensuing sensitivity equations. This is of particular significance where the system does not have an analytical framework to define a transfer function and consequently only a model that numerically evaluates this is appropriate. This method forms the basis of the *Direct Solution Technique* (DST) which is the subject of this thesis and will be discussed later in greater detail.

The direct approach for sensitivity analysis can be broadly classified into two categories [2.7]. The first is the *Coupled Direct Method* where the sensitivity equations are solved together with the rudimentary model equations. The second, the *Decoupled Direct Method*, is another alternative where the solutions to both equations are achieved independently in order to maximise computational efficiency.

The drawback to the direct method is that it requires access to explicit model equations and thus cannot be applicable to black-box problems where the governing model equations are not known. A common example of this is when an executable file is made available from numerical algorithms but the source code, that is responsible for the explicit relationship between input and output parameters, is inaccessible.

2.7   Applications of Statistical Techniques to EMC

2.7.1   Tolerances and Variability

The nature of practical systems is such that the stochastic nature of parameters that defines them renders deterministic assessment insufficient for expansive performance analysis. The requirement for precise manoeuvres to quantify uncertainty in loads, geometry, material properties, manufacturing processes and operational environments has become a growing necessity to allow for more competitive designs [2.48]. This is the reason motivating the incorporation of *tolerance* values in design to establish fluctuations around nominal system parameters due to the fabrication process, ambient temperature conditions, aging and other performance factors [2.49, 2.50].

The use of entity tolerance values can aid not only in the handling of variations in component characteristics from the manufacturing process (tolerance synthesis) but also provides an assessment on how it will affect the overall working of system in which that component is a part (tolerance analysis). As a result, there is an impetus to pursue statistical methods, in cases where the expected values of response from nominal input parameters are not adequate, for the characterisation of system behaviour. In fact, the tolerance of component values in design optimisation can now be expressed in terms of its mean or central value and the variance about it to facilitate statistical approximations of measured response parameters [2.49, 2.51]. This makes an attractive method to estimate the probability that prescribed system thresholds are exceeded given the statistical description of uncertain parameters.

There are four key aspects that are involved with the study of tolerances in engineering; namely size, form, orientation and position. The first two areas influence the shape and material behaviour of uncertain features while the later two govern the directionality and location respectively. The techniques that have been a focal point for this design include tolerance calculation, worst-case analysis, statistical analysis, design optimisation and constraint-based reasoning [2.51, 2.52]. The tolerance design is an essential part of manufacturing and plays

an integral role in the relation of performance to cost of a product. Therefore, it is necessary to ensure that the maximum range of tolerance is met while satisfying the functional requirement of the design process [2.51].

2.7.2 Tolerances in Selected Electrical Engineering Problems

The drive behind developing novel means to depict the random nature of system parameters has produced some encouraging dividends. There are many engineering case studies where some of the statistical techniques mentioned in this chapter have been profitably employed. This subsection highlights the progress that has been made with some examples.

The failure of conventional design methods to account for uncertainties of element values in design of integrated circuits have been solved via the application of practical and efficient statistical techniques. The reliability analysis and yield estimation in integrated circuit design has been improved through the use of MC sampling methods on an approximation strategy based on polynomial expansions of equivalent circuit parameters [2.53, 2.54]. The primary drawback here as stated before is the extensive amount of computation required to attain desired accuracy [2.55, 2.56]. Another problem with using a MC procedure (either in isolation or co-ordination with other statistical methods) is where the distribution of design parameters is unknown and the only available information is not beyond a central value and some tolerance related in some way to the variance of the input random variables [2.57]. These problems can be assuaged using the first-order second moment (FOSM) method from a truncated Taylor series expansion to calculate the variance of the output behaviour. This method requires, for its proper execution, the calculation of the sensitivities of the response with all the degrees of freedom. The performance of a linear-time invariant circuit was used to illustrate this in [2.56] where the response of a Butterworth low pass filter was considered. The required sensitivities from uncorrelated random entries were obtained using adjoint network procedures. The FOSM method was also found to be an alternative to the MC method in the calculation of the mean and variance of the frequency response of periodically

switched linear circuits such as switched capacitor networks and switching-mode power supplies. The cost of computation increases with the order of the derivatives [2.58]. Another proposed method for calculation of uncertainty in equivalent circuit model is known as *simulated annealing* (SA) which is similar in principle to the response surface method. This is basically a search method that conditionally explores a solution space and keeps track of the information on the sensitivities and uncertainties of random parameters. The SA method has been applied in the uncertainty analysis of high-speed devices [2.59].

The physical parameters of the components are affected by uncertainties from the construction process which is compounded by parasitics and actual operating conditions. The combined effect of uncertainty sources cause deviations from the nominal performance of adopted parameters [2.60]. The use of interval mathematics has been applied in the calculation of tolerances for switching converters and non-linear output functions that are used in electronic design [2.60 – 2.65]. A model approximation can be derived and interval mathematics applied to estimate the tolerance at a reduced computational effort [2.60]. The efficiency of the interval mathematics method for switching converters has been shown to improve using the genetic algorithm optimisation technique and it highlights its significance over the repeated analyses of the system while accounting for statistical distribution of parameter variations using the MC method [2.61].

The worst case circuit analysis is a nonlinear, multivariate and global optimisation problem that requires a thorough evaluation of system attributes against performance tolerance limits under the simultaneous existence of all the most unfavourable conditions. This method has been used strategically in the calculation of the gain of a band-pass filter with the tolerances of the passive components provided to determine if the circuit can withstand the changes in the environment. The MC method and Taylor series expansion approximation method can be used for worst case circuit analysis [2.65 – 2.66]. In situations where circuit equations cannot be used to explicitly determine tolerance responses the transformation into a set of linear equations using piecewise methods might be required prior to the application of interval mathematics.

However, the trade-off of the expansion error with ease of implementation has to be considered [2.65].

2.7.3   Statistics and EMC

The EMC analyses of complex systems conspicuously point to a statement that a lack of information stemming from uncertainty limits the extent to which deterministic prediction plays a role for a detailed investigation [2.67]. This creates a void in the feasibility of using nominal parameter simulations to get an insight into the internal physics in EMC applications inherently affected by variability. Probabilistic and statistical methods have the propensity to create a relationship between the accuracy of predicted features to the available data which cannot be achieved using deterministic modelling [2.68]. This subsection presents some case studies on the use of statistical methods in EMC.

The instrumentation and measurement of electromagnetic coupling mechanisms involves the challenge of suppressing electromagnetic interference (EMI) and enhancing EMC. Most of these EMC measurements are conducted in well-controlled coupling environments in facilities such as open-area test sites and anechoic chambers. The reverberation chamber can be used in a complementary role to the aforementioned measurement domains and is defined as a highly resonant cavity with metallic walls used to produce multi-mode fields with an average magnitude that tends towards a plane wave uniformly distributed throughout the entire volume. These conditions enable this enclosure to be used as a simple radiated, isotropic and randomly polarized test environment [2.69].

A variable scatter or paddle wheel is inserted as the mechanism to alter the modal excitation of the chamber [2.70]. The fields in the interior of the chamber are deterministic but owing to the changing boundary conditions, the ability of a given source to couple energy into certain modes can only be assessed statistically. A physical interpretation of the random field is that each member of the ensemble coincides with a different stirrer position [2.71]. The paddle wheel also forms a high quality factor with boundary conditions that are constantly

modified in the chamber making it exhibit a pass band characteristic [2.72, 2.73]. The quality factor is a useful parameter because it can predict the mean field strength from the input power [2.74]. The size of the paddle wheel determines the random nature of observed fields. There is a random modulation effect on the amplitude and frequency of fields for electrically large paddle wheels [2.75]. The stirring effect on modes achieved by mechanical means using the paddle wheel can equally be attained by sweeping the source of excitation over a narrow bandwidth [2.76]. Otherwise stated, the statistical interpretation of fields applied to equipment under test (EUT) in the reverberation chamber is an aftermath of either the stirring of the field modes electronically (from the source) or mechanically (using a paddle wheel or via vibration of the chamber walls) [2.77].

There are some paramount factors that determine whether a reverberation chamber is in the proper working configuration. These factors include the stirring ratio, field uniformity, the ratio of the maximum field to average field, and the underlying statistical characterisation of the fields. The PDF serves as a useful visualisation tool for underlying distributions of certain parameters of interest associated with a reverberation chamber. In a perfectly stirred chamber, the real and imaginary parts of the polarised (in-phase and quadrature components) electrical and magnetic fields have a normal distribution, the phase has a uniform distribution, the field magnitudes at the cut-off frequency of the modes are found to possess a Rayleigh distribution while the power (related to the square of the field amplitude) has an exponential distribution [2.71, 2.72, 2.78]. All the distributions associated with the reverberation chamber can be represented using MC techniques by mathematical manipulation of a uniform number generator [2.79, 2.80]. The advantage of using PDFs for field quantities is that estimators and their accuracy can be calculated. The quality factor of the chamber is directly proportional to the variance of the field components and the *maximum likelihood estimator* (the ratio of the mean square field to the number of degrees of freedom) whose statistical significance can be appreciated with large sample sizes [2.73]. The knowledge of these distributions can also be extended to the study of shielding effectiveness of an EUT within the chamber in a limited frequency range [2.81].

A statistical model for electromagnetic field variables in complex cavities can be obtained from the deterministic field expressions. The position vectors of fields in arbitrarily shaped cavities are treated as random variables distributed with a uniform distribution. The steady state field expression is adopted in conjunction with probability theory to obtain the statistical model. The eigenvectors of the arbitrarily shaped electrically large cavity with randomly crafted walls can be derived and used with the statistical model to acquire the volume averages of functions in the cartesian co-ordinates. The random cavity fields are interpreted to exhibit behaviour consistent with a superposition of a large number of photons with random locations and propagation direction. The attraction of statistical characterisation using this model has been illustrated in mode stirred chambers and RF system vulnerability assessment as incremental changes in test configuration or test object geometry can result in large deviations in measured responses [2.82].

EMI comes about as a result of unintentional coupling with an external source that degrades the effective performance of electrical/electronic devices. From a design perspective, it is important to limit the effects of EMI and this has lead to a surge in interest to construct analytically tractable, experimentally verifiable and statistical-physical models to achieve this goal [2.83]. There are three categories of electromagnetic noise distinguished by the comparison of the bandwidth of interference to that of the receptor system: Class A interference occurs in environments where the spectrum of noise is narrower than the bandwidth of the receptor, class B interference is seen when this situation is reversed and class C interference is a hybrid version combing the effects of the two previous classes [2.68, 2.83]. A useful way to observe the statistical impact of interference on the response of receptor is to place a typical narrow-band receiver in an electromagnetic environment [2.83]. A posteriori probability distributions are used to find out the chance that the envelope of a modulated waveform observed at the intermediate frequency (between that of the carrier and baseband signal) of the receiver exceeds a particular threshold that specifies the spectral range corresponding to a particular class of interference [2.68, 2.83].

Crosstalk is a type of EMI that is evident in wiring structures [2.68]. The random position of wires introduces a probabilistic aspect to the nature of crosstalk in transmission systems [2.67, 2.84]. This best describes the case when the problem described involves a bundle of wires in which their relative positions are unknown or vary in a haphazard manner. The method of interval mathematics is applied to experimental data to devise an empirical approach to find how coupling on cable harness matches with known statistical distributions via hypothesis tests [2.85]. The MC standpoint involves a single analysis output data as a random variable and considering several geometrical considerations to obtain a set of outcomes for substantial statistical treatment via repeated runs [2.68]. This is prevalent in cases where the information on the overall scale of non-uniformity is obtainable, the number of wires in the bundles is not high and the closed form expression of the cross talk PDF cannot be derived from random cable analysis because of arbitrary variation in cross section across the line axis [2.67, 2.68]. The efficacy of the MC method is also acknowledged in the uncertainty measurement of induced currents in a multiconductor transmission line (MTL). The source of illumination is a wave defined with random amplitude, polarisation or direction of incidence. The induced current magnitude is affected by the height above the ground, the cross-section and the load configurations of the MTL and this must be taken into account in its statistical interpretation [2.86].

On the other hand, a probabilistic model based on a purely analytical approach can be derived from the canonical circuit equations to calculate an implicit expression for crosstalk between a pair of wires above a ground plane separated by an unknown distance and at a random height above a ground plane both given by uniform distribution functions [2.84]. The constraint here is that the wires are straight, parallel and electrically-short [2.67, 2.84]. The distribution from both the empirical and analytical models for evaluating the coupling under these restrictions indicates a PDF with a lognormal characteristic [2.84, 2.85]. The crosstalk can be also investigated using a three conductor transmission line model in which a victim circuit integrates all the interference effects due to a generator circuit. The frequency behaviour of the mean and variance of the near and far end crosstalk voltage transfer ratio is derived in this paradigm using the

Taylor series method validated using the MC procedure as a benchmark [2.68, 2.87]. The perturbation theory is exploited, in the absence of closed-form expressions, to calculate useful statistical properties of wave propagation for quasi-random, inhomogeneous transmission lines [2.88].

Another important role of statistics in EMC is the characterisation of uncertainty associated with measurement systems. The quality of an EMC measurement can be tested and verified by repeating experimental procedures and improving the setup mechanism in order to suppress uncertainty. The process of identifying all the sources of error in measurement is called the *uncertainty budget* [2.68].

There are two types of error associated with measurement viz: *random errors* and *systemic errors*. The discrepancy between observed results and actual performance resulting from random errors is intrinsic to the measurement system. Upon closer scrutiny, it is evident that though this cannot be utterly eradicated, the effect of random can be minimised statistically to a large extent by repeated measurements using the MC method. The systemic errors also cannot be totally eliminated but the fluctuations about the nominal measurement values can be found thus allowing for appropriate amendments to data. The dispersion in measurement can be displayed using PDFs [2.68, 2.89]. The total uncertainty in a measurement system is expressed in decibels and is the accumulation of all the sources of uncertainty. This implies that the sources of uncertainty are a product of terms prior to the application of the logarithm to the base of ten. This leads to PDFs representing this type of uncertainty having normal and lognormal characteristics [2.68, 2.90]. The measurement of noise-parameters can also be subjected to uncertainty analysis. A low-noise amplifier has sources of uncertainty that are affected by the ambient temperature, reflection coefficients of terminations and variations in connection. The MC method can be used to elucidate the effect of these factors on the noise parameters. For instances where some factors are less dominant than others emphasis must be made on the parameters that cause maximum degradation in measurements [2.91].

2.8   Need for Alternative Uncertainty Analysis Methods

The ultimate objective behind this work is to explore the synergy between probabilistic and deterministic modelling tools to produce a seamless package unified into an organic whole. The use of statistical methods provides some information on the tolerance to be attributed to deterministic simulation results. This will be useful for yield analysis which can be defined as the number of system parameters that comply with imposed tolerance conditions [2.57]. The key feature of the effort behind this thesis is to cut down on the number of model runs required for MC simulations to obtain PDFs. Analytical methods are not as extensive or diverse as its MC counterpart but are good for problems where uncertainty is small and the system transfer function can be represented by mathematical equations. However, there is a need to find out ways to calculate higher order moments of responses as this will provide more information on the underlying distributions. These are the issues that will be addressed in this thesis using the DST method for electromagnetic modelling. The UT method is also used as a robust alternative that circumvents the need of transfer functions that are sometimes difficult to define.

2.9   References

[2.1]   S. Balakrishnan, A. Roy, M.G. Ierapetritou, G.P. Flach, and P.G. Georgopoulos, "Uncertainty Reduction and Characterization of Complex Environmental Fate and Transport Models: An Empirical Bayesian Framework Incorporating the Stochastic Response Surface Method," Water Resources Research, vol. 39, pp. 1350 – 1362, 2003.

[2.2]   A. Saltelli, S. Tarantola, and F. Campolongo, "Sensitivity Analysis as an Ingredient of Modelling," Statistical Science, vol. 15, pp. 377 – 395, 2000.

[2.3]   G.J. Klir, "The Many Faces of Uncertainty," In B.M Ayyub and M.M. Gupta, Editors, Uncertainty Modelling and Analysis: Theory and Applications, pp. 3 – 19, Elsevier Science, 1994.

[2.4]   J.C. Helton, "Alternative Representations of Epistemic Uncertainty," Reliability Engineering and Systems Safety, vol. 85, pp. 1 – 10, 2004.

[2.5]   G.J. Klir and T.A. Folger, "Fuzzy Sets, Uncertainty, and Information," Prentince-Hall, 1988.

[2.6]   J.C. Helton and F.J. Davis, "Latin Hypercube Sampling and the Propagation of Uncertainty in Analyses of Complex Systems," Sandia National Laboratories, 2002.

[2.7]   S.S. Isukapalli, "Uncertainty Analysis of Transport-Transformation Models," PhD Thesis, State University of New Jersey, New Brunswick, Rutgers, 1999.

[2.8]   W.L. Oberkampf, J.C. Helton, C.A. Joslyn, S.F. Wojkiewicz, and S. Ferson, "Challenge Problems: Uncertainty in System Response Given Uncertain Parameters," Reliability Engineering and System Safety, vol. 85, pp. 11 – 19, 2004.

[2.9]   J.C. Helton, J.D. Johnson, and W.L. Oberkampf, "An Exploration of Alternative Approaches to the Representation of Uncertainty in Model Predictions," Reliability Engineering and System Safety, vol. 85, pp. 39 – 71, 2004.

[2.10]   M.R. Spigel, J. Schiller, and R.A. Srinivasan, "Probability and Statistics," McGraw-Hill, 2000.

[2.11]   A. Papoulis, "Probability, Random Variables and Stochastic Processes," 2nd Edition, New York, NY: McGraw-Hill, 1984.

[2.12]   J.E. Freund, "Mathematical Statistics," Prentice Hall, Upper Saddle River, New Jersey, 1992.

[2.13]   H.E. Shaalan and R.P. Broadwater, "Using Interval Mathematics in Cost Benefit Analysis of Distribution Automation," Electric Power Systems Research, vol. 27, pp. 145 – 152, 1993.

[2.14]   Z. Pawlack, "Rough Sets," International Journal of Computer and Information Sciences, vol. 11, pp. 341 – 356, 1982.

[2.15] Z. Pawlack, "Rudiments of Rough Sets," Information Sciences, vol. 177, pp. 3 – 27, 2007.

[2.16] J.C. Helton and F.J. Davis, "Sampling Based Methods for Uncertainty and Sensitivity Analysis," Sandia National Laboratories, Albuquerque, NM, 2000.

[2.17] C. Christopoulos, "The Transmission-Line Modeling Method," IEEE Press, 1995.

[2.18] M.D. McKay, R.J. Beckman, and W.J. Conover, "A Comparison of Three Methods for Selecting Values of Output Variables in the Analysis of Output from a Computer Code," Technometrics, vol. 2, pp. 239 – 245, 1979.

[2.19] R.L. Iman and J.C. Helton, "An Investigation of Uncertainty and Sensitivity Analysis Techniques for Computer Models," Risk Analysis, vol. 8, pp. 71– 90, 1988.

[2.20] E.J. Pebesma and G.B.M. Heuvelink, "Latin Hypercube Sampling of Gaussian Random Fields," Technometrics, vol. 41, pp. 302 – 312, 1999.

[2.21] R.I. Cukier, C.M. Fortuin, K.E. Shuler, A.G. Petschek, and J.H. Schaibly, "Study of the Sensitivity of Coupled Reaction Systems to Uncertainties in Rate Coefficients. I. Theory," Journal of Chemical Physics, vol. 59, pp. 3873 – 3878, 1973.

[2.22] J. Hwang, E.P. Doughtery S. Rabitz and H. Rabitz, "The Green's function Method of Sensitivity Analysis in Chemical Kinetics," The Journal of Chemical Physics, vol. 69, pp. 5180 – 5191, 1978.

[2.23] A. Saaltelli, S. Tarantola, and K.P. Chan, "A Quantitative Model-Independent Method for Global Sensitivity Analysis of Model Output," Technometrics, vol. 41, pp. 39 – 56, 1999.

[2.24] T. Homma, and A. Saltelli, "Importance Measures in Global Sensitivity Analysis of Nonlinear Models," Reliability Engineering and System Safety, vol. 52, pp. 1 – 17, 1996.

[2.25] H.O. Madsen and T. Egeland, "Structural Reliability: Models and Applications," International Statistical Review, vol. 57, pp. 185 – 203, 1989.

[2.26] R.E. Melchers and M. Ahammed, "A Fast Approximate Method for Parameter Sensitivity Estimation in Monte Carlo Structural Reliability," Computers and Structures, vol. 82, pp. 55 – 61, 2004.

[2.27] A. Chiralaksanakul and S. Mahadevan, "First-Order Approximation Methods in Reliability-Based Design Optimisation," Journal of Mechanical Design, ASCE, vol. 127, pp. 851 – 857, 2005.

[2.28] K. Chan, S.J. Skerlos and P. Papalambros, "An Adaptive Sequential Linear Programming Algorithm for Optimal Design Problems with Probabilistic Constraints," Journal of Mechanical Design, ASCE, vol. 129, pp. 140 – 149, 2007.

[2.29] L. Cizelj, B. Mavko and H. Riesch-Oppermann, "Application of First and Second-Order Reliability Methods in the Safety Assessment of Cracked Steam Generator Tubing," Nuclear Engineering and Design, vol. 147, pp. 1 – 10, 1994.

[2.30] M. Hohenbichler, S. Gollwitzer, W. Kruse, and R. Rackwitz, "New Light on First and Second-Order Reliability Methods," Structural Safety, vol. 4, pp. 267 – 284, 1987.

[2.31] P. Bjerager, "On Computation Methods for Structural Reliability Analysis," Structural Safety, vol. 9, pp. 79 – 96, 1990.

[2.32] R. Ghanem and D. Ghiocel, "Comparative Analysis of FORM/SORM and Polynomial Chaos Expansions for Highly Nonlinear Systems," Proceedings of Engineering Mechanics, vol. 1, pp. 535 – 538, 1996.

[2.33] G.E.P. Box and K.B. Wilson, "On the Experimental Attainment of Optimum Conditions," Journal of the Royal Statistical Society, vol. 13, pp. 1 – 45, 1951.

[2.34] R.A. Fisher, "The Design of Experiments," Hafner Press, New York, 1971.

[2.35] A.I. Khuri and J.A. Cornell, "Response Surfaces: Design and Analyses," Marcel Dekker, New York, 1987.

[2.36] A.N. Freudenthal, "Safety and the Probability of Structural Failure," Trans. ASCE, vol. 121, pp. 1337 – 1397, 1956.

[2.37] F.E. Haskin, B.D. Staple, and C. Ding, "Efficient Uncertainty Analyses Using Fast Probability Integration," Nuclear Engineering and Design. vol. 166, pp. 225 – 248, 1996.

[2.38] M. Rosenblatt, "Remarks on a Multivariate Transformation," The Annals of Mathematical Statistics, vol. 23, pp. 470 – 472, 1952.

[2.39] S. Adhikari and C.S. Manohar, "Dynamic Analysis of Framed Structures with Statistical Uncertanities," International Journal of Numerical Methods in Engineering, vol. 44, pp. 1157 – 1178, 1999.

[2.40] L. Eyges, "The Classical Electromagnetic Field," Dover Publications, New York, 1972.

[2.41] J.G. Simmonds and J.E. Mann, "A First Look at Perturbation Theory," 2nd Edition, New York, NY: Dover Publications, 1997.

[2.42] E.P. Doughtery and H. Rabitz, "A Computational Algorithm for the Green's Function Method of Sensitivity Analysis in Chemical Kinetics," International Journal of Chemical Kinetics, pp. 1237 – 1249, 1979.

[2.43] R.G. Ghanem and P. Spanos, "Stochastic Finite Elements: A Spectral Approach," Springer-Verlag, New York, 1991.

[2.44] J. Villadsen and M.L. Michelsen, "Solution of Differential Equation Models by Polynomial Approximation," Prentice-Hall, Englewood Cliffs, New Jersey, 1978.

[2.45] M.A. Tatang, "Direct Incorporation of Uncertainty in Chemical and Environmental Engineering Systems," PhD Thesis, Massachusetts Institute of Technology, 1995.

[2.46] S.J. Julier and J.K. Uhlmann, "Unscented Filtering and Nonlinear Estimation," Proc. IEEE, vol. 92, pp. 401 – 422, Mar. 2004.

[2.47] J. Zhang, "The Calculating Formulae, and Experimental Methods in Error Propagation Analysis," IEEE Trans. on Reliability, vol. 55, pp. 169 – 181, Jun. 2006.

[2.48] S. Choi, R.V. Grandhi, R.A. Canfield and C.L. Pettit, "Polynomial Chaos Expansion with Latin Hypercube Sampling for Predicting Response Variablity," AIAA Journal., vol. 41, pp. 1191 – 1198, Jun. 2004.

[2.49] W.F. Curi and K. Ponnambalam, "Introductory Probabilistic and Stochastic Analysis and Design of Circuits," IEEE. Trans. on Education, vol. 36, pp. 51 – 56, Feb. 1993.

[2.50] F. Vallette and G. Vasilescu, "A Non-Statistical Approach to Tolerance Analysis of Microwave Circuits," Proceedings of the 40th Midwest Symposium on Circuits and Systems, vol. 2, pp. 1083 – 1086, Aug. 1997.

[2.51] C.C. Yang, M.M. Marefat and F.W. Ciarallo, "Tolerance Analysis and Synthesis by Interval Constraint Networks," Proc. of the IEEE International Conference on Robotics and Automation, pp. 2522 – 2527, Apr. 1997.

[2.52] H. Wang, N. Pramanik, U. Roy, R. Sudarsan, R.D. Sriram and K.W. Lyons, "A Scheme for Mapping Tolerance Specifications to Generalized Deviation Space for Use in Tolerance Synthesis and Analysis," IEEE Trans. on Automation Science and Engineering, vol. 3, pp. 81 – 91, Jan. 2006.

[2.53] J.F. Swidzinski and K. Chang, "Nonlinear Statistical Modeling and Yield Estimation Technique for Use in Monte Carlo Simulations," IEEE Trans. Microwave Theory Tech., vol. 48, pp. 2316 – 2324, Dec. 2000.

[2.54] F.N. Najm, I.N. Hajj, and P. Yang, "An Extension of Probabilistic Simulation for Reliability Analysis of CMOS VLSI Circuits," IEEE Trans. Computer-Aided Design, vol. 10, pp. 1372 – 1381, Nov. 1991.

[2.55] M.H.J. Bollen, "Method for Reliability Analysis of Industrial Distribution Systems," IEE Proceedings-C, vol. 140, pp. 497 – 502, Nov. 1993.

[2.56] F. Yuan, "Analysis of Stochastic Behaviour of Linear Circuits Using First-Order Second-Moment and Adjoint Network Techniques," Electronic Letters, vol. 33, pp. 766 – 768, Apr.1997.

[2.57] E. Laermans, F. Olyslager and D. De Zutter, "Sensitivity Based Statistical Analysis of Multiconductor Transmission Lines in Multilayered Media," Antennas and Propagation Society International Symposium, vol. 1, pp. 288 – 291, Jul. 1996.

[2.58] F. Yuan, "Efficient Non-Monte Carlo Method for Statistical Analysis of Periodically Switched Linear Circuits in Frequency Domain," IEE Proceedings-Circuits, Devices and Systems, vol. 150, pp. 423 – 428, Oct. 2003.

[2.59] M.-K. Vai, Y. Chen, S. Prasad, B. Meskoob and C. Bulutany, "Uncertainty and Sensitivity Analysis in High Speed Device Modelling," IEEE/Cornell Conference on Advanced Concepts in High Speed Semiconductor Devices and Circuits, pp. 75 – 83, 1991.

[2.60] A. Cirillo, N. Femia and G. Spagnuolo, "An Interval Mathematics Approach to Tolerance of Switching Converters," 27th Annual IEEE Power Electronics Specialists Conference, vol. 2, pp. 1349 – 1355, Jun. 1996.

[2.61] N. Femia, G. Spagnuolo and G. Vocca, "Genetic Optimisation of Interval Mathematics-Based Sensitivity Analysis of Switching Converters," 23rd International Conference on Industrial Electronics, Control and Instrumentation, vol. 2, pp. 639 – 644, Nov. 1997.

 [2.62] G. Shilo, O. Voropay and M. Gaponenko, "Interval-Statistical Analysis of Tolerances," The International Conference – Modern Problems of Radio Engineering, Telecommunications and Computer Science, pp. 575 – 578, Feb. 2004.

[2.63] A.F. Tsetkov, "Tolerance Calculation in Radio Electronic Devices," Ryazan: RRTI, 1970.

[2.64] L.V. Kolev, V.M. Mladenov, and S.S. Vladov, "Interval Mathematics Algorithms for Tolerance Analysis," IEEE. Trans. On Circuits and Systems, vol. 35, pp. 967 – 974, Aug. 1988.

[2.65] W.M. Smith, "Worst Case Circuit Analysis – An Overview (Electronic Parts/Circuit Tolerance Analysis)," Annual Reliability and Maintainability Symposium, pp. 326 – 334, Jan. 1996.

[2.66] W. Tian, X. Ling and R. Liu, "Novel Methods for Circuit Worst-Case Tolerance Analysis," IEEE. Trans. on Circuit and Systems, vol. 43, Apr.1996.

[2.67] A. Ciccolella and F.G. Canavero, "Stochastic Prediction of Wire Coupling Interference," International Symposium on Electromagnetic Compatibility, pp. 51 – 56 1995.

[2.68] S.A. Pignari, "Statistics and EMC," The Radio Science bulletin, March 2006.

[2.69] S.-P. Yu and C.F. Bunting, "Statistical Investigation of Frequency-Stirred Reverberation Chambers," IEEE International Symposium on Electromagnetic Compatibility, pp. 155 – 159, 2003.

[2.70] P.F. Wilson, "Advances in Radiated EMC Measurements Techniques," The Radio Science bulletin, December 2004.

[2.71] D.A. Hill, "Spatial Correlation Function for Fields in a Reverberation Chamber," IEEE Trans. on Electromagnetic Compatibility, vol. 37, pp. 138, Feb. 1995.

[2.72] C.F. Bunting, K.J. Moeller, C.J. Reddy, and S.A. Scearce, "A Two Dimensional Finite-Element Analysis of Reverberation Chambers," IEEE Trans. on Electromagnetic Compatibility, vol. 41, pp. 280 – 289, Nov. 1999.

[2.73] C.F. Bunting, "Statistical Characterization and the Simulation of a Reverberation Chamber Using Finite-Element Techniques," IEEE Trans. on Electromagnetic Compatibility, vol. 44, pp. 214 – 221, Feb. 2002.

[2.74] J.G. Kostas and B. Boverie, "Statistical Model of a Mode Stirred Chamber," IEEE Trans. on Electromagnetic Compatibility, vol. 33, pp. 214 – 221, Feb. 1991.

[2.75] D.L. Wu and D.C. Chang, "The Effect of an Electrically Large Stirrer in a Mode-Stirred Chamber," IEEE Trans. on Electromagnetic Compatibility, vol. 31, pp. 164–170, May 1989.

[2.76] D.A. Hill, "Electronic Mode Stirring for Reverberation Chambers," IEEE Trans. on Electromagnetic Compatibility, vol. 36, pp. 294 – 299, Nov. 1994.

[2.77] N.K. Kouveliotis, P.T. Trakadas, I.I. Hairetakis and C.N. Capsalis, "Experimental Investigation of the Field Conditions in a Vibrating Intrinsic Reverberation Chamber," Microwave and Optical Technology Letters, vol. 40, pp. 35 – 38, Jan. 2004.

[2.78] M. Migliaccio, "On the Phase Statistics of the Electromagnetic Field in Reverberating Chambers," IEEE Trans. on Electromagnetic Compatibility, vol. 43, pp. 694 – 695, Nov. 2001.

[2.79] J.M. Ladbury, "Monte Carlo Simulation of Reverberation Chambers," Digital Avionics Systems Conference Proceedings, vol. 2, pp. 10.C.1-1 – 10.C.1-8, Oct. 1999.

[2.80] L. Musso, F. Canavero, B. Demoulin, and V. Berat, "A Plane Wave Monte-Carlo Simulation Method for Reverberation Chamber," EMC Europe, Sorrento, Italy, 2002.

[2.81] C.F. Bunting, "Shielding Effectiveness in a Two-Dimensional Reverberation Chamber Using Finite-Element Techniques," IEEE Trans. on Electromagnetic Compatibility, vol. 35, pp. 548 – 552, Aug. 2003.

[2.82] T.H. Lehman, "A Statistical Theory of Electromagnetic Fields in Complex Cavities," Interaction Notes, May 1993.

[2.83] D. Middleton, "Statistical-Physical Models of Electromagnetic Interference," IEEE Trans. on Electromagnetic Compatibility, EMC-19, pp. 106 – 127, Aug. 1977.

[2.84] S. Shiran, B. Reiser and H. Cory, "A Probabilistic Model for Evaluation of Coupling Between Transmission Lines," IEEE Trans. on Electromagnetic Compatibility, vol. 35, pp. 387 – 393, Aug. 1993.

[2.85] G.T. Capararo and C.R. Paul, "A Probabilistic Approach to Wire Coupling Interference Prediction," International Zurich Symposium on Electromagnetic Compatibility, pp. 267 – 272, Feb. 1981.

[2.86] S. Pignari and D. Bellan, "Statistical Characterisation of Multiconductor Transmission Lines Illuminated by a Random Plane-Wave Field," IEEE International Symposium on Electromagnetic Compatibility, vol. 2, pp. 605 – 609, Aug. 2000.

[2.87] D. Bellan, S.A. Pignari and G. Spadacini, "Characterisation of Crosstalk in Terms of Mean and Standard Deviation," IEE Proceedings-Science, Measurement and Technology, pp. 289 – 295, vol.150, Nov. 2003.

[2.88] F. Wenger, T. Gustafsson, and L.J. Svensson, "Perturbation Theory for Inhomogeneous Transmission Lines," IEEE Trans. Circuits Systems – I: Fundamental Theory and Applications, vol. 49, pp. 289 – 297, Mar. 2002.

[2.89] IEC CISPR, "Specification for Radio Disturbance and Immunity Measuring Apparatus and Methods – Part 4-2: Uncertainties, Statistics and Limit Modelling – Uncertainty in EMC Measurements," International Electrotechnical Commission, vol. 16, Nov. 2003.

[2.90] E.L. Bronaugh and J.D.M. Osburn, "Estimating EMC Measurement Uncertainty Using Logarithmic Terms (dB)," IEEE International Symposium on Electromagnetic Compatibility, pp. 376 – 378, Aug. 1999.

[2.91] J. Randa and W. Wiatr, "Monte Carlo of Noise-Parameter Uncertainties IEE Proceedings-Science, Measurement and Technology, vol. 149, pp. 333 – 337, Nov. 2002.

Chapter 3   Basic Theory

The use of probabilistic techniques is the widely accepted approach for uncertainty analysis of mathematical models. In EMC studies, numerical solutions of equivalent circuit models simplify the rigorous differential equations describing their behaviour. The aims of this chapter are two fold. First, to provide an introduction to probability techniques used in this thesis. Second, to present the basic electromagnetic theory that explains the models used in later chapters. The combination of both independent areas of study will establish a firm foundation for stochastic EMC problems.

PART I

3.1   The Random Variable

The concept of a random variable entails a function that has a domain which is the sample space of experimental outcomes [3.1]. Alternatively, it is regarded as a mathematical quantity that depicts uncertainty. A random variable can describe, from the sample space of experimental outcomes, the range of values that the probabilities associated with an uncertainty quantity can assume [3.2, 3.3].

The random variable can take any value between plus and minus infinity provided that there are no physical restrictions. For example, the constitutive parameters defining relative permeability and permittivity of a material cannot be less than unity.

Mathematically, let X be a random variable that expresses all possible outcomes from an engineering system. This transformation is either a one-to-one or one-to-many mapping process [3.4]. The characteristic of the outcomes is such that

the set $\{X \le x\}$ is an event for any real number x. The probability of an event where X tends to an absolute value of infinity is zero [3.2]:

$$P\{X = +\infty\} = P\{X = -\infty\} = 0 \tag{3.1}$$

Random variables can be classified based on their features into two main types [3.1, 3.3, 3.4]:

- *Continuous Random Variables*: These typify the random variables that have continuous range of values within a specific interval. In this case, it is impossible to find an exact value of the random variable as there are an infinite number of possible values. This is the reason why intervals are used to ascertain what the likelihood is that a random variable is between two known values. The cumulative distribution function (CDF) $F(x)$ of a continuous random variable X is the probability of the event $\{X \le x\}$ and is represented by the expression [3.5]:

$$F(x) = P(X \le x) \tag{3.2}$$

The continuous cumulative distribution function has the following properties [3.1 – 3.6]:

(i)
$$F(x) = \begin{cases} 0 & x = -\infty \\ 1 & x = +\infty \end{cases} \tag{3.3}$$

(ii)
$$F(x_1) \le F(x_2) \qquad x_1 < x_2 \tag{3.4}$$

(iii)
$$\lim_{y \to 0^+} F(x + y) = F(x) \qquad \forall x \tag{3.5}$$

The properties shown in (3.3) – (3.5) above show that $F(x)$ is a continuous, monotonically increasing function from zero to one [3.5].

The derivative of $F(x)$ is another distribution function known as the probability density function (PDF) defined as:

$$f(x) = \frac{dF(x)}{dx}$$

(3.6)

Proceeding from the axiom of monoticity of the CDF, it is consistent to state that $f(x)$ is non-negative; that is [3.1],

$$f(x) \geq 0$$

(3.7)

The properties of $F(x)$ in (3.3) and (3.6) can be adapted to form an expression to represent the corresponding PDF as a definite integral over the range of real numbers ad infinitum [3.4]:

$$P(-\infty < X < +\infty) = F(\infty) - F(-\infty) = \int_{-\infty}^{+\infty} f(x)\,dx = 1$$

(3.8)

The CDF $F(x)$ can thus be given by an expression from (3.7):

$$F(x) = F(x) - 0 = F(x) - F(-\infty) = \int_{-\infty}^{x} f(u)\,du$$

(3.9)

The expression of $f(x)$ in (3.6) can be rewritten by taking into account that of $F(x)$ in (3.9):

$$f(x) = \frac{d}{dx} \int_{-\infty}^{x} f(u)\,du$$

(3.10)

The PDF $f(x)$ is expressed as a real-valued function of a random variable representative of the probability of each point within an interval and the total area under it must be one [3.1, 3.4]. The probability that a non-discrete random variable X lies within a range of two different values x_1 and x_2 is:

$$P(x_1 < X < x_2) = F(x_2) - F(x_1) = \int_{x_1}^{x_2} f(x)dx \qquad (3.11)$$

The probability of the event $\{X \geq x\}$ can easily be derived from the (3.8) and (3.9):

$$P(X \geq x) = \int_{x}^{+\infty} f(x)dx = 1 - P(X < x) = 1 - F(x) \qquad (3.12)$$

- *Discrete Random Variables*: These are random variables that arise from discrete values of a set [3.1]. These are distinct from the continuous types as the probability of occurrence of a discrete random variable X can be determined by a probability mass function (PMF) $P(x)$ in which the random variable is equal to an exact value denoted by [3.4]:

$$P(x_i) = P(X = x_i) \qquad (3.13)$$

where x_i is the ith value of X.

The PMF must obey the inequality [3.4]:

$$0 \leq P(x_i) \leq 1 \qquad (3.14)$$

In addition to the property in (3.14), the sum of all possible probabilities of the random variable must be equal be one. Let n be the total number of outcomes or the number of elements in the sample space of the random variable, then:

$$\sum_{i=1}^{n} P(x_i) = 1 \qquad (3.15)$$

The discrete cumulative distribution function in which X, as shown in (3.15), can take on a finite number of values x_1, x_2 ,..., x_n has the following properties [3.1, 3.4, 3.5]:

(i)

$$F(x) = \begin{cases} 0 & -\infty < x < x_1 \\ P(x_1) & x_1 \leq x < x_2 \\ P(x_1) + P(x_2) & x_2 \leq x < x_3 \\ \vdots \\ P(x_1) + \bullet \bullet \bullet \bullet + P(x_n) & x_n \leq x < \infty \end{cases} \qquad (3.16a)$$

(ii)

$$F(x_i) = P(X \leq x_i) = \sum_{j=1}^{i} P(x_j) \qquad (3.16b)$$

(iii)

$$F(x_1) \leq F(x_2) \qquad x_1 < x_2 \qquad (3.17)$$

(iv)

$$P(X = x_i) = F(x_i) - \lim_{y \to x_i^-} F(y) \qquad \forall x_i \qquad (3.18)$$

(v)

$$P(x_1 \leq X \leq x_2) = F(x_1) - \lim_{y \to x_2^-} F(y) \qquad (3.19)$$

The properties shown in (3.16a) − (3.19) above show that $F(x)$ is a discontinuous, monotonically increasing function from zero to one [3.5]. Consider an example distribution function with the features:

$$F(x) = \begin{cases} 0 & -\infty < x < 0 \\ 0.5 & 0 \leq x < 1 \\ 1 & 1 \leq x < 2 \end{cases} \qquad (3.20)$$

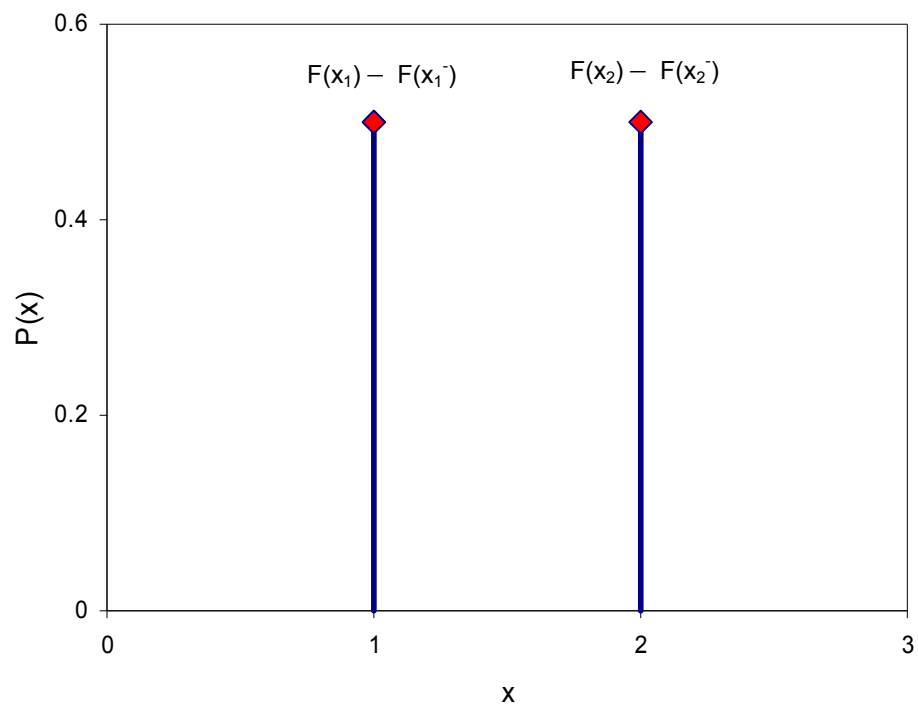From (3.18), the corresponding PMF $P(x) = \{0.5, 0.5\}$ as shown in Fig. 3.1-A.

Fig. 3-1A Probability mass function of a discrete random variable
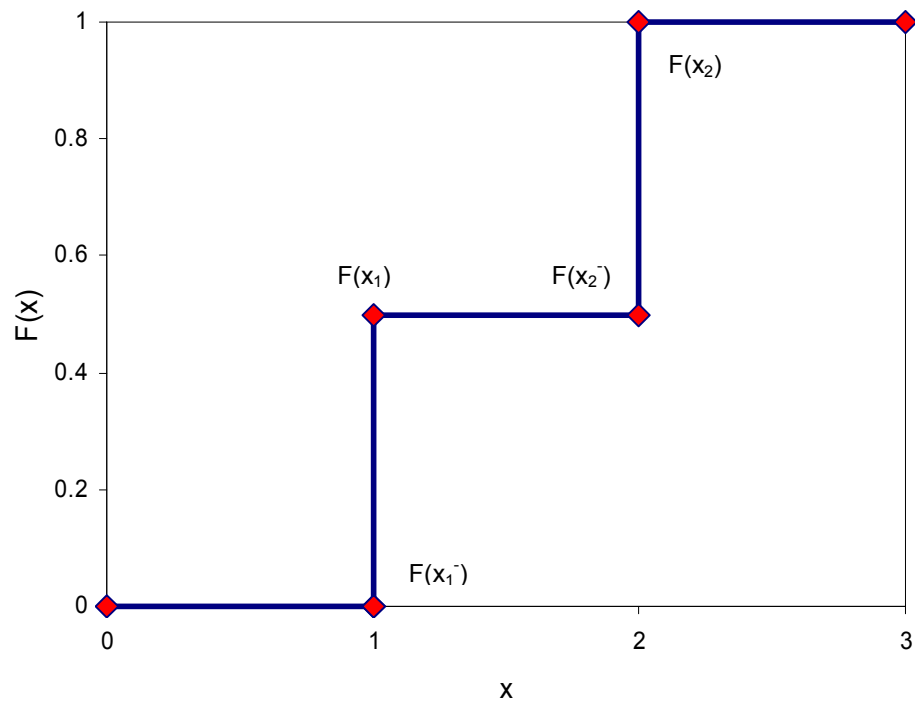

Fig. 3-1B Cumulative mass function of a discrete random variable

The cumulative mass function (CMF) in (3.20) is depicted in Fig. 3.1-B. From the diagram, it is clear that the jump at 1 and 2 is precisely the probabilities that the random variable is equal to either of these integer values, that is 0.5. From (3.19), it is seen that it is a sure event that the random variable selected per experiment is between 1 and 2.

The uncertainty analysis of electromagnetic problems usually involves the use of the MC method. The sample space of uncertain parameters has finitely many elements and as a result any random variable type must be of the discrete type and obey the axioms postulated above. However, it must be noted that the discrete random variable provides an approximation of the continuous distribution functions and a sufficiently large number of samples improves the precision of uncertainty measurement.

3.2   Normal Distribution and Central Limit Theorem

The normal or Gaussian random variable X is one defined by the PDF [3.1, 3.4 – 3.6]:

$$f(x) = \frac{1}{\sigma\sqrt{2\pi}} e^{-\frac{(x-\bar{x})^2}{2\sigma^2}} \quad -\infty < x < \infty \quad (3.21)$$

where $\bar{x}$ is the mean of the distribution and σ is the standard deviation. Both parameters will be studied in later sections.

The CDF of a normal distribution is given by [3.4, 3.6]:

$$F(x) = \frac{1}{\sigma\sqrt{2\pi}} \int_{-\infty}^{x} e^{-\frac{(x-\bar{x})^2}{2\sigma^2}} dx \quad (3.22)$$

The normal distribution has the following properties [3.4]:

(i)   The PDF tends to zero as the absolute value of the normal random variable approaches infinity.

(ii)   The PDF is symmetric about the mean $\overline{x}$. This implies for any real number x_0 then $f\left(\overline{x} - x_0\right) = f\left(\overline{x} + x_0\right)$.

(iii)   The mode, that is the value that occurs most in a data set, and the mean of the distribution are the same.

(iv)   The mean and variance are the parameters that describe the distribution.

(v)   The mean of the sum of normally disturbed independent variables is equal to the sum of the mean of each of the random variables.

(vi)   The variance of the sum of normally disturbed independent variables is equal to the sum of the variance of each of the random variables.

In Fig. 3-2A, the PDF of a normal distribution is shown for a random variable with a mean = 10 and standard deviation = 2. The corresponding CDF is presented in Fig. 3-2B.

From [3.5], the *central limit theorem* states that for a sum of independent N random variables that are distributed identically with a finite variance tends to a normal distribution as the N approaches infinity. This theorem is the main motivation for the choice of the normal distribution for most of the case studies presented in this thesis as the cumulative effect of many sources of uncertainty (without a dominant distribution type) can be modelled by a solitary random variable with a normal distribution [3.6].
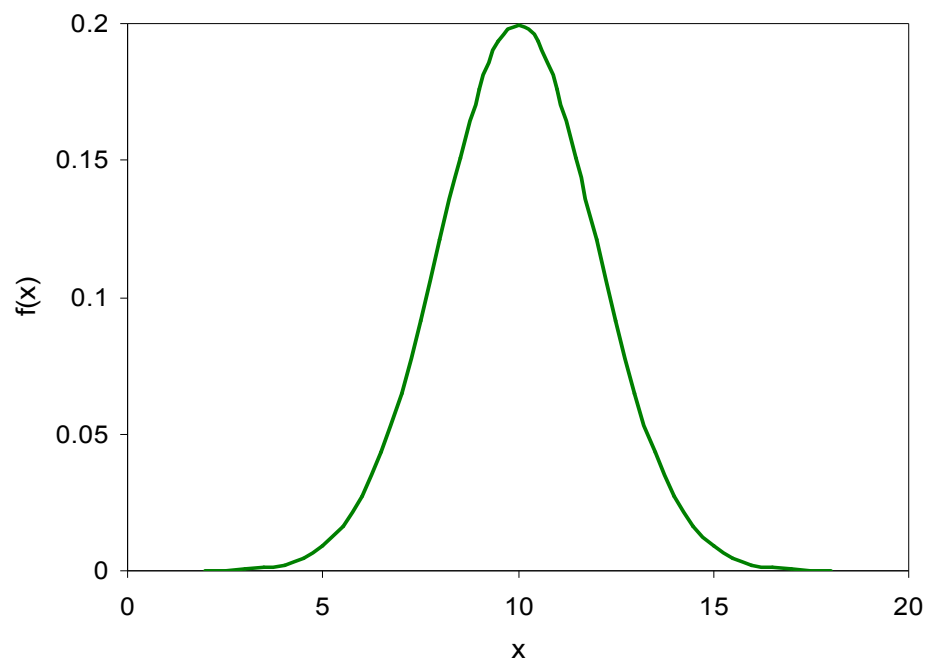
Fig. 3-2A Probability density function of the normal distribution
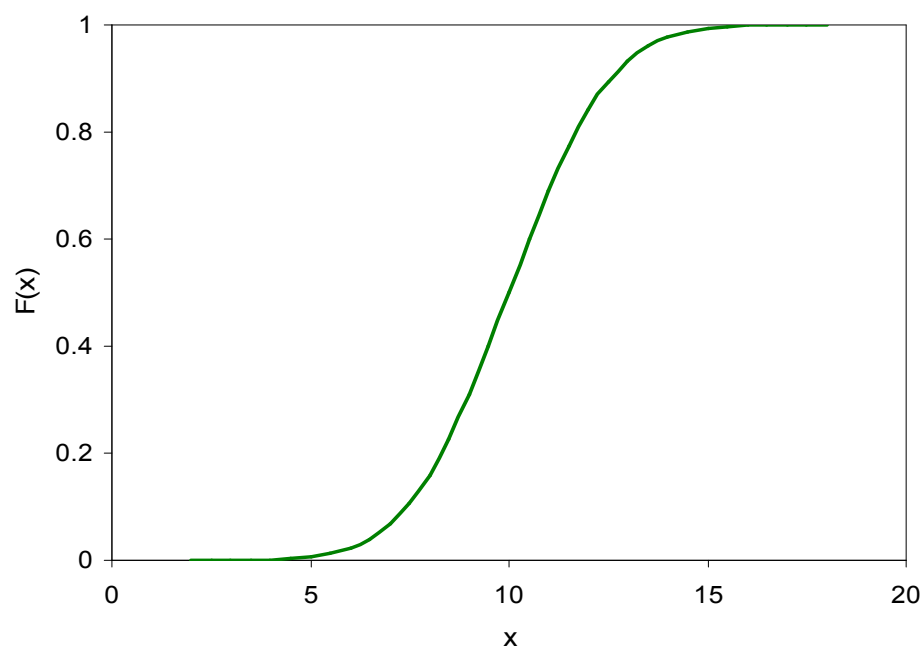
Fig. 3-2B Cumulative density function of the normal distribution

3.3   Exponential Distribution

The random variable X with an exponential distribution is defined by the PDF [3.1, 3.6]:

$$f(x) = \lambda e^{-\lambda x} U(x) \qquad \lambda > 0, x \geq 0. \tag{3.23}$$

where $U(x)$ is a unit step function and λ is a factor necessary to ensure (3.23) satisfies (3.8).

The cumulative distribution function is obtained by substituting (3.23) into (3.9) [3.1, 3.4]:

$$F(x) = 1 - e^{-\lambda x} \tag{3.24}$$

The PDF and CDF of an exponential distribution with $\lambda = 1$ are shown in Fig. 3-2A and Fig. 3-2B respectively.

The choice of the exponential distribution in this thesis is important as the random variable is non-negative and therefore typical of the examples used for the case studies. This also verifies that the proposed approximation techniques are not restricted to the more tractable normal distribution.

$\lambda = 1$

Fig. 3-3A Probability density function of the exponential distribution

$\lambda = 1$
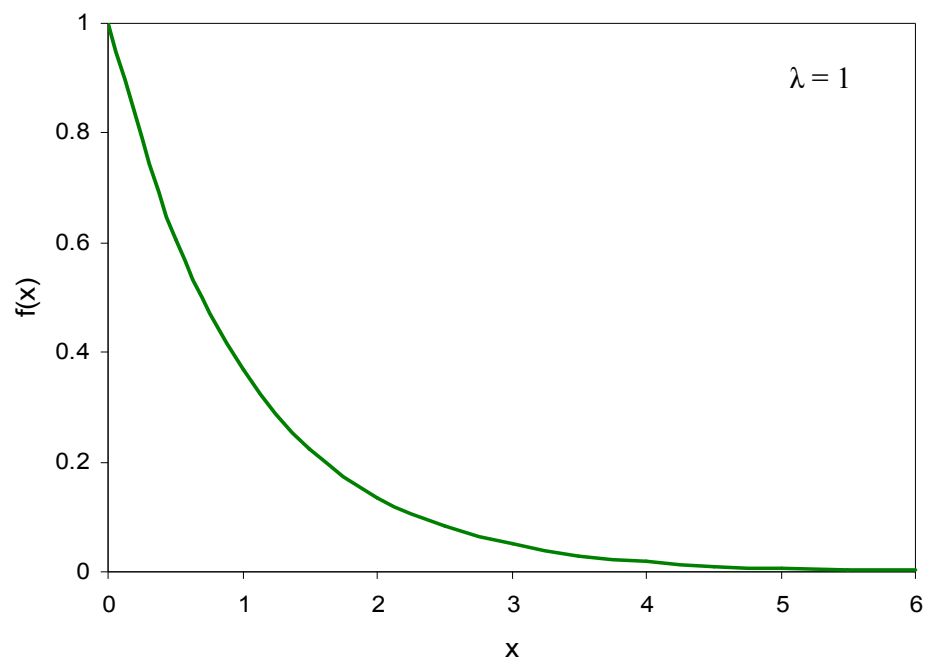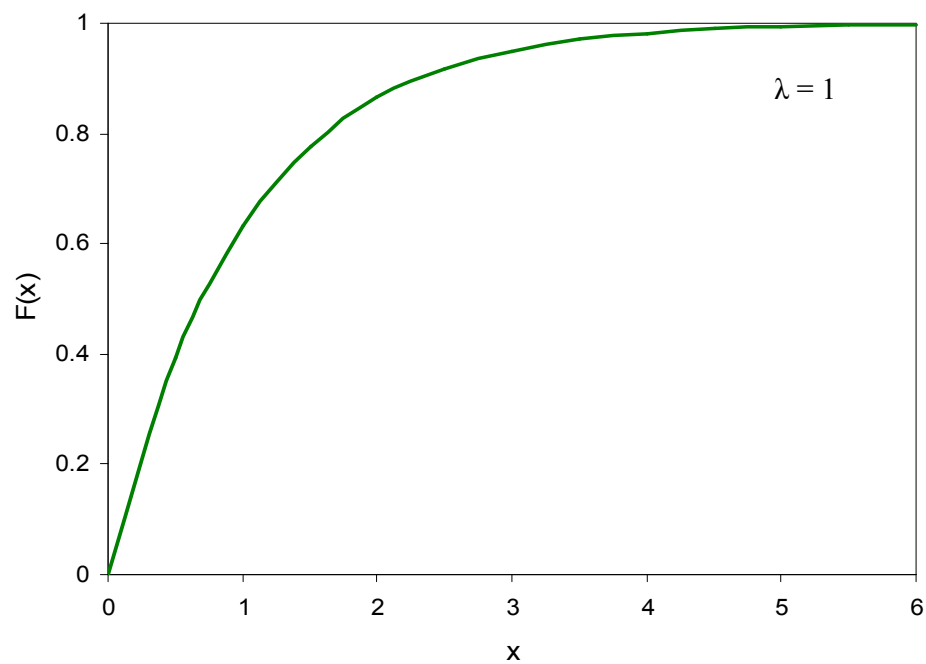
Fig. 3-3B Cumulative density function of the exponential distribution

3.4   The Expected Value and Moments of a Random Variable

The tendency of a sample of interest to cluster round a particular value can be sufficiently characterised using values associated with mathematical expectations called statistical moments. The moments of a particular set of values is the sum of integer powers of the values [3.7]. The importance of these parameters is innate in the ability to describe the shape of the probability distribution of a random variable

The concept of moments can be further elucidated upon analogy with area moments used in the calculation of quantities such as centroidal distance, first static moments and moment of inertia. In statistics, the origin and the mean are common reference points on the measurement axis for the calculation of moments. The statistical moments are regarded as a special case of mathematical expectation [3.4]. The definition of random variable is incomplete without the mention of the mathematical expectation [3.6]. In this section, the moments important for probabilistic and statistical studies are provided for both continuous and discrete random variables.

The kth moment about the origin, denoted m_k, of a continuous random variable X with a PDF $f(x)$ is the expected value for X^k and is given by [3.1 – 3.6]:

$$m_k = E\left[X^k\right] = \int_{-\infty}^{+\infty} x^k f(x)\, dx \qquad (3.25)$$

The corresponding equation for a discrete random variable X and PMF $P(x)$ is:

$$m_k = E\left[X^k\right] = \sum_{i=1}^{n} x_i^{\,k} P(x_i) \qquad (3.26)$$

In the following sub-sections, some moments used to describe the random variables are discussed [3.1 – 3.5].

3.4.1   The Expected Value or Mean

The mean is a very important concept in probability and statistics that denotes the average value of the distribution of a random variable [3.3, 3.5]. The mean is defined as the first moment about the origin which acts as a representative of the central value for the distribution. The mean of a discrete random variable that can take a set of values $x_1, x_2, \ldots, x_n$ provides an estimate to the position where central clustering occurs. Therefore, the mean is often referred to as the *measure of central tendency* of a set of values [3.5]. The proximity of the limiting central value to the arithmetic mean of an experiment depends on the number of samples considered. The same principle applies to higher order moments of the distribution.

A mathematical expression for the mean, denoted $\overline{x}$, of a continuous random variable X with a PDF $f(x)$ can be obtained via the substitution of $k = 1$ in (3.25):

$$\overline{x} = m_1 = E[X] = \int_{-\infty}^{+\infty} x f(x) dx \tag{3.27}$$

From (3.27), the mean of the exponential distribution in (3.23) is the reciprocal of the non-zero parameter λ.

For a discrete random variable X with a probability mass function $P(x)$ the substitution of $k = 1$ yields the expression [3.4]:

$$\overline{x} = m_1 = E[X] = \sum_{i=1}^{n} x_i P(x_i) \tag{3.28}$$

The concept of relative frequency from classical probability theory stipulates that the probability an event occurs is the ratio of its occurrences to the total number of trials [3.1, 3.4]. This standpoint allows for a modification, consistent with MC technique, to (3.28) if all observations are attributed equal weights, that is the $P(x_i) = \frac{1}{n}$:

$$\bar{x} = \tfrac{1}{n} \sum_{i=1}^{n} x_i \qquad (3.29)$$

The mean has the same units as the random variable. The median and mode are alternative estimators of this quantity especially in cases of poor mean convergence with an increased number of sample points. The median is the value of the 50th percentile of the distribution and the mode is the value where the distribution has the highest value [3.3]. The mean provides specific information about a random variable but does not fully characterise it. This is because two distinct distribution types might have the same mean. This leads to the exploration of other ways to characterise the underlying variable [3.4]. The next step upon the characterisation of the central value of a distribution will by convention be to define the spread of data around that value [3.7].

For more details on the shape of the distribution, higher order moments about the mean are required. In general terms, the kth moment about the mean $\bar{x}$ of a continuous random variable X in (3.28) is the expected value for $\left(X - \bar{x} \right)^{k}$ and is given by [3.4, 3.6]:

$$\mu_k = E\left[\left(X - \bar{x} \right)^{k} \right] = \int_{-\infty}^{+\infty} \left(x - \bar{x} \right)^{k} f\left(x \right) dx \qquad (3.30)$$

The corresponding equation for the discrete random variable X is [3.4]:

$$\mu_k = E\left[\left(X - \bar{x} \right)^{k} \right] = \sum_{i=1}^{n} \left(x_i - \bar{x} \right)^{k} P\left(x_i \right) \qquad (3.31)$$

The central moment for an exponential distribution of a continuous random variable is given by:

$$\mu_k = \frac{k!}{\lambda^{k}} \qquad (3.32)$$

3.4.2   Variance or Dispersion

The *second moment* is indicative of the width or variability of the distribution about the central value. In other words, it is an indicator for the closeness of the values in the distribution to the mean.

The *variance*, or its square root, the *standard deviation*, is a measure available for the second central moment of data [3.6]. The units of variance are the square of the units of the random variable [3.4]. A mathematical expression for the variance, denoted σ^2, of a continuous random variable can be obtained via the substitution of $k = 2$ in (3.30):

$$\sigma^2 = \mu_2 = E\left[\left(X - \overline{x}\right)^2\right] = \int_{-\infty}^{+\infty} \left(x - \overline{x}\right)^2 f(x)\,dx \tag{3.33}$$

For a discrete random variable with equal weights with a mean value as shown in (3.28), the variance with the substitution of $k = 2$ and $P(x_i) = \frac{1}{n}$ in (3.31) yields the expression [3.4]:

$$\sigma^2 = \mu_2 = E\left[\left(X - \overline{x}\right)^2\right] = \frac{1}{n}\sum_{i=1}^{n}\left(x_i - \overline{x}\right)^2 \tag{3.34}$$

The value of variance from equation (3.34) is a biased estimate [3.4] as the mean of the distribution is known *a priori* rather than being evaluated from data [3.7]. In this case, the average value of many sample estimates of the variance does not approach the true value. This situation is rectified using the unbiased estimate which is given as [3.4]:

$$\sigma^2 = \mu_2 = E\left[\left(X - \overline{x}\right)^2\right] = \frac{1}{n-1}\sum_{i=1}^{n}\left(x_i - \overline{x}\right)^2 \tag{3.35}$$

The standard deviation is defined as the *square root of the variance*. It has the same units as the mean of the distribution and the random variable and as a result is a better descriptor of dispersion or spread of a distribution function than the

variance [3.4]. The standard deviation, denoted σ, for a continuous random variable X is the square root of the expression in equation (3.35):

$$\sigma = \sqrt{E\left[\left(X - \bar{x}\right)^2\right]} = \sqrt{\int_{-\infty}^{+\infty} \left(x - \bar{x}\right)^2 f\left(x\right) dx} \qquad (3.36)$$

The standard deviation from an unbiased estimate of variance, in equation (3.35), for a discrete random variable X is:

$$\sigma = \sqrt{E\left[\left(X - \bar{x}\right)^2\right]} = \sqrt{\frac{1}{n-1} \sum_{i=1}^{n} \left(x_i - \bar{x}\right)^2} \qquad (3.37)$$

The coefficient of variation, CV, is a dimensionless quantity that is defined as the ratio of the dispersion of a data set to the central value. Mathematically, this is given by the expression [3.4]:

$$CV = \frac{\sigma}{\mu} \qquad (3.38)$$

In cases where there is no convergence with increasing data points then a more robust estimator for the width known as average deviation denoted A_d is prescribed. This is defined by the expression [3.7]:

$$A_d = E\left[\left|X - \bar{x}\right|\right] = \frac{1}{n} \sum_{i=1}^{n} \left|x_i - \bar{x}\right| \qquad (3.39)$$

3.4.3   Skew

The third central moment about the mean describes the symmetry or *skew* of the distribution. The skew unlike other lower order moments is defined in a way to make it dimensionless, that is, a pure number that signifies the degree of asymmetry of a distribution about its mean. Since the third moment about the mean has units of the cube of the random variable [3.4], the skew for a

continuous random variable, *X*, with a standard deviation σ shown in (3.36) is [3.6, 3.7] the ratio of the third moment measured about the mean to the cube of the standard deviation:

$$Skew = \frac{\mu_3}{\sigma^3} = E\left[\left(\frac{X - \bar{x}}{\sigma}\right)^3\right] = \int_{-\infty}^{+\infty}\left(\frac{x - \bar{x}}{\sigma}\right)^3 f(x)\,dx \qquad (3.40)$$

The skew for a discrete random variable, *X*, with $P(x_i) = \frac{1}{n}$ and a standard deviation σ shown in (3.37) is computed as [3.4, 3.7]:

$$Skew = \frac{\mu_3}{\sigma^3} = E\left[\left(\frac{X - \bar{x}}{\sigma}\right)^3\right] = \frac{1}{n}\sum_{i=1}^{n}\left(\frac{x_i - \bar{x}}{\sigma}\right)^3 \qquad (3.41)$$
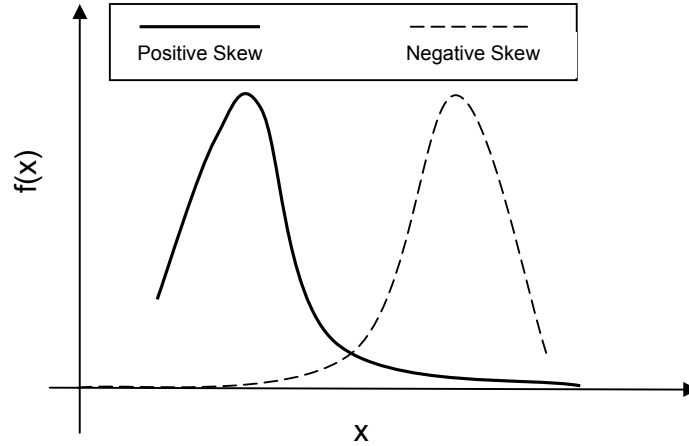
Fig. 3-4 Skewness of a probability distribution function

From the skewed probability distributions illustrated in Fig. 3-4, it can be seen that the positive (negative) value for skewness connotes a distribution with an asymmetric extremity extending outwards towards more positive (negative) axis of the random variable. Otherwise stated, the extreme tail of the distribution is more to the right (left) of the central value for distributions with a positive (negative) skew.

It is important to note that for any set of n values it is likely that the expression in equation (3.41) is non-zero even for an intrinsically symmetrical distribution. For an idealised case of a normal distribution, the standard deviation of (3.41) as an estimator for skewness is about $\sqrt{\frac{15}{n}}$. It is good practise to consider valid skewness that is many times as large as this [3.7]. The skewness of a continuous exponential distribution obtained by substituting $f(x)$ in (3.40) with that in (3.23) and gives a value of 2.

3.4.4   Kurtosis

The fourth central moment about the mean describes the relative *peakedness* or *flatness* of a probability density function relative to a normal distribution. This kurtosis is a non-dimensional quantity related to the fourth central moment. For a continuous random variable, X, it is defined by the expression [3.7]:

$$Kurt = \frac{\mu_4}{\sigma^4} - 3 = \left[E\left[\left(\frac{X - \overline{x}}{\sigma} \right)^4 \right] \right] - 3$$
$$= \left[\int_{-\infty}^{+\infty} \left(\frac{x - \overline{x}}{\sigma} \right)^4 f(x)\,dx \right] - 3$$

(3.42)

The corresponding expression for a discrete random variable X with $P(x_i) = \frac{1}{n}$ is:

$$Kurt = \frac{\mu_4}{\sigma^4} - 3 = \left[E\left[\left(\frac{X - \overline{x}}{\sigma} \right)^4 \right] \right] - 3$$
$$= \left[\frac{1}{n}\sum_{i=1}^{n} \left(\frac{x_i - \overline{x}}{\sigma} \right)^4 \right] - 3$$
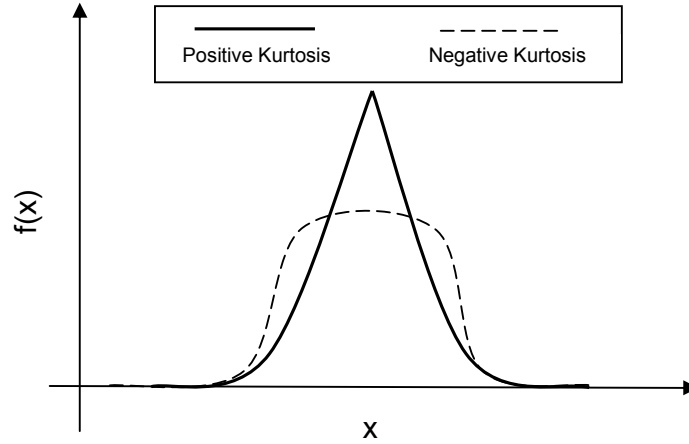
(3.43)

Fig. 3-5 Kurtosis of a probability distribution function

The −3 term in the above expressions makes the value of the kurtosis zero for a normal distribution. A distribution is *leptokurtic* in nature if it has a *positive* kurtosis and that with a *negative* kurtosis is termed *platykurtic* [3.7]. Fig 3-5 illustrates probability distributions with non-zero kurtosis. It can be seen that the peaked distribution has a positive kurtosis

The standard deviation of (3.43) for an essentially normal distribution is $\sqrt{\frac{96}{n}}$ but this tends to infinity for many practical distributions as the kurtosis depends on a high central moment [3.7]. The kurtosis of a continuous exponential distribution obtained by substituting $f(x)$ in (3.42) with that in (3.23) and this gives a value of 6.

3.5   Functions of a Random Variable

There are many electromagnetic problems that involve a dependent variable that is a function of one or more independent random variables. The probabilistic features exhibited by the dependent random variable are based on those of the independent random variables and the functional relationship between them [3.4]. The function of a random variable can only be a random variable if the following conditions are satisfied [3.1]:

   (i)   The domain must include the range of the independent random variables.

   (ii)   The probability at plus or minus infinity is zero.

   (iii)   The CDF of the function occurs at outcomes from the sample space of a countable number of intervals.

3.5.1   Probability Distribution of a Dependent Random Variable

Let X be a continuous random variable with PDF $f(x)$ and the function $Y = g(X)$ is also continuous with a PDF. $f(y)$ can also be calculated from the following [3.4]:

   (i)   An event $\{Y \le y\}$ can only be defined from a corresponding event $\{X \le x\}$.

   (ii)   The probability of the event $\{Y \le y\}$ is set to be the CDF $F(y)$.

   (iii)   The PDF $f(y)$ is the derivative of $F(y)$.

   (iv)   The range of Y for which $f(y)$ is valid is determined.

The random variable Y has the PDF [3.1, 3.4]:

$$f(y) = f\left(g^{-1}(y)\right)\left|\frac{\partial g^{-1}(y)}{\partial y}\right| \tag{3.44}$$

where $x = g^{-1}(y)$ and the Jacobian of the inverse is:

$$\frac{\partial g^{-1}(y)}{\partial y} = \left[\frac{\partial g(x)}{\partial x}\right]^{-1}\Bigg|_{x=g^{-1}(y)}$$

The CDF of Y is [3.1, 3.4]:

$$F(y) = \int_{-\infty}^{g^{-1}(y)} f(x)\, dx \tag{3.45}$$

For any value of $g^{-1}(y)$ where the function $g(x)$ has n roots then (3.45) can be rewritten as follows [3.1, 3.4, 3.6]:

$$f(y) = \sum_{i=1}^{n} f\left(g_i^{-1}(y)\right) \left| \frac{\partial g_i^{-1}(y)}{\partial y} \right| \tag{3.46}$$

3.5.2   Mean and Variance of a Dependent Random Variable

For certain problems, it is essential enough to know only the mean and variance of a dependent random variable $Y = g(X)$. This can be obtained from the probabilistic characteristics of the independent random variable X and the mapping properties defined by the function.

The mean or expected value of the function of a continuous random variable X is given by [3.1, 3.4 – 3.6]:

$$E\left[g(x)\right] = \int_{-\infty}^{+\infty} g(x) f(x) \, dx \tag{3.47}$$

The variance of the function of a continuous random variable X is given by [3.1, 3.4]:

$$\sigma^2_{\,g} = \int_{-\infty}^{+\infty} \left[g(x) - E\left[g(x)\right]\right]^2 f(x) \, dx \tag{3.48}$$

The standard deviation σ_g is the square root of (3.48).

The corresponding expressions for a discrete random variable of (3.47) and (3.48) can be obtained as (3.30) was from (3.31). The skew and kurtosis expressions for the function $g(X)$ can easily be derived by replacing $x, \overline{x}$ and σ with $g(x)$, E [g (x)], and σ_g in the relevant equations from (3.40) – (3.43).

3.5.3   Approximate Methods

The analytical solutions for the distribution and moments of a function of random variables can be acquired from expressions provided in the preceding sections. However, there are scenarios where these methods are not suitable since solutions to functions are not available in closed form. In this case, approximate methods based on Taylor series expansion can be used [3.4].

The Taylor series expression for $g(X)$ about the mean of X is:

$$g(x) = g(\overline{x}) + (x - \overline{x})\frac{dg}{dx}\bigg|_{x=\overline{x}} + (x - \overline{x})^2 \frac{d^2 g}{dx^2}\bigg|_{x=\overline{x}} \qquad (3.49)$$

A detailed description of derivations of approximations of the moments (using the Taylor series expansion in (3.49)) of the function of a random variable with normal and exponential distributions is presented in Appendix A. It is worthy to note that the derivations of the mean and variance of the normal distribution are well documented in literature [3.1, 3.4]. The mean and variance of the function of a random variable with an exponential distribution on the other hand, which is not readily available in literature, have been derived in this thesis. The approximations of the skew of the function of a random variable for both distributions and the kurtosis of the function of the random variable with normal distribution have also been derived.

PART II

3.6   Basic Theory on Electromagnetism

The theory behind electromagnetism is founded on the basic understanding that electric and magnetic fields are interdependent. In general, the time harmonic representation of electric and magnetic fields propagating at an angular frequency ω are given by [3.9]:

$$\boldsymbol{E} = E\,e^{j\omega t} \tag{3.50a}$$

$$\boldsymbol{H} = H\,e^{j\omega t} \tag{3.50b}$$

where t is the time variable, E and H are the phasor vectors of the complex electric and magnetic field expressions respectively. The boldface terms $\boldsymbol{E}$ (V/m) and $\boldsymbol{H}$ (A/m) are vector quantities that represent the electric and magnetic fields respectively.

The behaviour of electromagnetic fields is described by Maxwell's equations. The simplified time dependent form of these equations (in a source-free region) is [3.9 – 3.11]:

$$\nabla \cdot \boldsymbol{D} = 0 \tag{3.51a}$$

$$\nabla \cdot \boldsymbol{B} = 0 \tag{3.51b}$$

$$\nabla \times \boldsymbol{E} = -\frac{\partial \boldsymbol{B}}{\partial t} \tag{3.51c}$$

$$\nabla \times \boldsymbol{H} = \frac{\partial \boldsymbol{D}}{\partial t} \tag{3.51d}$$

where $\boldsymbol{D}$ (C/m) is the electric flux density and $\boldsymbol{B}$ (T) is the magnetic flux density.

The divergence relations in (3.51a) and (3.51b) are obtained from Gauss's law for electric field and magnetic flux conservation respectively. From Stoke's theorem, the contour integral versions of Faraday's law and Ampere's law yield the curl relations in (3.51c) and (3.51d) respectively [3.9].

The time-harmonic source free equations are obtained from (3.51c) and (3.51d) by assuming all quantities as phasors:

$$\nabla \times \boldsymbol{E} = -j\omega\boldsymbol{B} \qquad (3.52a)$$

$$\nabla \times \boldsymbol{H} = j\omega\boldsymbol{D} \qquad (3.52b)$$

The interaction between electromagnetic fields and the materials in linear, isotopic media are defined by the constitutive relations [3.9 – 3.11]:

$$\boldsymbol{D} = \varepsilon\,\boldsymbol{E} = \varepsilon_0\varepsilon_r\,\boldsymbol{E} \qquad (3.53a)$$

$$\boldsymbol{B} = \mu\,\boldsymbol{H} = \mu_0\mu_r\,\boldsymbol{H} \qquad (3.53b)$$

where ε (F/m) is the material permittivity, μ (H/m) is the material permeability, ε_r is relative material permittivity and μ_r is relative material permeability . The permittivity and permeability of free space are ε_0 and μ_0 respectively. The work presented in this thesis relates only to isotropic, non-magnetic materials where $\mu_r = 1$.

The wave equation for the electric field can be found by taking the curl on both sides of (3.52a) and using the relations in (3.52b), (3.53a) and (3.53b):

$$\nabla \times \nabla \times \boldsymbol{E} = -j\omega\nabla \times \boldsymbol{B} = -j\omega\mu\nabla \times \boldsymbol{H} = -\mu\left(j\omega\right)^2 \varepsilon\,\boldsymbol{E} \qquad (3.54)$$

The wave number $k = \omega\sqrt{\mu\varepsilon}$ (rads/m) is defined as the spatial analogue of angular frequency. Using k in (3.54) gives:

$$\nabla \times \nabla \times \boldsymbol{E} = k^2\boldsymbol{E} \qquad (3.55)$$

The left hand side of (3.55) can be rewritten using the well known vector identity [3.9]:

$$\nabla \times \nabla \times \boldsymbol{E} = \nabla\nabla.\boldsymbol{E} - \nabla^2\boldsymbol{E} \qquad (3.56)$$

From (3.51a) and (3.53a), it can be shown that the term $\nabla.\boldsymbol{E} = 0$. Therefore, (3.55) can be reformulated to give:

$$\nabla^2 \boldsymbol{E} + k^2 \boldsymbol{E} = 0 \qquad (3.57)$$

The wave equation for magnetic fields can also be obtained by taking the curl of both sides of (3.52b). After similar mathematical manipulations, this is found to be:

$$\nabla^2 \boldsymbol{H} + k^2 \boldsymbol{H} = 0 \qquad (3.58)$$

Both (3.57) and (3.58) are referred to as Helmholtz equations [3.9].

The cut-off frequency of resonant structures with rectangular cross-section and filled with homogenous dielectrics can be obtained from Helmholtz equations [3.9]. The idea in future chapters is to make ε a random variable and study the behaviour of cut-off frequency as a function of this random variable. The next chapter deals with the statistical analysis of 1-D electromagnetic problems using some of the theory reviewed here.

3.8   References

[3.1]   A. Papoulis, "Probability, Random Variables and Stochastic Processes," 2nd Edition, New York, NY: McGraw-Hill, 1984.

[3.2]   T. H. Lehman, "A Statistical Theory of Electromagnetic Fields in Complex Cavities," Interaction Notes, May 1993.

[3.3]   S.S. Isukapalli, "Uncertainty Analysis of Transport-Transformation Models," PhD Thesis, State University of New Jersey, New Brunswick, Rutgers, 1999.

[3.4]   B. M. Ayyub and R.H. McCuen, "Probability, Statistics and Reliability for Engineers and Scientists," 2nd Edition, Chapman and Hall / CRC Press, 2003.

[3.5]   M.R. Spiegel, J. Schiller and R. A. Srinivasan, "Schaum's Outline Series Theory and Problems of Probability and Statistics," McGraw-Hill, 2000.

[3.6]   X.R. Li, "Probability, Random Signals, and Statistics," CRC Press LLC, 1999.

[3.7]   W.H. Press, S.A. Teukolsky, W.T. Vetterling, and B.P. Flannery, "Numerical Recipes in C: The Art of Scientific Computing," 2nd Edition, Cambridge University Press, 1997.

[3.8]   J. Zhang, "The Calculating Formulae, and Experimental Methods in Error Propagation Analysis," IEEE. Trans. on Reliability, vol. 55, June 2006.

[3.9]   N. Ida, "Engineering Electromagnetics," New York, NY: Springer, 2000.

[3.10]   R.E. Collin, "Field Theory of Guided Waves," IEEE Press, 1991.

[3.11]   F. T. Ulaby, "Fundamentals of Applied Electromagnetics," 5th Edition, Pearson Prentice Hall, 2007.

Chapter 4   Statistical Analysis of 1-D problems

The Monte Carlo (MC) method is widely accepted as the conventional way to carry out statistical analysis. This involves the development of a computer-based model that illustrates the performance of the system under study. In this chapter, the one-dimensional (1-D) TLM technique will be introduced and applied to solving a simple electromagnetic problem. The MC method will be used to quantify the uncertainty of a stochastic model parameter. The constraints of using the method are discussed and a suitable alternative is proposed. The main motivation for restricting deterministic considerations in this chapter to one dimension is to make it possible to obtain direct predictions at reduced computational cost. This will be extended to higher dimensions in subsequent chapters.

4.1   One-Dimensional (1-D) TLM

Numerical modelling allows the solution of real world problems through the use of mathematical surrogates. This commences with a problem statement. Once this is understood, the features of the problem to be scrutinised are identified. The efficacy of the modelling process is linked with the simplicity it provides and how favourably it compares with the real behaviour of the system under analysis. Verification and ease of obtaining the results obtained are therefore of paramount importance [4.1].

The transmission line modelling (TLM) method is an established numerical technique exploited to solve electromagnetic field problems [4.1 – 4.2]. The technique is a differential method that can be implemented in both the time and frequency domains. In both domains, the problem space defined is discretised using transmission line segments connected at points referred to as nodes [4.1].

The basic line segment and its discrete TLM equivalent are shown in Fig. 4-1A and 4-1B respectively.
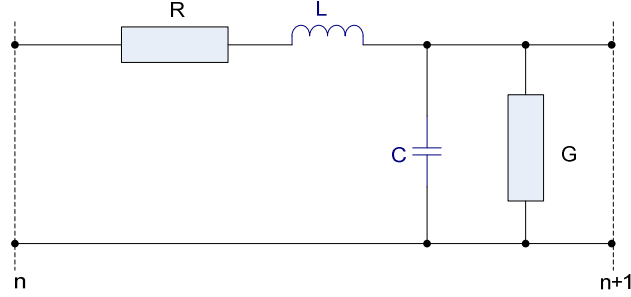

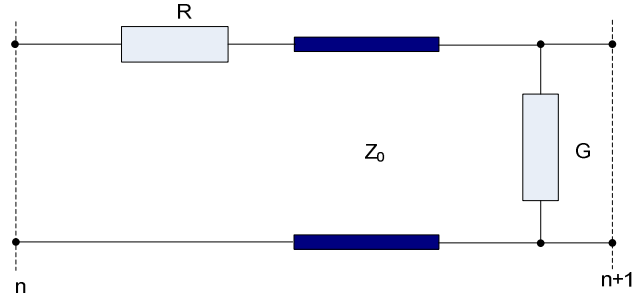**Fig. 4-1A Lumped circuit representation of basic line segment**

Fig. 4-1B Discrete TLM equivalent of basic line segment

The parameters R and G are passive circuit components denoting series resistance and shunt admittance. These can be introduced to incorporate losses in the transmission line. In this thesis, all the case studies assume these values to be negligible. The parameters L and C are the series inductance and shunt capacitance respectively. The link impedance Z_0 in Fig. 4-1B can be related to the lumped circuit parameters, in the lossless case, by the expression [4.1]:

$$Z_0 = \sqrt{\frac{L}{C}} \qquad (4.1a)$$

The velocity of propagation u of a wave that travels the length of the line segment Δx is [4.1]:

$$u = \sqrt{\frac{1}{\left(L/\Delta x\right)\left(C/\Delta x\right)}} = \Delta x \sqrt{\frac{1}{LC}} \qquad (4.1b)$$

Therefore, the time taken Δt for a wave to travel a line segment is:

$$\Delta t = \frac{\Delta x}{u} = \sqrt{LC} \qquad (4.1c)$$

The interaction between the sampling nodes interconnected by short lengths of commensurate transmission line is shown in Fig. 4-2. For notational convenience, the subscript n and k are used to represent quantities at that node and time step respectively. The superscript i denotes incident quantities and r reflected quantities.

The central node n is *connected* to its neighbours $n-1$ and $n+1$ at the left and right respectively. The incident voltages on the left and right of the node n at time step k are $_kVL^i_n$ and $_kVR^i_n$ respectively. At the point and instance of contact, the incident voltage at n are reflected in the opposite direction of transit. This is termed the *scattering* process. The sum of the forward and backward propagating pulses on each line segment constitutes the total node voltage.
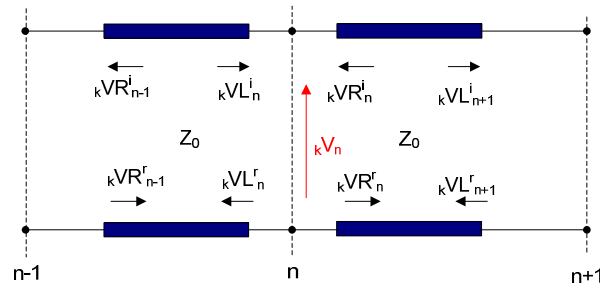
Fig. 4-2 Connection and scattering process between adjacent nodes

In order to derive the Thevenin circuit equivalent for the interaction at the node n, it is essential to resort to transmission line theory. The voltage pulse injected at either end of a line segment terminated by an open circuit is reflected so that the total voltage is twice that of the incident voltage. Hence, the Thevenin equivalent circuit at node n is presented as shown in Fig. 4-3.
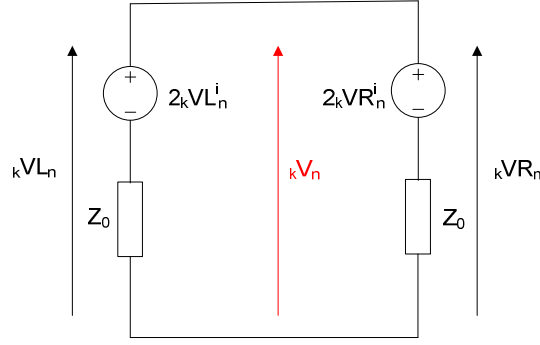
Fig. 4-3 Thevenin equivalent circuit for transmission line section in free space

The application of Millman's theorem [4.3] to the circuit in Fig. 4-3 makes the total node voltage to be:

$$_kV_n = \frac{\dfrac{2\,_kVL^i{}_n}{Z_0} + \dfrac{2\,_kVR^i{}_n}{Z_0}}{\dfrac{1}{Z_0} + \dfrac{1}{Z_0}} = {}_kVL^i{}_n + {}_k VR^i{}_n \qquad (4.2)$$

The total voltage to the left and right of the node n is the same and equal to the voltage at the node centre as shown in Fig.4-3:

$$_kVL_n = {}_kVR_n = {}_kV_n \qquad (4.3)$$

The total voltages on the left and right of the node n, from the scattering process, is known to be the sum of the pertinent incident and reflected voltages that is [4.1]:

$$_kVL_n = {}_kVL^i{}_n + {}_k VL^r{}_n \qquad (4.4a)$$

$$_kVR_n = {}_kVR^i{}_n + {}_k VR^r{}_n \qquad (4.4b)$$

The incident voltages a time step depend on the conditions imposed on the previous time step. The voltage incident to the right of the node n at a particular time step is equal to that reflected from the right of the subsequent node $n + 1$ at the previous time step. This concept is similar to the left of the node but in

reverse spatial orientation. The connection process can thus be described using the following relations [4.1]:

$$_{k+1}VL^i_n = {}_kVR^r_{n-1} \qquad (4.5a)$$

$$_{k+1}VR^i_n = {}_kVL^r_{n+1} \qquad (4.5b)$$

The different material properties in TLM are introduced by adding stubs. The link line impedance represents free space with unity relative permittivity and permeability. The stubs are only introduced to model materials when these parameters exceed unity. These are either capacitive stubs to model permittivity or inductive stubs to model permeability. The former is an open circuit stub while the later is a short circuit stub. The need to preserve synchronisation with the free space model is important to ensure that node pulses in either case are combined and updated at the same instant in time [4.1].
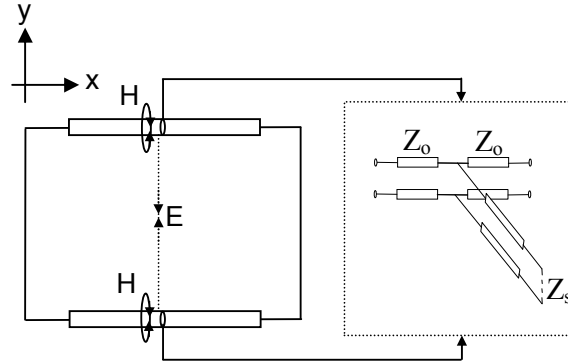

Fig. 4-4 1-D resonator and the TLM equivalent circuit of a segment

The arrangement considered for the application of stubs is indicated in Fig. 4-4. This illustrates the simple implementation of a 1-D stubbed resonator with a relative permittivity greater than one. The aim of this apparatus is to obtain the statistical properties of resonant frequency in the presence of a material with random relative permittivity. The boundary conditions to the problem are defined such that the voltage is short circuited. The round trip time of the capacitive stub must be the same as the transit time for each link line to maintain synchronisation. For the material shown, the modelled capacitance per unit

length C_d can be expressed in terms of the ratio of the link impedance to stub impedance:

$$C_d = \frac{1}{\Delta x}\left[\frac{\Delta t}{Z_0} + \frac{\Delta t}{2Z_S}\right] = \frac{1}{uZ_0}\left[1 + \frac{Z_0}{2Z_S}\right] \qquad (4.6a)$$

Given that C_d is the permittivity of the modelled medium [4.1], then the relationship between the stub impedance Z_S, the link impedance Z_0 and the relative permittivity ε_r using (4.6a) is:

$$Z_S = \frac{Z_0}{2(\varepsilon_r - 1)} \qquad (4.6b)$$

The Thevenin equivalent circuit for the node in the presence of a capacitive stub is presented in Fig. 4-5. The central branch is the part of the network represents the stub contribution. The total voltage at the node for this scenario is:

$$_kV_n = \frac{\dfrac{2_kVL^i_n}{Z_0} + \dfrac{2_kVR^i_n}{Z_0} + \dfrac{2_kV^i_{S\,n}}{Z_S}}{\dfrac{1}{Z_0} + \dfrac{1}{Z_0} + \dfrac{1}{Z_S}} \qquad (4.7)$$

where $_kV_s^i$ represents the incident voltage to the capacitive stub. The total node voltage can be substituted into (4.3) to determine the voltage reflected to neighbouring nodes. The voltage reflected from the stub into the node after the round trip time is [4.1]:

$$_kV_s^r = {_kV_n} - {_kV_s^i} \qquad (4.8)$$

The connection process for the open circuit stub is [4.1]:

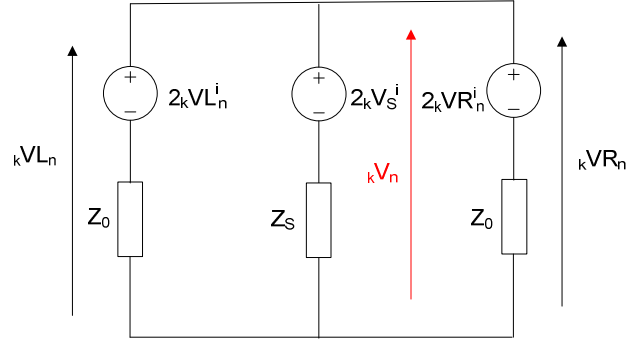$$_{k+1}V_s^i = {_kV_s^r} \qquad (4.9)$$

Fig. 4-5 Thevenin equivalent circuit for transmission line with capacitive stub

The electric field is polarised in the y – direction if the direction of propagation is x as shown in Fig. 4-4. This field quantity is related to the total node voltage [4.1]:

$$E_y = -\frac{{}_k V_n}{\Delta x} \tag{4.10}$$

The frequency response of the problem defined in Fig. 4-4 can be obtained using the Fast Fourier Transform (FFT), of the TLM field or voltage computation. The general expression for the resonant frequency of interest f_r is:

$$f_r = g\left(\varepsilon_r\right) = \frac{n' c}{2L\sqrt{\varepsilon_r}} \tag{4.11}$$

where c is the speed of light in m/s, L is the length of the transmission line in m and n' is a positive integer representing the harmonic number. Fig. 4-6A shows the frequency response using TLM with modelling parameters of 100 nodes and 32,768 time steps. The relative permittivity $\varepsilon_r = 2$ and the length of the cavity $L = 1$m.
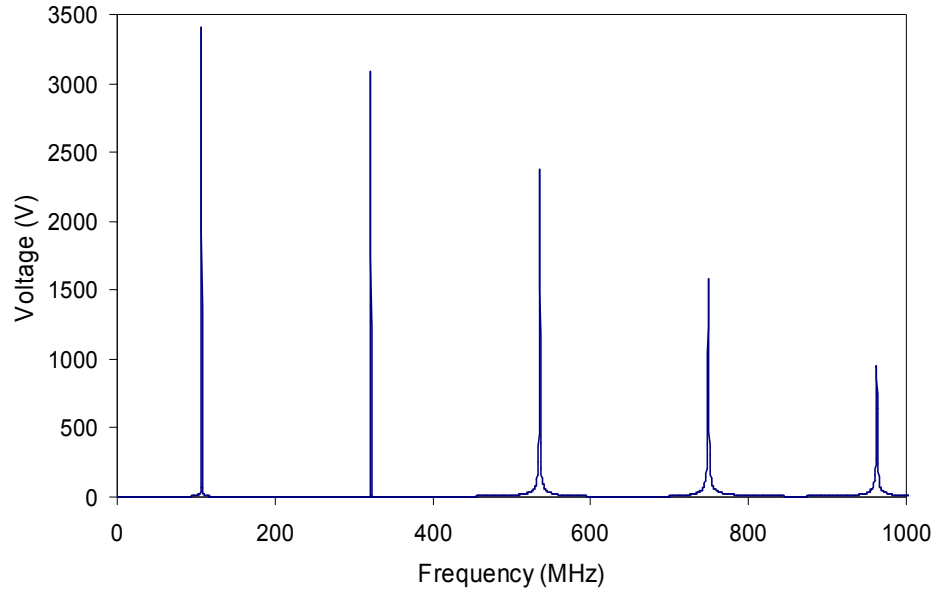
Fig. 4-6A Frequency response of stubbed resonator with $\varepsilon_r = 2$ and $L = 1\text{m}$

The percentage difference between the results derived via simulation and analysis is shown in Fig. 4-6B. From the results obtained, it is clear that the numerical dispersion errors in the model increase with frequency. This limitation can be mitigated by selecting Δx to be at most one-tenth of the smallest wavelength of interest [4.1]. In this thesis, spectral analysis is restricted to $n' = 1$ where the error is smallest.

Fig. 4-6B Percentage difference between analytic and simulated results

4.2   1-D Resonator with Stochastic Permittivity

The starting point for statistical analysis is a deterministic treatment of the model relevant to the interactions of parameters under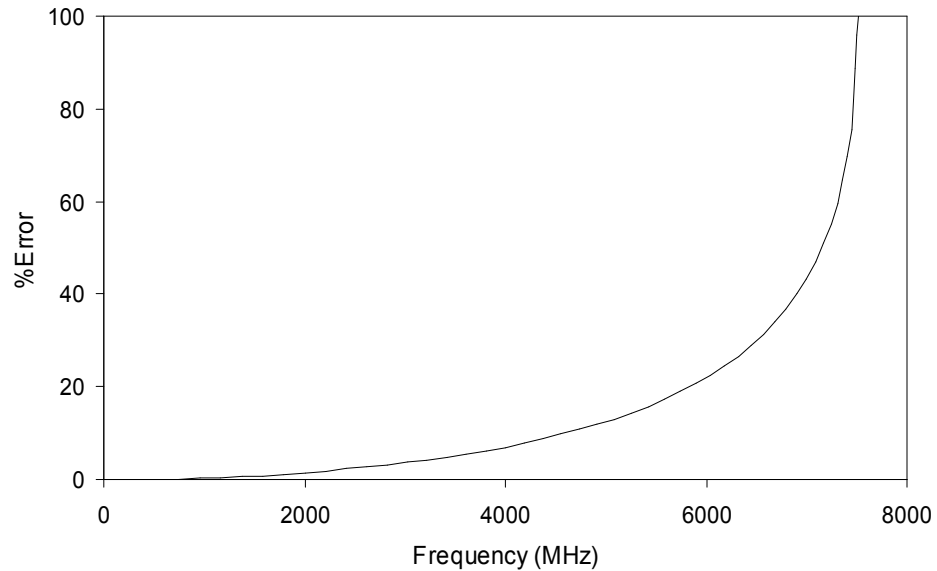 examination. This has been dealt with using the TLM technique in the previous section. The aim here is to use the stubs introduced earlier as means for introducing permittivity.

4.2.1   Monte Carlo Analysis

The MC method can be used to assess a problem of a 1-D resonator with normally distributed uniform stochastic permittivity. The random variables representing the relative permittivity are generated from uniform random variates transformed into normal variates. The results are repeatable as a seed is used to begin the random number generation. This is important for debugging simulation and for comparison with design alternatives [4.4].
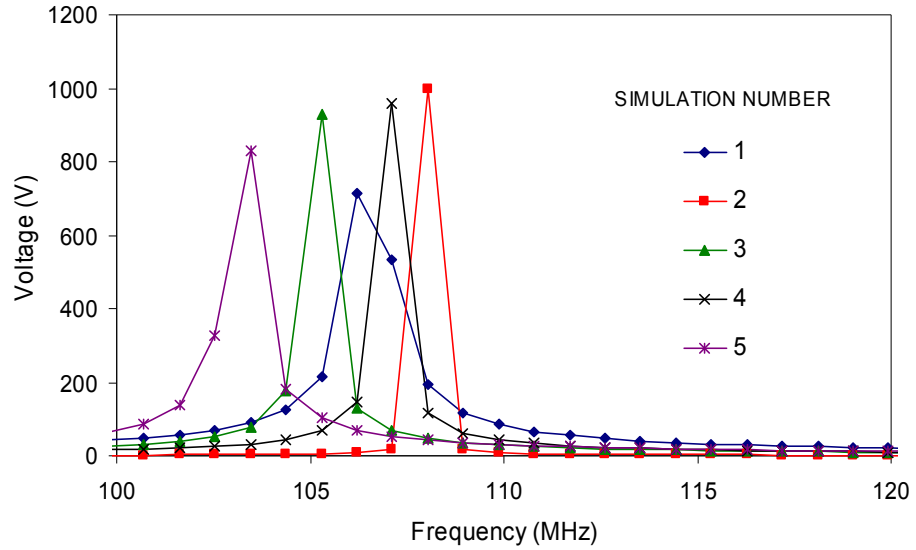

Fig. 4-7 Frequency responses at first harmonic using the MC method

The mean relative permittivity $\overline{\varepsilon}_r = 2$ and the length of the cavity $L = 1$m. The corresponding fundamental resonance is evaluated for each relative permittivity sample. The result for the standard deviation in relative permittivity $\sigma_{\varepsilon r}$ of 0.05 after first five MC simulations, using 100 TLM stubbed nodes and 32,768 time steps, is presented in Fig. 4-7. The PDFs of cavity resonances defined for a range of standard deviations, $\sigma_{\varepsilon r}$ is shown in Fig. 4-8. Each curve is the result of 100,000 MC simulations. Even with this number of simulations, the peaks of the PDFs are not perfectly aligned for different $\sigma_{\varepsilon r}$. This illustrates the need for approximate methods with less stringent computational demands.

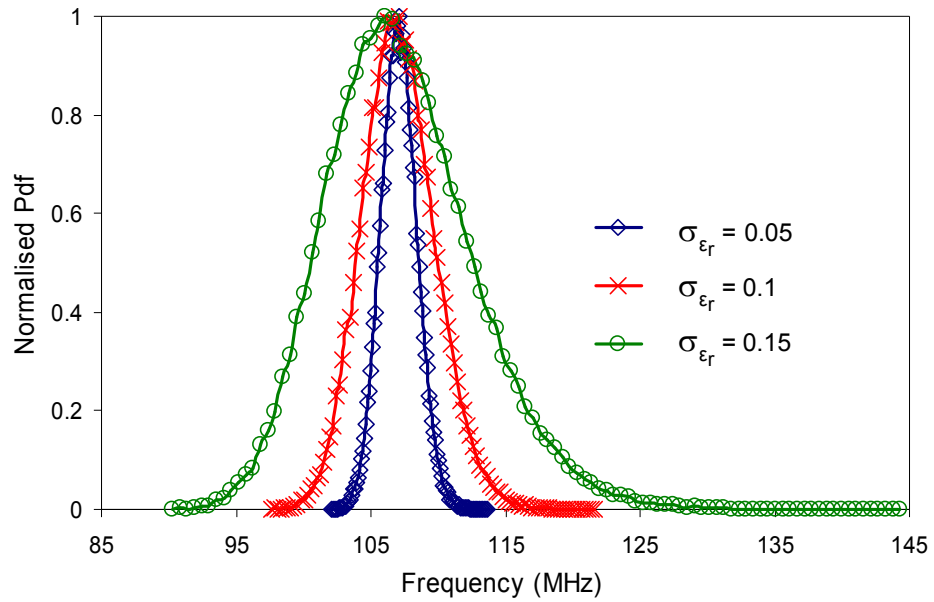**Fig. 4-8 Frequency PDFs of fundamental resonance at different values of $\sigma_{\varepsilon r}$**

The relationship between the statistical moments of the resonant frequency with $\sigma_{\varepsilon r}$, obtained from the MC simulations, is shown in Fig. 4-9. The quasi-linear behaviour clearly observed for small $\sigma_{\varepsilon r}$ can be used as the basis of comparison with approximate methods.
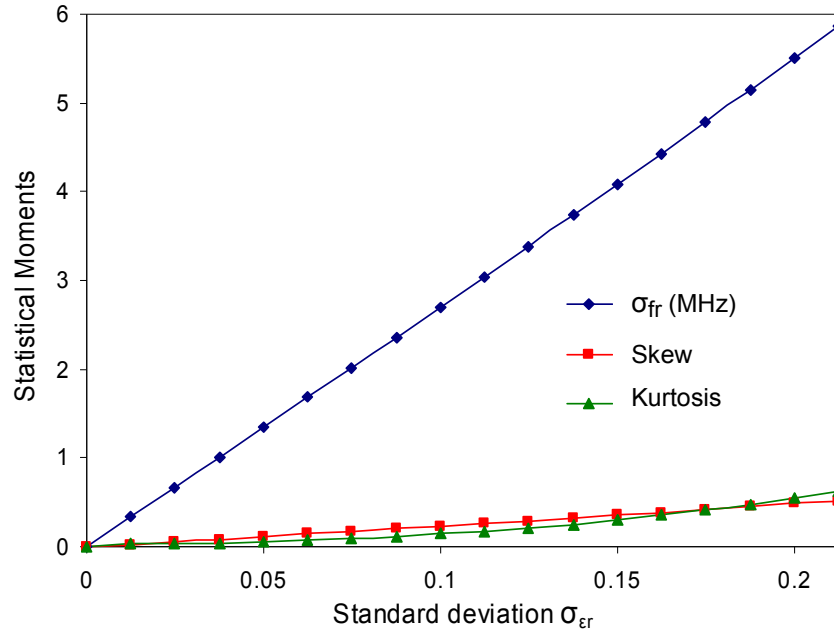
Fig. 4-9 Effect of changing $\sigma_{\varepsilon r}$ on the moments of the frequency PDF

The study of convergence of moments of the distribution is important in determining the number of MC simulations that would be necessary. Fig. 4-10 shows the convergence of the MC analysis with the number of simulations performed. From the simple example of a 1-D resonator and at $\sigma_{\varepsilon r} = 0.1$ the convergence is very slow, and consequently, the approach becomes rapidly intractable for even moderately sized problems. The order of the moments determines the rate of convergence. The higher the order, the more simulations needed for convergence to be obtained. 20,000 simulations of this example requires a run time of over 5 hours on a PC with a AMD Athlon 2.01GHz processor. The inexpensive approach of a single computational run in 1-D soon becomes more time consuming for numerous simulations using the MC method. The onus is now to adopt approximate method that can drastically reduce computation costs. The results obtained here will be compared with approximate technique based on Taylor series expansions.

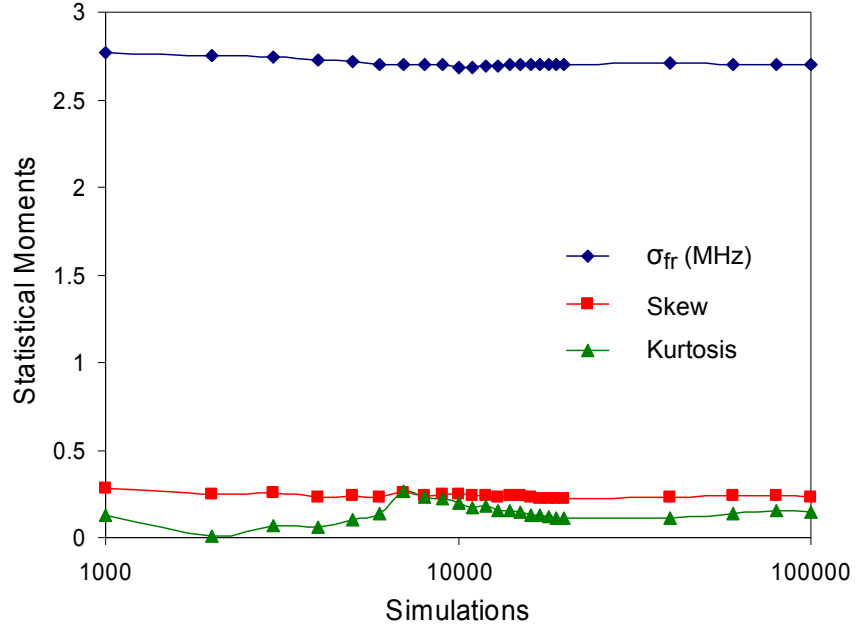**Fig. 4-10 Convergence of the statistical moments of the first cavity resonance obtained from Monte Carlo analysis simulations with $\sigma_{\varepsilon r} = 0.1$**

4.2.2   Approximate Method

The approximation of moments was discussed in chapter 2 of this thesis. The aim of this sub-section is to illustrate the efficacy of using the Taylor series approach. The equations deployed are those derived in section A of the appendix. For the case study of the 1-D stubbed resonator, the same deterministic and stochastic parameters given in sub-section 4.2.1 are used. The agreements between the analytic considerations and MC method for the statistical moments are shown in Fig. 4.11A – C.

The standard deviation of the frequency PDF σ_{fr} measured from the MC method and the fourth order Taylor series approximation using (A.23) in Appendix A are compared in Fig. 4.11A. The discrepancy as expected would increase with the standard deviation $\sigma_{\varepsilon r}$. The percentage difference between both methods for measuring σ_{fr} at $\sigma_{\varepsilon r} = 0.2125$ is 1.26%. Similarly, the measurement of the skew and kurtosis of the frequency PDF also deteriorates with an increase in $\sigma_{\varepsilon r}$. The fourth order Taylor series approximations of the skew and kurtosis are used from

(A.26) and (A.31) in Appendix A respectively. The percentage difference between the MC and fourth order Taylor series approximations of both moments at $\sigma_{\varepsilon r} = 0.2125$ are 2.43% and 2.55% respectively.

Fig. 4-11A Comparison of the Monte Carlo and analytic methods for measuring σ_{fr} of the frequency PDF as $\sigma_{\varepsilon r}$ changes
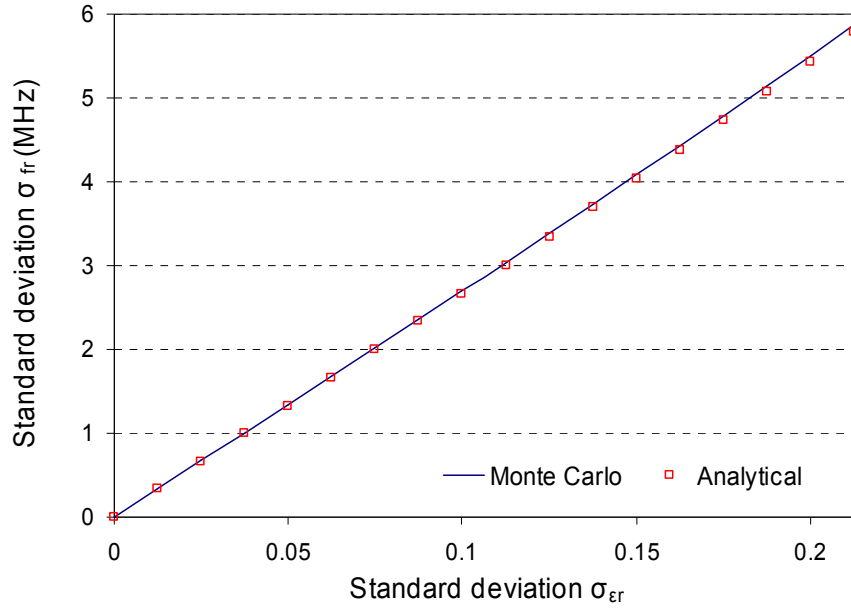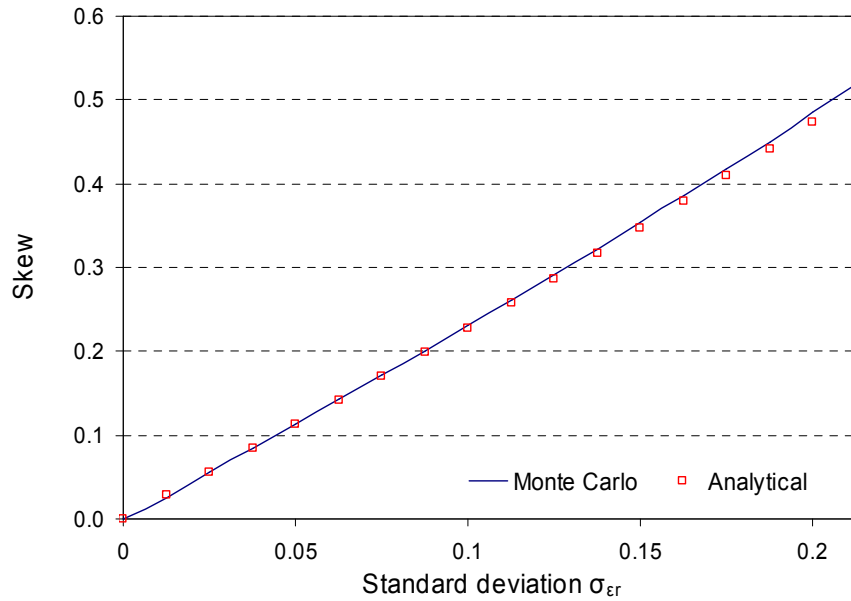

Fig. 4-11B Comparison of the Monte Carlo and analytic methods for measuring skew of the frequency PDF as $\sigma_{\varepsilon r}$ changes
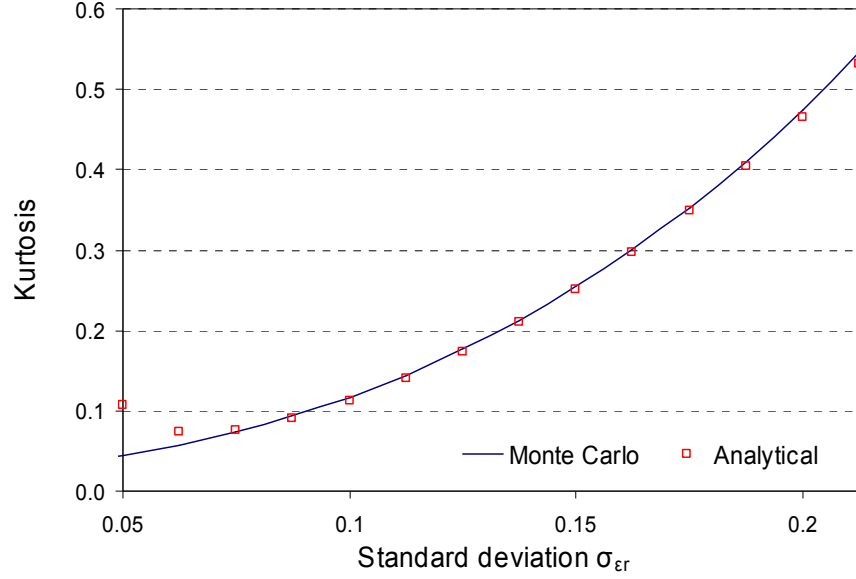
Fig. 4-11C Comparison of the Monte Carlo and analytic methods for measuring kurtosis of the frequency PDF as σ$_{\varepsilon r}$ changes

The discrepancy between the measurements of the kurtosis between both methods is increased for σ$_{\varepsilon r}$ less than 0.1. The reason for this is that when σ$_{\varepsilon r}$ approaches zero the distribution behaves like a delta function with a very sharp peak.

4.3   Material Correlation Effects in Random Media

In the previous section, analysis was based on the sampling a relative random variable from a normal distribution. The medium of propagation was specified as a homogenous layer of relative dielectric permittivity at different MC simulations. Each sample defines the relative permittivity of the entire line during simulation and the fundamental resonance of resonating signal is extracted after steady state is reached.

This section deals with the generation of random relative dielectric permittivity with a given spatial correlation function which characterises the degree of roughness of the medium. For this purpose two statistical parameters are of

importance and will feature as input to the theoretical model. These are the *root mean square* (or standard deviation) of the permittivity values and the *correlation length*.

The model of the randomly inhomogeneous medium is defined in the form of a set of localised relative permittivity of different scales, that is correlation length [4.5]. The correlation length is introduced in the stochastic representation of random nodal distribution in the discretised TLM model. The correlation length is so called, as the relative permittivity is now a function of distance along the direction of propagation.

The relative permittivity in the previous section had infinite correlation length as the entire line is homogenous. For the condition of zero correlation length, the permittivity is locally homogenous and isotropic on a nodal scale. Consideration of continuously spatial variations in material parameters requires some care, if convergence with mesh density is to be observed. Quantification of the correlation of, for example, the relative permittivity at different spatial locations, can proceed from the autocorrelation function $R(a)$,

$$R(a) = \lim_{L \to \infty} \frac{1}{L} \int_{-\frac{L}{2}}^{-\frac{L}{2}} \varepsilon_r(x)\, \varepsilon_r(x+a)\, dx \qquad (4.12)$$

Here, an exponential autocorrelation function [4.7], which is typical of many physical scenarios, is adopted for the purposes of illustration,

$$R(a) = \varepsilon^2_{RMS}\, e^{\left(-|a|/L_c\right)} \qquad (4.13)$$

where L_c is the correlation length and ε_{RMS} is the root mean square of the central permittivity value. Appendix B shows the derivations of how to generate a set of inhomogeneous relative permittivity values with a known mean from a uniform random number generator using an exponential autocorrelation function.

For time domain simulations, it is difficult to keep track of changes to propagating pulses in inhomogeneous media even for deterministic conditions. This situation makes it challenging to devise analytical methods that can account for the points where the pulses have been and the time when this event occurred. An illustration of this can be seen from a simple numerical experiment. The aim is to see if the spread of a propagating Gaussian pulse in a 1-D stubbed resonator (case I) with a fixed length is commensurate with that of another longer line (case II) after provided the distance covered by the pulse is the same while keeping L_c and ε_{RMS} unchanged. The Gaussian pulse V_s injected at the end of the line in both scenarios is:

$$V_s = e^{\left(\Delta t - t_p \big/ HW \right)^2} \tag{4.14}$$

where t_p is the time step where the peak of the pulse occurs and HW is the number of time steps that indicates pulse half-width. For $t_p = HW = 30\Delta t$, the Gaussian pulse is presented in Fig. 4-12. The source resistance for both case I and II is 50 Ω.

In case I the following parameters were used to define inhomogeneity: $L_c =$ 0.1 and $\varepsilon_{RMS} = 0.0025$. The summation of the relative permittivity at each node divided by the total number of nodes gives a central value of 2. The length of the cavity is 1m and a total of 100 nodes were used. This implies that $\Delta x = 0.01$m. The distribution of the permittivity under these conditions is shown in Fig. 4-13A. This can be obtained from (B.20) and (B.21) in Appendix B.

The voltage profile after 750 time steps as observed at point $n = 50$ is shown in Fig. 4-13B. The amplitude of the pulse and how wide it is are also indicated. As the pulse propagates the amplitude reduces while the width increases with distance.
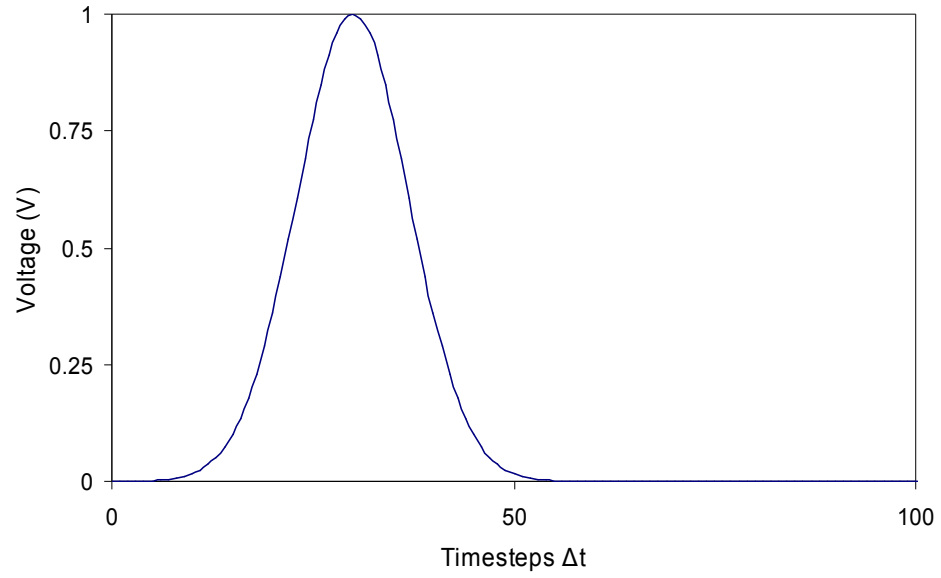
Fig. 4-12 Gaussian pulse with unit amplitude and parameters $t_p = HW = 30\ \Delta t$
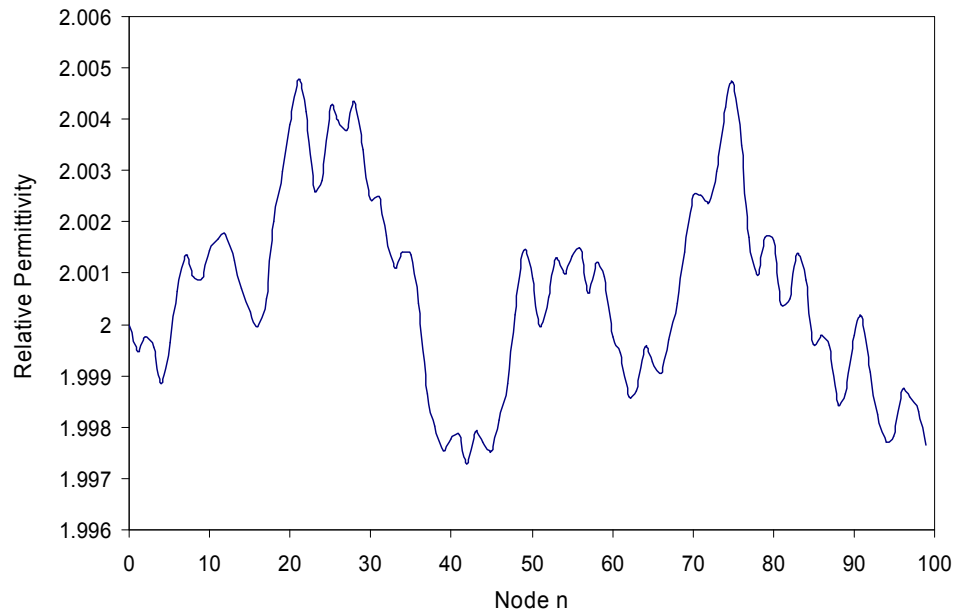
Fig. 4-13A Distribution of relative permittivity in case I with $L_c = $ 0.1 and $\varepsilon_{RMS} = 0.0025$
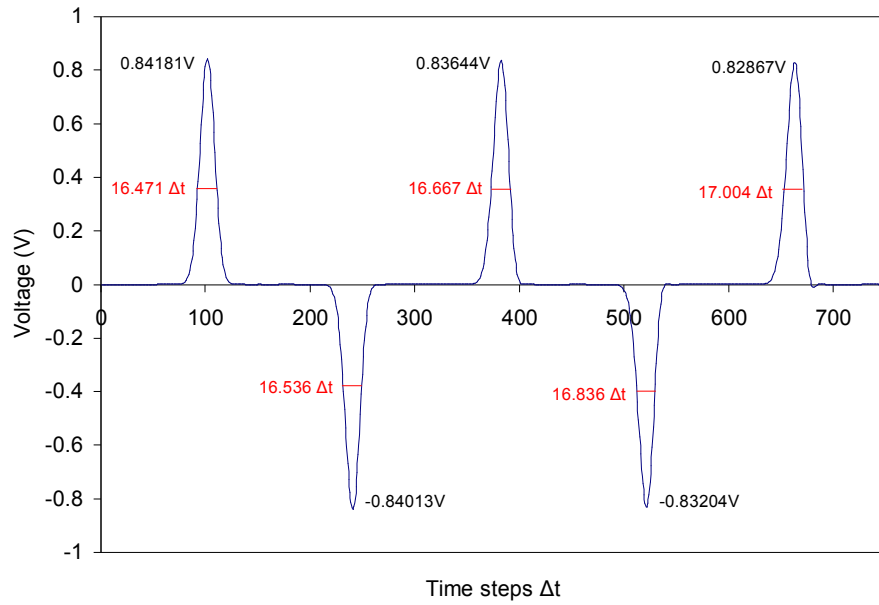
Fig. 4-13B Pulse propagating in case I observed at *n* = 50 after 750 Δ*t*

In case II, there are six conjoined lines each of the same geometric length and roughness characteristics as case I. The choice of samples are however dissimilar due to the random selection process. The diagram of the transmission line arrangement used in case II is shown in Fig. 4-14A.
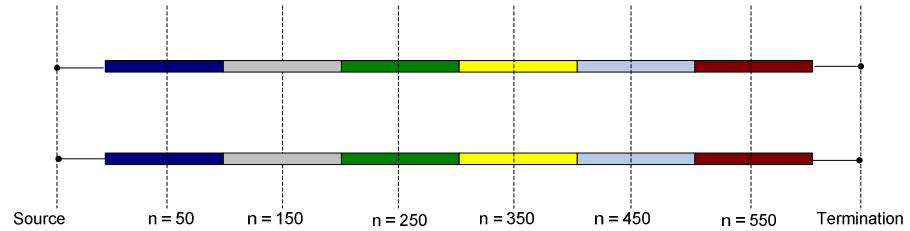
Fig. 4-14A Transmission line arrangement for case II

The central relative permittivity in each line is 2. The distribution of the permittivity in case II is shown in Fig. 4-14B with spatial parameters in are Δ*x* = 0.01m with a total of 600 nodes.
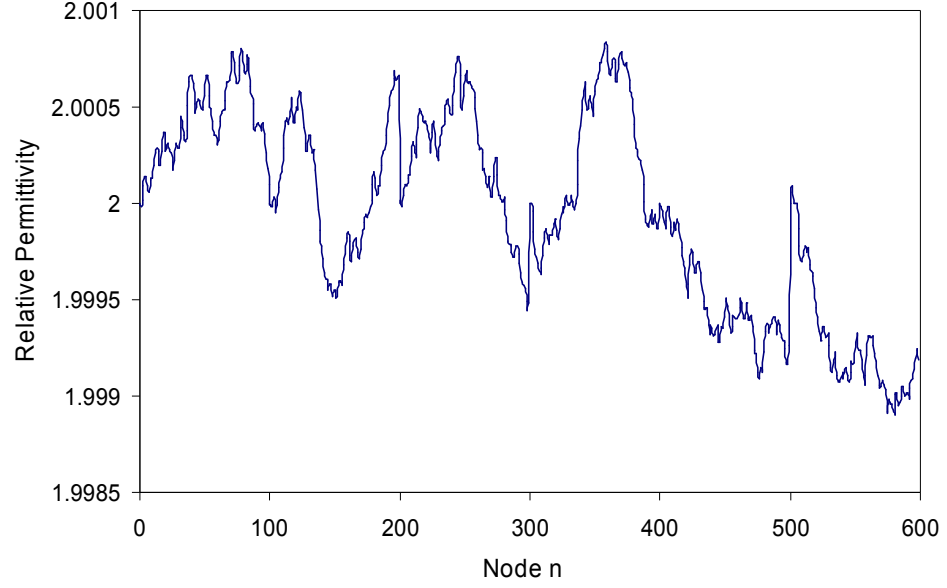
Fig. 4-14B Distribution of relative permittivity in case II with L_C = 0.1 and ε_{RMS} = 0.0025

The pulse propagating in case II is shown in Fig. 4-14C. The observation point that corresponds to the pulse after the fourth reflection in case I is n = 450 in case II. The voltage profile after 900 time steps, as observed at this point, is shown in Fig. 4-14D. The pulse spreads in both cases due to *material dispersion* [4.1]. From the results, it is observed that the pulse in case II is wider after the same distance travelled as case I but with smaller amplitude. This might be because the reverberating pulse case I becomes correlated with the medium and as such does not spread as adversely as the forward propagation in case II. This behaviour gets progressively worse with increasing time steps. This would make it difficult to derive approximate expressions for the statistical behaviour of a propagating pulse in the time domain for inhomogeneous stochastic media.
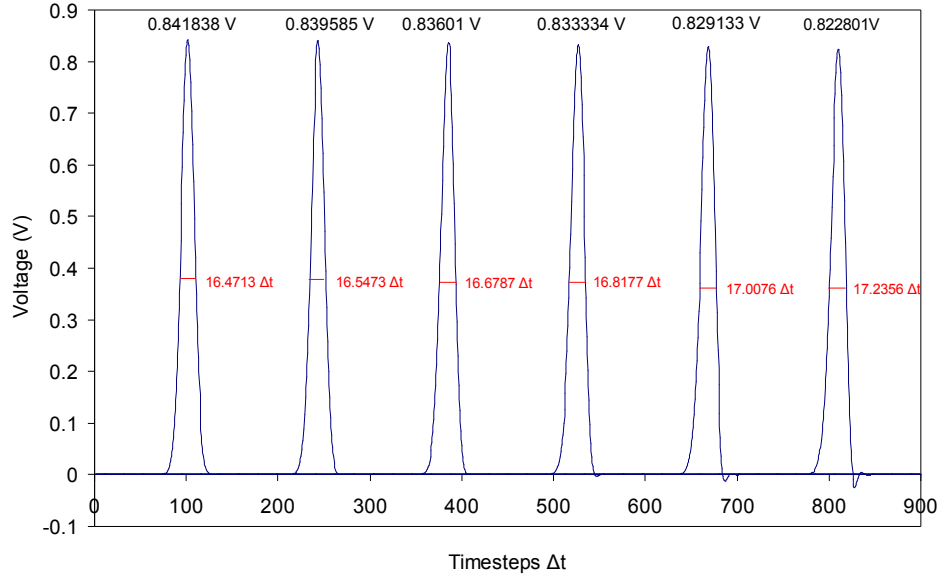
Fig. 4-14C Pulse propagating in case II after 900 Δ*t*
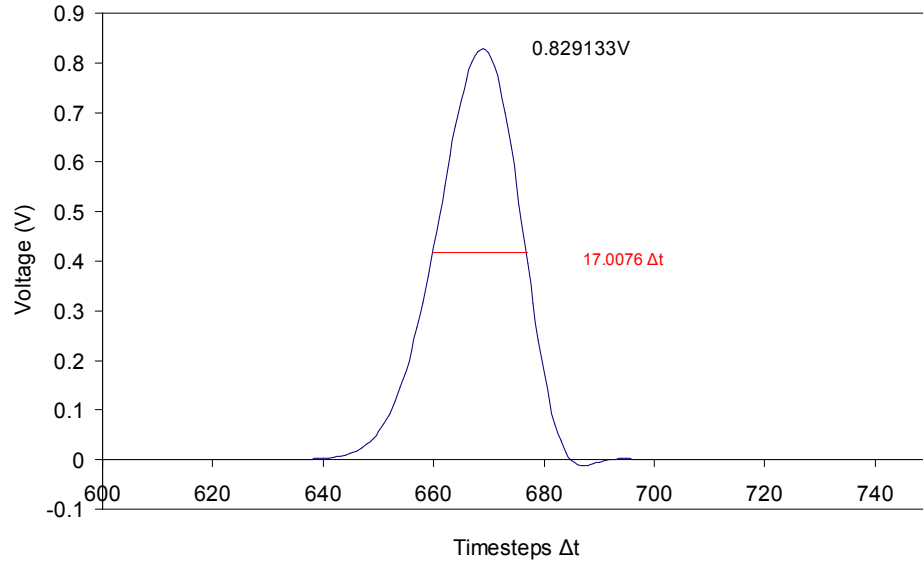
Fig. 4-14D Pulse propagating in case II observed at *n* = 450 after 900 Δ*t*

The simulation in case I is repeated 100,000 times to assess the statistical significance of the standard deviation of the changes in pulse width $\sigma\Delta w$ between the original pulse and reflections after some time steps. As the relative permittivity samples are selected from a random number generator, the data set generated during each simulation is different. Fig. 4-15 shows how $\sigma\Delta w$ converges with increasing simulations for each reflection. From the results, it is observed that the pulse width increases after each reflection. The difference

between σΔw at the first and second reflection is more than that at the second and third reflection. This could be due to the fact that as the signal transverses the line back and forth it becomes correlated with the medium of propagation. As numerical dispersion becomes more prominent, it is observed that the difference between σΔw at the penultimate and final reflections does not follow the expected trend. This suggests more complications in deriving analytical models for statistical behaviour in the time domain. For this reason, most of the subsequent case studies are considered in the frequency domain.
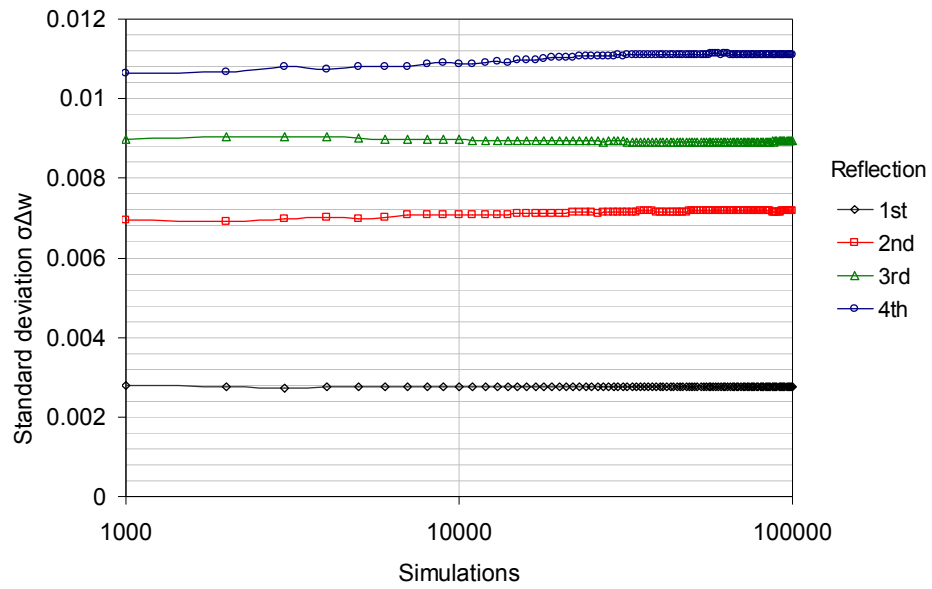
Fig. 4-15 Convergence of the standard deviation of the changes in pulse width

The next chapter deals with the mesh analysis of transmission line with random impedances in the frequency domain. The results obtained are to be used in the extension of approximation paradigm discussed in this chapter to higher dimensions.

4.4   References

[4.1]   C. Christopoulos, "The Transmission-Line Modelling Method," IEEE Press, 1995.

 [4.2]   P. B. Johns and R. L Beurle, "Numerical Solution of 2-Dimensional Scattering Problems using a Transmission Line Matrix," Proc. of the IEE, vol. 118, pp. 1203 – 1208, May 1993.

[4.3]   S.A. Boctor, "Electric Circuit Analysis," Englewood Cliffs, NJ: Prentice-Hall, 1999.

[4.4]   B. M. Ayyub and R.H. McCuen, "Probability, Statistics and Reliability for Engineers and Scientists," 2nd Edition, Chapman and Hall / CRC Press, 2003.

[4.5]   N.T. Afanasiev, S.N. Kolesnik, M.V. Tinin, "Simulation Modelling of Statistical Characteristics of the Radio Wave in a Layer with Random Inhomogeneities of Dielectric Permittivity," MMET Proceedings, pp. 334-336, Sep. 2000.

[4.6]   N. Barabanentov, A. Kravtsov, S.M. Rytov, V.I. Tamarskii, "Status of the Theory of Propagation of Waves in a Randomly Inhomogeneous Medium," Soviet Physics Uspekhi, vol. 13, pp. 551-575, March-April 1971.

[4.7]   F. Ladouceur, J. D. Love, T.J. Senden, "Effect of Side Wall Roughness in Buried Channel Waveguides," IEE Proceedings, vol. 141, pp. 242 – 248, Aug. 1994.

Chapter 5   Direct Solution Technique

This chapter involves the use of an approximate method based upon Taylor series expansions for statistical circuit analysis. This method is referred to as the Direct Solution Technique (DST). The development of this method will be illustrated by its application to a simple circuit network that represents a transmission line in the frequency domain. The results are presented for showing the behaviour of mesh currents as the impedance in the network varies stochastically. The method is then applied on a more complex circuit network to assess the degradation of the technique with increasing complexity. Finally, the impact of including higher order moments into the approximation model is discussed.

5.1   Stochastic Circuit Analysis

In this section an approach is presented that allows the moments of output quantities to be evaluated directly using a Taylor series approximation on a matrix representation of an electromagnetic problem. The method will be initially developed using the simple electrical circuit example of Fig. 5-1 [5.1] and subsequently extended to the case of the 2-D TLM algorithm in the next chapter. The approach is referred to as the Direct Solution Technique (DST) [5.1].
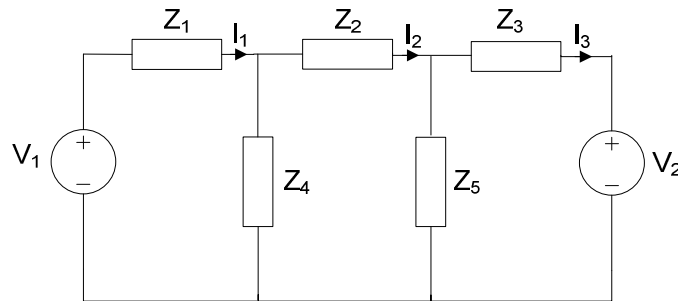
Fig. 5-1 Generic circuit configuration with random impedances

The circuit in Fig. 5-1 is the lumped equivalent circuit of a transmission line. In accordance with the circuit topology, the impedances Z_1, Z_2 and Z_3 have the same nominal inductive reactance while Z_4 and Z_5 have the same nominal capacitive reactance. The impedances Z_1 to Z_5 are defined to be normally distributed independent random variables and the voltage sources to be precisely specified. Mesh analysis yields a matrix equation for the unknown loop currents. This matrix is a simple example of the more general form

$$\underline{\underline{Z}}.\underline{I} = \underline{V} \tag{5.1}$$

where $\underline{\underline{Z}}$ is the random impedance matrix, $\underline{I}$ is a column vector of mesh currents and $\underline{V}$ is a column vector of source voltages. By definition, each element of $\underline{\underline{Z}}$ is known and specified in terms of the statistical moments of the individual impedances. The objective is to obtain the statistical moments of the mesh currents. Let $\underline{\underline{Y}}$ be the admittance matrix which is the inverse of the impedance matrix $\underline{\underline{Z}}$, then pre-multiplying both sides of (5.1) by $\underline{\underline{Y}}$ gives:

$$\underline{\underline{Y}}.\underline{V} = \underline{I} \tag{5.2}$$

For simplicity, consider that only one impedance, Z_n, is statistically variable. Given that $\underline{V} = \underline{\underline{Z}}.\underline{\underline{Y}}.\underline{V}$ then

$$\underline{V}' = \underline{0} = \left(\underline{\underline{Z}}.\underline{\underline{Y}}' + \underline{\underline{Z}}'.\underline{\underline{Y}} \right).\underline{V} \tag{5.3}$$

where $'$ denotes differentiation with respect to Z_n.

The derivative of the current in the *kth* mesh I_k with respect to Z_n using (5.2) and (5.3) is:

$$I_k' = \left(\underline{\underline{Y}}'.\underline{V} \right)_k = -\left(\underline{\underline{Y}}.\,\underline{\underline{Z}}'.\underline{\underline{Y}}.\underline{V} \right)_k \tag{5.4}$$

The first order second moment of I_k can be found from (A.23) in Appendix A:

$$\sigma^2_{I_k} \cong \sigma^2_{Z_n}\left(I_k{}'\right)^2 \qquad (5.5)$$

Similarly,

$$\underline{V}'' = \underline{0} = \left(\underline{\underline{Z}}.\underline{Y}'' + \underline{\underline{Z}}''.\underline{Y} + 2\underline{\underline{Z}}'.\underline{Y}'\right).\underline{V} \qquad (5.6)$$

and hence

$$I_k{}'' = \left(\underline{\underline{Y}}''.\underline{V}\right)_k = -\left(\left(\underline{Y}.\underline{\underline{Z}}''.\underline{Y} - 2\underline{Y}.\underline{\underline{Z}}'.\underline{Y}.\underline{\underline{Z}}'.\underline{Y}\right).\underline{V}\right)_k \qquad (5.7)$$

The second order first moment of I_k can be found from (A.8) in Appendix A:

$$\overline{I_k} \cong I_k\left(\overline{Z}_n\right) + \frac{\sigma^2_{Z_n}}{2}\left(I_k{}''\right) \qquad (5.8)$$

where $I_k\left(\overline{Z}_n\right)$ denotes the *kth* current when all impedances take their mean values.

The expressions in (5.4) and (5.8) can be extended to cases where all the impedances vary independently,

$$\sigma^2_{I_k} \cong \sum_n \sigma^2_{Z_n}\left(I_k{}'\right)^2 \qquad (5.9)$$

$$\overline{I_k} \cong \sum_n I_k\left(\overline{Z}_n\right) + \frac{\sigma^2_{Z_n}}{2}\left(I_k{}''\right) \qquad (5.10)$$

The equivalent expressions if all random impedances vary independently according to an exponential distribution can be found respectively from (A.23) and (A.10) in Appendix A:

$$\sigma^2_{I_k} \cong \sum_n \sigma^2_{Z_n}\left(I_k{}'\right)^2 \qquad (5.11)$$

$$\overline{I}_k \cong \sum_n \left[\begin{array}{c} I_k\left(\overline{Z}_n\right) + \sigma_{Z_n}\left(I_k{'}\right) + \sigma^2_{Z_n}\left(I_k{''}\right) \\ -\sigma_{Z_n}\left(\overline{Z}_n.I_k{''}\right) - \left(\overline{Z}_n.I_k{'}\right) + \frac{\sigma_{Z_n}}{2}\left(\overline{Z}_n{}^2.I_k{''}\right) \end{array} \right] \tag{5.12}$$

These derivations will be applied to the circuit under analysis and the results compared to the benchmark results from converged MC simulations.

5.1.1   Stochastic Impedances with a Normal Distribution

The mesh current analysis for the circuit in Fig. 5-1 is:

$$\begin{pmatrix} \left(Z_1 + Z_4\right) & -Z_4 & 0 \\ -Z_4 & \left(Z_2 + Z_3 + Z_4\right) & -Z_5 \\ 0 & -Z_5 & \left(Z_3 + Z_5\right) \end{pmatrix} \begin{pmatrix} I_1 \\ I_2 \\ I_3 \end{pmatrix} = \begin{pmatrix} V_1 \\ 0 \\ -V_2 \end{pmatrix} \tag{5.13}$$

The term $Z{'}$ can be expressed in terms of the random impedances $Z_1 - Z_5$ in the circuit network all resulting in symmetric and sparse matrices:

$$\frac{d\underline{\underline{Z}}}{dZ_1} = \begin{pmatrix} 1 & 0 & 0 \\ 0 & 0 & 0 \\ 0 & 0 & 0 \end{pmatrix} (5.14\text{a}) \quad \frac{d\underline{\underline{Z}}}{dZ_2} = \begin{pmatrix} 0 & 0 & 0 \\ 0 & 1 & 0 \\ 0 & 0 & 0 \end{pmatrix} (5.14\text{b}) \quad \frac{d\underline{\underline{Z}}}{dZ_3} = \begin{pmatrix} 0 & 0 & 0 \\ 0 & 0 & 0 \\ 0 & 0 & 1 \end{pmatrix} (5.14\text{c})$$

$$\frac{d\underline{\underline{Z}}}{dZ_4} = \begin{pmatrix} 1 & -1 & 0 \\ -1 & 1 & 0 \\ 0 & 0 & 0 \end{pmatrix} (5.14\text{d}) \quad \frac{d\underline{\underline{Z}}}{dZ_5} = \begin{pmatrix} 0 & 0 & 0 \\ 0 & 1 & -1 \\ 0 & -1 & 1 \end{pmatrix} (5.14\text{e})$$

The first and second columns of matrix in (5.14d) and the second and third of (5.14e) are collinear as both random impedances Z_4 and Z_5 are common to the central mesh. The term $Z{'}$ is evidently a null matrix when expressed in terms of all the random impedances.

In this section, all the impedances are independent stochastic variables that are normally distributed. The impedances Z_1, Z_2 and Z_3 have a mean of $20j\Omega$ while

Z_4 and Z_5 have a mean of $-30j\Omega$. The voltage sources are $V_1 = 24V$ and $V_2 = -12V$. The standard deviation, σ_{Zn}, is assumed to be the same for all impedances. The standard deviation and mean of each mesh current can be found from (5.9) and (5.10) respectively. The comparison between the DST and the converged MC method for 100,000 simulations is shown in Fig. 5-2. From the results obtained, it is seen that the difference in both methods for the standard deviation of mesh currents gets larger with increasing values of σ_{Zn}. The difference between the DST and MC approaches is less than 1% when the standard deviation of the circuit impedances is below 0.5 Ω, corresponding to variations of 1.7 – 2.5% about the absolute central impedance value of 20 – 30 Ω.

Fig. 5-2 Percentage difference between the DST and MC methods for circuit with stochastic impedances with a normal distribution

5.1.2   Stochastic Impedances with an Exponential Distribution

The impedances in the circuit configuration in Fig. 5-1 are taken in this section to have an exponential distribution. The impedances have the same nominal values and tolerances as the previous section to compare both distributions. The exponential distribution used is taken from (A.9) in Appendix A. The DST method approximates the standard deviation and mean of mesh currents using

(5.11) and (5.12) respectively. The converged MC method used was based on 100,000 repeated runs of the exponential impedance variates. The percentage difference between the DST and MC methods is presented in Fig. 5-3.
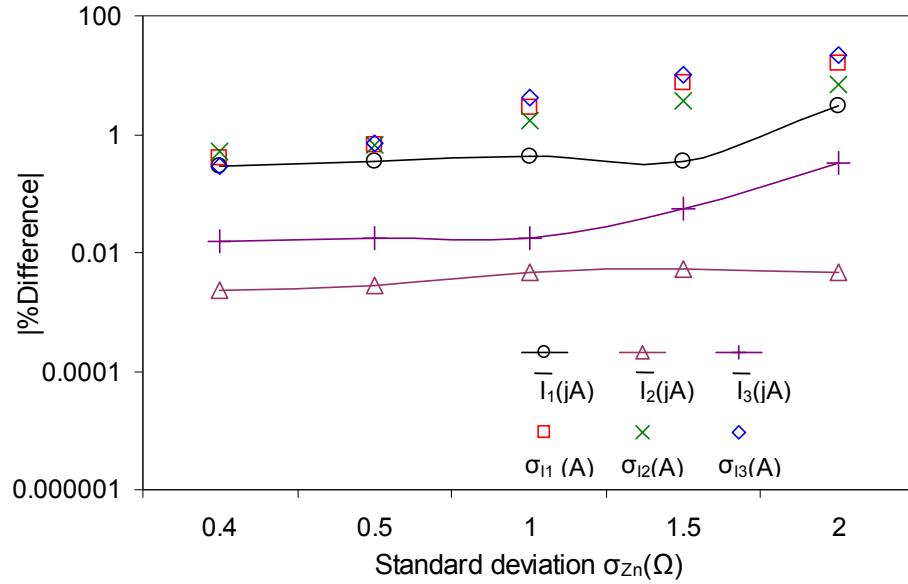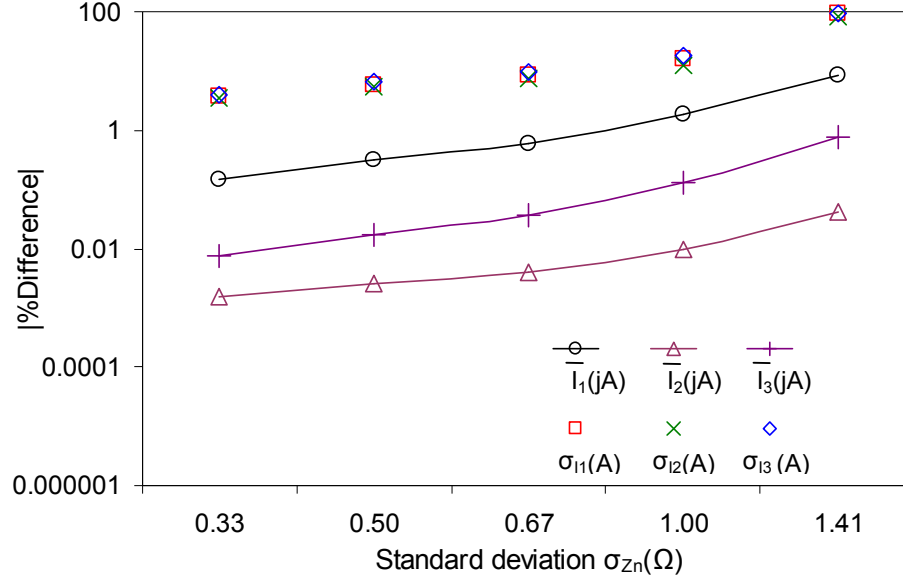

Fig. 5-3 Percentage difference between the DST and MC methods for circuit with stochastic impedances with an exponential distribution

The results obtained show that the percentage difference between both methods here yields a wider discrepancy when compared with normal distributions. The percentage difference between the methods when measuring σ_{I1}, σ_{I2} and σ_{I3} at $\sigma_{Zn} = 0.5\Omega$, are 0.66 %, 0.65 % and 0.69 % respectively. The corresponding values in the case of the normal distribution are 5.85 %, 5.34 % and 6.53 % respectively. Due to the mathematical tractability of the later, the effect of the higher order moments on DST particularly for low standard deviations would have a lower impact on accuracy than in the case for exponential distributions. This is because the odd moments for normal distributions are zero and so make no contribution to the DST approach. The conclusion drawn here is that the type of distributions of stochastic variables plays an important role in the accuracy approximation methods. Other distributions could be studied but most have properties similar to the two cases considered here.

5.2   Impact of Complexity on DST Accuracy

In this section, the effect of increased circuit complexity on the accuracy of the DST method is studied. The circuit in Fig. 5-1 is modified slightly by introducing an additional branch. The resulting circuit configuration is shown in Fig. 5-4 [5.1]. The impedances are all independent normal random variables. The impedances Z_1, Z_2, Z_3 and Z_4 have a mean of $20j\Omega$ while Z_5 and Z_6 have a mean of $-30j\Omega$.
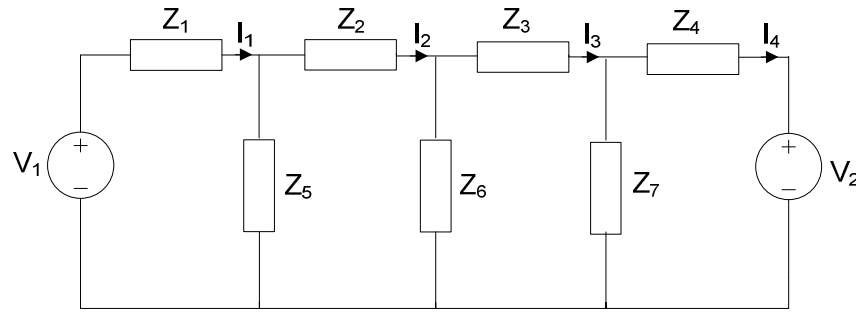
Fig. 5-4 A more extensive circuit for the application of DST.

The results in Fig. 5-5 show the percentage difference in the mean and standard deviation of mesh currents between DST and the MC method for 100,000 simulations. From the difference between the DST and Monte Carlo approaches, it is clear that there is a closer agreement with small standard deviations as expected. This degrades with both increased standard deviation and circuit complexity. The percentage difference between the methods when measuring σ_{I1}, σ_{I2} , σ_{I3} and σ_{I4} at $\sigma_{Zn} = 0.5\Omega$, are 7.63 %, 7.48 %, 7.70 % and 8.07 % respectively. This is worse than results obtained from the simpler case studied in section 5.1. The conclusion from these results is that even if a tractable distribution is used, the DST method will need an improvement to cope with enhanced complexity. An improvement in accuracy should be achievable with higher order approximations as will be shown in the next section.
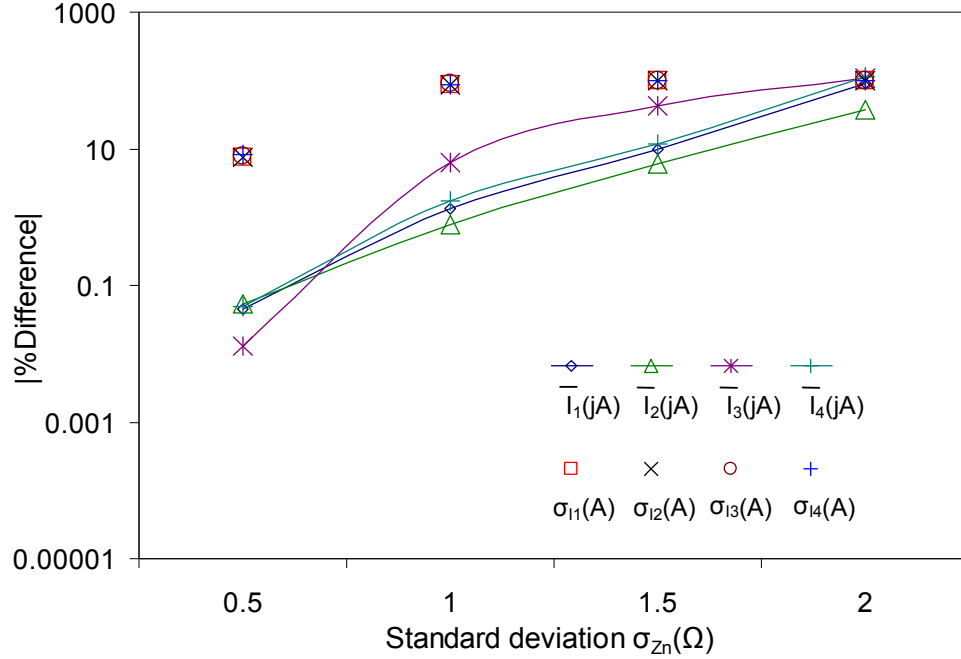
Fig. 5-5 Percentage difference between the DST and MC methods for circuit with enhanced complexity

5.3   Improving Accuracy of DST Using Higher Order Terms

Until this point, only first and second order moments were retained in the DST analysis. This section will now generalise to higher order terms and demonstrate that improved accuracy may be available, albeit at some extra computational effort. From the expansion in (A.5) of Appendix A:

$$\overline{f}(\beta) = f\left(\overline{\beta}\right) + \frac{\mu_2}{2!}\left.\frac{\partial^2 f}{\partial \beta^2}\right|_{\beta=\overline{\beta}} + \frac{\mu_3}{3!}\left.\frac{\partial^3 f}{\partial \beta^3}\right|_{\beta=\overline{\beta}} + \dots \tag{5.15}$$

where β is a random variable of mean $\overline{\beta}$ and *nth* central moment at μ_n given by:

$$\mu_n = \int_{-\infty}^{\infty}\left(\beta - \overline{\beta}\right)^n P(\beta)\, d\beta \tag{5.16}$$

where $P(\beta)$ is the probability density function of β. The first central moment has been excluded from (5.15) above because it is zero as seen from substituting $n = 1$ in (5.16). This has been shown in (A.6) of Appendix A. The expression in (5.15) can be generalised by truncating the expansion at the *rth* term:

$$\overline{f} = f\left(\overline{\beta}\right) + \sum_{j=2}^{r}\left(\frac{\mu_j}{j!}\frac{\partial^j f}{\partial\beta^j}\bigg|_{\beta=\overline{\beta}}\right) \tag{5.17}$$

Specifically applying this formula to the mesh circuit of Fig. 5-1 and summing over the influences of all the impedances, the mean of the *kth* current is:

$$\overline{I}_k = \sum_{n=1}^{5}\left(I_k\left(\overline{Z_n}\right) + \sum_{j=2}^{r}\left(\frac{\mu_{jZ_n}}{j!}\left(\frac{d^j I_k}{dZ_n^j}\right)\right)\right) \tag{5.18}$$

Using the identity for variance [5.2]:

$$\sigma_f^2 = \overline{f^2(\beta)} - \overline{f}^2 \tag{5.19}$$

and with a substantial amount of algebra as shown in [5.3] the following formulae are recovered as the generalisations of (5.18):

$$\sigma_f^2 = \sum_{j=2}^{r}\left(\frac{\mu_j}{j!}\sum_{i=1}^{j-1}\left[\binom{j}{i}f^i f^{j-i}\right]\right) - \left(\sum_{j=2}^{r}\left[\frac{\mu_j}{j!}f^j\right]\right)^2 \tag{5.20}$$

Here $f^i = \dfrac{\partial^i f}{\partial\beta^i}\bigg|_{\beta=\overline{\beta}}$ and $\binom{j}{i} = {}^j C_i$ is a binomial coefficient.

Applying (5.20) to the mesh circuit of Fig. 5-1 and summing over the influences of all the impedances, the variance of the *kth* current is:

$$\sigma_{I_k}^2 = \sum_{n=1}^{5}\left[\sum_{j=2}^{r}\left(\frac{\mu_{jZ_n}}{j!}\sum_{i=1}^{j-1}\left[\binom{j}{i}\frac{d^i I_k}{dZ_n^i}\frac{d^{j-i}I_k}{dZ_n^{j-i}}\right]\right) - \left(\sum_{j=2}^{r}\left[\frac{\mu_{jZ_n}}{j!}\frac{d^j I_k}{dZ_n^j}\right]\right)^2\right] \tag{5.21}$$

where μ_{jZ_n} is the *jth* central moment of Z_n, vector products are performed as piecewise multiplications and derivatives are evaluated at the mean values of Z_n. The main results of this section, (5.18) and (5.21), were presented in [5.4] and shall now be employed for the problem of Fig. 5-1.

Fig. 5-6A and 5-6B show the improvement in the predicted current standard deviation as the number of moments is increased. The cases of both small and large standard deviations of normally distributed impedance values are considered. The percentage difference for all the results in this section is from the DST and converged MC method after 100,000 simulations.

Fig. 5-6A Effect of increasing moments on the accuracy of the DST for random impedances with $\sigma_{Zn} = 0.1$
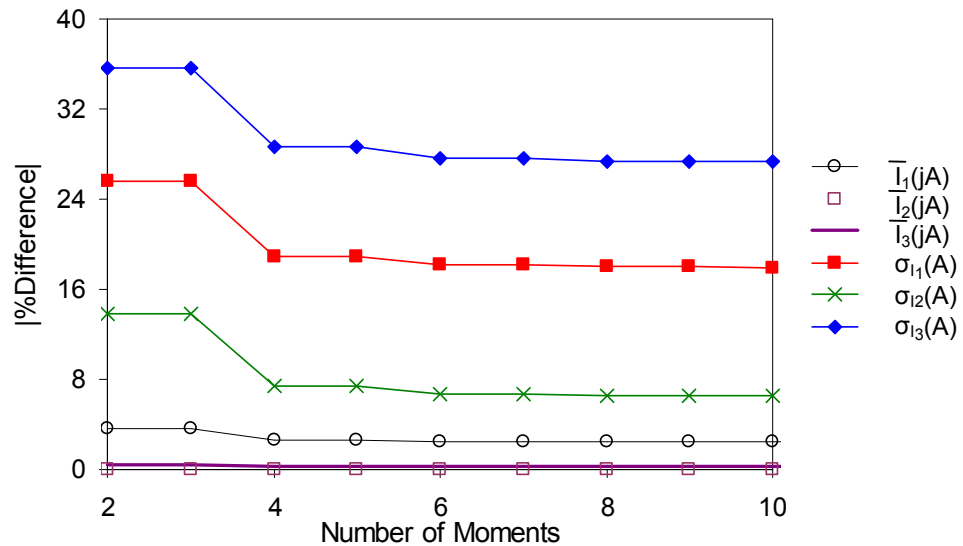
Fig. 5-6B Effect of increasing moments on the accuracy of the DST for random impedances with $\sigma_{Zn} = 2$

Although there is an initial improvement and the curves do asymptotically approach zero theoretically, it is clear that the rate of convergence is very slow, particularly above four moments. The percentage difference in the mean is much smaller than that of the standard deviations. Fig. 5-7A and 5.7B repeat this test using exponentially distributed impedances.
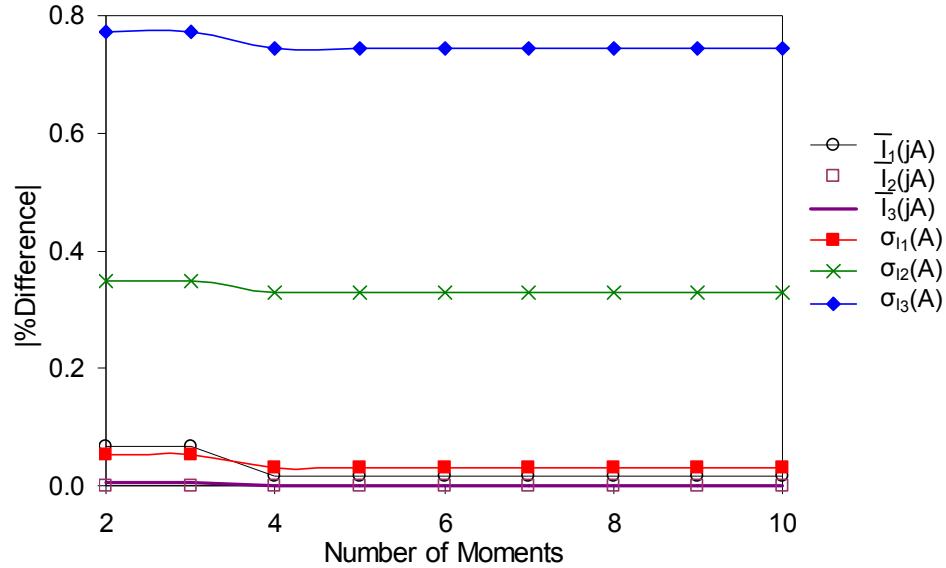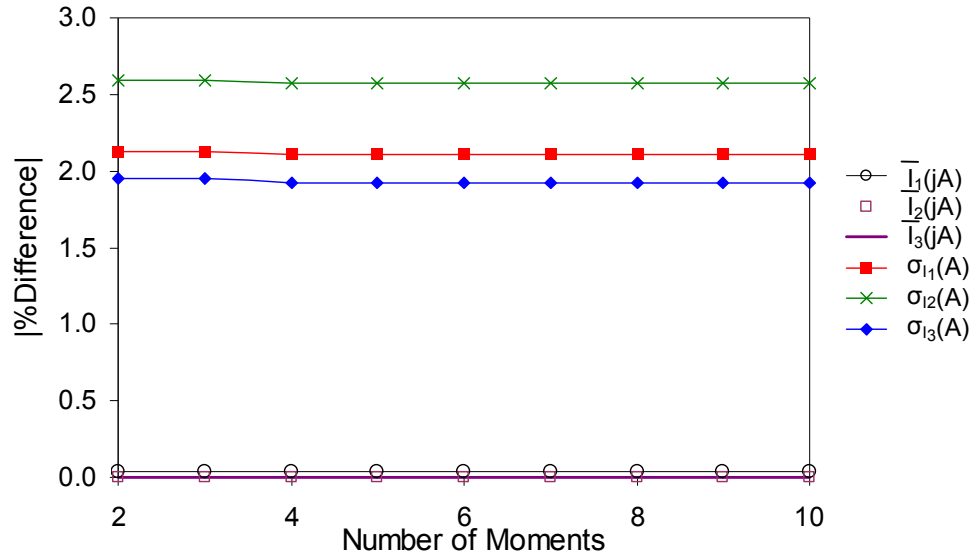

Fig. 5-7A Effect of increasing moments on the accuracy of the DST for random impedances with σ_{Zn} = 0.1
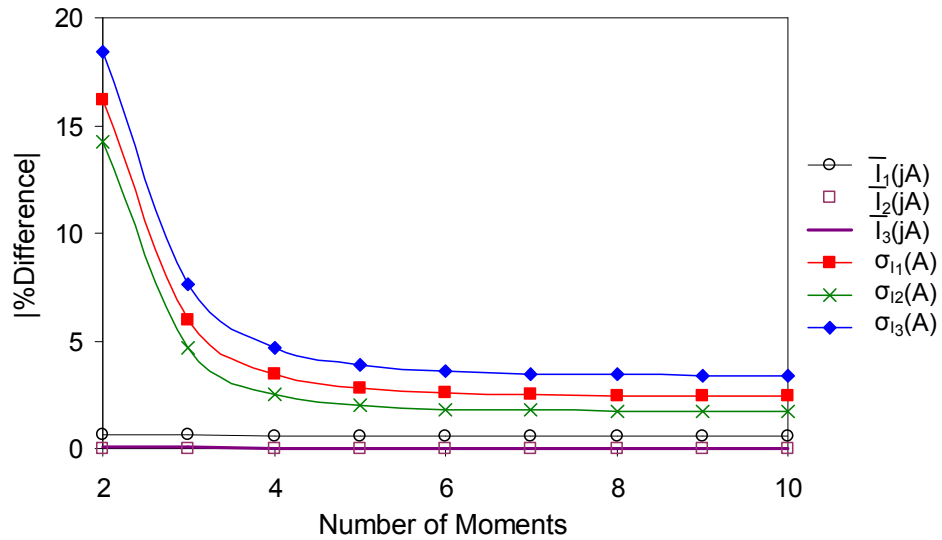
Fig. 5-7B Effect of increasing moments on the accuracy of the DST for random impedances with σ_{Zn} = 0.67

The initial convergence is better, but again the asymptotic convergence is very slow above four moments. The relationship between the number of moments and standard deviation on the percentage difference between the DST and MC approaches is shown in the 3-D plot in Fig. 5-8. As anticipated, the discrepancy between both techniques reduces with increasing moments and reducing standard deviations.
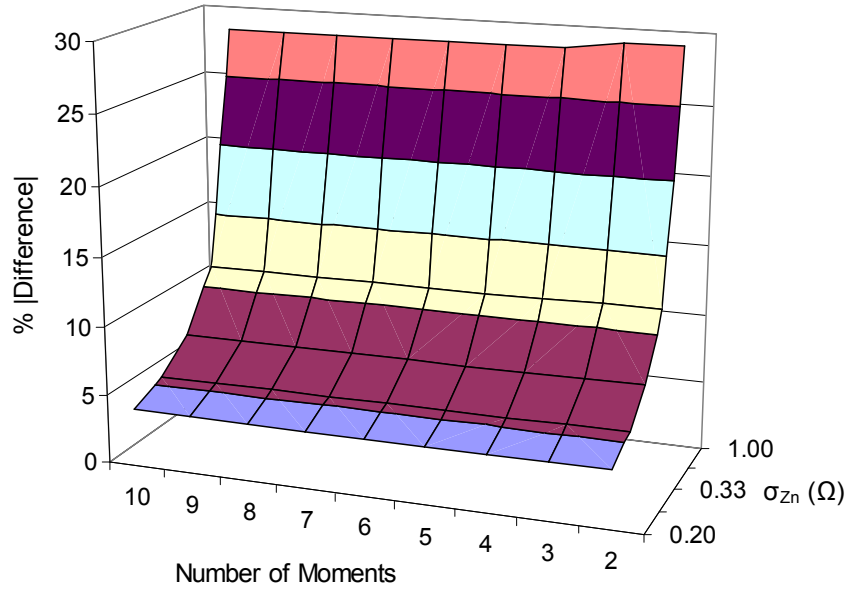
Fig. 5-8 Effect of increasing moments and standard deviation on the accuracy of the DST

The accuracy of the DST method with increasing moments was tested in a scenario having mixed distributions in [5.3]. The circuit in Fig. 5-1 is used for this analysis. The impedances Z_1, Z_3 and Z_4 were chosen to be normal variates while Z_2 and Z_5 were exponential variates. There cases of small and large standard deviation values were considered assessed.

For the first case, the mean and standard deviation of stochastic impedances used are: $\bar{Z}_1 = 20j\Omega$, $\bar{Z}_2 = 15j\Omega$, $\bar{Z}_3 = 18j\Omega$, $\bar{Z}_4 = -30j\Omega$, $\bar{Z}_5 = -25j\Omega$, $\sigma_{Z1} = 0.1\Omega$, $\sigma_{Z2} = 0.1\Omega$, $\sigma_{Z3} = 0.2\Omega$, $\sigma_{Z4} = 0.15\Omega$, and $\sigma_{Z5} = 0.067\Omega$. Fig. 5-9A and 5-9B show the effect of increasing moments on DST accuracy when measuring the mean and standard deviations of mesh currents respectively.

For the second case, the mean and standard deviation of stochastic impedances used are: $\overline{Z}_1 = 20j\Omega$, $\overline{Z}_2 = 15j\Omega$, $\overline{Z}_3 = 18j\Omega$, $\overline{Z}_4 = -30j\Omega$, $\overline{Z}_5 = -25j\Omega$, $\sigma_{Z1} = 0.9\Omega$, $\sigma_{Z2} = 0.5\Omega$, $\sigma_{Z3} = 1.5\Omega$, $\sigma_{Z4} = 0.85\Omega$, and $\sigma_{Z5} = 0.33\Omega$. Fig. 5-10A and 5-10B show the effect of increasing moments on DST accuracy when measuring the mean and standard deviations of mesh currents respectively. The percentage difference between the DST and MC methods in the second case is more than the first case as the variations of stochastic parameters is higher. The results obtained in both cases also showed that beyond four moments the asymptotic convergence is slow.
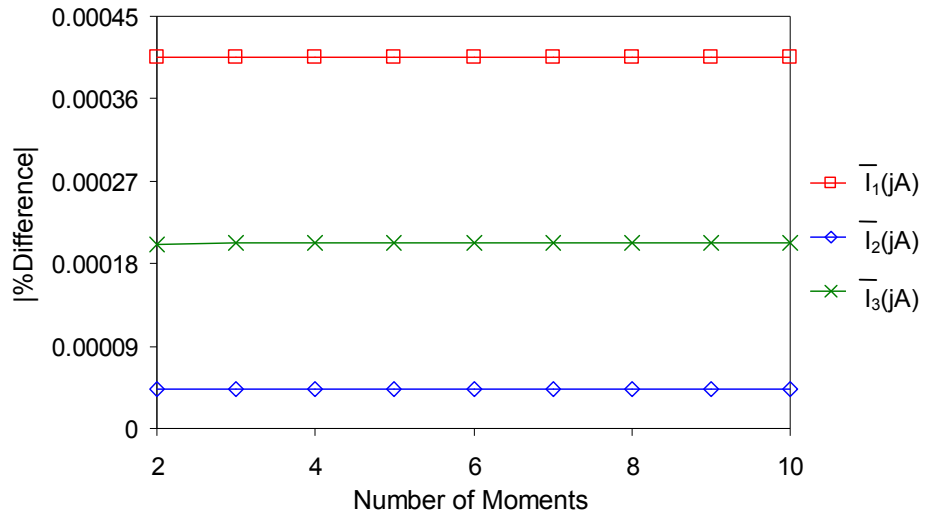
Fig. 5-9A Effect of increasing moments on the accuracy of the mean using DST for random impedances with mixed distributions with small variations
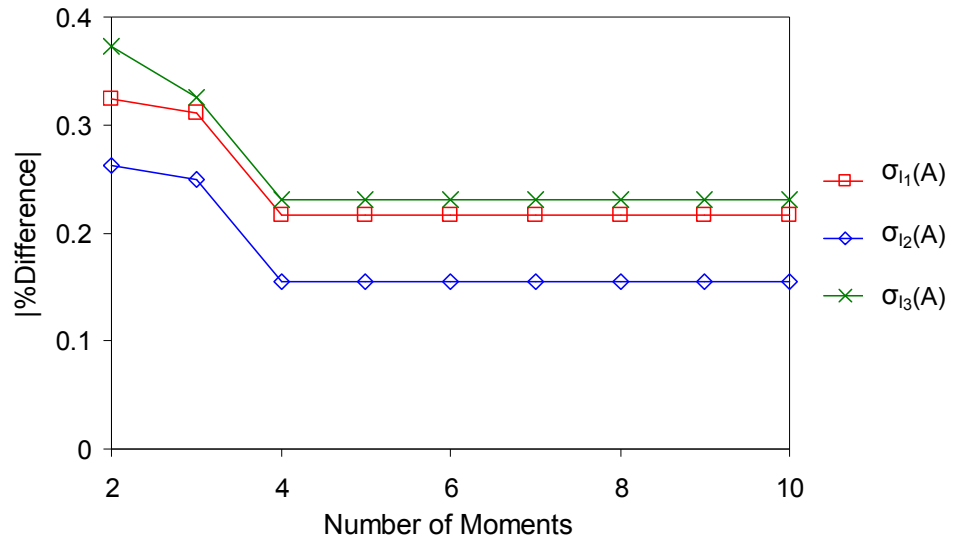
Fig. 5-9B Effect of increasing moments on the accuracy of the standard deviation using DST for random impedances with mixed distributions with small variations
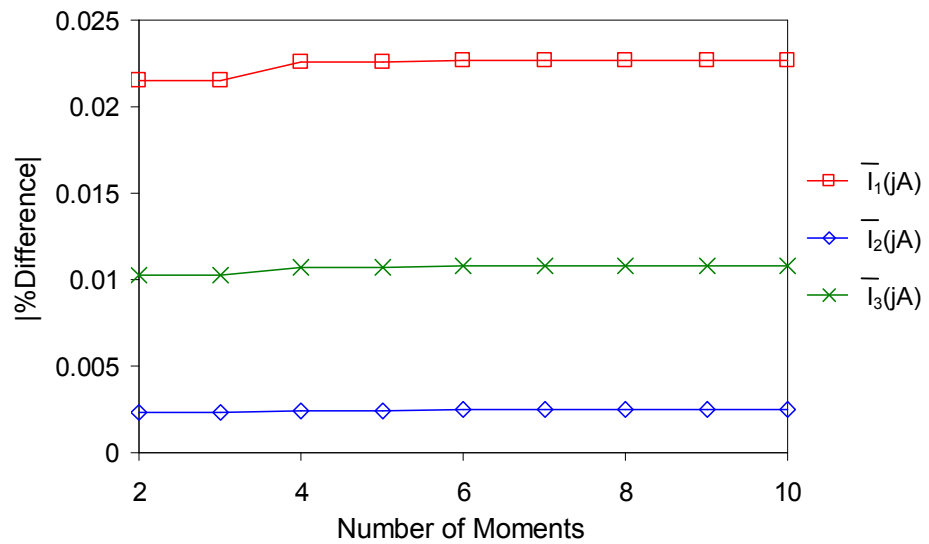
Fig. 5-10A Effect of increasing moments on the accuracy of the mean using DST for random impedances with mixed distributions and large variations
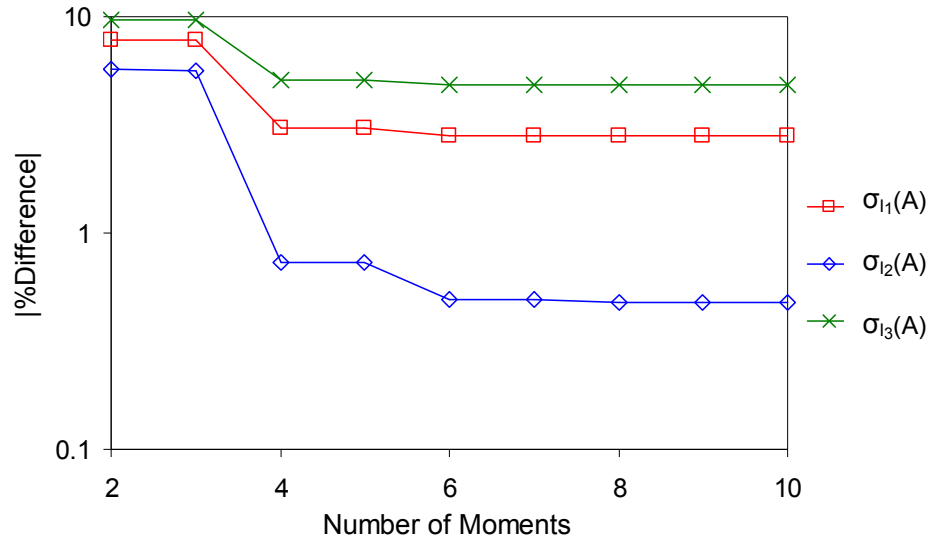
Fig. 5-10B Effect of increasing moments on the accuracy of the standard deviation using DST for random impedances with mixed distributions and large variations

The conclusion for both distributions is that use of a few higher order terms may extend the accuracy of the overall approach to larger standard deviations in the problem parameters, but that the use of higher terms does not always yield practically better results.

5.4   References

[5.1]   A. Ajayi, C, Christopoulos and P. Sewell, "Direct Computations of Statistical Variations in Electromagnetic Problems," EMC Europe 2008 International symp. on Electromag. Comp., Barcelona-Spain, Sep. 2006.

[5.2]   A. Papoulis, "Probability, Random Variables and Stochastic Processes," 2nd Edition, New York, NY: McGraw-Hill, 1984.

[5.3]   P. Ingrey, "Higher Order Approximations for Stochastic Electromagnetism," University of Nottingham, Jun. 2007.

[5.4]   A. Ajayi, P. Ingrey, C. Christopoulos and P. Sewell, "Direct Computations of Statistical Variations in Electromagnetic Problems," IEEE Trans. on Electromagnetic Compatibility, May 2008.

Chapter 6   Statistical Analysis in 2-D Problems

This chapter presents the application of the DST to two-dimensional (2-D) stochastic problems. These provide a better illustration of real-life examples than the 1-D examples, albeit at a higher computational overhead. The 2-D TLM technique is used to solve for the fields in the case studies presented. The MC method is then be used to generate random samples of stochastic variables and the statistical moments are acquired. The results are compared with the DST applied to TLM models depicting parameters of interest. The impact of including higher order approximations to improve the DST is also discussed.

6.1   Two-Dimensional (2-D) TLM

In chapter 4, the 1-D TLM model had only two ports per node junction. This restricts the field components that could be studied. In this section the 2-D TLM technique is introduced.

The 2-D TLM model involves the discretisation of the problem space in two orthogonal directions which constitute a reference plane. This is achieved by using a mesh of interconnected transmission lines on the planar structure under analysis [6.1].

There are two field configurations that can be examined from the discretised structure. The first allows modelling the magnetic field component in the direction orthogonal, while the electric fields are parallel to the reference plane. This is referred to as the TE mode and is modelled using a series node. The second configuration is the dual of the first which implies that the electric field component is orthogonal while the magnetic fields are parallel to the reference plane. This is denoted as the TM case and is modelled using a shunt node. The later case is considered in this chapter.

For the illustration of this technique, the majority of examples here deal with the effect of stochastic permittivity on the resonance of the first harmonic in resonant structures. The schematic illustration of a discretised 2-D dielectric space is shown in Fig 6-1. The *x*-*y* plane is used as the frame of reference. There are *NX* nodes and *NY* nodes in the *x* and *y*-directions respectively. The total number of nodes is the product of *NX* and *NY*. The order of numbering the co-ordinates (*x*, *y*) is found by scanning each node along the *x*-axis. The selected nodes in Fig. 6-1 are closest to the edges of the problem space.

Let the subscripts *x*, *y* and *z* represent the direction of the field components and circuit parameters. For the TM case, the non-zero field components are H_x, H_y and E_z. Given that there is no field variation in the *z*-direction for 2-D problems, the wave equation can be derived as [6.1]:

$$\frac{\partial^2 E_z}{\partial x^2} + \frac{\partial^2 E_z}{\partial y^2} = \mu\varepsilon \frac{\partial^2 E_z}{\partial t^2} \tag{6.1}$$
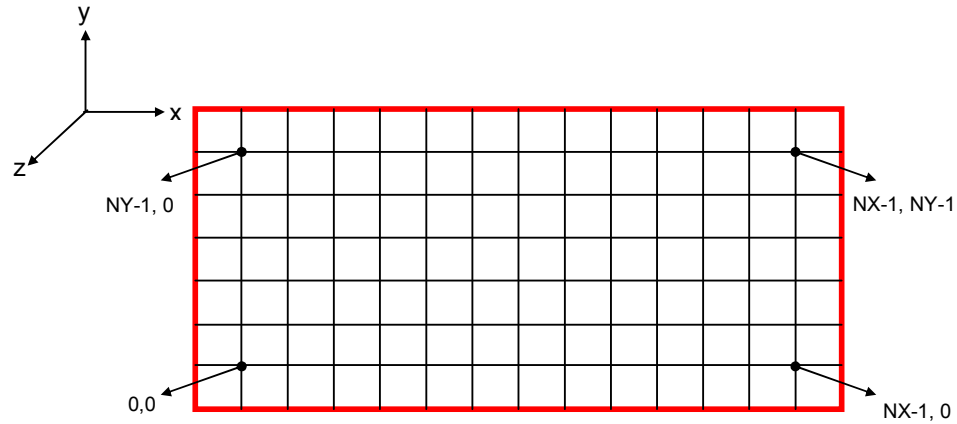
Fig. 6-1 2-D dielectric resonator in the *x*-y plane

The lumped circuit representation of the shunt node located at (*x*, *y*) is shown in Fig. 6-2A. The structure is such that each node comprises four ports which are exchange channels with neighbours in the *x*-*y* plane. All the inductive circuit parameters are connected between a port and the node centre. The total inductance per unit length for propagation in the *x* and *y*-directions is *L* (*H/m*) while the total capacitance per unit length in the *z*-direction is 2*C* (*F/m*).The

discrete TLM equivalent for the shunt node is depicted in Fig. 6-2B with the incident and reflected port voltages.
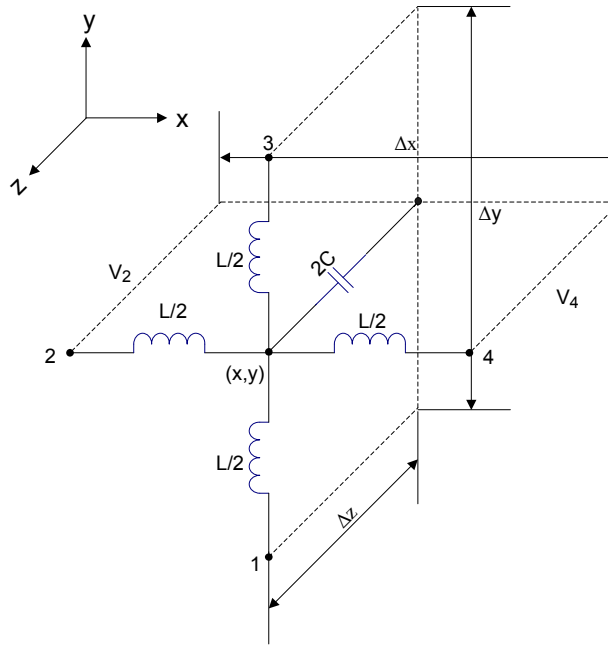
Fig. 6-2A Lumped circuit representation of shunt node [6.1]
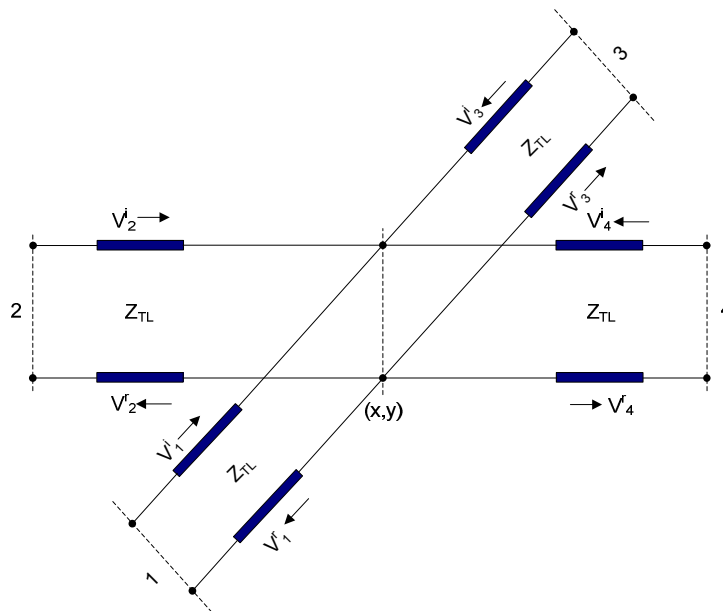
Fig. 6-2B Discrete TLM equivalent of shunt node

105

The space dimensions of the node from Fig. 6-2A are Δx, Δy and Δz in the x, y and z-directions respectively. It is assumed for simplicity that these parameters are of the same length Δl. The relationship between currents and voltages associated in time and space in the shunt node is given by [6.1]:

$$\frac{\partial V_z}{\partial x} = -\frac{L}{\Delta l}\frac{\partial I_x}{\partial t} \tag{6.2a}$$

$$\frac{\partial V_z}{\partial y} = -\frac{L}{\Delta l}\frac{\partial I_y}{\partial t} \tag{6.2b}$$

$$\frac{\partial I_x}{\partial x} = -\frac{C}{\Delta l}\frac{\partial V_z}{\partial t} \tag{6.2c}$$

$$\frac{\partial I_y}{\partial y} = -\frac{C}{\Delta l}\frac{\partial V_z}{\partial t} \tag{6.2d}$$

Differentiating (6.2a) and (6.2c) with respect to x and t respectively and combining the results gives:

$$LC\frac{\partial^2 V_z}{\partial t^2} = \left(\Delta l\right)^2\frac{\partial^2 V_z}{\partial x^2} \tag{6.3}$$

Differentiating (6.2b) and (6.2d) with respect to y and t respectively gives a similar expression to (6.3). Both results can be combined to give:

$$\frac{\partial^2 V_z}{\partial x^2} + \frac{\partial^2 V_z}{\partial y^2} = 2\mu\varepsilon\frac{\partial^2 V_z}{\partial t^2} \tag{6.4}$$

The parameters *inductance and capacitance per unit length* are by definition the permeability μ and permittivity ε respectively. Dividing (6.4) through by Δl and comparing with (6.1), the voltage per unit length is equal to the electric field. The same relationship applies for the current per unit length and magnetic field. Also, it is seen that the permittivity being modelled is twice that required by the medium from theory. This value must be scaled accordingly in the model parameters.

The link impedance Z_{TL} in Fig. 6-1B is related to the lumped circuit parameters in free space by the expression [6.1]:

$$Z_{TL} = \sqrt{\frac{2\mu_0}{\varepsilon_0}}$$

(6.5a)

The velocity of propagation u_{TL} of a wave that travels the length of the line segment Δl for time step Δt in free space is [6.1]:

$$u_{TL} = \frac{\Delta l}{\Delta t} = \sqrt{\frac{2}{\mu_0 \varepsilon_0}}$$

(6.5b)

The connection and scattering process between a node located at (x, y) and its immediate neighbours is shown in Fig. 6-3.
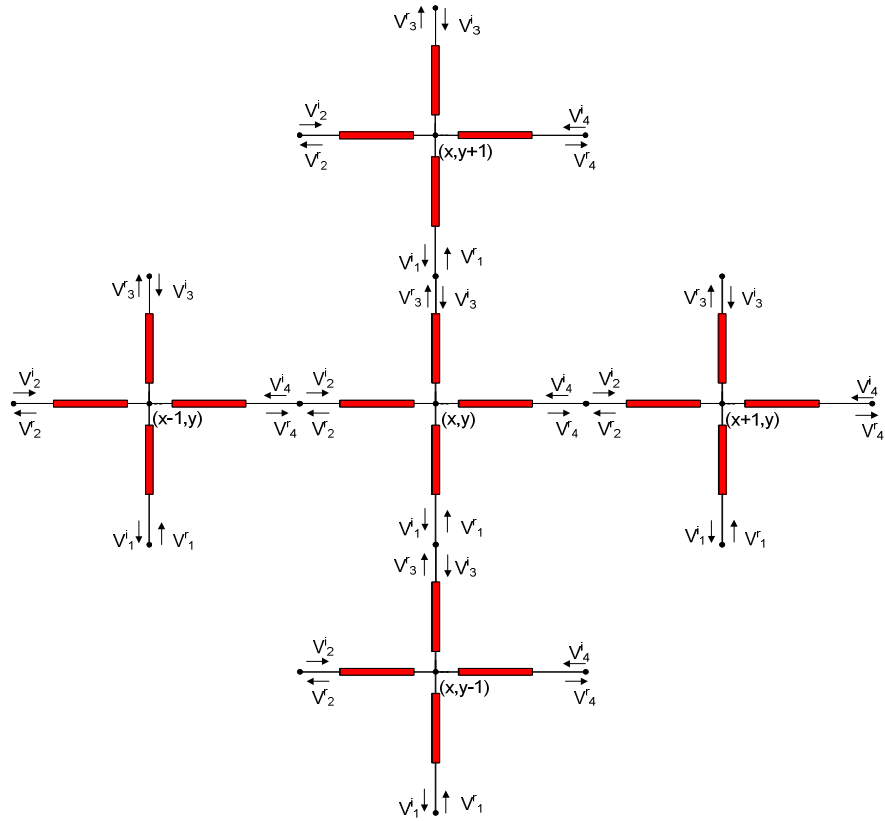
Fig. 6-3 Connection and scattering process between adjacent nodes

Voltage pulses at a particular port are reflected or *scattered* back towards neighbouring node centres and vice-versa. In every TLM simulation, it is essential to define boundaries. The process of connection is simply a *handshake* between coupled ports away from boundaries. The ports linked directly with boundaries have the incident voltage reflected back in conformity with transmission line theory.

In the previous chapter, material properties were modelled using 1-D stubs. The 2-D stub architecture is based on the same principle. The lumped circuit arrangement for the application of capacitive stubs is illustrated in Fig. 6-4A. The stub capacitance C_S is added to the original model. This is connected at the node centre to represent lossless materials with relative permittivity that is more than one.   The discrete TLM equivalent is depicted in Fig. 6-4B.
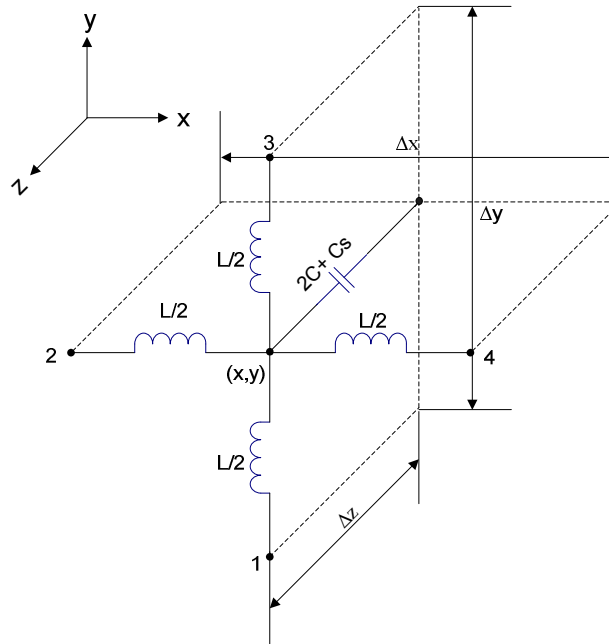
Fig. 6-4A Lumped circuit representation of shunt node with stub capacitance
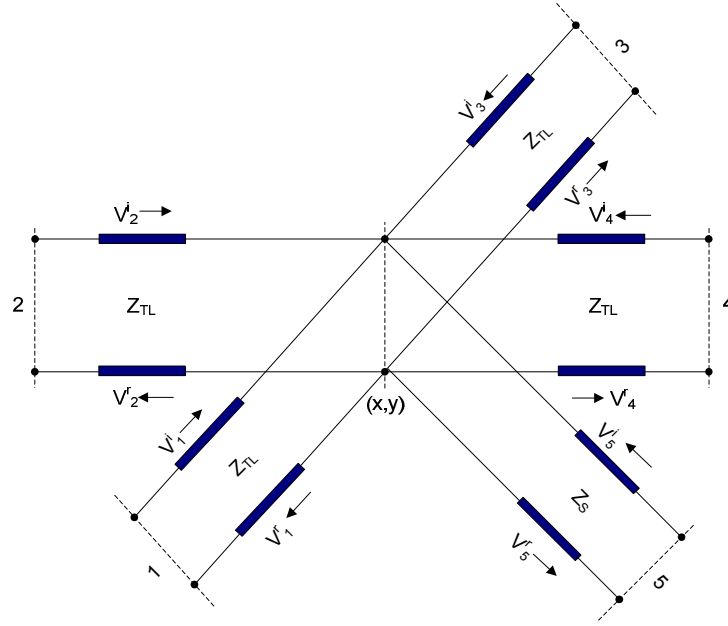
Fig. 6-4B Discrete TLM equivalent of shunt node with capacitive stub

The round trip propagation time in a stub should be the same as the time to transverse a node. The relationship between the stub capacitance C_S and stub impedance Z_S is given by [6.1]:

$$C_S = \frac{\Delta t}{2Z_S}$$

(6.6)

The relationship between link capacitance C and link impedance Z_{TL} is:

$$C = \frac{\Delta t}{Z_{TL}}$$

(6.7)

The overall capacitance represented by the shunt node from Fig. 6-4A is thus:

$$C_{tot} = 2C + C_S = \frac{2\Delta t}{Z_{TL}}\left(1 + \frac{Z_{TL}}{4Z_S}\right)$$

(6.8)

As stated earlier, the permittivity of the medium is the total capacitance per unit length. This can be related to the modelling parameters in (6.8) using (6.5a) and (6.5b) to give:

$$\varepsilon = \varepsilon_0 \varepsilon_r = \frac{C_{tot}}{\Delta l} = \varepsilon_0 \left(1 + \frac{Z_{TL}}{4Z_S} \right) \tag{6.9}$$

From (6.9), the relationship between the stub impedance of a material and relative permittivity ε_r is:

$$Z_S = \frac{Z_{TL}}{4(\varepsilon_r - 1)} \tag{6.10}$$

The Thevenin equivalent circuit for the shunt node in the presence of a capacitive stub is presented in Fig. 6-5. Branch 5 represents the stub contribution to the network. The total voltage V_Z at the node centre for this scenario is:

$$V_Z = \frac{\dfrac{2\left(V^i_1 + V^i_2 + V^i_3 + V^i_4\right)}{Z_{TL}} + \dfrac{2V^i_5}{Z_S}}{\dfrac{4}{Z_{TL}} + \dfrac{1}{Z_S}} \tag{6.11a}$$
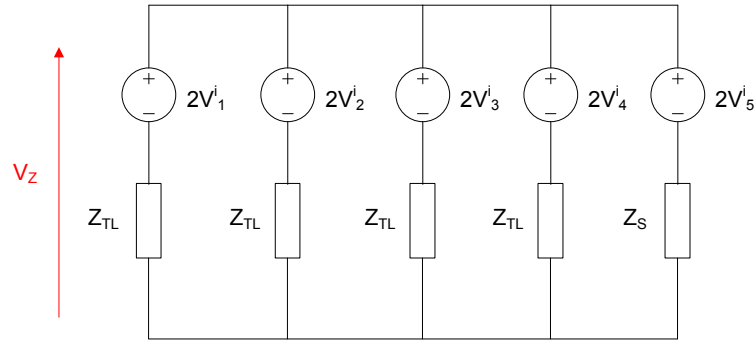
Fig. 6-5 Thevenin equivalent circuit for shunt node with capacitive stub

The expression in (6.11) can be multiplied through by Z_{TL} to give:

$$V_z = \frac{2\left(V^i_1 + V^i_2 + V^i_3 + V^i_4\right) + 2V^i_5 \hat{Y}_S}{4 + \hat{Y}_S} \tag{6.11b}$$

where $\hat{Y}_S = \dfrac{Z_{TL}}{Z_S}$

The reflected voltage at any port is the difference between V_Z and the incident voltage at that port. The scatter sub-matrix relates the vector of incident voltages with that of the reflected voltage of each node (x, y) of the problem space at a time step k:

$$_k\underline{V}^r_{x,y} = \underline{\underline{S}}_{x,y} \cdot {}_k\underline{V}^i_{x,y} \tag{6.12}$$

For a shunt node with a stub, the scatter sub-matrix is a 5 × 5 matrix [6.1]:

$$\underline{\underline{S}}_{x,y} = \frac{1}{\hat{Y}}\begin{pmatrix} 2-\hat{Y} & 2 & 2 & 2 & 2\hat{Y}_S \\ 2 & 2-\hat{Y} & 2 & 2 & 2\hat{Y}_S \\ 2 & 2 & 2-\hat{Y} & 2 & 2\hat{Y}_S \\ 2 & 2 & 2 & 2-\hat{Y} & 2\hat{Y}_S \\ 2 & 2 & 2 & 2 & 2\hat{Y}_S-\hat{Y} \end{pmatrix} \tag{6.13}$$

where $\hat{Y} = 4 + \hat{Y}_S$

The *global scatter matrix* is given by a sparse matrix with diagonal entries consisting of the scatter sub-matrices. This provides the relationship between the incident and reflected voltages of all the nodes. The expression for this at a particular time step k is:

$$_k V^r = \underline{\underline{S}} \cdot {}_k V^i \tag{6.14}$$

where $_k\underline{V}^r$ and $_k\underline{V}^i$ are global vectors that contain all the reflected and incident port voltages respectively at time step k.

The problem with *NP* ports per node has a global scatter matrix $\underline{\underline{S}}$ of the order *NX x NY x NP*. Using the designated numbering arrangement in Fig. 6-1, $\underline{\underline{S}}$ is given by the expression:

$$
\underline{\underline{S}} =
\begin{pmatrix}
\underline{\underline{S}}_{0,0} & \underline{\underline{0}} & \underline{\underline{0}} & & \underline{\underline{0}} & \underline{\underline{0}} & . & . & \underline{\underline{0}} \\
\underline{\underline{0}} & . & \underline{\underline{0}} & & \underline{\underline{0}} & \underline{\underline{0}} & \underline{\underline{0}} & . & \underline{\underline{0}} \\
\underline{\underline{0}} & \underline{\underline{0}} & . & & \underline{\underline{0}} & \underline{\underline{0}} & \underline{\underline{0}} & . & \underline{\underline{0}} \\
\underline{\underline{0}} & \underline{\underline{0}} & \underline{\underline{0}} & & \underline{\underline{S}}_{NX-1,0} & . & . & . & . \\
. & . & . & . & . & . & . & & . \\
. & . & . & . & . & . & . & & . \\
. & . & . & . & . & . & . & & . \\
\underline{\underline{0}} & \underline{\underline{0}} & \underline{\underline{0}} & \underline{\underline{0}} & . & . & . & & \underline{\underline{S}}_{NX-1,NY-1}
\end{pmatrix}
\tag{6.15}
$$

where $\underline{0}$ is a null *NP x NP* matrix. For a 2-D shunt node, *NP* = 5.

This global matrix formulation is important for solving 2-D frequency domain problems. This can be achieved by translating voltage expressions from the time domain into the frequency domain using a Fourier transform.

The connection sub-matrix can also be attained by taking into account that pulses incident on a port are either coupled into adjacent ports or reflected according to boundary conditions. For a shunt node (*x, y*) away from the boundary, the incident link line voltages at a current time step *k* + 1 depend on those reflected from adjacent ports at a previous time step *k*. The port associated with the capacitive stub is terminated with an open circuit boundary and connected to the node centre. By inspection, the following expressions are obtained:

$$
{}_{k+1}V^i_1(x,y) = {}_k V^r_3(x,y-1)
\tag{6.16a}
$$

$$
{}_{k+1}V^i_2(x,y) = {}_k V^r_4(x-1,y)
\tag{6.16b}
$$

$$
{}_{k+1}V^i_3(x,y) = {}_k V^r_1(x,y+1)
\tag{6.16c}
$$

$$
{}_{k+1}V^i_4(x,y) = {}_k V^r_2(x+1,y)
\tag{6.16d}
$$

$$
{}_{k+1}V^i_5(x,y) = {}_k V^r_5(x,y)
\tag{6.16e}
$$

For nodes connected to metallic boundaries, the associated port p will be terminated with a short circuit boundary and the incident voltage at the time step $k + 1$ is:

$$_{k+1}V^{\,i}_{\ p}\left(x,y\right)=-\,_{k}V^{\,r}_{\ p}\left(x,y\right)$$

(6.17)

where $(0,\ y)$, $(NX-1,\ y)$, $(x,\ 0)$ and $(x,\ NY-1)$ are the pertinent co-ordinates of (x,y) in (6.17).

The global connection matrix relates all the incident voltages at a current timestep with the reflected voltages at the previous timestep for all the ports in the problem space. This is given by:

$$_{k+1}V^{\,i}=\underline{\underline{C}}\cdot\,_{k}V^{\,r}$$

(6.18)

The order of the global connection matrix is sparse and of the same order as that of the global scatter matrix. The entries of this matrix are shown in Appendix C.

6.1.1   Frequency Domain TLM (FDTLM) for Problems with Reflecting Boundaries

For waveguide problems, a frequency domain interpretation of the TLM matrix is obtained using the following steps:

STEP 1: Substitution of the vector of reflected voltages $\underline{V}^{r}(t)$ in (6.18) with its representation in (6.14). The resulting expression is written in terms of Δt to give:

$$\underline{V}^{\,i}\left(t+\Delta t\right)=\underline{\underline{C}}.\underline{\underline{S}}.\underline{V}^{\,i}\left(t\right)$$

(6.19)

STEP 2: Find the Fourier transform of both sides (6.19):

$$\underline{V}^{\,i}e^{\,j\omega\Delta t}=\underline{\underline{C}}.\underline{\underline{S}}.\underline{V}^{\,i}$$

(6.20)

where $\underline{V}^{\,i}$ is the is an eigenvector of $\underline{\underline{C}}.\underline{\underline{S}}$ and the Fourier transform of $\underline{V}^{\,i}(t)$. The corresponding eigenvalue is $e^{\,j\omega\Delta t}$ and ω is the angular resonant frequency.

6.1.2 Frequency domain TLM for problems with non-reflecting boundaries

For problems with non-reflecting boundaries, the frequency domain interpretation of the TLM matrix is obtained using the following steps:

STEP 1: A vector of all voltage sources $\underline{Vs}(t)$ is included to (6.19) to give:

$$\underline{V}^{i}(t) = \underline{Vs}(t) + \underline{\underline{C}}.\underline{\underline{S}}.\underline{V}^{i}(t - \Delta t) \tag{6.21}$$

STEP 2: Find the Fourier transform of both sides (6.21):

$$\underline{Vs} = \left(\underline{\underline{I}} - \underline{\underline{C}}.\underline{\underline{S}}e^{j\omega\Delta t}\right).\underline{V}^{i} \tag{6.22a}$$

where $\underline{Vs}$ is the Fourier transform of $\underline{Vs}(t)$, and $\underline{\underline{I}}$ is an identity matrix of order *NX x NY x NP*.

Making a substitution $\underline{\underline{A}} = \underline{\underline{I}} - \underline{\underline{C}}.\underline{\underline{S}}\,e^{\,j\omega\Delta t}$ in (6.22a), a Fourier expression for the voltage source can be found [6.2]:

$$\underline{Vs} = \underline{\underline{A}}.\underline{V}^{i} \tag{6.22b}$$

6.2   Application of the DST to Stochastic Waveguide Problems

In many applications, where the response of a system is a function of several design parameters, it is important to know how the eigensolutions of a matrix change as it elements change [6.3]. A statistical model can be derived from the electromagnetic constitutive variables. The derivatives of eigenvalues in particular are useful in the calculation of the statistics of eigenvalue location in stochastic applications [6.4]. This feature is exploited here in the application of DST to TLM waveguide analyses. This is shown using the steps below:

STEP 1: Differentiate both sides of (6.20) with respect to the random variable, which in this case is relative permittivity, ε_r. There are two variables here that are identified as functions of ε_r namely: resonant frequency f_r and scatter matrix $\underline{S}$.

$$\underline{\underline{C}} \cdot \frac{d\underline{\underline{S}}}{d\varepsilon_r} \cdot \underline{V}^i + \underline{\underline{C}} \cdot \underline{\underline{S}} \cdot \frac{d\underline{V}^i}{d\varepsilon_r} = \frac{de^{j\omega\Delta t}}{d\varepsilon_r} \underline{V}^i + e^{j\omega\Delta t} \frac{d\underline{V}^i}{d\varepsilon_r} \tag{6.23}$$

STEP 2: Let $\underline{U}^i$ represent the eigenvector of the transpose of the connect and scatter matrix product. This is defined in (6.24). From matrix algebra, the eigenvectors, $\underline{U}^i$ and $\underline{V}^i$ have identical eigenvalues. The eigenvectors are generated to satisfy the boundary conditions on the metallic walls of the guide.

$$\underline{U}^{iT} \cdot \underline{\underline{C}} \cdot \underline{\underline{S}} = e^{j\omega\Delta t} \underline{U}^{iT} \tag{6.24}$$

STEP 3: Pre-multiply both sides of (6.23) with the transpose of the eigenvector $\underline{U}^i$:

$$\underline{U}^{iT} \left(\underline{\underline{C}} \cdot \frac{d\underline{\underline{S}}}{d\varepsilon_r} \cdot \underline{V}^i + \underline{\underline{C}} \cdot \underline{\underline{S}} \cdot \frac{d\underline{V}^i}{d\varepsilon_r} \right) = \underline{U}^{iT} \left(\frac{de^{j\omega\Delta t}}{d\varepsilon_r} \underline{V}^i + e^{j\omega\Delta t} \frac{d\underline{V}^i}{d\varepsilon_r} \right) \tag{6.25}$$

STEP 4: Substitute the (6.24) into (6.25) and eliminate the product of $e^{j\omega\Delta t}$ and $\underline{U}i^T.d\underline{V}i \,/d\varepsilon_r$ which appears on both sides of the equation. This can be rearranged to make the derivative of the eigenvalue with respect to relative permittivity subject of the formula:

$$\frac{de^{j\omega\Delta t}}{d\varepsilon_r} = \frac{\underline{U}^{iT} \cdot \underline{\underline{C}} \cdot \frac{d\underline{\underline{S}}}{d\varepsilon_r} \cdot \underline{V}^i}{\underline{U}^{iT} \cdot \underline{V}^i} \tag{6.26}$$

STEP 5: As for problems involving inhomogenously loaded dielectric waveguide, an explicit relationship between f_r and ε_r is not readily obvious and can only be assessed via the solution of a set of transcendental equations [6.4].

This issue can be obviated via the introduction of an auxiliary derivative term $d/d f_r$ to obtain the rate of change of f_r with ε_r.

$$\frac{df_r}{d\varepsilon_r} = \frac{\underline{U}^{iT} . \underline{\underline{C}} . \dfrac{d\underline{\underline{S}}}{d\varepsilon_r} . \underline{V}^i}{\underline{U}^{iT} \left(j2\pi\Delta t \right) e^{j\omega\Delta t} \underline{V}^i} \tag{6.27}$$

STEP 6: The first order approximation for the variance of the resonant frequency for a distribution of ε_r and N_{RV} random variables can be found via the relation [6.5]:

$$\sigma^2_{\,fr} \cong \sum_{j=1}^{N_{RV}} \sigma^2_{\,\varepsilon rj} \left(\frac{df_r\left(\overline{\varepsilon_{r\,j}}\right)}{d\varepsilon_{r\,j}} \right)^2 \tag{6.28}$$

where the overbar denotes the mean of the parameter under consideration.

6.3   Application of the DST to Stochastic Problems with Absorbing Boundaries

Consider a set of wires (whose exact radii are unknown) suspended in an enclosure with absorbing boundaries. The DST now has to be modified to take these boundary conditions into account. The equations derived in sub-section 6.1.2 are used with the DST approach to approximate the mean and variance of observed voltages.

The variance of TLM port voltages are contained in a single covariance matrix. This can be obtained from differential analysis. The method described here involves the use of the perturbation method as shown:

$$\underline{\underline{A}}'(r) = \underline{\underline{A}}'\left(\overline{r} + \delta_r\right) \cong \underline{\underline{A}}'\left(\overline{r}\right) + \delta_r \frac{d\underline{\underline{A}}'\left(\overline{r}\right)}{dr} + \frac{\delta^2_r}{2} \frac{d^2\underline{\underline{A}}'\left(\overline{r}\right)}{dr^2} + \dots \tag{6.29}$$

where r is the stochastic wire radius, $\overline{r}$ is the mean wire radius, δ_r is the perturbation parameter and $\underline{\underline{A}}'$ is the inverse of $\underline{\underline{A}}$.

Applying the perturbation term to (6.22b):

$$\underline{V}^{i} = \underline{\underline{A}}'\left(\overline{r} + \delta_{r}\right)\underline{Vs} \cong \left[\underline{\underline{A}}'\left(\overline{r}\right) + \delta_{r}\frac{d\,\underline{\underline{A}}'\left(\overline{r}\right)}{dr} + \frac{\delta_{r}^{2}}{2}\frac{d^{2}\,\underline{\underline{A}}'\left(\overline{r}\right)}{dr^{2}} + \ldots\right]\underline{Vs} \qquad (6.30a)$$

where

$$\underline{\underline{A}}'\left(\overline{r}\right) \cong \left(\underline{\underline{I}} - \underline{\underline{C}}\left(\overline{r}\right).\underline{\underline{S}}\left(\overline{r}\right)e^{-j\omega\Delta t}\right)^{-1} \qquad (6.30b)$$

$$\frac{d\,\underline{\underline{A}}'\left(\overline{r}\right)}{dr} = -\underline{\underline{A}}'\left(\overline{r}\right).\frac{d\,\underline{\underline{A}}\left(\overline{r}\right)}{dr}.\underline{\underline{A}}'\left(\overline{r}\right) \qquad (6.30c)$$

The rate of change of the vector $\underline{V}^{i}$ with respect to r is:

$$\frac{d\underline{V}^{i}\left(\overline{r}\right)}{dr} = \frac{d\,\underline{\underline{A}}'\left(\overline{r}\right)}{dr}\underline{Vs} \qquad (6.31)$$

The covariance matrix to approximate the variances in each of the ports for N_{RV} random variables is:

$$\underline{\underline{\sigma}}^{2}_{Vi} \cong \sum_{j=1}^{N_{RV}}\sigma^{2}_{rj}\left[\frac{d\underline{V}^{i}\left(\overline{r}\right)}{dr_{j}}\right]^{2} = \sum_{j=1}^{N_{RV}}\sigma^{2}_{rj}\left[\frac{d\,\underline{\underline{A}}'\left(\overline{r}_{j}\right)}{dr_{j}}\right].\underline{Vs}.\underline{Vs}^{T}.\left[\frac{d\,\underline{\underline{A}}'\left(\overline{r}_{j}\right)}{dr_{j}}\right]^{T} \qquad (6.32)$$

The covariance matrix $\underline{\underline{\sigma}}^{2}_{Vi}$ is a symmetric one defined as follows [6.6]:

$$\underline{\underline{\sigma}}^{2}_{Vi} = \begin{pmatrix} \sigma_{V^{i}_{11}} & \sigma_{V^{i}_{12}} & \cdots & \sigma_{V^{i}_{1n}} \\ \sigma_{V^{i}_{21}} & \sigma_{V^{i}_{22}} & \cdots & \sigma_{V^{i}_{2n}} \\ \vdots & \vdots & \cdots & \vdots \\ \sigma_{V^{i}_{n1}} & \sigma_{V^{i}_{n1}} & \cdots & \sigma_{V^{i}_{nn}} \end{pmatrix} \qquad (6.33)$$

where $\sigma_{V}{}^{i}_{ab}$ gives the covariance between incident voltages between port a and port b which must be equal to $\sigma_{V}{}^{i}_{ba}$. The variance on port a independent of other influences is given by the expression $\sigma_{V}{}^{i}_{aa}$ and is found in the ath position on the leading diagonal of the covariance matrix.

Now, it is has been established that each shunt node consists of a 5 x 5 sub-matrix depicting the 5 port network that act as links to neighbouring nodes. The total voltage on a particular node *m* from (6.11b) is:

$$V_m = 2 \left[\frac{V^i_{m1} + V^i_{m2} + V^i_{m3} + V^i_{m4} + \hat{Y}_{sm} V^i_{m5}}{4 + \hat{Y}_{sm}} \right] \tag{6.34}$$

where m_1 - m_4 are the link line orthogonal ports and m_5 is the open circuit stub modelling permittivity with normalised admittance $\hat{Y}_{sm}$.

Given the variances and covariance of all the ports from (6.33), the first order variance approximation of the total voltage at node *m* can be found in [6.6]:

$$\sigma^2_{Vm} \cong \frac{4}{\left(4 + \hat{Y}_{sm}\right)^2} \left(\begin{array}{l} \sigma^2_{V^i_{m1}} + \sigma^2_{V^i_{m2}} + \sigma^2_{V^i_{m3}} + \sigma^2_{V^i_{m4}} + \hat{Y}_{sm}^{\,2} \sigma^2_{V^i_{m5}} \\[2mm] +2 \left(\begin{array}{l} \sigma_{V^i_{m1m2}} + \sigma_{V^i_{m1m3}} + \sigma_{V^i_{m1m4}} \\[1mm] +\sigma_{V^i_{m2m3}} + \sigma_{V^i_{m2m4}} + \sigma_{V^i_{m3m4}} \\[1mm] + \hat{Y}_{sm} \left(\sigma_{V^i_{m1m5}} + \sigma_{V^i_{m2m5}} + \sigma_{V^i_{x3x5}} + \sigma_{V^i_{x4x5}} \right) \end{array} \right) \end{array} \right) \tag{6.35}$$

The second derivative of $\underline{V}^i$ with respect to *r* can be found from (5.7) to be:

$$\frac{d^2 \underline{V}^i}{dr^2} = \left(\frac{d^2 \underline{\underline{A}}'}{dr^2} \right) \underline{V}_S = - \left[\left(\underline{\underline{A}}' \cdot \frac{d^2 \underline{\underline{A}}'}{dr^2} \cdot \underline{\underline{A}}' \right) - 2 \left(\underline{\underline{A}}' \frac{d \underline{\underline{A}}}{dr} \cdot \underline{\underline{A}}' \cdot \frac{d \underline{\underline{A}}}{dr} \cdot \underline{\underline{A}}' \right) \right] \tag{6.36}$$

The second order approximation for the mean of incident voltages is:

$$\overline{V}^i \cong \sum_{j=1}^{N_{RV}} \underline{V}^i\left(\overline{r}_j\right) + \frac{\sigma^2_{r_j}}{2} \left(\frac{d^2 \underline{V}^i}{dr_j^2} \right) \tag{6.37}$$

The mean total voltage can be found from (6.34):

$$\overline{V}_m \cong 2\left[\frac{\overline{V}^i{}_{m1} + \overline{V}^i{}_{m2} + \overline{V}^i{}_{m3} + \overline{V}^i{}_{m4} + \hat{Y}_{sm}\,\overline{V}^i{}_{m5}}{4 + \hat{Y}_{sm}}\right] \qquad (6.38)$$

6.4   Case Studies for the Application of the DST to Electromagnetic Problems

This section deals with the application of the theory developed in sections 6.2 and 6.3. The case studies here deal with stochastic electromagnetic problems analysed using the MC method and then compared with the DST alternative. For each scenario the problem space in sub-sections 6.41 – 6.43 is discretised using 24 nodes (*NX*) in the horizontal direction and 12 nodes (*NY*) in the vertical direction.   To validate the DST approach, the resonances of a number of canonical boxed dielectrics are considered. This will use the DST equations derived in section 6.2. There are additional examples with wires suspended in a deterministic medium with absorbing boundaries. This will use the DST equations derived in section 6.3.

6.4.1   Resonances in Structures with Homogenous Normally Distributed Random Dielectrics

Although it would suffice to use conventional methods to estimate how homogenous random dielectric affects resonance distribution, calculations are shown here based on the DST and comparisons are made.

From the expression of fundamental resonant frequency for homogenous dielectric resonators provided in [6.7], the rate of change of f_r with ε_r is found to be:

$$\frac{df}{d\varepsilon_r} = \frac{c}{4\varepsilon_r{}^{3/2}}\sqrt{\left(\frac{1}{L_X}\right)^2 + \left(\frac{1}{L_Y}\right)^2} \qquad (6.39)$$

where c is the speed of light L_X and L_Y are the length and height of the resonator respectively.

Consider a normally distributed random dielectric with a central relative permittivity of 2.01 and a standard deviation of 0.05. The resonator dimensions are L_X = 1m and L_Y = ½ m. The MC simulation is performed by using 100,000 repeated runs of the FDTLM algorithm described in [6.8]. The fundamental frequency converges to a standard deviation of 2.9541MHz. Using a substitution of (6.39) into (6.28), the analytic approximation of this standard deviation is 2.9426MHz. The DST for the same experiment in 2D-TLM involves using the derivative in (6.27). This gives a standard deviation of 2.94304 MHz which is very close to the closed form result. The difference between the DST and the closed form approximations is the manner in which sensitivity is calculated. The comparison between both techniques is shown in Fig. 6-6 for different central relative permittivity values but the same standard deviation of 0.05. The speed of propagating fields would decrease with increasing relative permittivity. Therefore, the approximate variance from (6.28) of the field must also decrease as seen in Fig. 6-6. For a problem with N_{RV} random variables, the DST approach requires N_{RV} + 1 simulations to obtain results which are considerably less than the number required by the MC method. Each simulation for both approaches takes about 2s on a PC with a AMD Athlon 2.01GHz processor.

The effect of increasing standard deviation on the accuracy of both the DST and analytical methods is also studied. The same parameters from the previous paragraphs are retained with $\sigma_{\varepsilon r}$ the only changing variable. The converged MC simulations take 100,000 repeated runs. From the results obtained, the agreement between the MC and the first order approximation methods degrades with increasing standard deviation. This is shown in Fig. 6-7.
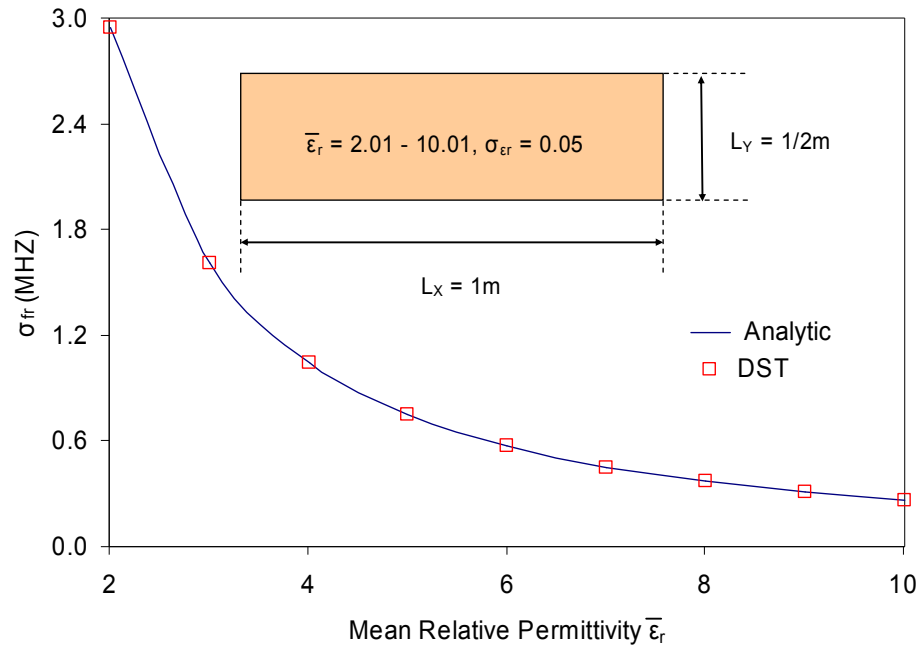
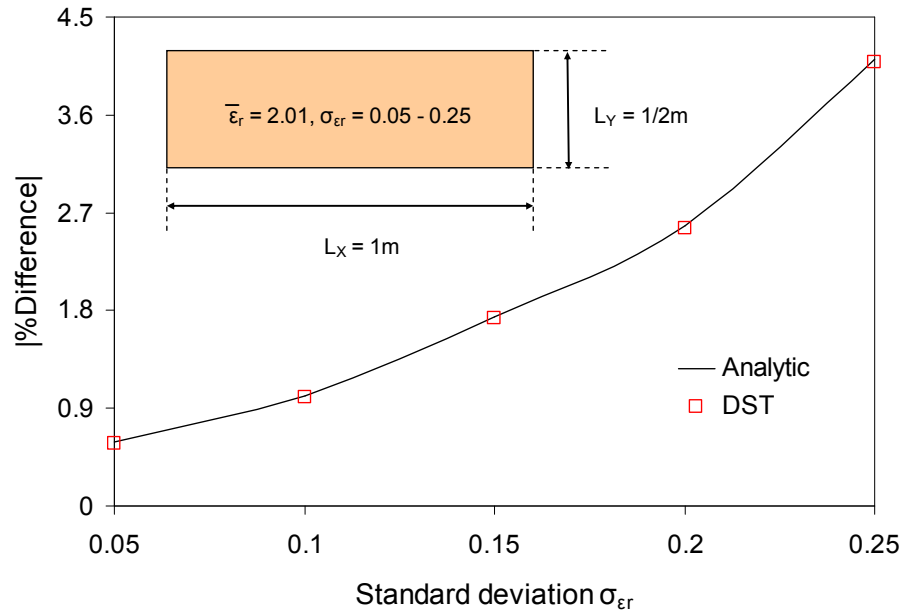**Fig. 6-6 Comparison between the analytic and DST approximation methods for homogeneous resonators**

Fig. 6-7 Percentage difference between the converged MC simulations and approximation methods

6.4.2 Resonances in Structures with Normally Distributed Inhomogeneous Random Dielectrics

Numerical modelling has been seen to be a suitable way for the deterministic modelling of inhomogenously filled waveguides [6.9]. One reason for this is the drawback in the analytic approach which involves solving transcendental equation [6.5], and consequently contriving an expression for $df_r/d\varepsilon_r$ is difficult or impossible to handle. The DST approach used for TLM has a unique way of navigating this obstacle by providing sensitivity parameters in terms of known connection and scatter matrices.

The dielectric slab with rectangular cross section, illustrated in Fig. 6-8A, does not yield closed form results even from a deterministic viewpoint [6.5]. However, the proximity between the analytic and DST methods for the homogeneous case gives the confidence to apply the latter in this section. The dimensions of the partially-filled resonator and the position of the slab are also provided. The central slab is stochastic with a normal distribution of mean relative permittivity of 2.01 with increasing standard deviation values. The surrounding medium is not a random variable with relative permittivity ε_{r1} of 1.01. The results show that applying the DST in a TLM modelling environment yields satisfactory results when compared with the MC technique. Intuitively, as seen in Fig. 6-8A, the changes in $\sigma_{\varepsilon r2}$ affect the standard deviation of fundamental resonance σ_{fr}. The percentage difference between the DST and MC approximations of σ_{fr} increases with the variability of the problem as shown in Fig. 6-8B.
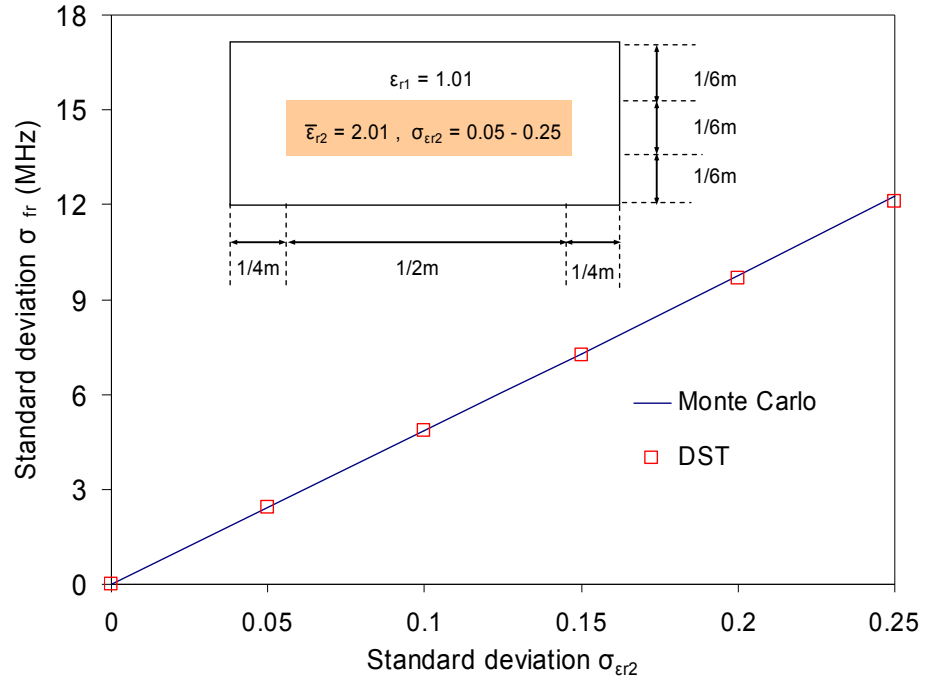
Fig. 6-8A Comparison between the DST and MC approximation methods for a floating dielectric slab in a resonator
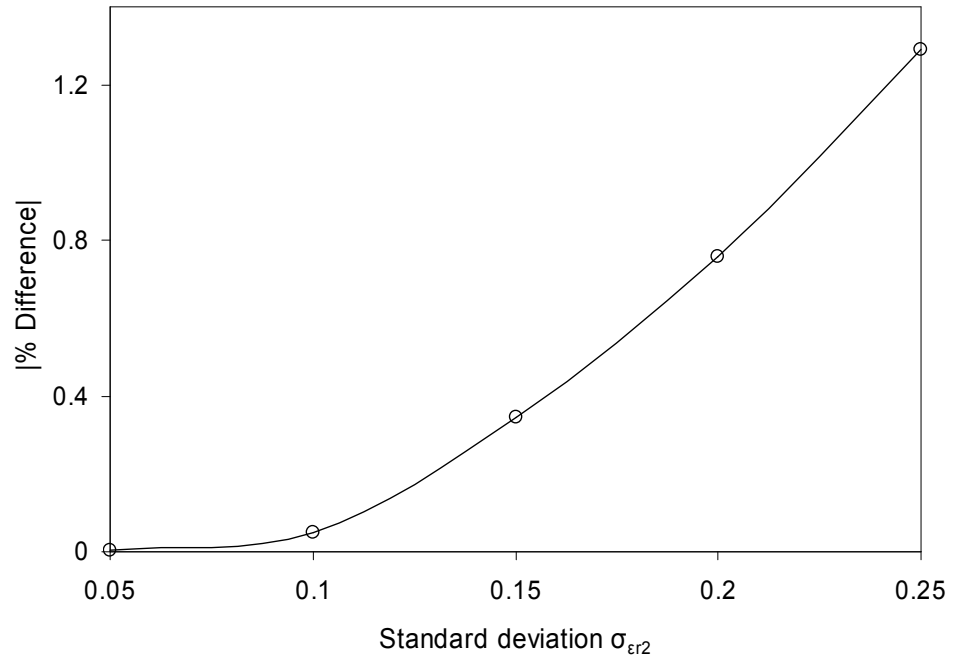
Fig. 6-8B Percentage difference between the converged MC simulations and DST methods for the structure shown in Fig. 6-8A

The DST can be applied to situations where N_{RV} is greater than one. For the problem defined in Fig. 6-9A, the number of random dielectric variables in the resonator is increased. The geometry of the dielectric materials and their respective positions are also shown. The four slabs are uncorrelated materials 1, 2, 3 and 4 that have the same central relative permittivity, of 2.01, and standard deviation $\sigma_{\varepsilon r}$. The central surrounding medium is deterministic and retains the relative permittivity ε_{r1} of 1.01.

The relationship between the standard deviation of relative permittivity and fundamental resonance is shown in Fig. 6-9A. For the DST approach, the independent sensitivity of all the slabs is taken into account when calculating the output frequency variance. The percentage difference between the DST and MC methods is presented in Fig. 6-9B. As with the other results, there is a growing discrepancy between both approaches with rising input variability.
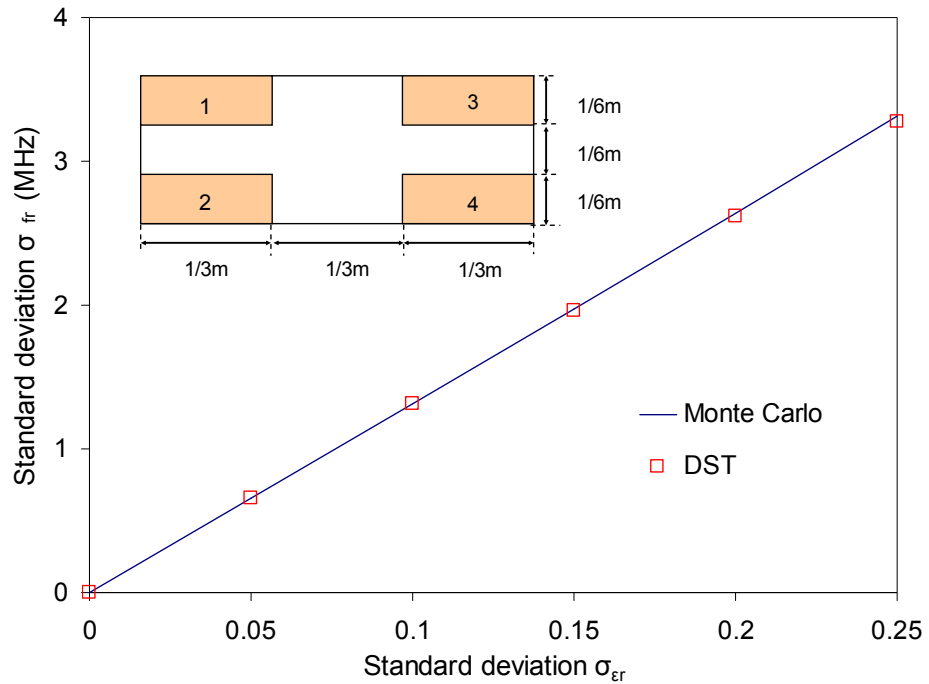
**Fig. 6-9A Comparison between the MC and DST approximation methods for a four dielectric slabs with rectangular cross-section**
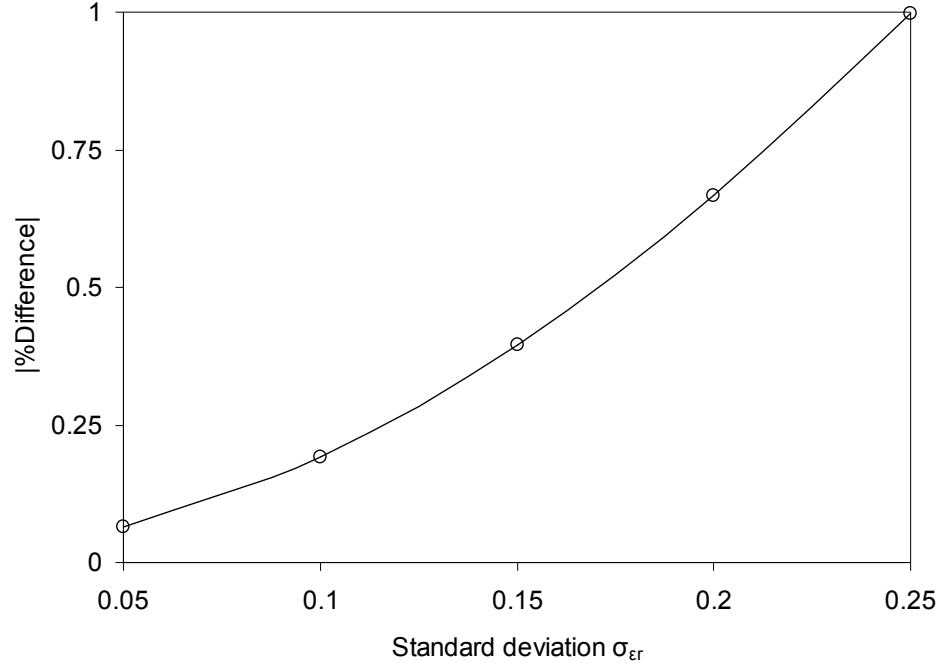
Fig. 6-9B Percentage difference between the converged MC simulations and DST methods for the structure shown in Fig. 6-9A

In the examples just considered, the materials are assumed to be piecewise homogeneous. However, in a practical inhomogeneous case caused by non-uniform fabrication, it is apparent that samples of the same piece of material are no longer independent and similar observations can be made regarding surface roughness and boundary placements. Such cases require that the statistical variations of two or more problem parameters are dependent, necessitating the introduction of covariances in the analysis presented above.

A convenient normalised measure of the dependence of two parameters is provided by the correlation coefficient. This can be readily used to extend the DST approach to treat the case of dependent statistical parameters. For the example in Fig. 6-10A, the correlation coefficient ρ_{13} between the two dielectric materials, with relative permittivity ε_{r1} and ε_{r3} is:

$$\rho_{13} = \frac{\sigma_{\varepsilon_{r13}}}{\sigma_{\varepsilon_{r1}}\sigma_{\varepsilon_{r3}}} \tag{6.40}$$

where $\sigma_{\varepsilon r13}$ is the covariance between them and $-1 \leq \rho_{13} \leq 1$. Correlation can be included in, for example, by generalising (6.28) to give [6.6]:

$$\sigma_f \cong \sqrt{\sigma^2_{\varepsilon r1}\left(\frac{df_r}{d\varepsilon_{r1}}\right)^2 + 2\left(\frac{df_r}{d\varepsilon_{r1}}\right)\left(\frac{df_r}{d\varepsilon_{r3}}\right)\left(\rho_{13}\,\sigma_{\varepsilon r1}\sigma_{\varepsilon r3}\right) + \sigma^2_{\varepsilon r3}\left(\frac{df_r}{d\varepsilon_{r3}}\right)^2} \qquad (6.41)$$

Fig. 6-10B shows the percentage difference between converged MC simulations and the DST approach as the correlation coefficient between the two discrete dielectric materials is varied. From the results, the discrepancy is minimum when both variables are uncorrelated, that is when $\rho_{13} = 0$, and remains acceptably low across the complete range of correlations. The general efficiency of this approach is illustrated by the fact that the maximum difference for the example in Fig. 6-10A is not more than 0.22% for the different degrees of statistical dependency considered.
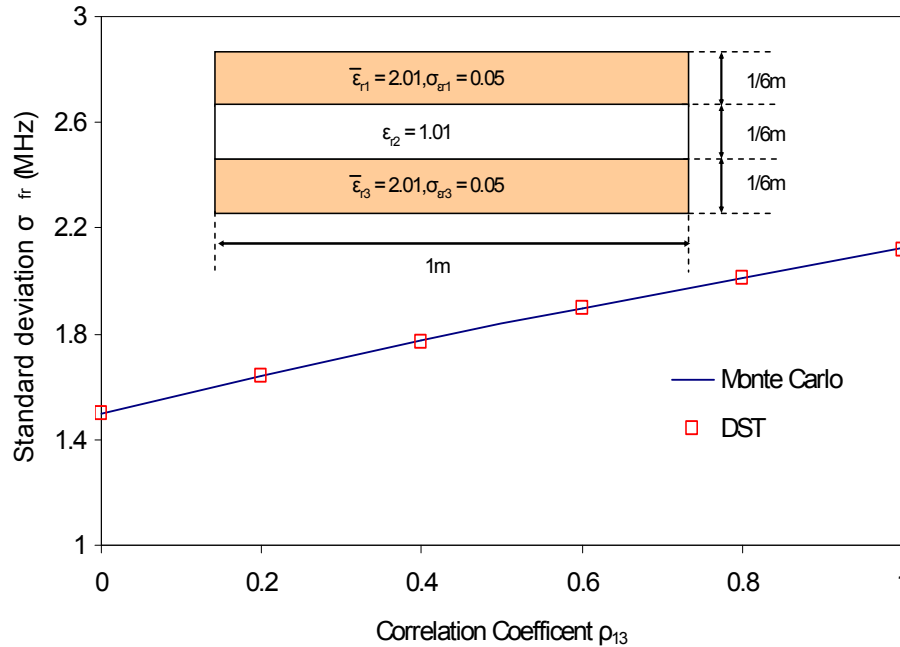
**Fig. 6-10A Effect of statistical dependency of two dielectric slabs using the correlation coefficient between them**
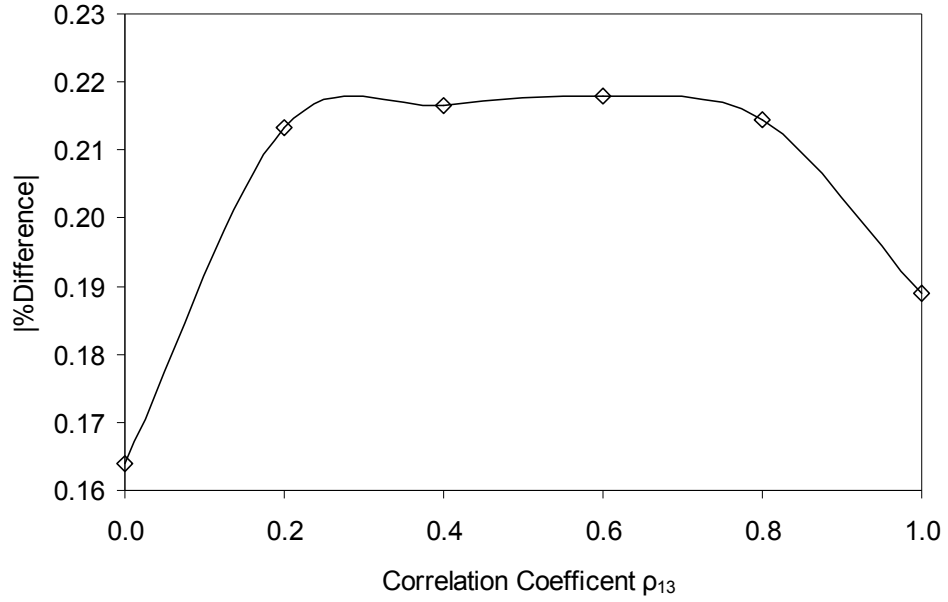
Fig. 6-10B Percentage difference between the converged MC simulations and DST methods for the structure shown in Fig. 6-10A

Consideration of continuously spatial variations in material parameters requires some care, if convergence with mesh density is to be observed. Quantification of the correlation of, for example, the relative permittivity at different spatial locations, can proceed from the autocorrelation function given in (4.12). The structure in Fig. 6-11A models a single dielectric material, sampled at eight points as eight uniform layers of correlated relative permittivity values generated using (4.13) with $L_c = 0.125$m and $\varepsilon_{RMS} = 0.05$. The slabs have a combined mean relative permittivity of 2.01 and the same standard deviation. Fig. 6-11B shows the percentage difference between converged MC simulations and the DST approach.
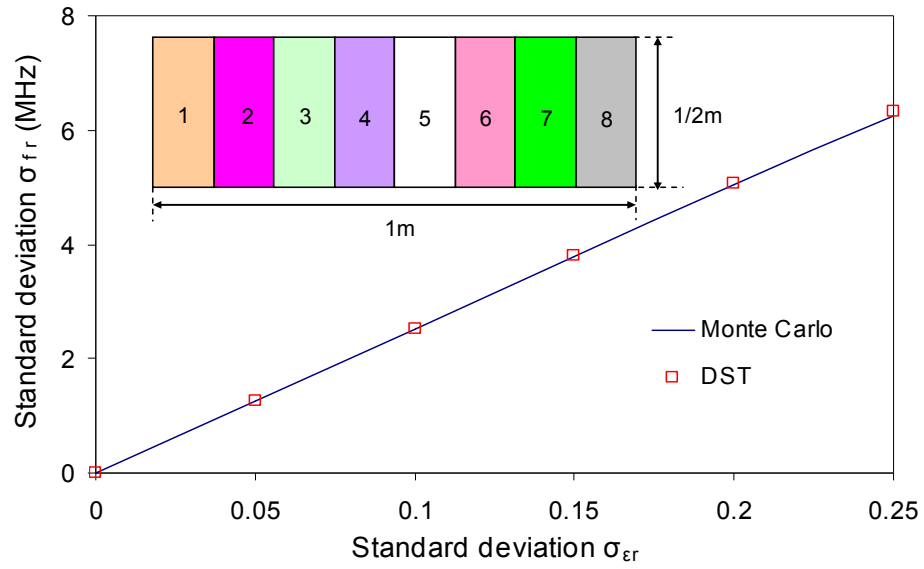
Fig. 6-11A Eight correlated dielectric slabs modelling a single dielectric block as eight layers with correlated relative permittivities

Fig. 6-11B Percentage difference between the converged MC simulations and DST methods for the structure shown in Fig. 6-11A

6.4.3 Resonances in Structures with Normally Distributed Stochastic Boundaries

The exact position of boundaries allows for accurate modelling of waveguide problems. This is difficult to attain in cases where dimensions of structure under analysis is not a multiple of the mesh size. The method proposed in [6.10] addresses this constraint by allowing for boundaries to be adjusted in infinitesimal dimensions compared with overall size of the structure. The modelling advantage of this approach is that there is a simple modification to the scatter matrix and no alteration to the connect matrix. Fig. 6-12 illustrates a resonator that has a highlighted movable boundary.
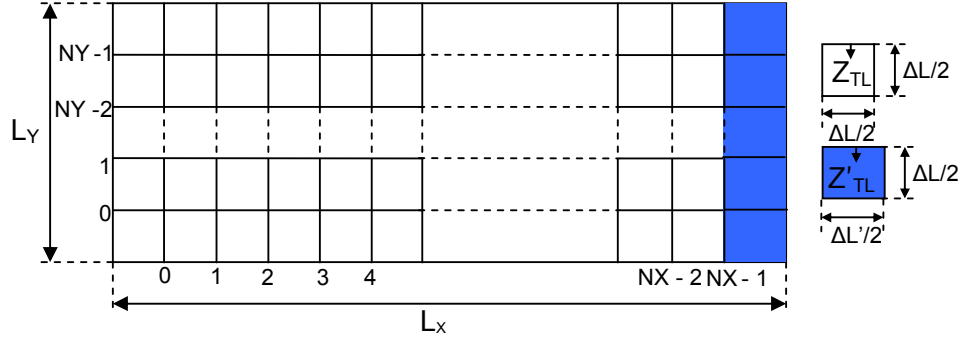
Fig. 6-12 Resonator with an infinitesimally adjustable boundary

Let ΔL be the size of the mesh in the problem space away from the adjustable boundary. This is related to the height of the resonator L_Y by the expression:

$$L_Y = \Delta L.NY \tag{6.42}$$

A variation parameter α is introduced consistent with the physics of the problem. This is related to the length of the resonator L_X by the expression [6.10]:

$$L_X = (NX - 1)\Delta L + (1 + \alpha)\frac{\Delta L}{2} \tag{6.43}$$

where $0 < \alpha < 2$.

129

The constitutive and geometric parameters of cells at the adjustable boundary are related to those away from it as shown [6.10]:

$$\Delta L' \cong \alpha \Delta L \tag{6.44a}$$

$$Z'_{TL} \cong \alpha Z_{TL} \tag{6.45b}$$

where $\Delta L'$ and Z'_{TL} are the length and characteristic impedance of link lines connecting terminal nodes to the movable boundary respectively.

The corresponding Thevenin equivalent circuit of the adjustable boundary model is shown in Fig. 6-13.
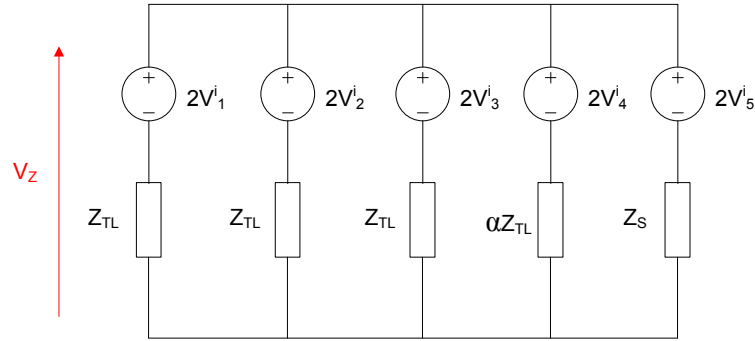
Fig. 6-13 Thevenin equivalent circuit for shunt node connected to an adjustable boundary

The expression of total node voltage V_z from the circuit model in Fig. 6-13 is:

$$V_Z = \frac{2\left(V^i_1 + V^i_2 + V^i_3 + \dfrac{V^i_4}{\alpha}\right) + 2V^i_5 \hat{Y}_S}{3 + \dfrac{1}{\alpha} + \hat{Y}_S} \tag{6.46}$$

The expression of V_z in (6.46) would only affect entries of the scatter sub-matrix of associated with the movable boundary. This is a 5 x 5 matrix as shown:

$$\underline{\underline{S}}_{x,y} = \frac{1}{\hat{Y}_m} \begin{pmatrix} 2-\hat{Y}_m & 2 & 2 & 2 & 2\hat{Y}_S \\ 2 & 2-\hat{Y}_m & 2 & 2 & 2\hat{Y}_S \\ 2 & 2 & 2-\hat{Y}_m & 2 & 2\hat{Y}_S \\ 2 & 2 & 2 & \frac{2}{\alpha}-\hat{Y}_m & 2\hat{Y}_S \\ 2 & 2 & 2 & 2 & 2\hat{Y}_S-\hat{Y}_m \end{pmatrix} \qquad (6.47)$$

where $\hat{Y}_m = 3 + \dfrac{1}{\alpha} + \hat{Y}_S$

In a homogenous resonator with an uncertain boundary, the standard deviation of resonant frequency σ_{fr} can be derived analytically from the standard deviation of sub-nodal variations σ_α:

$$\sigma_{fr} \cong \left| L_X^{-3} \left(\frac{-c\Delta L (\varepsilon_r)^{-0.5}}{4} \right) \left(\left(\frac{1}{L_X} \right)^2 + \left(\frac{1}{L_Y} \right)^2 \right) \right| \sigma_\alpha \qquad (6.48)$$

The DST for moving boundaries simply entails the substitution of ε_r, in section 6.2, with α and the introduction of $\Delta L'$ and Z'_{TL} as appropriate. The comparison between approximation methods is shown in Fig. 6-14A for a mean variation parameter of 0.5 with different standard deviation values. Consistent with results earlier, there is a growing discrepancy between approximation techniques as the standard deviation of α increase. This is illustrated in Fig. 6-14B.

Surface roughness can be achieved by applying (4.12) and (4.13) to the variation parameter α. In Fig. 6-15A, the combined mean of the variation parameters of all six random variables shown is 0.5, $L_c = 0.167$ m and the root mean square of α is 0.05. The example here has ε_r fixed at 2.01. Again, it is apparent that the DST approach provides excellent agreement with the converged MC analysis. Fig. 6-15B shows the percentage difference between converged MC simulations and the DST approach.
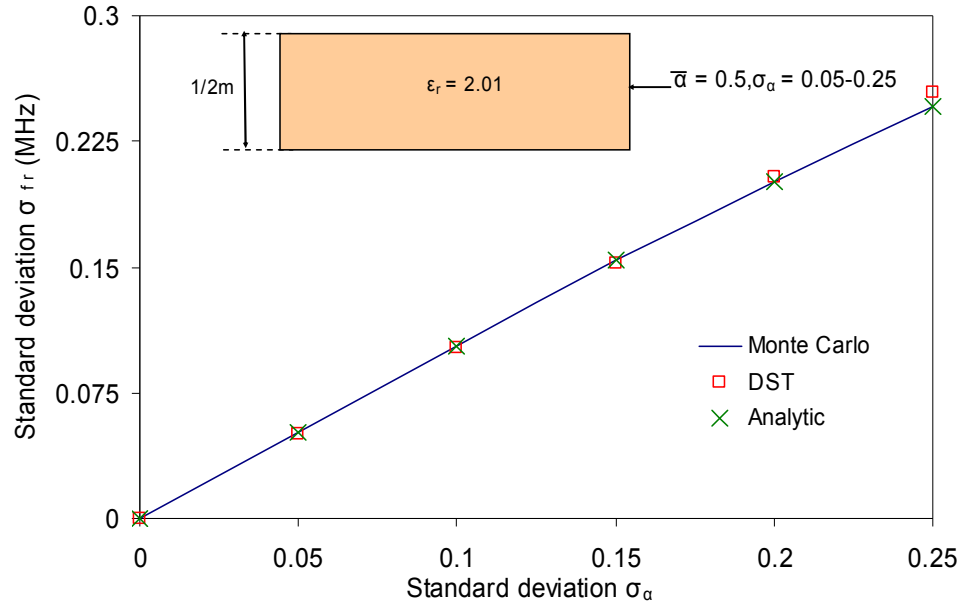
Fig. 6-14A Comparison between the MC, DST and analytic approximation methods for a resonator with movable boundaries.

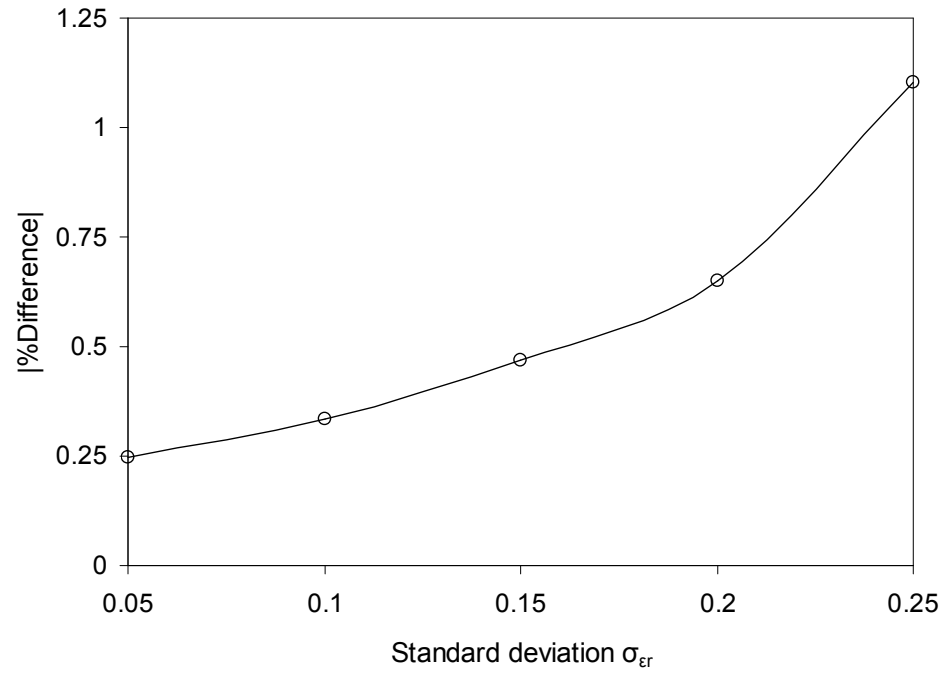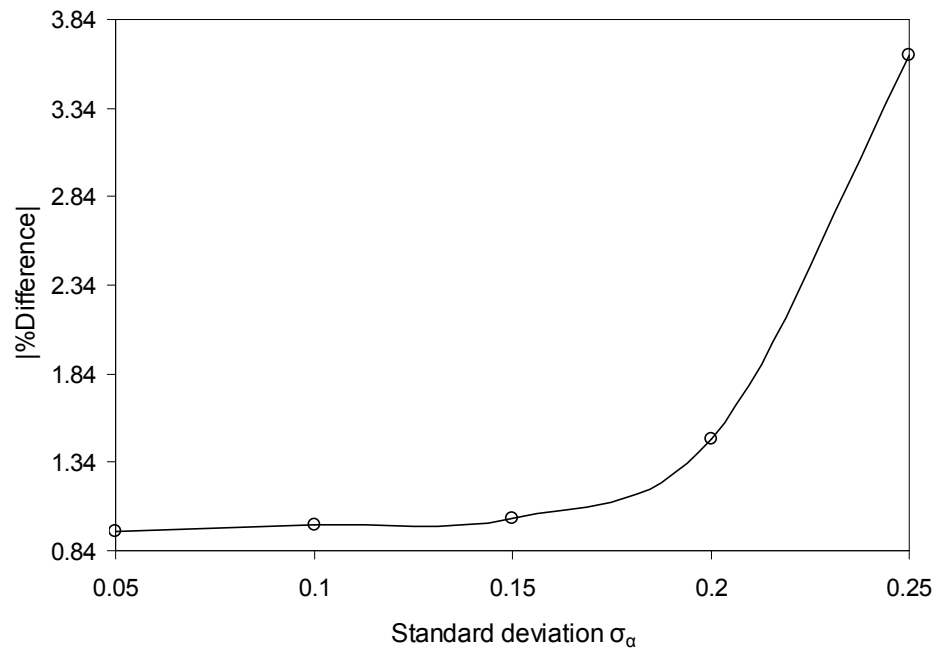**Fig. 6-14B Percentage difference between the converged MC simulations and DST methods for the structure shown in Fig. 6-14A.**
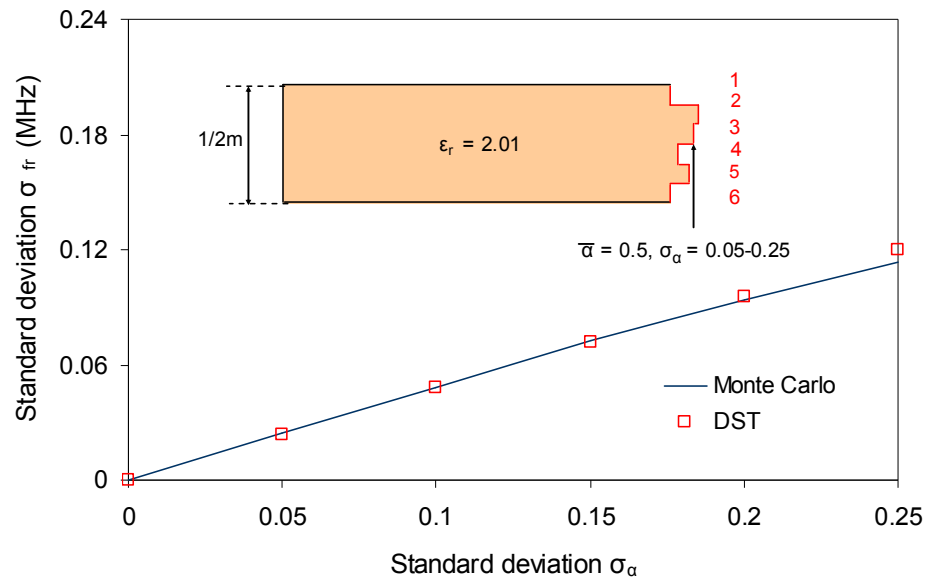
Fig. 6-15A An approximation of surface roughness using six correlated variation parameters
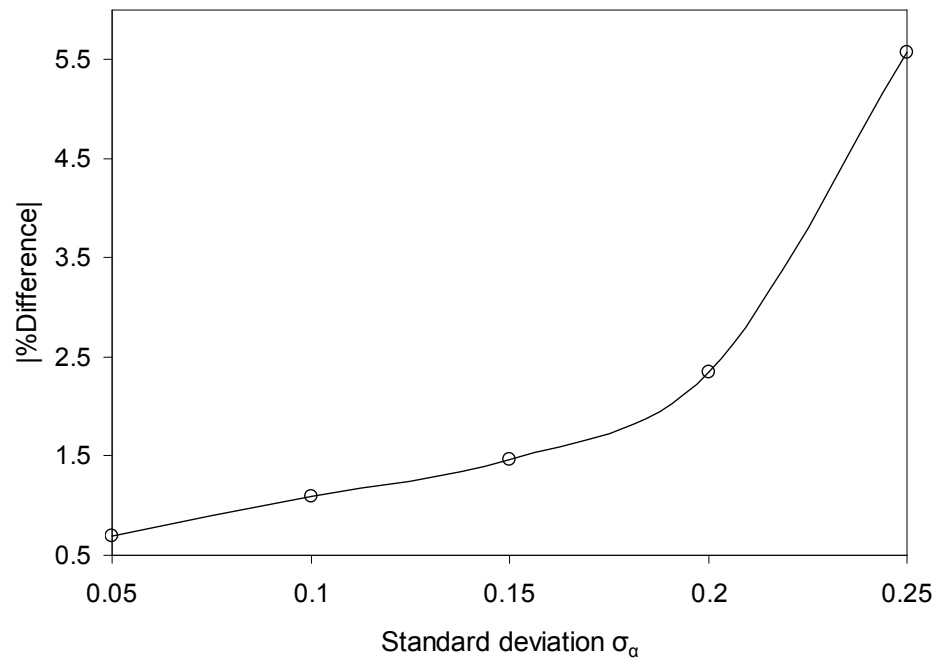
Fig. 6-15B Percentage difference between the converged MC simulations and DST methods for the structure shown in Fig. 6-15A

6.4.4 Wires with Stochastic Radius in Deterministic Medium with Absorbing Boundaries

One of the most important aspects of the EMC design process is the ability to accurately measure the shielding effectiveness (SE) of an enclosure. This is to ensure that unwanted interference is restricted to avoid disturbing the performance of equipment under test. The calculation of SE has to take variability into account to predict its performance in cases where the structure under analysis has non-deterministic features. As described in the section 6.3, an approximation paradigm such as the DST is suitable for this type of case study.

The TLM model of a wire node is shown in Fig. 6-16. This was obtained by mapping the analytic field behaviour of a thin wire onto the numerical model. Complete derivation and validation of the thin wire model can be found in [6.11]. In this sub-section, a set of wires with stochastic radii are arranged in enclosure with deterministic boundaries as shown later. The wires formulate a screen and the variability on SE is assessed in the presence of a plane wave illumination.
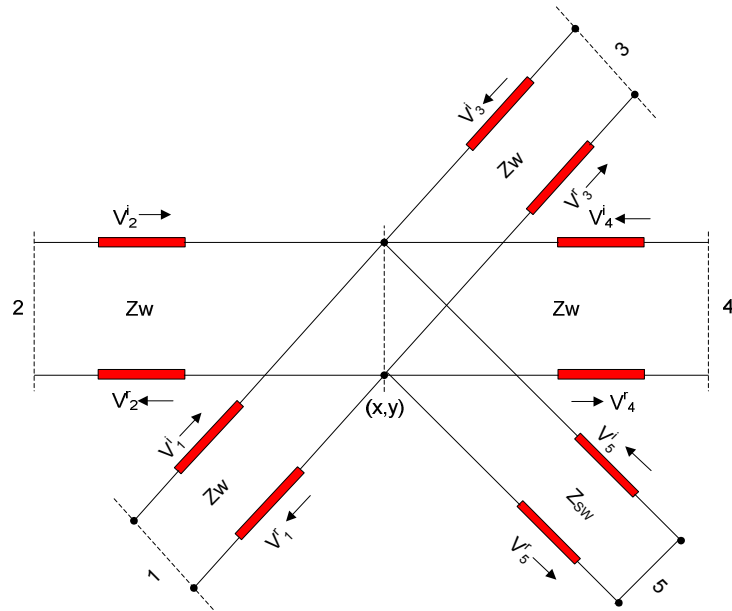
Fig. 6-16 Discrete TLM model of wire shunt node

The relationship between the link line impedance Z_w of a node with a thin wire to that of the surrounding medium Z_{TL} is given by [6.11]:

$$Z_w = Z_{TL}\left(\frac{\Delta^2 - r^2}{\Delta^2 + r^2}\right) \tag{6.49}$$

where Δ is the cell radius, that is $\Delta L/2$, and r is the wire radius.

The stub impedance of the wire model Z_{sw} has a short circuit termination with incident and reflected voltages following the relation in (6.17). Z_{sw} is related to Z_{TL} via the expression [6.11]:

$$Z_{sw} = \frac{Z_{TL}}{4}\ln\left(\frac{\Delta}{r}\right) \tag{6.50}$$

The scatter sub-matrix of the wire node is given by:

$$\underline{\underline{S}}_{x,y} = \frac{1}{\hat{Y}}\begin{vmatrix} 2-\hat{Y}_w & 2 & 2 & 2 & 2\hat{Y}_{sw} \\ 2 & 2-\hat{Y}_w & 2 & 2 & 2\hat{Y}_{sw} \\ 2 & 2 & 2-\hat{Y}_w & 2 & 2\hat{Y}_{sw} \\ 2 & 2 & 2 & 2-\hat{Y}_w & 2\hat{Y}_{sw} \\ 2 & 2 & 2 & 2 & 2\hat{Y}_{sw}-\hat{Y}_w \end{vmatrix} \tag{6.51}$$

where $\hat{Y}_w = 4 + \hat{Y}_{sw}$ and $\hat{Y}_{sw} = \dfrac{4Z_w}{Z_{sw}}$.

The connection matrix has to be modified to illustrate the mismatch in impedance between the wire and the surrounding medium. The discrete TLM model depicting connection between horizontal link lines is shown in Fig. 6-17A. The corresponding Thevenin equivalent circuit is provided in Fig. 6-17B.
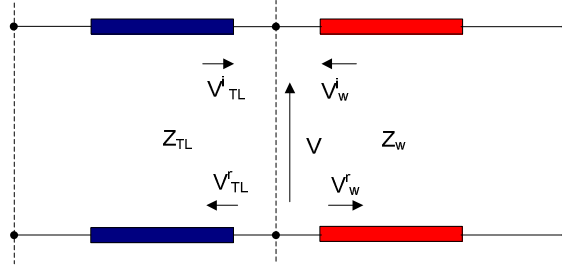
Fig. 6-17A Connection between the link lines of wire (right) and surrounding medium (left)
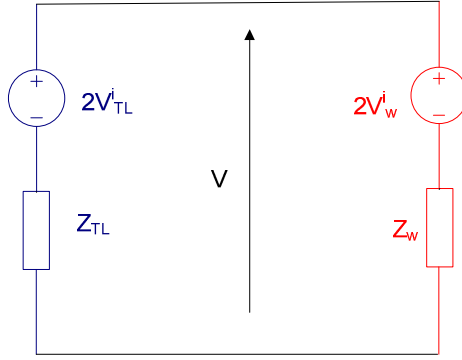
Fig. 6-17B Thevenin equivalent circuit for connection between wire and surrounding medium

The total voltage V in Fig. 6-17B is:

$$V = \left(\frac{2V^i_{TL}}{Z_{TL}} + \frac{2V^i_w}{Z_w} \right) \left(\frac{1}{Z_{TL}} + \frac{1}{Z_w} \right)^{-1} \tag{6.52}$$

where V^i_{TL} and V^i_w are the incident voltages to the medium and wire nodes respectively.

The reflected voltages from the medium and wire can be found from the difference between the total voltage and respective incident voltages:

$$V^r_{TL} = \frac{2V^i_w Z_{TL} - (Z_{TL} - Z_w)}{Z_{TL} + Z_w} \tag{6.53a}$$

$$V^r_w = \frac{2V^i_{TL} Z_w - 2(Z_{TL} - Z_w)}{Z_{TL} + Z_w} \tag{6.53b}$$

where V^r_{TL} and V^r_w are the reflected voltages to the medium and wire nodes respectively.

From (6.53a) and (6.53b), it is clear that the reflected voltages depend on Z_w which is a function of r. This implies that the connection matrix must also have entries relating wire and medium quantities which are functions of r. Therefore, the DST for wires with stochastic radii, as derived in section 6.3, take account of this property.

The structure in Fig. 6-18 comprises four wires suspended in free space with vertical absorbing walls and horizontal reflecting walls. The absorbing walls have a reflection coefficient is the ratio of $1 - \sqrt{2}$ to $1 + \sqrt{2}$ [6.1]. The problem space here is discretised with $NX = 23$ and $NY = 11$. The cell size ΔL for this problem is $\frac{1}{23}$ m. The dimensions of the wires, their position and the size of the surrounding structure are shown in Fig. 6-18. The mean radius of each wire is 0.125. The excitation of amplitude 1V is made at all the ports of the nodes located at $2\Delta L$ from the left absorbing wall. The wires would act as a partial shield and the spaces between them are effectively apertures through which fields penetrate. An observation point is defined at $6\Delta L$ from the bottom reflecting wall and $7\Delta L$ from the right absorbing wall.
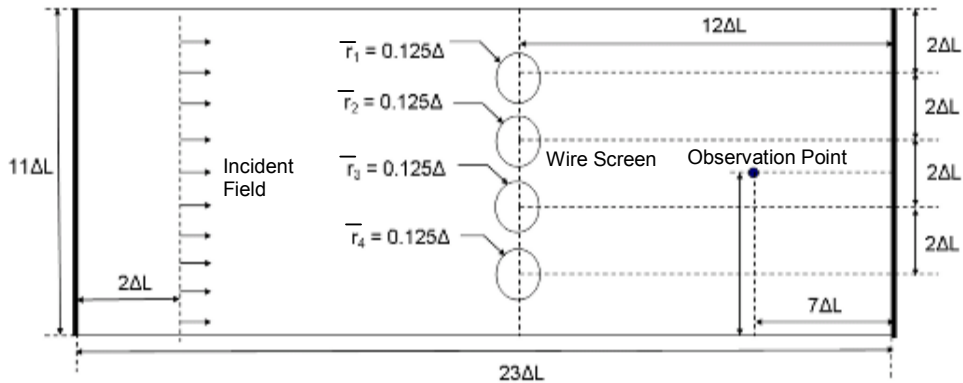
Fig. 6-18 Wires suspended in a free space medium with vertical absorbing and horizontal reflecting walls

The coefficient of variation (the ratio of the standard deviation to the mean) of each wire radius is fixed at 0.05. The MC method involves the application for nominal design to a large number of randomly perturbed radii values of each

wire. For the purposes here, a total of 20,000 runs per wire radius are performed to assess the field behaviour against increasing frequency. The results are compared then with the DST. The analysis is confined to the lower frequency range to as dispersion affects analysis at the higher end of the spectrum.

The mean total voltage (related to electric field) at observation point in Fig. 6.18 can be found using (6.38). Fig. 6-19A shows how the real part of expected voltage relates with frequency for the MC and DST methods. Fig. 6-19B illustrates how the imaginary part of expected voltage relates with increasing frequency both methods. The standard deviation of total voltage at the observation point can be approximated using (6.34). Fig. 6-19C shows how the standard deviation, approximated from statistical methods, of observed voltage changes with increasing frequency values. All these results show how applicable the DST is to situations of different boundary conditions. This is a good alternative that uses the derivatives to each random variable which is cheaper to compute across the frequency band considered here. The favourable comparison with the benchmark MC method validates the results. Further investigation on the statistical behaviour the SE using both techniques can now be confidently implemented.
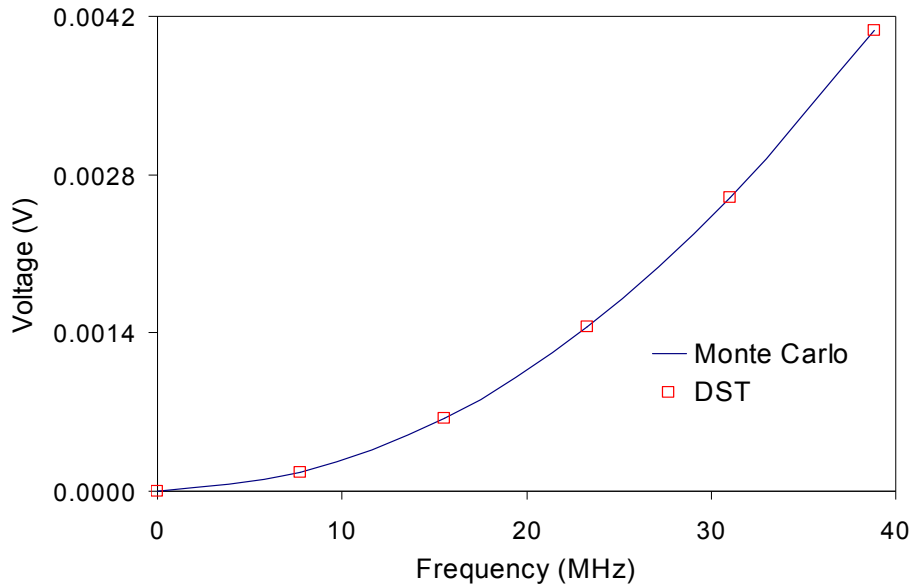
Fig. 6-19A Relationship between real part of expected voltage and frequency
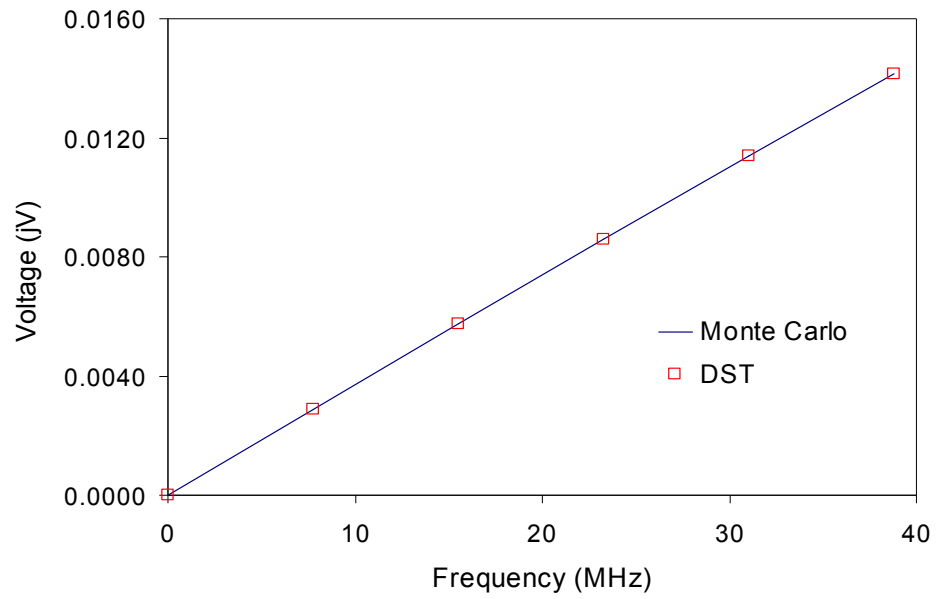
Fig. 6-19B Relationship between imaginary part of expected voltage and frequency
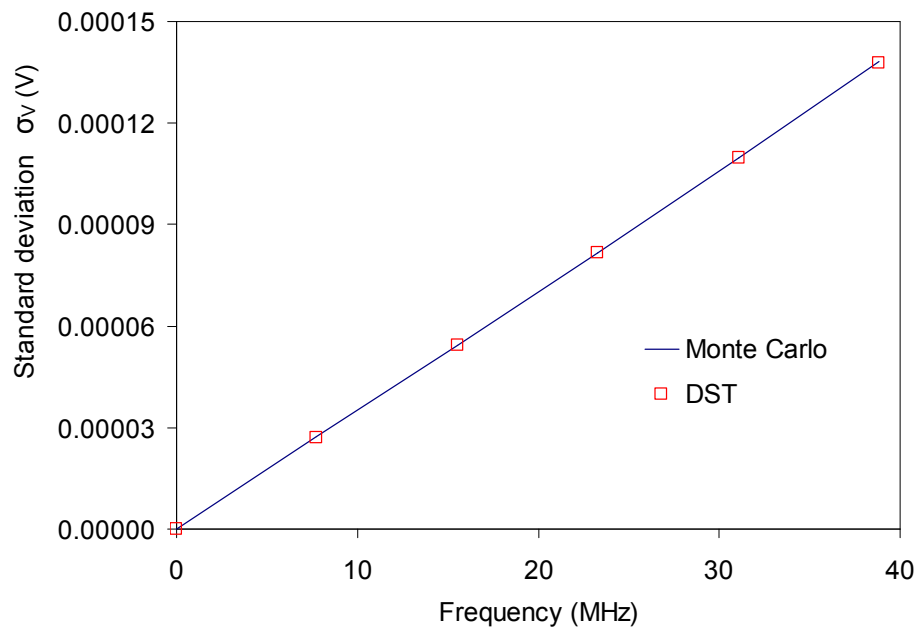
Fig. 6-19C Relationship between standard deviation of voltage and frequency

The SE of the wire structure in an enclosure shown in Fig. 6-18 is:

$$SE = 20 \, log \frac{\left|V_{ref}\right|}{\left|V\right|} \tag{6.54}$$

where V_{ref} and V are the total voltages at the observation point with the wires absent and present respectively.

The first order average shielding effectiveness $\overline{SE}$ is:

$$\overline{SE} \cong 20 \, log \frac{\left|V_{ref}\right|}{\left|\overline{V}\right|} \tag{6.55}$$

where $\overline{V}$ is the mean total voltage at observation point. Both MC and DST approximations of $\overline{SE}$ are compared for a range of frequencies as shown in Fig. 6-20A. The percentage difference between both methods is about 0.0027%.
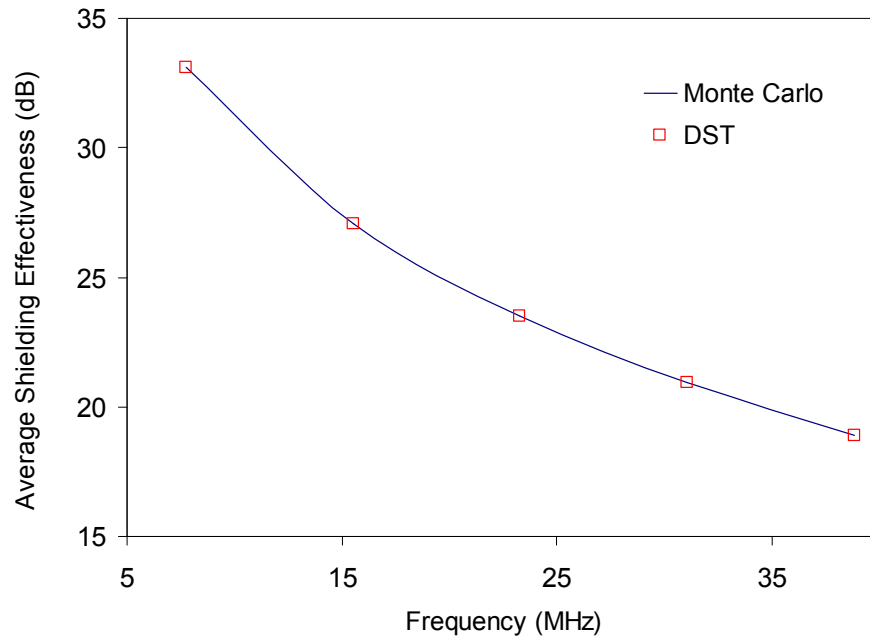
Fig. 6-20A Relationship between expected shielding effectiveness and frequency

The first order standard deviation of shielding effectiveness is σ_{SE}:

$$\sigma_{SE} \cong \sigma_V \left| \frac{\partial SE}{\partial V} \right|_{V=\bar{V}} = \frac{20}{ln\,10} \frac{\sigma_V}{\left| \bar{V} \right|} \tag{6.56}$$

where σ_V is the standard deviation of total voltage at observation point shown in Fig. 6-18. From (6.56) it is seen that σ_{SE} has a dependency on the coefficient of variation of total voltage. The standard deviation σ_{SE} is approximated using both approximations of σ_V from MC and DST as shown in Fig. 6-20B. The percentage difference between both methods is about 0.023%.
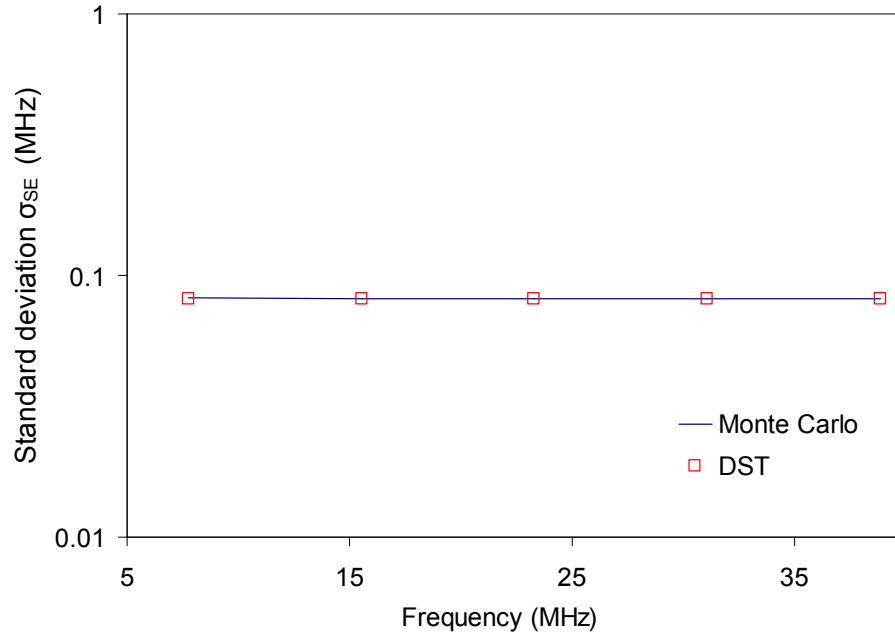
Fig. 6-20B Relationship between standard deviation of shielding effectiveness and frequency

6.4.5 Impact of Higher Order Derivatives on the DST Approach

In the previous sub-sections, the DST was applied using the first and second order derivatives to approximate the mean and standard deviation of random parameters of interest. This technique can be improved via consideration of higher order sensitivity values although this involves additional solutions of the

global FDTLM matrix equations. This can be particularly expensive when iterative methods are adopted for waveguide problems [6.12]. However, although this could be prohibitive, it is useful for approximating higher order statistical moments. This sub-section entails an iterative algorithm to compute higher order derivatives of random variables about nominal values. The effect of this on the approximation of statistical moments and the choice of random variable distribution are discussed.

Higher order DST approximations to waveguide problems are based on the steps below:

STEP 1: Differentiate both sides of (6.23) with respect to the ε_r random variable:

$$\underline{\underline{C}} \cdot \frac{d^2 \underline{\underline{S}}}{d\varepsilon_r^2} \cdot \underline{V}^i + 2\underline{\underline{C}} \cdot \frac{d\underline{\underline{S}}}{d\varepsilon_r} \cdot \frac{d\underline{V}^i}{d\varepsilon_r} + \underline{\underline{C}} \cdot \underline{\underline{S}} \cdot \frac{d^2 \underline{V}^i}{d\varepsilon_r^2}$$
$$= \frac{d^2}{d\varepsilon_r^2} e^{j\omega\Delta t} \underline{V}^i + 2\frac{de^{j\omega\Delta t}}{d\varepsilon_r} \cdot \frac{d\underline{V}^i}{d\varepsilon_r} + e^{j\omega\Delta t} \frac{d^2 \underline{V}^i}{d\varepsilon_r^2} \tag{6.57}$$

STEP 2: The equation (6.57) can be readily extended to the nth derivative:

$$\sum_{m=0}^{n} \binom{n}{m} \underline{\underline{C}} \cdot \frac{d^{n-m} \underline{\underline{S}}}{d\varepsilon_r^{n-m}} \cdot \frac{d^m \underline{V}^i}{d\varepsilon_r^m} = \sum_{m=0}^{n} \binom{n}{m} \frac{d^{n-m} e^{j\omega\Delta t}}{d\varepsilon_r^{n-m}} \cdot \frac{d^m \underline{V}^i}{d\varepsilon_r^m} \tag{6.58}$$

STEP 3: Pre-multiply both sides of (6.57) with the transpose of the eigenvector $\underline{U}^i$:

$$\underline{U}^{iT} \cdot \left(\underline{\underline{C}} \cdot \frac{d^2 \underline{\underline{S}}}{d\varepsilon_r^2} \cdot \underline{V}^i + 2\underline{\underline{C}} \cdot \frac{d\underline{\underline{S}}}{d\varepsilon_r} \cdot \frac{d\underline{V}^i}{d\varepsilon_r} \right)$$
$$= \underline{U}^{iT} \cdot \left(\frac{d^2}{d\varepsilon_r^2} e^{j\omega\Delta t} \underline{V}^i + 2\frac{de^{j\omega\Delta t}}{d\varepsilon_r} \frac{d\underline{V}^i}{d\varepsilon_r} \right) \tag{6.59}$$

STEP 4: The equation (6.59) can also be readily extended to the nth derivative:

$$\sum_{m=0}^{n} \binom{n}{m} \underline{U}^{iT} \cdot \left(\underline{\underline{C}} \cdot \frac{d^{n-m}\underline{\underline{S}}}{d\varepsilon_r^{n-m}} \cdot \frac{d^m \underline{V}^i}{d\varepsilon_r^m} \right)$$
$$= \sum_{m=0}^{n} \binom{n}{m} \underline{U}^{iT} \cdot \left(\frac{d^{n-m} e^{j\omega\Delta t}}{d\varepsilon_r^{n-m}} \frac{d^m \underline{V}^i}{d\varepsilon_r^m} \right) \tag{6.60}$$

It is important to note that when $m = n$, both sides of (6.60) would cancel each other out.

STEP 5: The second derivative of $e^{j\omega\Delta t}$ with respect to ε_r is:

$$\frac{d^2 e^{j\omega\Delta t}}{d\varepsilon_r^2} = \left(j2\Delta t \right) \left(\frac{d^2 f}{d\varepsilon_r^2} e^{j\omega\Delta t} + \frac{df}{d\varepsilon_r} \frac{de^{j\omega\Delta t}}{d\varepsilon_r} \right) \tag{6.61}$$

STEP 6: In general, the nth derivative of $e^{j\omega\Delta t}$:

$$\frac{d^n e^{j\omega\Delta t}}{d\varepsilon_r^n} = \left(j2\Delta t \right) \sum_{m=0}^{n-1} \binom{n-1}{m} \left(\frac{d^{n-m} f}{d\varepsilon_r^{n-m}} \frac{d^m e^{j\omega\Delta t}}{d\varepsilon_r^m} \right) \tag{6.62}$$

From (6.62), it is possible to find the nth derivative of f_r with respect to ε_r . This is useful in deriving higher order approximations and is shown in Appendix A.

The impact of higher order derivatives is demonstrated here using the dielectric slab with rectangular cross section in Fig. 6-8A. The third order terms are not included for normal distributions as all odd moments are zero in this case. The fourth order DST approximation of the mean is seen in (A.8) in Appendix A. The percentage difference between the results obtained for the mean fundamental resonance and the MC method is shown in Fig. 6-21A. It is observed that the discrepancy between both methods as $\sigma_{\varepsilon r2}$ increases is most apparent when the first order estimation is used. The second and fourth order methods significantly reduce this effect as more terms are considered from (A.8). There is no considerable difference between the second and fourth order results. Due to the computational expense required to go from second order derivatives to fourth order, it is recommended that for this scenario the second order technique should

143

be sufficient. The fourth order DST approximation of standard deviation σ_{fr} can be found from (A.23). As with the values for the mean, the higher order terms have better agreement with the converged MC methods. Fig. 6-21B shows the percentage difference between DST and MC methods as the order increases. The third and fourth order contributions do not have any noticeable differences between the results. This would imply that the third order approximation should be more computationally cost effective.
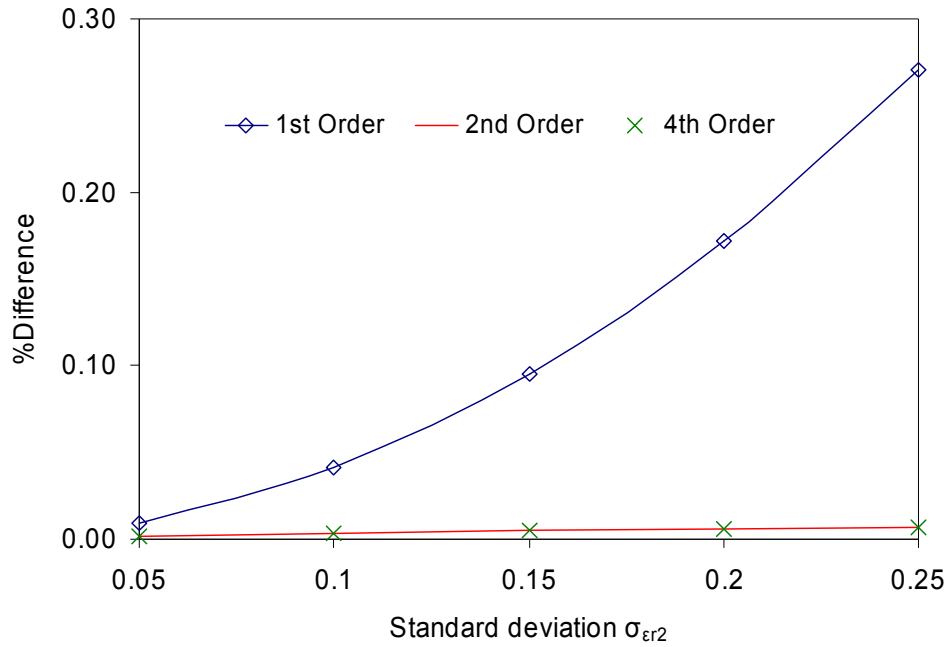
Fig. 6-21A Impact of higher order derivatives on the DST approximation of the average fundamental resonance of the structure in Fig. 6-8A
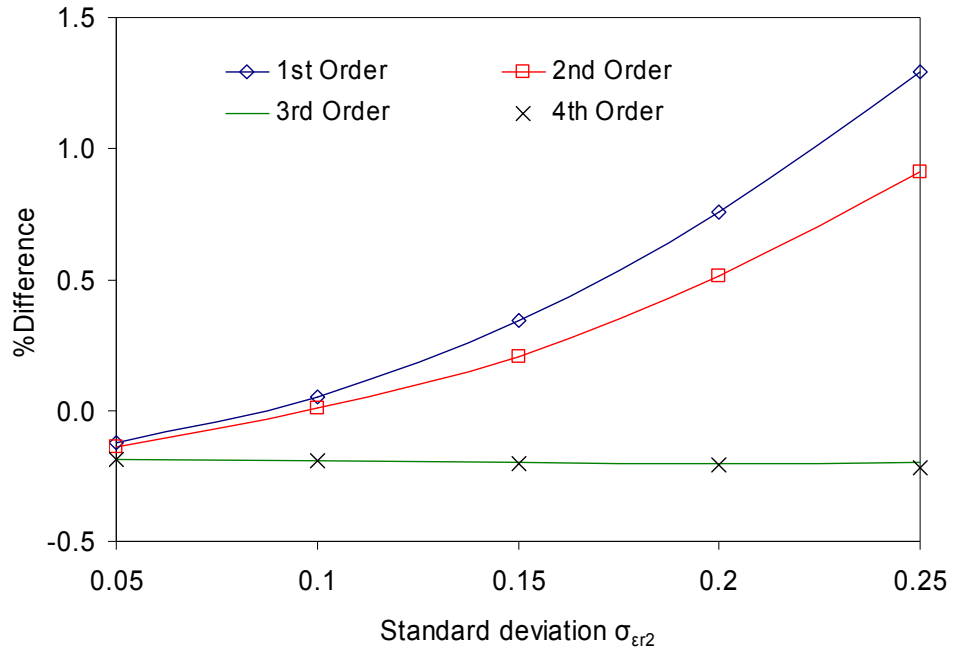
Fig. 6-21B Impact of higher order derivatives on the DST approximation of the standard deviation of fundamental resonance of the structure in Fig. 6-8A

The higher order derivatives are also useful in producing better approximations of higher order moments such as the skew and kurtosis of a distribution as shown in Fig. 6-21C and Fig. 6-21D respectively.

The DST approximation of the skew is found from (A.29) in Appendix A. From the results shown in Fig. 6-21C, the fourth order contributions provide the best agreement with the MC method. The same applies for the kurtosis, shown in Fig 6-21D which is found from (A.33) in Appendix A.
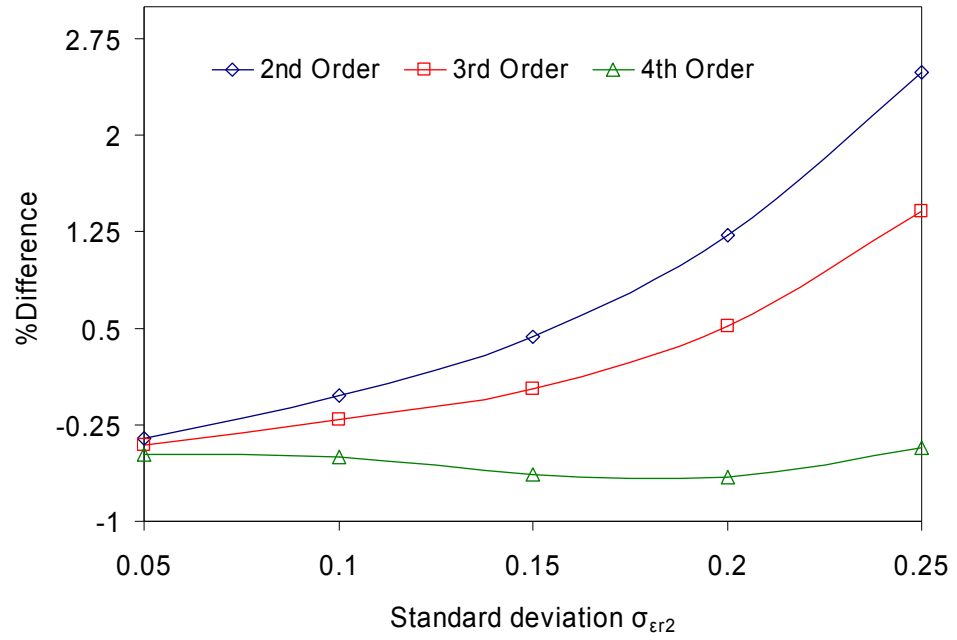
Fig. 6-21C Impact of higher order derivatives on the DST approximation of the skew of fundamental resonance of the structure in Fig. 6-8A
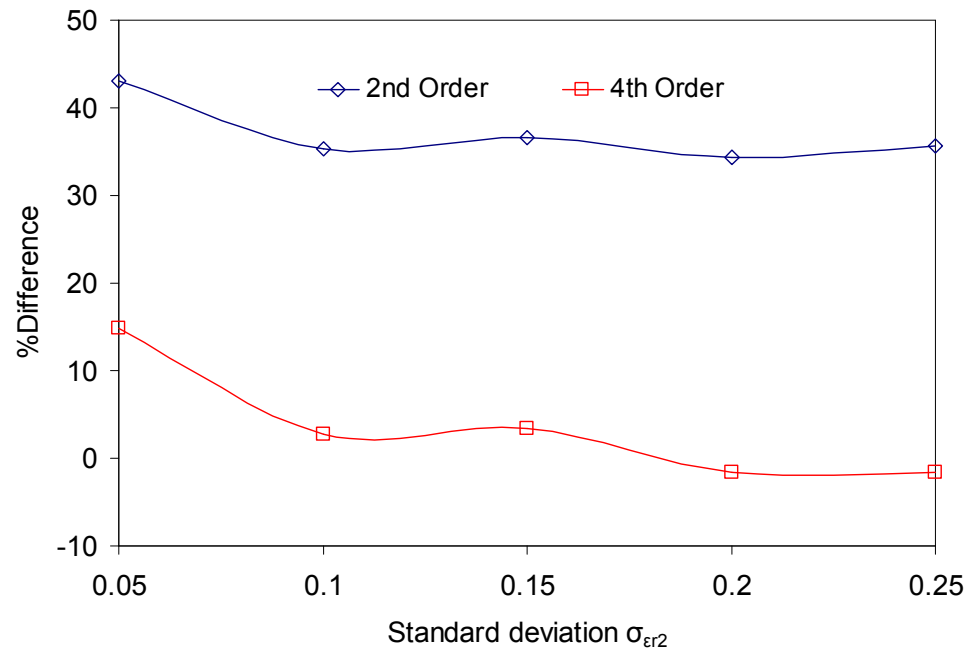
Fig. 6-21D Impact of higher order derivatives on the DST approximation of the kurtosis of fundamental resonance of the structure in Fig. 6-8A

The impact of higher order derivatives could also be useful when dealing with exponential random variables. In general, this kind of distribution requires a higher order approximation than the normal distribution with identical statistical parameters. This is because the odd moments are non-zero for exponential distributions and would add more terms to the DST approximation. To obtain meaningful results for the structure in Fig. 6-8A with an exponential distribution of ε_{r2}, at least a fourth order approximation is required. The results for the percentage difference between the fourth order DST and MC methods are shown in Figs. 6-22A – C. The percentage difference between both methods for the same standard deviation increases as the order of the moment considered increases. The fourth DST approximation of the mean, standard deviation and skew can be found from (A.10), (A.24) and (A.28) respectively.
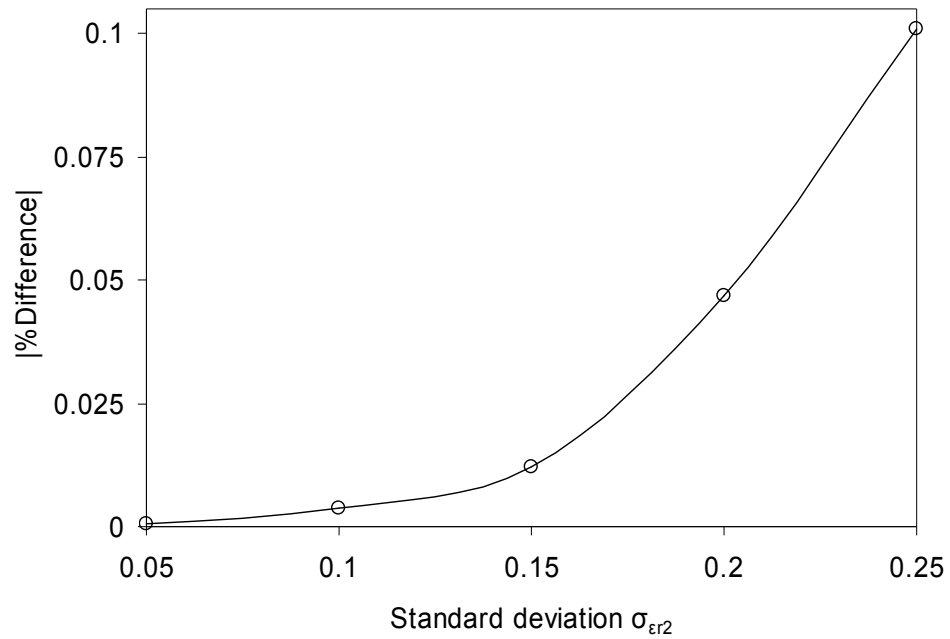
Fig. 6-22A Percentage difference between DST and MC approximations of the average fundamental resonance of the structure in Fig. 6-8A with exponential distribution of ε_{r2}
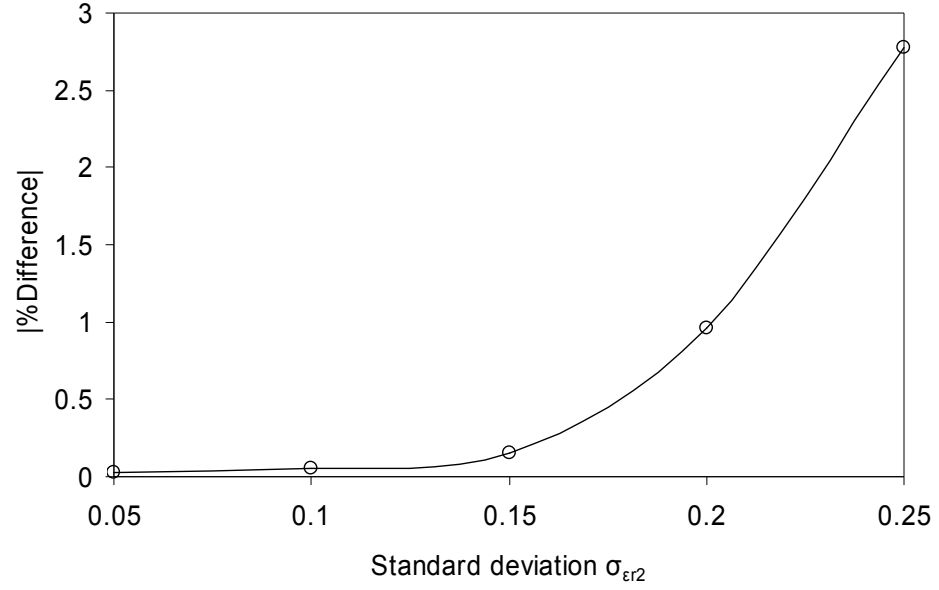
Fig. 6-22B Percentage difference between DST and MC approximations of the standard deviation of fundamental resonance of the structure in Fig. 6-8A with exponential distribution of ε_{r2}
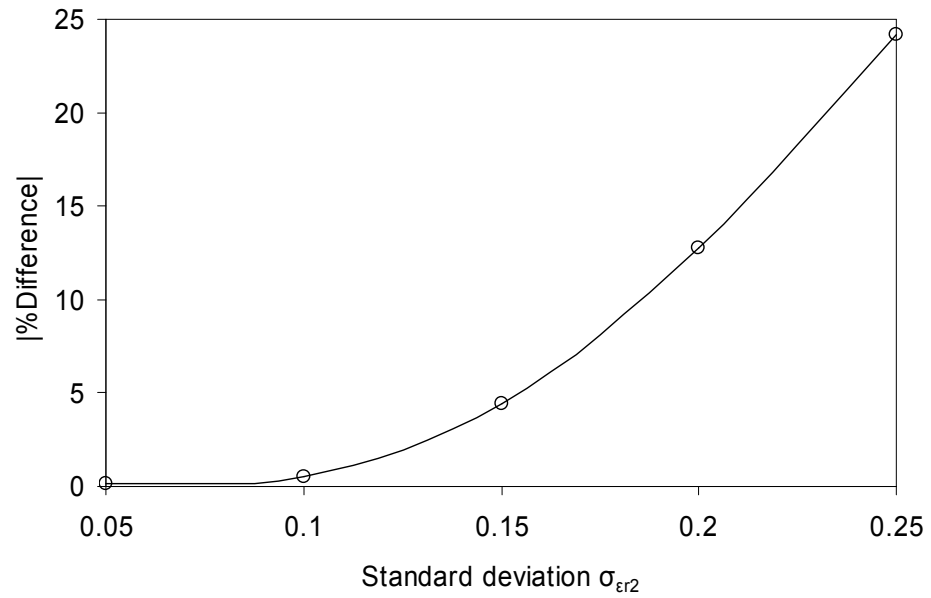
Fig. 6-22C Percentage difference between DST and MC approximations of the skew of fundamental resonance of the structure in Fig. 6-8A with exponential distribution of ε_{r2}

The next chapter deals with the application of DST to 3-D TLM problems. This is done simply to scale up the use of the method to realistic case studies.

6.5   References

[6.1]   C. Christopoulos, "The Transmission-Line Modelling Method," IEEE Press, 1995.

[6.2]   D.P. Johns, "A Three-Dimensional Frequency Domain Transmission-Line Modelling Method," PhD Thesis, University of Nottingham, 1996.

[6.3]   S. Garg, "Derivatives of Eigensolutions of a General Matrix," AIAA Journal., vol. 11, pp. 1191 – 1194, August 1973.

[6.4]   D. Murty, "Derivatives of Eigenvalues and Eigenvectors of a General Complex matrix," AIAA Journal., vol. 26, pp. 293 – 311, August 1988.

[6.5]   R.E. Collin, "Field Theory of Guided Waves," IEEE Press, 1991.

[6.6]   B.M. Ayyub and R.H. McCuen, "Probability, Statistics and Reliability for Engineers and Scientists," 2nd Edition, Chapman and Hall / CRC Press, 2003.

[6.7]   N. Ida, "Engineering Electromagnetics," Springer-Verlag, 2000.

[6.8]   J. Hesselbarth, R. Vahldieck, "Resonance Frequencies Calculated Efficiently with the Frequency-Domain TLM Method," IEEE Microw. Wireless Comp. Lett., vol. 13, pp. 190 – 192, May 2003.

[6.9]   P.B. Johns, "The Solution of Inhomogeneous Waveguide Problems Using a Transmission-Line Matrix," IEEE Trans. Microwave Theory Tech., vol. MTT-22, pp. 209 – 215, March 1974.

[6.10]   F.J. German, "Infinitesimally Adjustable Boundaries in Symmetrical Condensed Node TLM Simulations," 9th Annual Review of Progress in Applied Electromagnetics (ACES), March 1993, Monterey, CA, USA, pp. 482 – 490.

[6.11]   Y.K. Choong, P. Sewell and C. Christopoulos, "New Thin Wire Formulation for Time-Domain Differential-Equation Models," Int. J. Numer. Model., vol. 15, pp. 489 – 501, 2002.

[6.12]   J.P. Webb, "Finite-Element Analysis of the Effect of Geometric Tolerances on Performance Over a Frequency Band," IEEE Trans. Microwave Theory Tech., vol. 52, pp. 306 – 310, Jan. 2004.

Chapter 7   Statistical Analysis in 3-D Problems

This chapter presents the application of the DST to three-dimensional (3-D) stochastic problems. In comparison with 1-D or 2-D problems, the 3-D approach provides the best depiction of realistic scenarios at the cost of substantially increased computational effort. As with the previous chapters, the TLM method is used to numerically assess field behaviour. The MC method is compared with the DST for 3-D problems.

7.1   Three-Dimensional (3-D) TLM

The 3-D TLM technique is used to scale up the size of a corresponding 2-D problem by introducing more ports into the computational domain. This increases the coverage of field behaviour in a defined electromagnetic problem. The 3-D TLM node is constructed by combining 2-D series and shunt nodes [7.1]. The most successful approach is the symmetrical condensed node [7.2] which is described in the next section.

7.2   The Symmetrical Condensed Node

The 3-D symmetrical condensed node (SCN) is illustrated in Fig. 7-1. This is developed by using transmission lines without resorting to the conventional lumped and Thevenin equivalent circuits. Two directions of polarisation in the *x-y*, *y-z* or *x-z* planes are carried on two pairs of transmission lines joined together at a common node centre [7.2, 7.3].
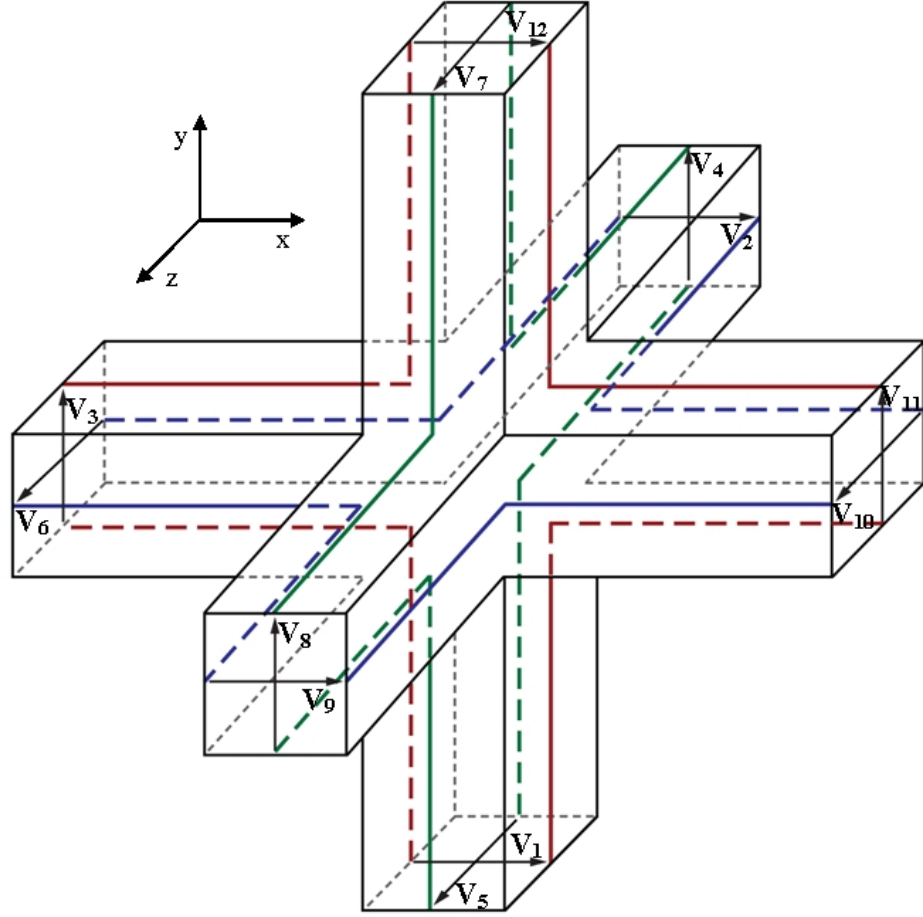
Fig. 7-1 The symmetrical condensed node [7.4]

For a SCN without stubs, all transmission lines have the same characteristic impedance Z_{TL}. This SCN is used for modelling free space and has 12 ports which represent two orthogonal field polarisations in each of the x, y or z-directions. The total voltage across any port p is denoted by V_p. The ports of a particular node (x, y, z) connect to those of its neighbours with the same polarisation. For example, port 1 of a particular node couples with port 12 of its neighbour while port 2 couples with port 9. This same pattern remains for all the ports with except those connected with boundaries. The incident link line voltages at a current time step $k + 1$ depend on those reflected from adjacent ports at a previous time step k. By inspection, the following expressions are obtained:

$$_{k+1}V^i_1(x,y,z) = {}_k V^r_{12}(x, y-1, z) \qquad (7.1a)$$

$$_{k+1}V^i{}_2\left(x,y,y\right)=_k V^r{}_9\left(x,y,z-1\right) \tag{7.1b}$$

$$_{k+1}V^i{}_3\left(x,y,z\right)=_k V^r{}_{11}\left(x-1,y,z\right) \tag{7.1c}$$

$$_{k+1}V^i{}_4\left(x,y,z\right)=_k V^r{}_8\left(x,y,z-1\right) \tag{7.1d}$$

$$_{k+1}V^i{}_5\left(x,y,z\right)=_k V^r{}_7\left(x,y-1,z\right) \tag{7.1e}$$

$$_{k+1}V^i{}_6\left(x,y,z\right)=_k V^r{}_{10}\left(x-1,y,z\right) \tag{7.1f}$$

$$_{k+1}V^i{}_7\left(x,y,z\right)=_k V^r{}_5\left(x,y+1,z\right) \tag{7.1g}$$

$$_{k+1}V^i{}_8\left(x,y,z\right)=_k V^r{}_4\left(x,y,z+1\right) \tag{7.1h}$$

$$_{k+1}V^i{}_9\left(x,y\right),z =_k V^r{}_2\left(x,y,z+1\right) \tag{7.1i}$$

$$_{k+1}V^i{}_{10}\left(x,y,z\right)=_k V^r{}_6\left(x+1,y,z\right) \tag{7.1j}$$

$$_{k+1}V^i{}_{11}\left(x,y,z\right)=_k V^r{}_3\left(x+1,y,z\right) \tag{7.1k}$$

$$_{k+1}V^i{}_{12}\left(x,y,z\right)=_k V^r{}_1\left(x,y+1,z\right) \tag{7.1l}$$

For nodes connected to metallic boundaries, the associated ports *p* are terminated with a short circuit boundary and the incident voltage at the time step *k* + 1 is:

$$_{k+1}V^i{}_p\left(x,y,z\right)=-_k V^r{}_p\left(x,y,z\right) \tag{7.2}$$

For an incident pulse on a particular port to scatter to other ports on the same node, there must be a relationship between one or both field quantities associated with them. This scattering sub-matrix $\underline{S}_{x,y,z}$ at a node (*x, y ,z*) in free space is a 12 *x* 12 matrix derived in [7.2, 7.3] to be:

$$\underline{\underline{S}}_{x,y,z} = 0.5 \begin{pmatrix} 0 & 1 & 1 & 0 & 0 & 0 & 0 & 0 & 1 & 0 & -1 & 0 \\ 1 & 0 & 0 & 0 & 0 & 1 & 0 & 0 & 0 & -1 & 0 & 1 \\ 1 & 0 & 0 & 1 & 0 & 0 & 0 & 1 & 0 & 0 & 0 & -1 \\ 0 & 0 & 1 & 0 & 1 & 0 & -1 & 0 & 0 & 0 & 1 & 0 \\ 0 & 0 & 0 & 1 & 0 & 1 & 0 & -1 & 0 & 1 & 0 & 0 \\ 0 & 1 & 0 & 0 & 1 & 0 & 1 & 0 & -1 & 0 & 0 & 0 \\ 0 & 0 & 0 & -1 & 0 & 1 & 0 & 1 & 0 & 1 & 0 & 0 \\ 0 & 0 & 1 & 0 & -1 & 0 & 1 & 0 & 0 & 0 & 1 & 0 \\ 1 & 0 & 0 & 0 & 0 & -1 & 0 & 0 & 0 & 1 & 0 & 1 \\ 0 & -1 & 0 & 0 & 1 & 0 & 1 & 0 & 1 & 0 & 0 & 0 \\ -1 & 0 & 0 & 1 & 0 & 0 & 0 & 1 & 0 & 0 & 0 & 1 \\ 0 & 1 & -1 & 0 & 0 & 0 & 0 & 0 & 1 & 0 & 1 & 0 \end{pmatrix} \tag{7.3}$$

The scattering sub-matrix relates the vector of incident voltages with that of the reflected voltage of each node (x, y, z) of the problem space at a time step k:

$$_k\underline{V}^r_{x,y,z} = \underline{\underline{S}}_{x,y,z} \cdot _k\underline{V}^i_{x,y,z} \tag{7.4}$$

The law of energy conservation demands that the total incident power must equal the total reflected power [7.2]. As all the link lines have the same characteristic impedance, this relationship is given by:

$$\left(_k\underline{V}^r_{x,y,z} \right)^T \cdot _k\underline{V}^r_{x,y,z} = \left(_k\underline{V}^i_{x,y,z} \right)^T \cdot _k\underline{V}^i_{x,y,z} \tag{7.5}$$

where the superscript T represents the transpose of a matrix.

From the transpose of both sides of (7.4), the expression $(_k\underline{V}^r_{x,y,z})^T = (_k\underline{V}^i_{x,y,z})^T \cdot \underline{\underline{S}}^T_{x,y,z}$ is obtained. Substituting this into the right hand side of (7.5) gives:

$$\left(_k\underline{V}^r_{x,y,z} \right)^T \cdot _k\underline{V}^r_{x,y,z} = \left(_k\underline{V}^i_{x,y,z} \right)^T \cdot \underline{\underline{S}}^T_{x,y,z} \cdot _k\underline{V}^r_{x,y,z} \tag{7.6}$$

Comparing the right hand sides of (7.5) and (7.6), the relationship between incident and reflected voltages becomes:

$$_k\underline{V}^{\,i}_{\,x,y,z} = \underline{\underline{S}}^{\,T}_{\,x,y,z} \cdot {}_k\underline{V}^{\,r}_{\,x,y,z} \tag{7.7}$$

From (7.4) and (7.7) it is clear the scattering sub-matrix has a unitary property. This is because the transpose of $\underline{\underline{S}}_{x,y,z}$ is equal to its inverse.

The *global scattering matrix* is given by a sparse matrix with diagonal entries consisting of the scattering sub-matrices as shown in the last chapter. This provides the relationship between the incident and reflected voltages of all the nodes. This expression for this at a particular time step k is:

$$_k\underline{V}^{\,r} = \underline{\underline{S}} \cdot {}_k\underline{V}^{\,i} \tag{7.8}$$

where $_k\underline{V}^r$ and $_k\underline{V}^i$ are global vectors that contain all the reflected and incident port voltages respectively at time step k.

Assume a 3-D electromagnetic problem requires *NX*, *NY*, and *NZ* nodes in the x, y and z-directions respectively. A SCN with *NP* ports per node has a global scattering matrix of the order *NX x NY x NZ x NP*. Using a similar numbering scheme with the last chapter, the global scattering matrix is:

$$\underline{\underline{S}} = \begin{pmatrix} \underline{\underline{S}}_{0,0,0} & \underline{\underline{0}} & \underline{\underline{0}} & & \underline{\underline{0}} & \underline{\underline{0}} & . & . & \underline{\underline{0}} \\ \underline{\underline{0}} & . & \underline{\underline{0}} & & \underline{\underline{0}} & \underline{\underline{0}} & \underline{\underline{0}} & . & \underline{\underline{0}} \\ \underline{\underline{0}} & \underline{\underline{0}} & . & & \underline{\underline{0}} & \underline{\underline{0}} & \underline{\underline{0}} & . & \underline{\underline{0}} \\ \underline{\underline{0}} & \underline{\underline{0}} & \underline{\underline{0}} & & \underline{\underline{S}}_{NX-1,0,0} & . & . & . & \\ . & . & . & . & . & \underline{\underline{S}}_{0,1,0} & & & . \\ . & . & . & . & . & . & & & . \\ . & . & . & . & . & . & & & . \\ \underline{\underline{0}} & \underline{\underline{0}} & \underline{\underline{0}} & \underline{\underline{0}} & . & . & & \underline{\underline{S}}_{NX-1,NY-1,NZ-1} \end{pmatrix} \tag{7.9}$$

As mentioned earlier, free space media requires a SCN with $NP = 12$. This does not apply when relative permittivity or permeability exceeds unity. This case is dealt with in the Appendix D.

7.3   Application of DST to 3-D Electromagnetic Problems

The application of DST to the SCN stub model is quite straightforward. The frequency domain method simply entails using the exact formulation derived in Chapter 6. The global 2-D scattering and connection matrices are replaced with the corresponding 3-D SCN equivalent. The running of deterministic 3-D SCN stub models is quite demanding on computational resources. This constitutes a severe handicap in the use of MC methods to carry out multiple simulations for 3-D stochastic problems. For this reason, only two examples are presented in this section. For each case study, the problem space is a waveguide discretised using 24 nodes (*NX*) in the horizontal direction and 12 nodes (*NY*) in the vertical direction. The 3-D SCN mesh has been used successfully to model the rectangular cross-section of waveguides. The slice of the 3-D SCN is one cell thick. A schematic representation of this node across the cross-section of a rectangular waveguide is illustrated in Fig. 7-2.
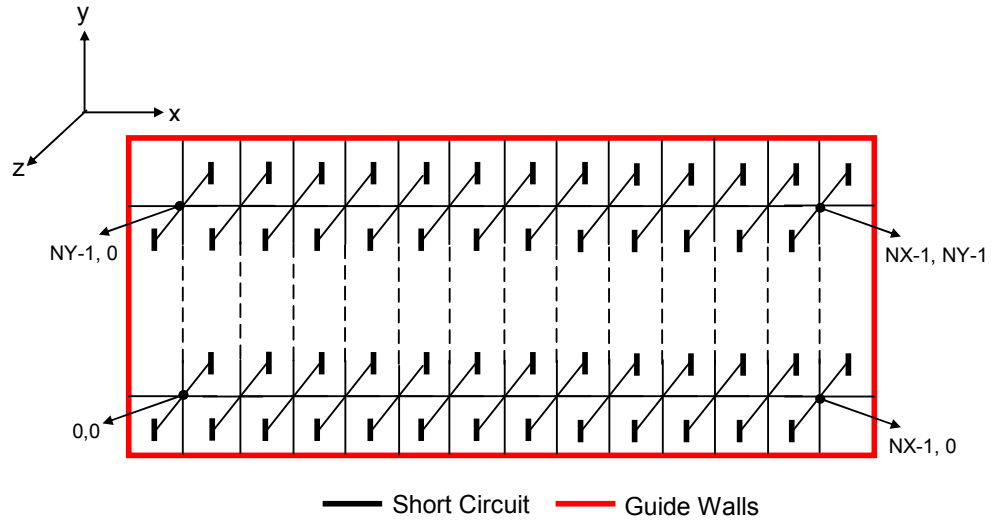
Fig. 7-2 2-D cross-section of dielectric waveguide in the x-y plane using a slice of the 3-D SCN

Ports 2, 4, 8 and 9 of all the SCNs are terminated by short circuit boundaries. The same procedure applies to ports 7 and 12 of the SCN connected to the top, 1 and 5 to the bottom, 3 and 6 to the left and 10 and 11 to the right waveguide walls. This yielded better agreement when compared with 2-D analytical results than the 2-D shunt node [7.6].

For 3-D SCN model of a problem with N_{RV} random variables, the DST approach (described in section 6.2) requires $N_{RV} + 1$ simulations to obtain results which are significantly less than the number required by the MC method. Each simulation for both approaches takes about 8s on a PC with a AMD Athlon 2.01GHz processor. The converged MC simulations take 100,000 repeated runs which is about 9 days on the same platform.

The first case study is of three dielectric slabs with rectangular cross section in the structure illustrated in Fig. 7-3A. The top and bottom slabs are stochastic and uncorrelated with a normal distribution of mean relative permittivity of 2.01 and increasing standard deviation values $\sigma_{\varepsilon r1} = \sigma_{\varepsilon r3} = \sigma_{\varepsilon r}$. The central medium is not a random variable with relative permittivity ε_{r2} of 1.01. The results show that applying the DST to a 3-D SCN yields good results when compared with the MC technique. The changes in $\sigma_{\varepsilon r}$ affect the standard deviation of fundamental resonance σ_{fr}. The percentage difference between the DST and MC approximations of σ_{fr} is shown in Fig. 7-3B. As expected the percentage difference between both methods increases with the variability of the problem.
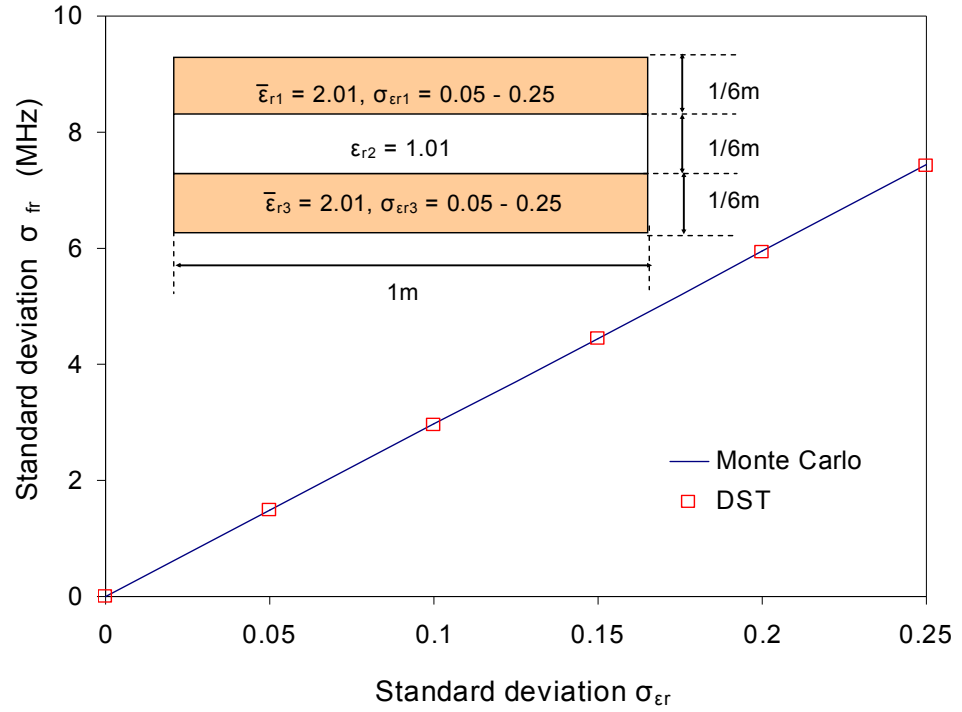
Fig. 7-3A Comparison between the DST and MC approximation methods for two dielectric slabs in a resonator
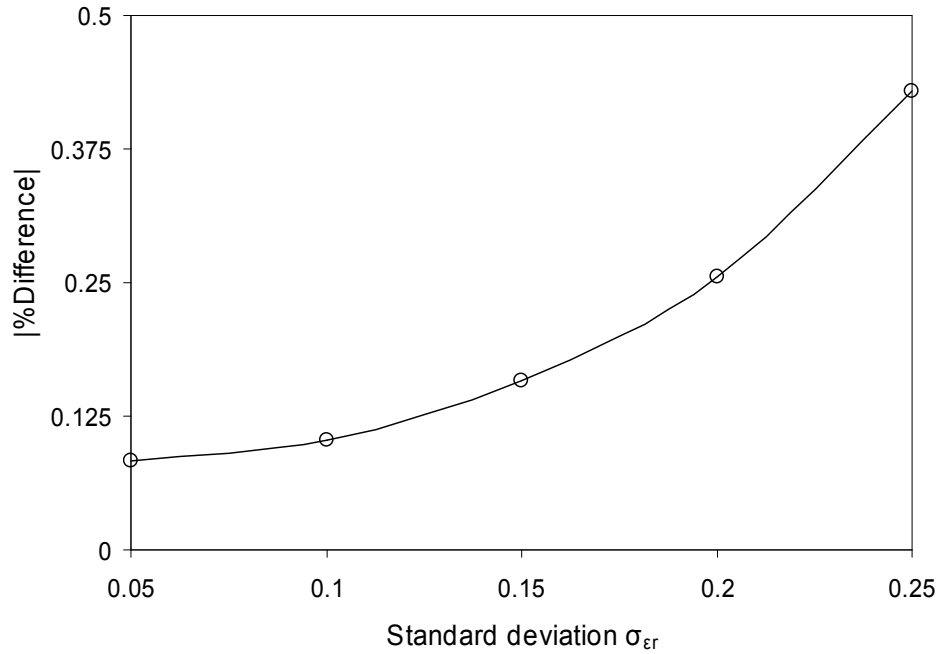
Fig. 7-3B Percentage difference between the converged MC simulations and DST methods for waveguide in Fig. 7-3A

The second case study using the SCN is the structure in Fig. 7-4A. The problem involves modelling eight dielectric slabs that are piecewise homogenous with correlated mean relative permittivity values generated using (4.13). The correlation length L_c = 0.125m and the root mean square of relative permittivity ε_{rms} = 0.05. The slabs have a combined mean relative permittivity of 2.01 and the same standard deviation. The 2-D model for this problem, shown in Fig. 6-11B, was examined in the last chapter. The results follow the same trend for both approaches. Fig. 7-4B shows the percentage difference between converged MC simulations and the DST approach. The 3-D SCN has better dispersion characteristics than the 2-D node [7.5] and thus offers better agreement between the DST and MC methods. For $\sigma_{\varepsilon r}$ = 0.25 in each slab, the percentage difference for the 2-D node in Fig. 6-11B is 1.103% while in the 3-D node this is reduced to 0.606%. This proves that improving on model accuracy provides a superior platform for comparative analysis. However, the computational resources required to achieve this are a major deterrent, particularly for statistical analysis based on repeated runs. The DST approach proposes a cost effective way to deal with stochastic problems with high complexity in 3-D.
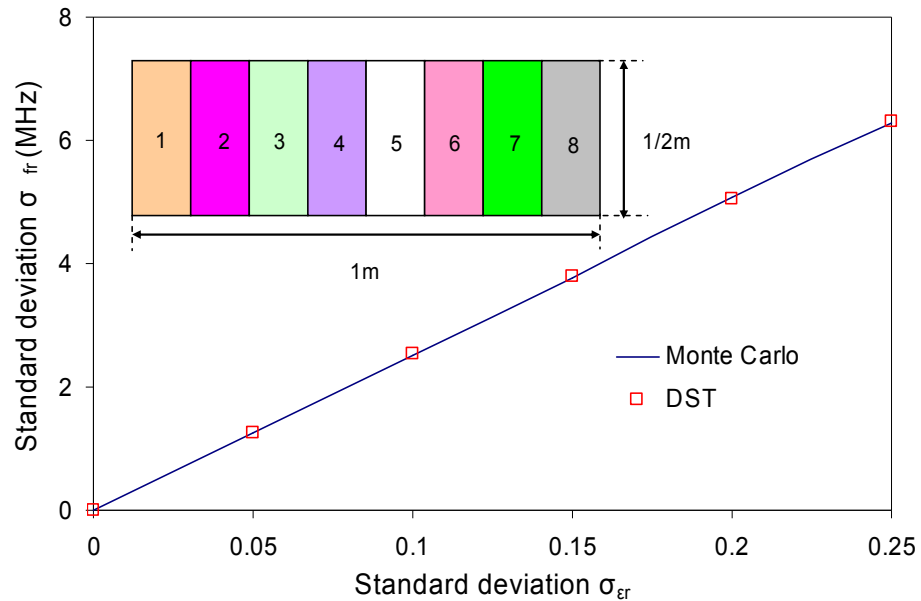
Fig. 7-4A Eight correlated dielectric slabs modelling a single dielectric block as eight layers with correlated relative permittivities
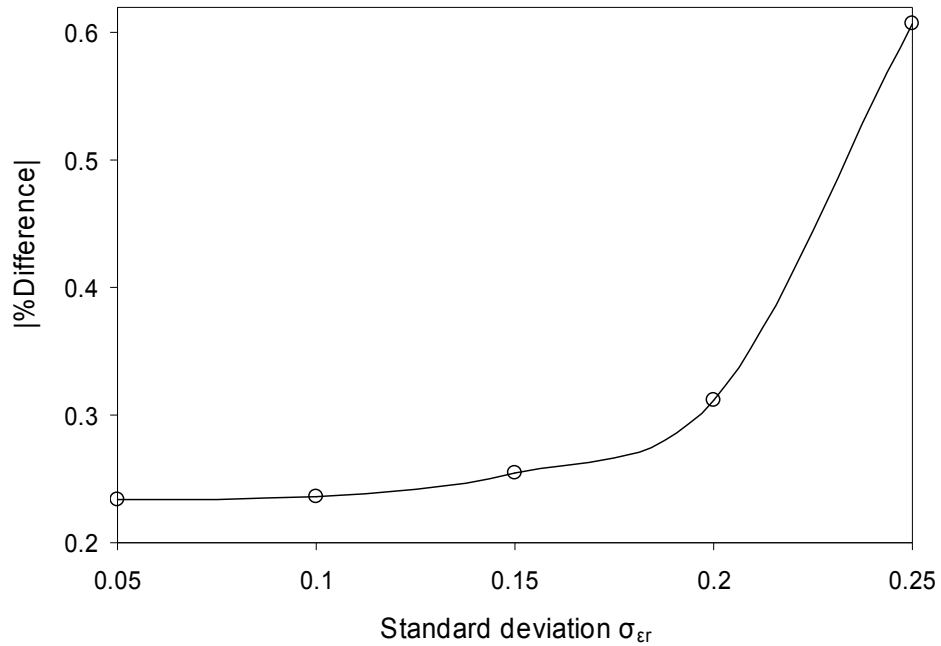
Fig. 7-4B Percentage difference between the converged MC simulations and DST methods for waveguide in Fig. 7-4A

The DST for performing electromagnetic simulations in the presence of statistically defined parameters has been shown to be useful for 1-D, 2-D and 3-D problems. The next chapter proposes an alternative means to carry out these statistical approximations.

7.4   References

[7.1]   W.J.R. Hoefer, "The Transmission-Line Matrix Method-Theory and Applications," IEEE Trans. Microwave Theory Tech., vol. MTT-33, pp. 882 – 893, Oct. 1985.

[7.2]   P.B. Johns, "A Symmetrical Condensed Node for the TLM Method," IEEE Trans. Microwave Theory Tech., vol. MTT-35, pp. 370 – 377, April 1987.

[7.3]   C. Christopoulos, "The Transmission-Line Modelling Method," IEEE Press, 1995.

[7.4]   K.P. Biwojno, "Embedding of Fine Features in Multi-scale Electromagnetic Models," PhD thesis, University of Nottingham, 2006.

[7.5]   R. Allen, A. Mallik and P.B. Johns, "Numerical Results for the Symmetrical Condensed TLM Node," IEEE Trans. Microwave Theory Tech., vol. MTT-35, pp. 378 – 382, Apr. 1987.

Chapter 8　　　The Unscented Transform Method

This chapter introduces an alternative method for estimation of statistical moments based on experimental design techniques. This method is referred to as the unscented transform method. This is particularly useful for functions which are calculable but not differentiable. The theory behind this technique is discussed here and applied to selected case studies in the next chapter.

8.1　Theory of the Unscented Transform (UT) Method

The Unscented Transform (UT) was developed in [8.1] as a practical estimator to the probability distribution function instead of the traditional MC method. The principle behind this approach is based on the moment design technique described in [8.2]. The first step to implementing UT is to identify the sources of variability in the system under consideration. A set of deterministically selected input (sigma) points are then transformed via a nonlinear mapping process. The number of sigma points depends on the order of approximation required. These points are much fewer in number when compared to the number required to attain convergence using the MC method. The mapped sigma points or design values are weighted in a commensurate manner to the probability distribution of stochastic input parameters. Therefore, it is possible to find the relationship between the moments of input parameters and the weights of the sigma points. Fig. 8-1 illustrates a continuous normal distribution and its discrete equivalent with 3 and 7 sigma points.
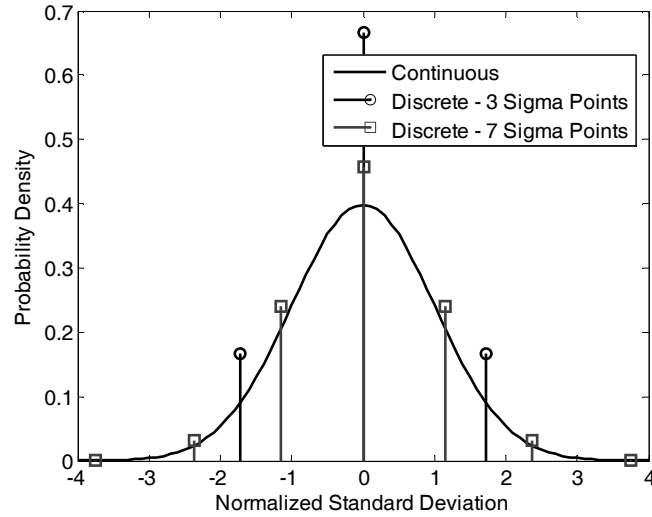
Fig. 8-1 Representation of the standard normal distribution and the discrete approximation

The DST developed in the preceding chapters requires that the function of stochastic variables is differentiable and as such is intimately connected with sensitivity analysis. The UT method however has the advantage of working with an existing model without an explicit transfer function. This makes it tailor made for applications to black-box models. However, the number of sigma points required increases exponentially with the number of random variables to obtain the same order of accuracy as the DST approximation. This section takes a look at the definition of sigma points and associated weights as well as how they both relate to the number of random variables and the choice of input distribution types.

8.1.1   Application of UT to Problems with One Random Variable

Let x be a random variable with a mean $\overline{x}$ and standard deviation σ_x. Then, a standardised random variable $\hat{x}$ can be defined with zero mean and the same standard deviation as x. Therefore, x is given by the expression:

$$x = \overline{x} + \hat{x} \tag{8.1}$$

The Taylor's series approximation for a function of x is:

$$f(x) = f(\overline{x} + \hat{x}) = f(\overline{x}) + \left(\frac{df}{dx}\Big|_{x=\overline{x}}\right)\hat{x} + \frac{1}{2!}\left(\frac{d^2 f}{dx^2}\Big|_{x=\overline{x}}\right)\hat{x}^2 + \frac{1}{3!}\left(\frac{d^3 f}{dx^3}\Big|_{x=\overline{x}}\right)\hat{x}^3 + \dots \quad (8.2)$$

The non-linear mapping process commences by attributing coefficients to stochastic variables to form a power series. This is attained by replacing the derivative terms in (8.2) with coefficients similar to the regression polynomial model adopted in [8.3]. Thus, (8.2) can be rewritten to give:

$$f(\overline{x} + \hat{x}) = a_0 + a_1\hat{x} + a_2\hat{x}^2 + \dots + a_n\hat{x}^n = a_0 + g(\hat{x}) \quad (8.3)$$

where $a_n = \dfrac{1}{n!}\left(\dfrac{d^n f}{dx^n}\Big|_{x=\overline{x}}\right)$ and n is the order of the polynomial. Comparing (8.2) and (8.3), it is clear that $a_0 = f(\overline{x})$.

The expected value of $f(x)$ is:

$$\overline{f} = E\left[f(\overline{x} + \hat{x})\right] = a_0 + E\left[g(\hat{x})\right] = f(\overline{x}) + \overline{g} \quad (8.4)$$

The variance of $f(x)$ is:

$$\sigma^2_{f} = E\left[\left(f(x) - \overline{f}\right)^2\right] = E\left[g^2(\hat{x})\right] - \overline{g}^2 \quad (8.5)$$

The sigma points S_i used in the UT calculations are defined at specific values and designated with weights w_i. As these are discrete values of stochastic variables, the expected value of $f(x)$ in terms of these parameters is [8.1]:

$$\overline{f} = w_0 f(\overline{x} + S_0) + \sum_{i=1}^{m-1} w_i f(\overline{x} + S_i) \quad (8.6a)$$

where *m* is the number of sigma points considered and $S_0 = 0$ for an odd number of sigma points and an even distribution. Substituting (8.3) into (8.6a) for this case and collecting like terms:

$$\overline{f} = \left[w_0 + \sum_{i=1}^{m-1} w_i \right] f(\overline{x}) + \sum_{i=1}^{m-1} w_i g(S_i) \tag{8.6b}$$

Comparing (8.4) and (8.6b), the following relations are obtained:

$$\left[w_0 + \sum_{i=1}^{m-1} w_i \right] = 1 \tag{8.6c}$$

$$\sum_{i=1}^{m-1} w_i g(S_i) = \overline{g} \tag{8.6d}$$

From (8.6c), the weights designated in UT are deterministic and must sum up to one. This implies that probability axioms are obeyed in UT. Similarly, the variance of $f(x)$ in terms of weights and sigma points is [8.1]:

$$\sigma^2_f = w_0 \left[f(\overline{x}) - \overline{f} \right]^2 + \sum_{i=1}^{m-1} w_i \left[f(\overline{x} + S_i) - \overline{f} \right]^2 \tag{8.7a}$$

Substituting (8.4) into (8.7a):

$$\sigma^2_f = w_0 \overline{g}^2 + \sum_{i=1}^{m-1} w_i \left[g(S_i) - \overline{g} \right]^2 \tag{8.7b}$$

Expanding (8.7b):

$$\sigma^2_f = \left[w_0 + \sum_{i=1}^{m-1} w_i \right] \overline{g}^2 + \sum_{i=1}^{m-1} w_i \left[g^2(S_i) - 2\overline{g}g(S_i) \right] \tag{8.7c}$$

Substituting (8.6c) and (8.6d) into (8.7c):

$$\sigma^2_f = \sum_{i=1}^{m-1} w_i \left[g^2(S_i) \right] - \overline{g}^2 \tag{8.7d}$$

Comparing (8.5) and (8.7d) gives the relation:

$$E\left[g^2\left(\hat{x}\right)\right] = \sum_{i=1}^{m-1} w_i g\left(S_i\right)^2 \tag{8.8}$$

In general, the sigma points and weights in UT are related to the moments of a random variable x by:

$$E\left[\hat{x}^k\right] = \sum_{i=1}^{m-1} w_i S_i^k \tag{8.9}$$

The first four moments of any distribution provide information on the mean, variance, skew and kurtosis. From these moments the following sets of equations are obtained:

$$E\left[\hat{x}\right] = \sum_{i=1}^{m-1} w_i S_i = 0 \tag{8.10a}$$

$$E\left[\hat{x}^2\right] = \sum_{i=1}^{m-1} w_i S_i^2 = \sigma^2{}_x \tag{8.10b}$$

$$E\left[\hat{x}^3\right] = \sum_{i=1}^{m-1} w_i S_i^3 = \gamma_1 \sigma^3{}_x \tag{8.10c}$$

$$E\left[\hat{x}^4\right] = \sum_{i=1}^{m-1} w_i S_i^4 = \left(\gamma_2 + 3\right)\sigma^4{}_x \tag{8.10d}$$

where γ_1 and γ_2 are the skew and kurtosis of the input distribution.

The sigma points and weights can be obtained by solving (8.10a) – (8.10d) using the Maple software. The first two terms for both parameters are [8.4]:

$$S_1 = \frac{1}{2}\left[\gamma_1 - \sigma_x \sqrt{4\left(\gamma_2 + 3\right) - 3\gamma_1{}^2}\right]\sigma_x$$

$$S_2 = \frac{1}{2}\left[\gamma_1 + \sigma_x \sqrt{4\left(\gamma_2 + 3\right) - 3\gamma_1{}^2}\right]\sigma_x$$

$$w_1 = \frac{-2}{\sqrt{4\left(\gamma_2 + 3\right) - 3\gamma_1{}^2}\left[\gamma_1 - \sqrt{4\left(\gamma_2 + 3\right) - 3\gamma_1{}^2}\right]}$$

$$w_2 = \frac{-2}{\sqrt{4\left(\gamma_2 + 3\right) - 3\gamma_1{}^2}\left[\gamma_1 + \sqrt{4\left(\gamma_2 + 3\right) - 3\gamma_1{}^2}\right]} \tag{8.11}$$

The weights and sigma points obtained are substituted into (8.6a) and (8.7a) to obtain the second order mean and standard deviation respectively. The more UT terms that are considered, the better the accuracy of the approximation.

The knowledge of the weights and sigma points can also be extended to find the skew and kurtosis of the output distribution [8.7]:

$$Skew = \frac{\sum_{i=1}^{m-1} w_i \left[f\left(\overline{x} + S_i\right) - \overline{f}\right]^3}{\sigma_f^3} \tag{8.12a}$$

$$Kurt = \frac{\sum_{i=1}^{m-1} w_i \left[f\left(\overline{x} + S_i\right) - \overline{f}\right]^4}{\sigma_f^4} - 3 \tag{8.12b}$$

8.1.2   Application of UT to Problems with Two Random Variables

For a problem with two random variables $\hat{x}_1$ and $\hat{x}_2$, the Taylor series in terms of regression coefficients is:

$$g\left(\hat{x}_1, \hat{x}_2\right) = a_1 \hat{x}_1 + a_2 \hat{x}_2 + a_3 \hat{x}_1 \hat{x}_2 + a_4 \hat{x}_1^2 + a_5 \hat{x}_2^2 + \ldots \tag{8.13}$$

The product terms in (8.13) leads to a modification in (8.9). The relationship between sigma points and moments is:

$$E\left[\hat{x}_1^{\,k} \hat{x}_2^{\,l}\right] = \sum_{i=1}^{m-1} w_i \left(^1 S_i^{k\,2} S_i^l\right) \tag{8.14}$$

For a second order approximation, the combination of k and l leads to a system of fourteen equations:

$$\sum_{i=1}^{m-1} w_i \left({}^1S_i \right) = E\left[\hat{x}_1 \right] \qquad\qquad \sum_{i=1}^{m-1} w_i \left({}^2S_i \right) = E\left[\hat{x}_2 \right]$$

$$\sum_{i=1}^{m-1} w_i \left({}^1S_i \right)^2 = E\left[\hat{x}_1^{\,2} \right] \qquad\qquad \sum_{i=1}^{m-1} w_i \left({}^2S_i \right)^2 = E\left[\hat{x}_2^{\,2} \right]$$

$$\sum_{i=1}^{m-1} w_i \left({}^1S_i \right)^3 = E\left[\hat{x}_1^{\,3} \right] \qquad\qquad \sum_{i=1}^{m-1} w_i \left({}^2S_i \right)^3 = E\left[\hat{x}_2^{\,3} \right]$$

$$\sum_{i=1}^{m-1} w_i \left({}^1S_i \right)^4 = E\left[\hat{x}_1^{\,4} \right] \qquad\qquad \sum_{i=1}^{m-1} w_i \left({}^2S_i \right)^4 = E\left[\hat{x}_2^{\,4} \right]$$

$$\sum_{i=1}^{m-1} w_i \left({}^1S_i \right)\left({}^2S_i \right) = E\left[\hat{x}_1\hat{x}_2 \right] \qquad \sum_{i=1}^{m-1} w_i \left({}^1S_i \right)\left({}^2S_i \right)^2 = E\left[\hat{x}_1\hat{x}_2^{\,2} \right]$$

$$\sum_{i=1}^{m-1} w_i \left({}^1S_i \right)^2\left({}^2S_i \right) = E\left[\hat{x}_1^{\,2}\hat{x}_2 \right] \qquad \sum_{i=1}^{m-1} w_i \left({}^1S_i \right)^2\left({}^2S_i \right)^2 = E\left[\hat{x}_1^{\,2}\hat{x}_2^{\,2} \right]$$

$$\sum_{i=1}^{m-1} w_i \left({}^1S_i \right)^3\left({}^2S_i \right) = E\left[\hat{x}_1^{\,3}\hat{x}_2 \right] \qquad \sum_{i=1}^{m-1} w_i \left({}^1S_i \right)\left({}^2S_i \right)^3 = E\left[\hat{x}_1\hat{x}_2^{\,3} \right] \quad (8.15)$$

Each sigma point has three variables (w_i, ${}^1S_i$ and ${}^2S_i$). This system has fourteen equations and therefore requires at least five sigma points to satisfy all the conditions in (8.15). This leads to the equations:

$$w_1\,{}^1S_1 + w_2\,{}^1S_2 + w_3\,{}^1S_3 + w_4\,{}^1S_4 + w_5\,{}^1S_5 = E\left[\hat{x}_1 \right]$$

$$w_1\,{}^2S_1 + w_2\,{}^2S_2 + w_3\,{}^2S_3 + w_4\,{}^2S_4 + w_5\,{}^2S_5 = E\left[\hat{x}_2 \right]$$

$$w_1\,{}^1S_1^2 + w_2\,{}^1S_2^2 + w_3\,{}^1S_3^2 + w_4\,{}^1S_4^2 + w_5\,{}^1S_5^2 = E\left[\hat{x}_1^{\,2} \right]$$

$$w_1\,{}^2S_1^2 + w_2\,{}^2S_2^2 + w_3\,{}^2S_3^2 + w_4\,{}^2S_4^2 + w_5\,{}^2S_5^2 = E\left[\hat{x}_2^{\,2} \right]$$

$$w_1\,{}^1S_1^3 + w_2\,{}^1S_2^3 + w_3\,{}^1S_3^3 + w_4\,{}^1S_4^3 + w_5\,{}^1S_5^3 = E\left[\hat{x}_1^{\,3} \right]$$

$$w_1\,{}^2S_1^3 + w_2\,{}^2S_2^3 + w_3\,{}^2S_3^3 + w_4\,{}^2S_4^3 + w_5\,{}^2S_5^3 = E\left[\hat{x}_2^{\,3} \right]$$

$$w_1\,{}^1S_1^4 + w_2\,{}^1S_2^4 + w_3\,{}^1S_3^4 + w_4\,{}^2S_4^4 + w_5\,{}^1S_5^4 = E\left[\hat{x}_1^{\,4} \right]$$

$$w_1\,{}^2S_1^4 + w_2\,{}^2S_2^4 + w_3\,{}^2S_3^4 + w_4\,{}^2S_4^4 + w_5\,{}^2S_5^4 = E\left[\hat{x}_2^{\,4} \right]$$

$$w_1\,{}^1S_1\,{}^2S_1 + w_2\,{}^1S_2\,{}^2S_2 + w_3\,{}^1S_3\,{}^2S_3 + w_4\,{}^1S_4\,{}^2S_4 + w_5\,{}^1S_5\,{}^2S_5 = E\left[\hat{x}_1\hat{x}_2 \right]$$

$$w_1\,{}^1S_1^2\,{}^2S_1 + w_2\,{}^1S_2^2\,{}^2S_2 + w_3\,{}^1S_3^2\,{}^2S_3 + w_4\,{}^1S_4^2\,{}^2S_4 + w_5\,{}^1S^2\,{}^2S_5 = E\left[\hat{x}_1^{\,2}\hat{x}_2 \right]$$

$$w_1\,{}^1S_1\,{}^2S_1^2 + w_2\,{}^1S_2\,{}^2S_2^2 + w_3\,{}^1{}^1S_3\,{}^2S_3^2 + w_4\,{}^1S_4\,{}^2S_4^2 + w_5\,{}^1S_5\,{}^2S_5^2 = E\left[\hat{x}_1\hat{x}_2^{\,2} \right]$$

$$w_1\,{}^1S_1^2\,{}^2S_1^2 + w_2\,{}^1S_2^2\,{}^2S_2^2 + w_3\,{}^1S_3^2\,{}^2S_3^2 + w_4\,{}^1S_4^2\,{}^2S_4^2 + w_5\,{}^1S_5^2\,{}^2S_5^2 = E\left[\hat{x}_1^{\,2}\hat{x}_2^{\,2} \right]$$

$$w_1\,{}^1S_1^3\,{}^2S_1 + w_2\,{}^1S_2^3\,{}^2S_2 + w_3\,{}^1S_3^3\,{}^2S_3 + w_4\,{}^1S_4^3\,{}^2S_4 + w_5\,{}^1S_5^3\,{}^2S_5 = E\left[\hat{x}_1^{\,3}\hat{x}_2 \right]$$

$$w_1\,{}^1S_1\,{}^2S_1^3 + w_2\,{}^1S_2\,{}^2S_2^3 + w_3\,{}^1S_3\,{}^2S_3^3 + w_4\,{}^1S_4\,{}^2S_4^3 + w_5\,{}^1S_5\,{}^2S_5^3 = E\left[\hat{x}_1\hat{x}_2^{\,3} \right] \quad (8.16)$$

The general equation for an nth order approximation with N_E equations and n_{RV} random variables is [8.4]:

$$N_E = \sum_{i=1}^{2n} \frac{(n_{RV} - i + 1)!}{i!\,(n_{RV} - 1)!} \qquad (8.17)$$

Each sigma point adds $n_{RV} + 1$ unknowns to each of the N_E equations. Therefore, the number of sigma points m is the next integer to the ratio between N_E and $n_{RV} + 1$:

$$m = \frac{N_E}{n_{RV} + 1} \qquad (8.18)$$

From (8.17) and (8.18), it can be seen that N_E increases rapidly with n_{RV}.

The sigma points for the random variables can be expressed in an orthogonal geometric plane. For two random variables $\hat{x}_1$ and $\hat{x}_2$, a position vector $({}^1S, {}^2S)$ is defined such that a point in this plane is:

$$\vec{P} = {}^1S\hat{a}_{x1} + {}^2S\hat{a}_{x2} \qquad (8.19)$$

where $\hat{a}_{x1}$ and $\hat{a}_{x2}$ are unit vectors in the $\hat{x}_1$ and $\hat{x}_2$ directions respectively.

The magnitude of the position vector $({}^1S, {}^2S)$ is:

$$R = \sqrt{{}^1S^2 + {}^2S^2} \qquad (8.20)$$

The second moments about the origin can be found from:

$$\sum_{i=1}^{m-1} w_i \left(\vec{P}_i . \vec{P}_i \right) = \sum_{i=1}^{m-1} w_i \left(x_{1i}^2 \hat{a}_{x1}.\hat{a}_{x1} + 2x_{1i}x_{2i}\hat{a}_{x1}.\hat{a}_{x2} + x_{2i}^2 \hat{a}_{x2}.\hat{a}_{x1} \right) \qquad (8.21)$$

For normal independent random variables with zero mean and unity standard deviation, (8.21) can be simplified to:

168

$$\sum_{i=1}^{m-1} w_i \left(\vec{P}_i . \vec{P}_i \right) = \sum_{i=1}^{m-1} w_i R^2 = E\left[\hat{x}_1^2 \right] + E\left[\hat{x}_2^2 \right] = \sum_{i=1}^{n_{RV}} E\left[\hat{x}_i^2 \right] \qquad (8.22)$$

Now, R^4 can be found from (8.20):

$$R^4 = {}^1S^4 + 2 \, {}^1S^2 \, {}^2S^2 + {}^2S^4 \qquad (8.23)$$

The fourth moments about the origin from (8.23) are:

$$\sum_{i=1}^{m-1} w_i R^4 = E\left[\hat{x}_1^4 \right] + 2E\left[\hat{x}_1^2 \hat{x}_2^2 \right] + E\left[\hat{x}_2^4 \right] = \sum_{i=1}^{n_{RV}} E\left[\hat{x}_i^4 \right] + 2\sum_{i\neq j}^{n_{RV}} E\left[\hat{x}_i^2 \hat{x}_j^2 \right] \qquad (8.24)$$

The radius about the origin R is the the ratio of (8.24) and (8.22):

$$R = \left(\frac{\sum_{i=1}^{n_{RV}} E\left[\hat{x}_i^4 \right] + 2\sum_{i\neq j}^{n_{RV}} E\left[\hat{x}_i^2 \hat{x}_j^2 \right]}{\sum_{i=1}^{n_{RV}} E\left[\hat{x}_i^2 \right]} \right)^{\frac{1}{2}} \qquad (8.25)$$

For uniformly distributed weights, w can be found by substituting (8.25) into (8.22):

$$w = \frac{\left(\sum_{i=1}^{n_{RV}} E\left[\hat{x}_i^2 \right] \right)^2}{n_{RV} \left(\sum_{i=1}^{n_{RV}} E\left[\hat{x}_i^4 \right] + 2\sum_{i\neq j}^{n_{RV}} E\left[\hat{x}_i^2 \hat{x}_j^2 \right] \right)} \qquad (8.26)$$

Now, as the random variables are normally distributed with unity standard deviation, then $E[\hat{x}_i^2] = E[\hat{x}_i^2] = 1$ and $E[\hat{x}_i^4] = 3$.

For two random variables, five sigma points are equidistant round a plane circle at an angle:

$$\alpha = \frac{2\pi p}{5} = cos^{-1}\left(\frac{{}^1S}{R} \right) = sin^{-1}\left(\frac{{}^2S}{R} \right) \qquad 0 \le p < 5 \qquad (8.27)$$

As the standard deviation considered is unity, the sigma points can be scaled by multiplying ^1S and ^2S by σ_{x1} and σ_{x2} respectively.

For normally distributed random variables the solution of (8.16) using (8.25), (8.26) and (8.27) is [8.4]:

$$w_i = \frac{1}{10} \qquad\qquad 1 \leq i \leq 5$$

$$^1S_1 = 2\cos\left(0\frac{2\pi}{5}\right)\sigma_{x1} \qquad ^2S_1 = 2\sin\left(0\frac{2\pi}{5}\right)\sigma_{x2}$$

$$^1S_2 = 2\cos\left(\frac{2\pi}{5}\right)\sigma_{x1} \qquad ^2S_2 = 2\sin\left(\frac{2\pi}{5}\right)\sigma_{x2}$$

$$^1S_3 = 2\cos\left(2\frac{2\pi}{5}\right)\sigma_{x1} \qquad ^2S_3 = 2\sin\left(2\frac{2\pi}{5}\right)\sigma_{x2}$$

$$^1S_4 = 2\cos\left(3\frac{2\pi}{5}\right)\sigma_{x1} \qquad ^2S_4 = 2\sin\left(3\frac{2\pi}{5}\right)\sigma_{x2}$$

$$^1S_5 = 2\cos\left(4\frac{2\pi}{5}\right)\sigma_{x1} \qquad ^2S_5 = 2\sin\left(4\frac{2\pi}{5}\right)\sigma_{x2} \qquad (8.28)$$

where σ_{x1} and σ_{x2} are the standard deviation of random variables $\hat{x}_1$ and $\hat{x}_2$ respectively.

The effects of correlation between two normally distributed random variables can be taken into account by using the covariance matrix transformation [8.8].

$$\begin{bmatrix} \dfrac{^1S'}{\sigma_{x1}} \\[2ex] \dfrac{^2S'}{\sigma_{x2}} \end{bmatrix} = \begin{bmatrix} \sqrt{\dfrac{1+\rho}{2}} & \sqrt{\dfrac{1-\rho}{2}} \\[2ex] \sqrt{\dfrac{1+\rho}{2}} & -\sqrt{\dfrac{1-\rho}{2}} \end{bmatrix} \begin{bmatrix} \dfrac{^1S}{\sigma_{x1}} \\[2ex] \dfrac{^2S}{\sigma_{x2}} \end{bmatrix} \qquad (8.29)$$

where $^1S'$ and $^2S'$ are the sigma points if $\hat{x}_1$ and $\hat{x}_2$ are statistically dependent with a correlation coefficient of ρ.

The solution of (8.16) for the scenario in (8.29) becomes:

$$w_i = \frac{1}{10} \qquad\qquad 1 \le i \le 5$$

$$^1S_1 = 2\left[T_1\cos\left(0\frac{2\pi}{5}\right)\sigma_{x1} + T_2\sin\left(0\frac{2\pi}{5}\right)\sigma_{x1}\right] \qquad ^2S_1 = 2\left[T_1\cos\left(0\frac{2\pi}{5}\right)\sigma_{x2} - T_2\sin\left(0\frac{2\pi}{5}\right)\sigma_{x2}\right]$$

$$^1S_2 = 2\left[T_1\cos\left(\frac{2\pi}{5}\right)\sigma_{x1} + T_2\sin\left(\frac{2\pi}{5}\right)\sigma_{x1}\right] \qquad ^2S_2 = 2\left[T_1\cos\left(\frac{2\pi}{5}\right)\sigma_{x2} - T_2\sin\left(\frac{2\pi}{5}\right)\sigma_{x2}\right]$$

$$^1S_3 = 2\left[T_1\cos\left(2\frac{2\pi}{5}\right)\sigma_{x1} + T_2\sin\left(2\frac{2\pi}{5}\right)\sigma_{x1}\right] \qquad ^2S_3 = 2\left[T_1\cos\left(2\frac{2\pi}{5}\right)\sigma_{x2} - T_2\sin\left(2\frac{2\pi}{5}\right)\sigma_{x2}\right]$$

$$^1S_4 = 2\left[T_1\cos\left(3\frac{2\pi}{5}\right)\sigma_{x1} + T_2\sin\left(3\frac{2\pi}{5}\right)\sigma_{x1}\right] \qquad ^2S_4 = 2\left[T_1\cos\left(3\frac{2\pi}{5}\right)\sigma_{x2} - T_2\sin\left(3\frac{2\pi}{5}\right)\sigma_{x2}\right]$$

$$^1S_5 = 2\left[T_1\cos\left(4\frac{2\pi}{5}\right)\sigma_{x1} + T_2\sin\left(4\frac{2\pi}{5}\right)\sigma_{x1}\right] \qquad ^2S_5 = 2\left[T_1\cos\left(4\frac{2\pi}{5}\right)\sigma_{x2} - T_2\sin\left(4\frac{2\pi}{5}\right)\sigma_{x2}\right]$$

$$(8.30)$$

where $T_1 = \sqrt{\dfrac{1+\rho}{2}}$ and $T_2 = \sqrt{\dfrac{1-\rho}{2}}$

8.1.3   Application of UT to Problems Using Non-Uniform Weights

For non-uniform weights, a geometric approach can also be deployed to obtain sigma points. The simplest manner to achieve this is to define random variables in a Euclidean space. n_{RV} axes are defined at the geometric centre of a n_{RV}-dimensional unit cube. Fig. 8-2 shows that the total number of sigma points (red and black dots) using this method is $2^{n_{RV}} + 2\,n_{RV}$.

2 Random variables   **3 Random variables**
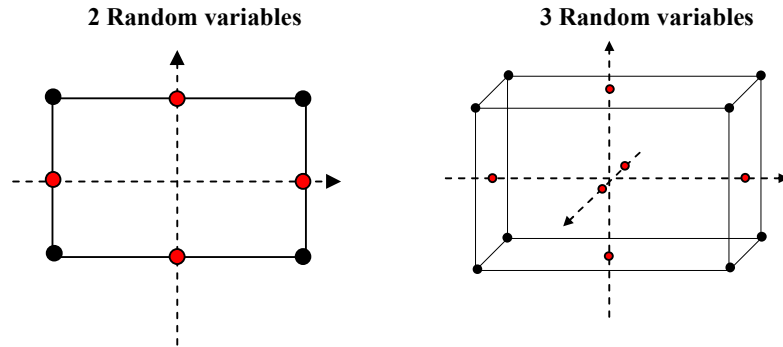
Fig. 8-2 Shapes (not to scale) illustrating the number of sigma points allocated for a problem with two and three random variables.

The 2^{nRV} sigma points that correspond to the black dots in Fig. 8-2 have co-ordinates given by the expression [8.4]:

$$\vec{P}_j = \sqrt{\frac{n_{RV}+2}{n_{RV}}} \left(i_1, i_2, \dots i_{n_{RV}} \right) \qquad 1 \le j < 2^{nRV} \qquad \text{(8.31a)}$$

where $i_1 = i_2 = \dots = i_{n_{RV}} = \pm 1$

The weights for the sigma points in (8.31a) are [8.4]:

$$w_j = \frac{1}{2^{nRV}} \left(\frac{n_{RV}}{n_{RV}+2} \right)^2 \qquad 1 \le j \le 2^{nRV} \qquad \text{(8.31b)}$$

The $2\,n_{RV}$ points represented by the red dots have co-ordinates given by the expression [8.4]:

$$\vec{P}_j = \sqrt{n_{RV}+2} \left(i_1, i_2, \dots i_{n_{RV}} \right) \qquad 2^{nRV}+1 \le j \le 2n_{RV}+2^{nRV} \qquad \text{(8.32a)}$$

where $i_1 = i_2 = \dots = i_{n_{RV}} = 0$ or ± 1

The weights for the sigma points in (8.31b) are [8.4]:

$$w_j = \left(\frac{1}{n_{rv}+2} \right)^2 \qquad 2^{nRV}+1 \le j < 2^{nRV}+2n_{RV} \qquad \text{(8.32b)}$$

8.1.4   Higher Order Approximations Using UT

The accuracy of the UT method can be improved by taking more terms into account from the Taylor series approximation in (8.3). The polynomial $g(\hat{x})$ for a fourth order approximation is:

$$g(\hat{x}) = a_1\hat{x} + a_2\hat{x}^2 + a_3\hat{x}^3 + a_4\hat{x}^4 \qquad \text{(8.33)}$$

From (8.17), a fourth order approximation requires eight equations required to find the weights and sigma points. The moments of a normally distributed random variable can be found in [8.9]. These are substituted in (8.9) to give:

$$E[\hat{x}] = \sum_{i=1}^{m-1} w_i S_i = 0$$

$$E[\hat{x}^2] = \sum_{i=1}^{m-1} w_i S_i^2 = \sigma_x^2$$

$$E[\hat{x}^3] = \sum_{i=1}^{m-1} w_i S_i^3 = 0$$

$$E[\hat{x}^4] = \sum_{i=1}^{m-1} w_i S_i^4 = 3\sigma_x^4$$

$$E[\hat{x}^5] = \sum_{i=1}^{m-1} w_i S_i^5 = 0$$

$$E[\hat{x}^6] = \sum_{i=1}^{m-1} w_i S_i^6 = 15\sigma_x^6$$

$$E[\hat{x}^7] = \sum_{i=1}^{m-1} w_i S_i^7 = 0$$

$$E[\hat{x}^8] = \sum_{i=1}^{m-1} w_i S_i^8 = 105\sigma_x^8 \tag{8.34}$$

There are four weights and four sigma points required to solve (8.34). These equations could not be solved directly using MAPLE software. Therefore, it is important to use an alternative means to simplify the calculation of the UT parameters. The method proposed here is to find a relationship between the UT technique and the integral calculation of moment.

The Gaussian Quadrature (GQ) method [8.10, 8.11] approximates the integral by selecting the optimal abscissas at which to evaluate the function. For a function $f(x)$, this is given by:

$$\int_{-\infty}^{+\infty} f(x)W(x)\,dx \cong \sum_{i=1}^{m-1} w_i f(S_i) = E[f(x)] \tag{8.35}$$

where $W(x)$ is the weighting function representing the continuous PDF, w_i are the weights and S_i are the optimal abscissas which correspond to the sigma points in UT.

Orthogonal polynomials $p_n(x)$ are a class of polynomials defined in a closed interval $[x_1, x_2]$ and are related to the weighting function by the equation [8.10]:

$$\int_{x_1}^{x_2} W(x) p_a(x) p_b(x) dx = 0 \qquad a \neq b \; ; a,b = 0,1,2,.. \qquad (8.36)$$

Using the method, the zeros of $p_n(x)$ of degree n are the optimal abscissas and correspond to the sigma points. The number of sigma points is equal to n. $p_n(x)$ is defined by the Rodrigues' formula [8.10]:

$$p_n(x) = \frac{1}{a_n W(x)} \frac{d^n}{dx^n} \left[W(x) Q^n(x) \right] \qquad (8.37)$$

where a_n is a constant and $Q(x)$ is a polynomial independent of n. Both these terms are documented in [8.10] and change according to different types of $W(x)$.

$p_n(x)$ is called a Hermite polynomial if $W(x)$ is a Gaussian distribution and a Laguerre polynomial if it is an exponential distribution. The weights for any distribution are calculated from $p_n(x)$ using the relation [8.11]:

$$w_i = \frac{1}{\left. \dfrac{dp_n}{dx} \right|_{x=S_i}} \int_{x_1}^{x_2} \frac{p_n(x)}{x - S_i} W(x) dx \qquad (8.38)$$

The generating function for a Hermite polynomial $H_n(x)$ from (8.37) is [8.10]:

$$H_n(x) = (-1)^n e^{\frac{x^2}{2}} \frac{d^n}{dx^n} \left[e^{-\frac{x^2}{2}} \right] \qquad (8.39a)$$

The recurrence relation for $H_n(x)$ from (8.39a) is [8.10]:

$$H_{n+1}(x) = x H_n(x) - n H_{n-1}(x) \qquad (8.39b)$$

These fourth order UT parameters for (8.34) are found using the Hermite polynomial at $n = 5$ within the range $(-\infty, +\infty)$:

$$S_0 = 0$$

$$S_1 = \sqrt{5 - \sqrt{10}}\,\sigma_x \quad S_2 = -\sqrt{5 - \sqrt{10}}\,\sigma_x$$

$$S_3 = \sqrt{5 + \sqrt{10}}\,\sigma_x \quad S_4 = -\sqrt{5 + \sqrt{10}}\,\sigma_x$$

$$w_0 = \frac{120}{\left(-5 + \sqrt{10}\right)^2 \left(5 + \sqrt{10}\right)^2}$$

$$w_1 = \frac{3}{4\left(5 - \sqrt{10}\right)^2} \quad w_2 = \frac{3}{4\left(5 - \sqrt{10}\right)^2}$$

$$w_3 = \frac{3}{4\left(5 + \sqrt{10}\right)^2} \quad w_4 = \frac{3}{4\left(5 + \sqrt{10}\right)^2} \qquad (8.40)$$

The generating function for a Laguerre polynomial $L_n(x)$ from (8.37) is [8.10]:

$$L_n(x) = \frac{e^x}{n!} \frac{d^n}{dx^n}\left[x^n e^{-x}\right] \qquad (8.41a)$$

The recurrence relation for $L_n(x)$ from (8.39a) is [8.10]:

$$(n + 1) L_{n+1}(x) = (2n + 1 - x) L_n(x) - n L_{n-1}(x) \qquad (8.41b)$$

The fourth order UT parameters for an exponential distribution with standard deviation σ_x are found from Laguerre polynomial at $n = 5$ at within the range $(0, +\infty)$:

$$S_0 = 3.596425771\sigma_x$$

$$S_1 = 0.2635603197\sigma_x \quad S_2 = 1.413403059\ \sigma_x$$

$$S_3 = 12.64080084\sigma_x \quad S_4 = 7.085810006\sigma_x$$

$$w_0 = 0.7594244976 \times 10^{-1}$$

$$w_1 = 0.5217556100 \quad w_2 = 0.3986668121$$

$$w_3 = 0.3611758646 \times 10^{-2} \quad w_4 = 0.2336997028 \times 10^{-4} \qquad (8.42)$$

The higher the order of an approximation, the more the weights and sigma points needed to satisfy the moment equations. There is a trade-off between computational demands and degree of accuracy.

8.1.5   Approximating the PDF of Random Variable Functions

The PDF of a function *y* can be found from that of the independent random variable *x*. Given that y has *n* roots, its PDF is defined by [8.12]:

$$f_y(y) = \frac{f_x(x_1)}{\left|\dfrac{dy}{dx}\right|_{x=x_1}} + \frac{f_x(x_2)}{\left|\dfrac{dy}{dx}\right|_{x=x_2}} + \ldots + \frac{f_x(x_n)}{\left|\dfrac{dy}{dx}\right|_{x=x_n}} \qquad (8.43)$$

where $f_x(x)$ and $f_y(y)$ are the PDFs of x and y respectively. $x_1, x_2, \ldots x_n$ are the roots of y which is a function of *x*.

For a second order UT approximation, the polynomial in (8.3) can be written as:

$$y - a_0 + a_1 x + a_2 x^2 = 0 \qquad (8.44)$$

The derivative of *y* with respect *x* is:

$$\frac{dy}{dx} = a_1 + 2a_2 x \qquad (8.45)$$

The roots of (8.37) are:

$$x = \frac{-a_1 \pm \sqrt{a_1^2 - 4a_2(y-a_0)}}{2a_2} \tag{8.46}$$

From (8.39), *dy/dx* is:

$$\frac{dy}{dx} = \pm\sqrt{a_1^2 - 4a_2(y-a_0)} \tag{8.47}$$

Assuming *x* is a normally distributed random variable, then $f_y(y)$ from (8.36) is:

$$f_y(y) = \frac{1}{\sigma_x\sqrt{2\pi}} \frac{\left[e^{-\frac{1}{2\sigma_x^2}\left(\frac{-a_1+\sqrt{a_1^2-4a_2(y-a_0)}}{2a_2}-\bar{x}\right)^2} + e^{-\frac{1}{2\sigma_x^2}\left(\frac{-a_1-\sqrt{a_1^2-4a_2(y-a_0)}}{2a_2}-\bar{x}\right)^2} \right]}{\sqrt{a_1^2-4a_2(y-a_0)}} \tag{8.48}$$

where $\bar{x}$ is the mean and σ_x is the standard deviation of *x*.

From (8.11a) and (8.11b) the sigma points are $S_1 = \sigma_x\sqrt{3}$ and $S_2 = -\sigma_x\sqrt{3}$. The weights are calculated from (8.6c), (8.11c) and (8.11d) are: $w_0 = 2/3$, $w_1 = w_2 = 1/6$. Therefore, the mean of *y* can be expressed in terms of the polynomial coefficients. This is compared with (8.6b) to give:

$$\bar{y} = a_0 + a_2\sigma_x = \frac{2}{3}y(\bar{x}) + \frac{1}{6}y(\bar{x}-\sigma_x\sqrt{3}) + \frac{1}{6}y(\bar{x}+\sigma_x\sqrt{3}) \tag{8.49a}$$

Similarly, the variance of *y* in terms of the polynomial coefficients is compared with (8.7b):

$$\sigma_y^2 = a_1\sigma_x^2 + 2a_2\sigma_x^4$$

$$= \frac{2}{3}\left[y(\bar{x})-\bar{y}\right]^2 + \frac{1}{6}\left[y(\bar{x}-\sigma_x\sqrt{3})-\bar{y}\right]^2 + \frac{1}{6}\left[y(\bar{x}+\sigma_x\sqrt{3})-\bar{y}\right]^2 \tag{8.42b}$$

From (8.2) and (8.3), $a_0 = y(\bar{x})$. The polynomial coefficients a_1 and a_2 can be found from solving (8.42a) and (8.42b) to give:

$$a_1 = \frac{1}{2\sqrt{3}}\left[y\left(\bar{x} + \sigma_x \sqrt{3}\right) - y\left(\bar{x} - \sigma_x \sqrt{3}\right)\right] \qquad (8.43a)$$

$$a_2 = \frac{1}{6}\left[y\left(\bar{x} + \sigma_x \sqrt{3}\right) - 2y\left(\bar{x}\right) + y\left(\bar{x} - \sigma_x \sqrt{3}\right)\right] \qquad (8.43b)$$

(8.43a) and (8.43b) show that the polynomial coefficients can be calculated from the weights and sigma points. The polynomial coefficients can now be used to approximate the distribution of y using (8.41). Higher order UT schemes follow a similar procedure by adopting pertinent root finding procedures. This can be obtained using in-built functions in MATLAB.

The next chapter deals with the application of the UT theory to stochastic electromagnetic problems. This is done to establish the method as a viable alternative to MC techniques. The potential drawback comes with the rapid increase in the number of design points required as the random variables and the degree of accuracy increases.

8.2   References

[8.1]   S.J. Julier and J.K. Uhlmann, "Unscented Filtering and Nonlinear Estimation," Proc. IEEE, vol. 92, pp. 401 – 402, Mar. 2004.

[8.2]   J. Zhang, "The Calculating Formulae and Experimental Methods in Error Propagation Analysis," IEEE Trans. on Reliability, vol. 55, pp. 169 – 181, June 2006.

[8.3]   B.M. Ayyub and R.H. McCuen, "Probability, Statistics and Reliability for Engineers and Scientists," 2nd Edition, Chapman and Hall / CRC Press, 2003.

[8.4]   L. R.A.X. de Menezes, A. Ajayi, C. Christopoulos, P. Sewell and G.A. Borges "Efficient Computation of Stochastic Electromagnetic Problems Using Unscented Transforms," IET Science, Measurement and Technology, vol. 2, pp. 88 – 95, Mar. 2008.

[8.5]   L. R.A.X. de Menezes, A. Ajayi, C. Christopoulos, P. Sewell and G.A. Borges, "Efficient Extraction of Statistical Moments in Electromagnetic Problems Solved with the Method of Moments" IEEE Microwave and Optoelectronics Conference, 2007.

[8.6]   L. R.A.X. de Menezes, A. Ajayi, C. Christopoulos, P. Sewell and G.A. Borges, "Extracting Statistical Moments of Output Quantities from a Small Number of Time-Domain Simulations," Proc. on Comp. Electromag. in Time-Domain, Perugia, Italy, 2007.

[8.7]   L. R.A.X. de Menezes, A. Ajayi, C. Christopoulos, P. Sewell and G.A. Borges, "Recent Advances in the Combination of the Unscented Transform (UT) with the Transmission Line Modelling Method (TLM)," Proc. of the Symp. in Honour of Prof. Wolfgang J. R. Hoefer, Technical University of Munich, May 2007.

[8.8]   E.W. Weisstein, "Bivariate Normal Distribution," From MathWorld – A Wolfram Web Resource, April 2007. Available Online:

http://mathworld.wolfram.com/BivariateNormalDistribution.html

[8.9]   E.W. Weisstein, "Normal Distribution," From MathWorld – A Wolfram Web Resource, April 2007. Available Online:

http://mathworld.wolfram.com/NormalDistribution.html

[8.10]   M. Abramowitz, and I.A. Stegun, "Handbook of Mathematical Functions with Formulas, Graphs, and Mathematical Tables", New York: Dover, pp. 887-888, 1972.

[8.11]   E.W. Weisstein, "Gaussian Quadrature," From MathWorld – A Wolfram Web Resource, July 2007. Available Online:

http://mathworld.wolfram.com/GaussianQuadrature.html

[8.12]   A. Papoulis, "Probability, Random Variables and Stochastic Processes," 2nd Edition, New York, NY: McGraw-Hill, 1984.

Chapter 9   Application of UT to Stochastic Problems

This chapter presents the application of the UT theory to stochastic electromagnetic problems. The case studies here are analysed in the time and frequency domains. The approximation of moments using UT is compared with the benchmark MC method.

9.1   Application of UT to Time Domain Problems

This section presents the measurement of uncertainty in electromagnetic problems modelled the time domain. The elegance of the UT approach is that it does not require any modifications to the preferred modelling algorithm. A deterministic set of sigma points and weights constitute the UT parameters to be identified. These depend on the number of random variables and the order of approximations to be attained. The overall number of simulations needed is much smaller than required when using the classical MC method. The UT parameters are then used to approximate the statistical moments of interest.

In the time domain, the interaction between neighbouring nodes in a discretised problem space can be characterised using the global matrix equation in (6.19). This can be rewritten as:

$$_k\underline{V}_i = \underline{\underline{C}} \cdot \underline{\underline{S}} \cdot {}_{k-1}\underline{V}_i \qquad (9.1)$$

where $\underline{\underline{C}}$ and $\underline{\underline{S}}$ are the global connect and scatter matrices respectively. $_k V_i$ is global vector that contains incident port voltages at time step k.

It is possible to further simplify (9.1). This involves the elimination of the dependency on the previous time step:

$$_k\underline{V}_i = \left[\underline{\underline{C}} \cdot \underline{\underline{S}}\right]^k \cdot {}_0\underline{V}_i \qquad (9.2)$$

For time domain problems with stochastic parameters, it is clear that a finite series approximation of (9.2) would deteriorate with increasing number of time steps. Therefore, the accuracy of the UT method will be better for a smaller number of time steps.

The case study shown in Fig. 9-1A comprises of a TEM line modelled using the time domain MEPHISTO TLM solver in [9.1]. The line has a spatial discretisation Δl of 1 mm and is terminated at either end with absorbing boundaries. The dimensions of the guide are 30 X 1 mm. Material 1 is deterministic with relative permittivity of 1. Material 2 is represented by a random variable with mean relative permittivity of 8 varying normally with a variance of 0.4. The geometry of the dielectric materials and their respective positions are also shown. Both dielectrics are 10 mm apart and are separated from either end of the guide by 5 mm. Input and output points in the TEM guide are defined for the excitation and observation of fields respectively. These are shown in Fig. 9-1B. A unit impulse function is applied at the input point and the voltage is sampled at the observation point.
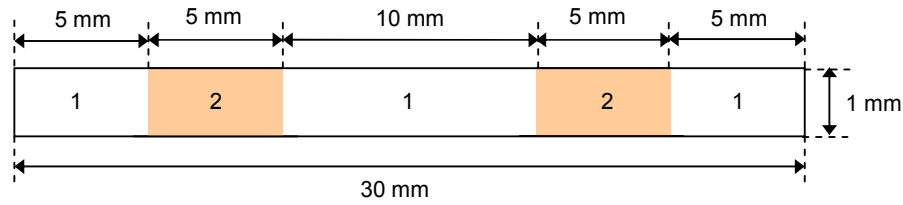
Fig. 9-1A TEM line with two stochastic dielectric materials
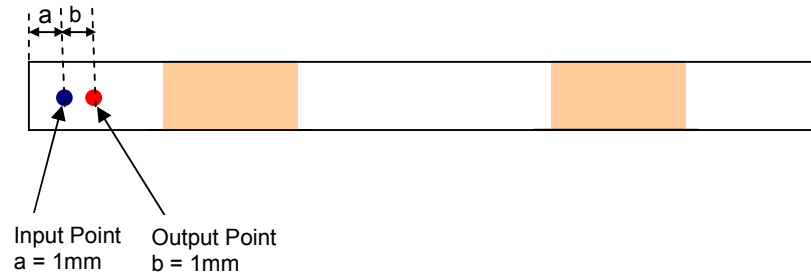
Fig. 9-1B TEM waveguide with input and output points

The second order UT method uses the parameters defined in (8.11) while the fourth order approach uses (8.35). The second order and fourth methods require three and five sigma points respectively. These second and fourth UT methods are applied to the observed voltage and are compared with 40,000 MC simulations. Each simulation for both methods takes 0.72s on a PC with a AMD Athlon 2.01GHz processor. The mean voltage at the output point for the first 120 time steps is shown in Fig. 9-2A.
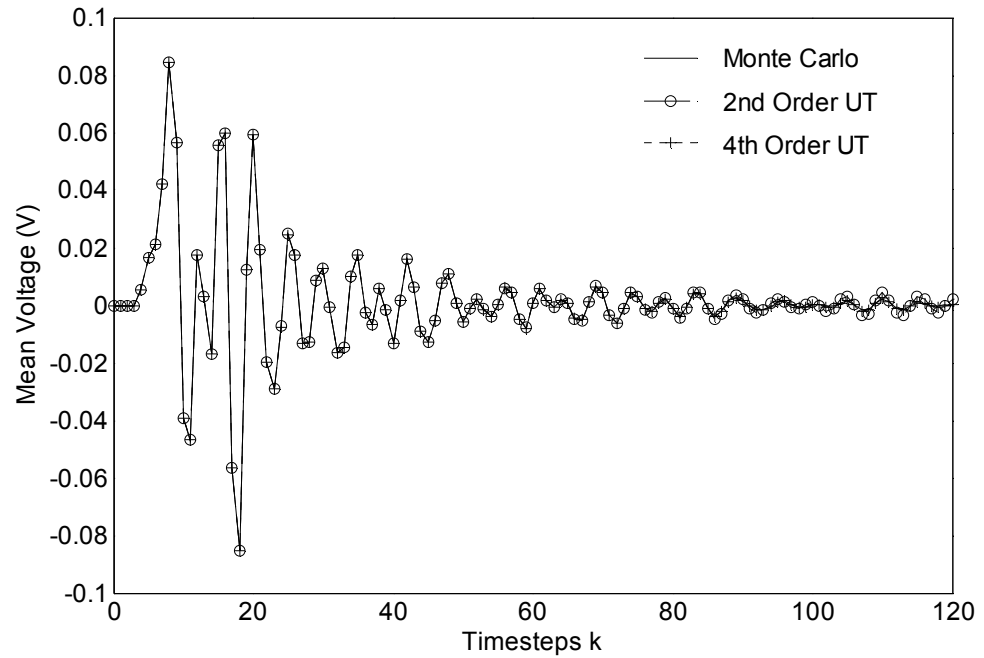
Fig. 9-2A Comparison between the MC and UT approximations of mean voltage for TEM guide

The agreement between the methods is found to deteriorate with increasing time steps k. This is not clear from Fig. 9-2A. To illustrate this effect, the mean voltage is shown from between time steps $k = 60$ and $k = 120$ in Fig. 9-2B. The second order UT approach begins to deviate from the MC method after $k = 85$. The fourth order UT deviates after $k = 115$. Therefore, the higher the order of the UT method the longer it is in agreement with the MC simulations in the time domain.
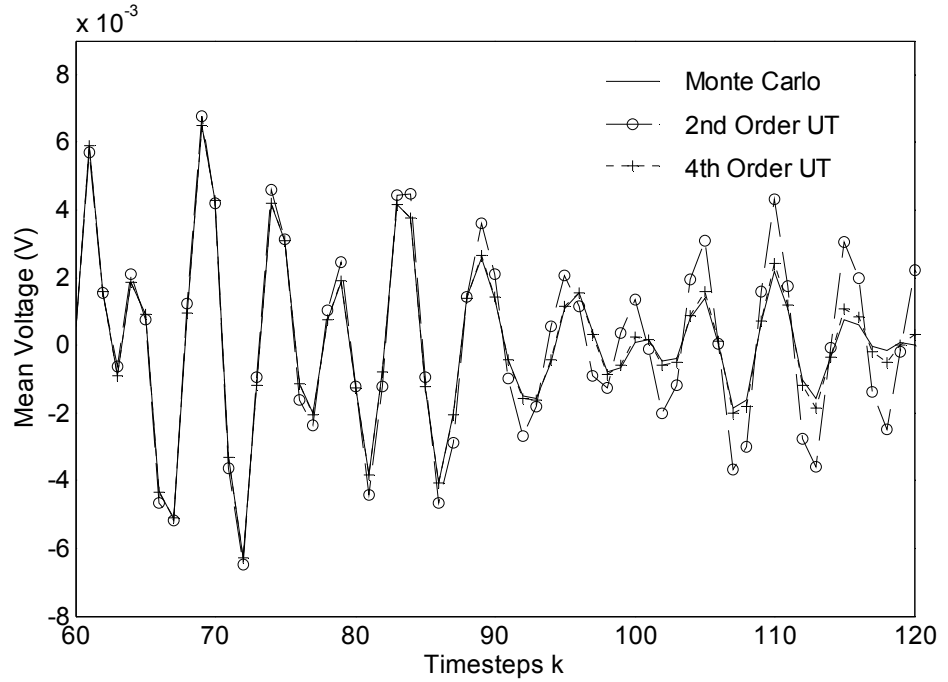
Fig. 9-2B Comparison between the MC and UT approximations of mean voltage for TEM guide between k = 60 and k = 120

The standard deviation of voltage at the output point is also approximated using both the UT and MC methods. The results are shown after the first 120 time steps in Fig. 9-3A. The agreement between methods here also deteriorates with increasing time steps. However, as the standard deviation is a higher order moment than the mean, it is expected that disagreement occurs in a shorter period. The standard deviation σ_V is shown from between the $k = 60$ and $k = 120$ in Fig. 9-2B. The second order UT approach begins to deviate from the MC method after $k = 70$ and the fourth order UT deviates after $k = 75$. These results pose a challenge on how to increase the order of UT approximations with time steps. This is not dealt with here but is a challenging problem for future research.
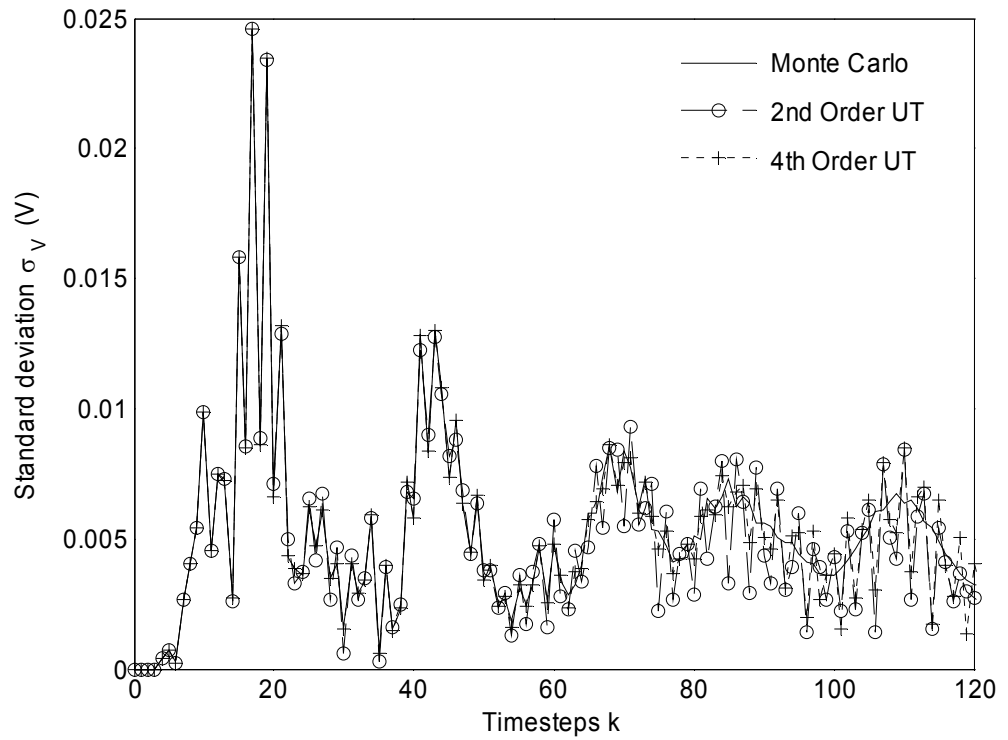
Fig. 9-3A Comparison between the MC and UT approximations of standard deviation of voltage for TEM guide
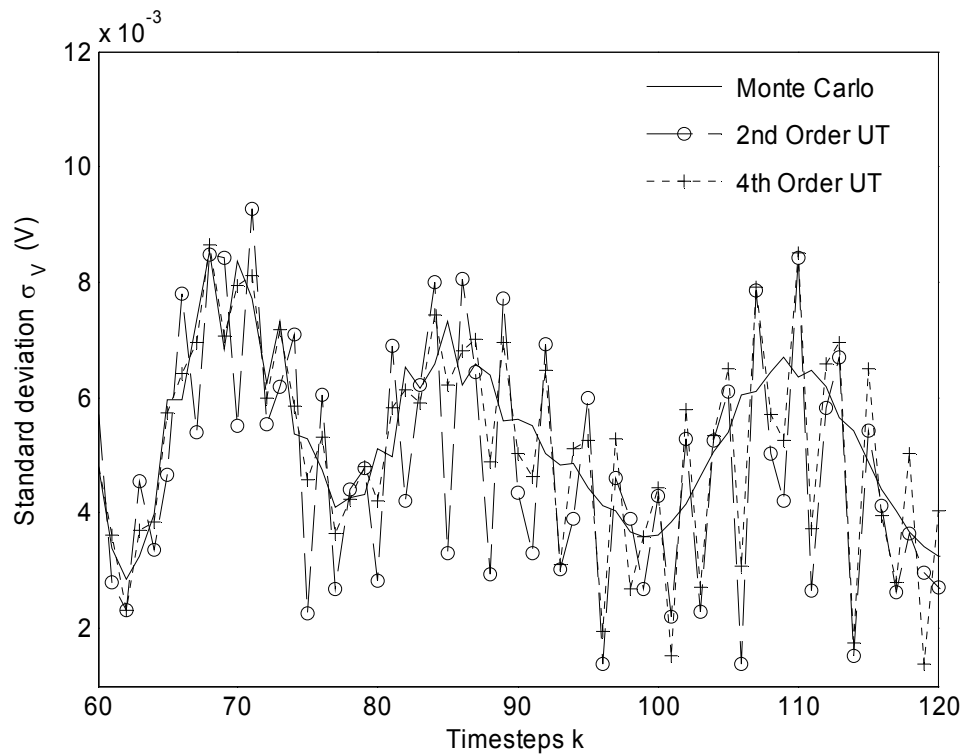
Fig. 9-3B Comparison between the MC and UT approximations of standard deviation of voltage for TEM guide between k = 60 and k = 120

The electric field at the output point is the ratio of the observed voltage to the cell size. This quantity randomly varies with stochastic relative permittivity. The probability density function (PDF) of electric field is approximated using the UT approach described in sub-section 8.1.3. The second and seventh order UT approximations are compared with the PDF obtained using the MC method at $k = 10$. The results from these comparisons are shown in Fig. 9-4. The agreement between methods further endorses the UT as a good alternative to time consuming MC method.
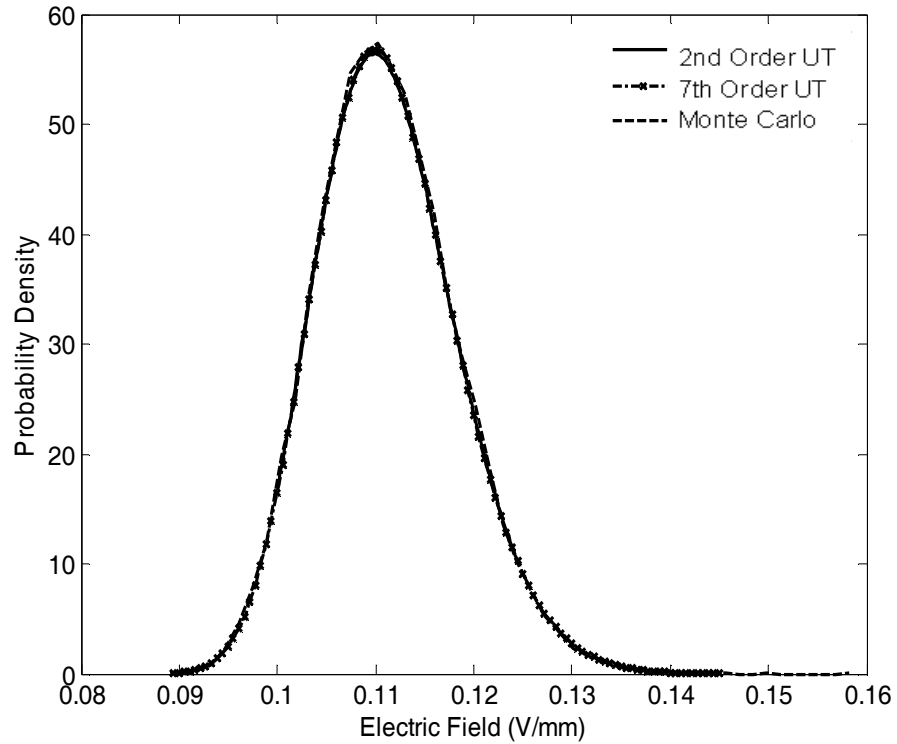
Fig. 9-4 Comparison between the MC and UT approximations of the probability distribution function at k = 10

The impact of increased time steps on the PDF of the electric field is now considered. From the results obtained when $k = 30$ in Fig. 9-5, it is clear that the moments of the PDF change. The discrepancy between the UT and MC methods becomes more pronounced. This is consistent with the behaviour observed before where the UT approximation degrades with increasing time steps.
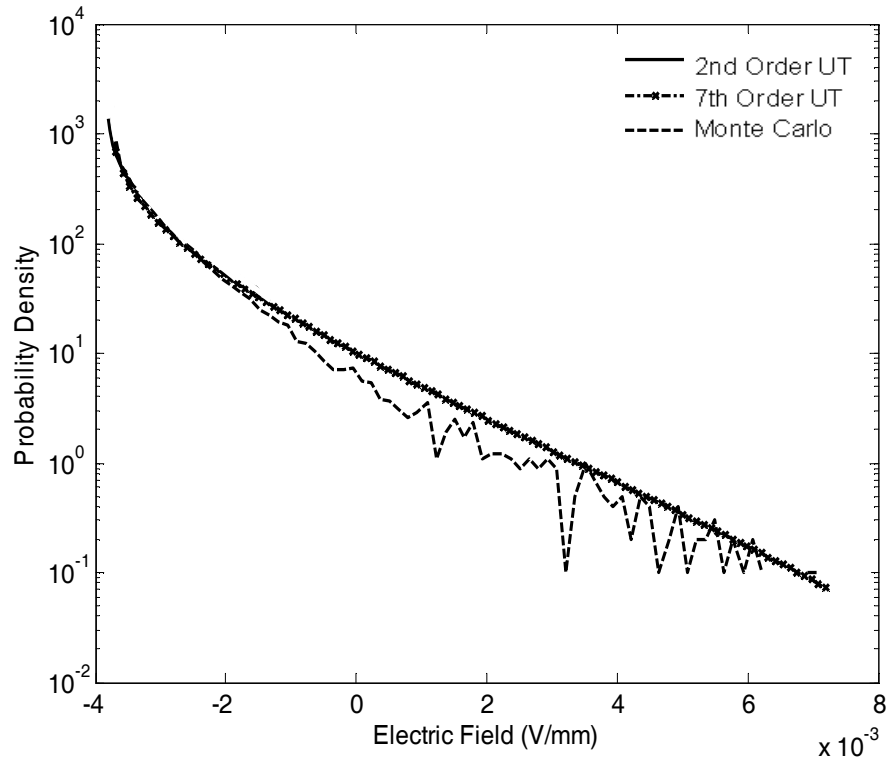
Fig. 9-5 Comparison between the MC and UT approximations of the probability distribution function at k = 30

9.2   Application of UT to Frequency Domain Problems

The problem defined in Fig. 9-1A is now assessed over a range of frequencies. The maximum frequency of the problem is inversely proportional to two times the total number of time steps. This is consistent with the Nyquist criterion for sampling. The scattering parameter S_{11} describes the reflection coefficient at the input point. This is given by the expression:

$$S_{11} = \frac{FFT\left(V_1\right) - FFT\left(V_2\right)}{FFT\left(V_1\right)} \tag{9.3}$$

where $FFT\left(V_1\right)$ is the frequency response in the TEM line with material 2 absent and $FFT\left(V_2\right)$ the frequency response with material 2 present.

S_{11} is calculated at certain frequencies f for the UT sigma points and 40,000 MC simulations of random relative permittivity. The maximum frequency for this problem is f_{max}. The mean of S_{11} magnitude and phase is computed from these results and is presented in Fig. 9-6A and Fig. 9-6B respectively.

There is good agreement between the UT and MC approximation methods. The fourth order UT method gives better results throughout the range displayed than the second order method. The second order UT mean of S_{11} magnitude begins to deviate from the MC method when the normalised frequency ratio f/f_{max} is 0.096. The same approximation of the mean of S_{11} phase shows a similar trend at the same frequency ratio. The fourth order approximation of the mean of S_{11} magnitude is good throughout the range of frequencies considered. The same however cannot be said of the mean of S_{11} phase which deviates when the normalised frequency ratio is 0.096.

The approximation of standard deviation of S_{11} magnitude and phase is considered in Fig. 9-7A and Fig. 9-7B respectively. The discrepancies between UT and MC results now occur at an earlier stage than that of the mean. For the case of S_{11} magnitude this occurs at the normalised frequencies of 0.05 and 0.07 for the second and fourth order UT results respectively. The S_{11} phase shows a noticeable deviation from the MC results at normalised frequencies of 0.044 and 0.088 for the second and fourth order UT results respectively.
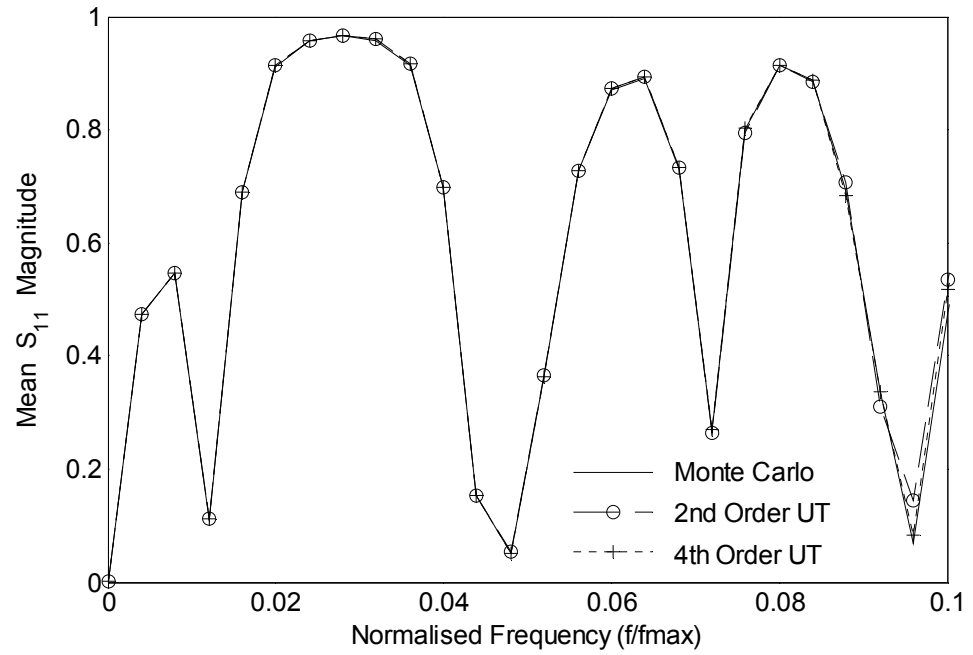
Fig. 9-6A Comparison between the MC and UT approximations of the mean S_{11} Magnitude
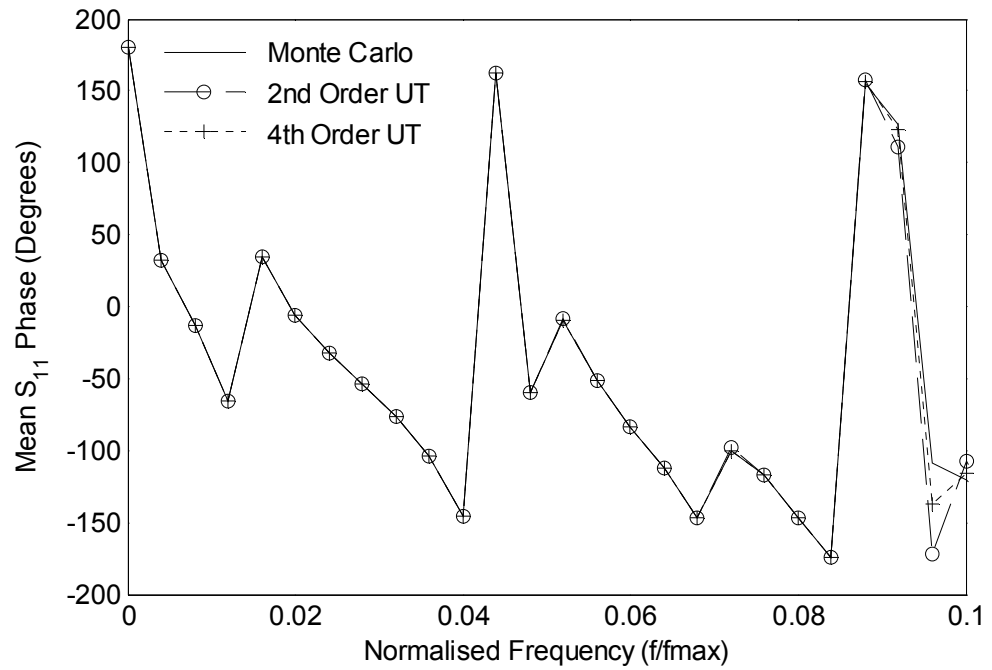
Fig. 9-6B Comparison between the MC and UT approximations of the mean S_{11} Phase
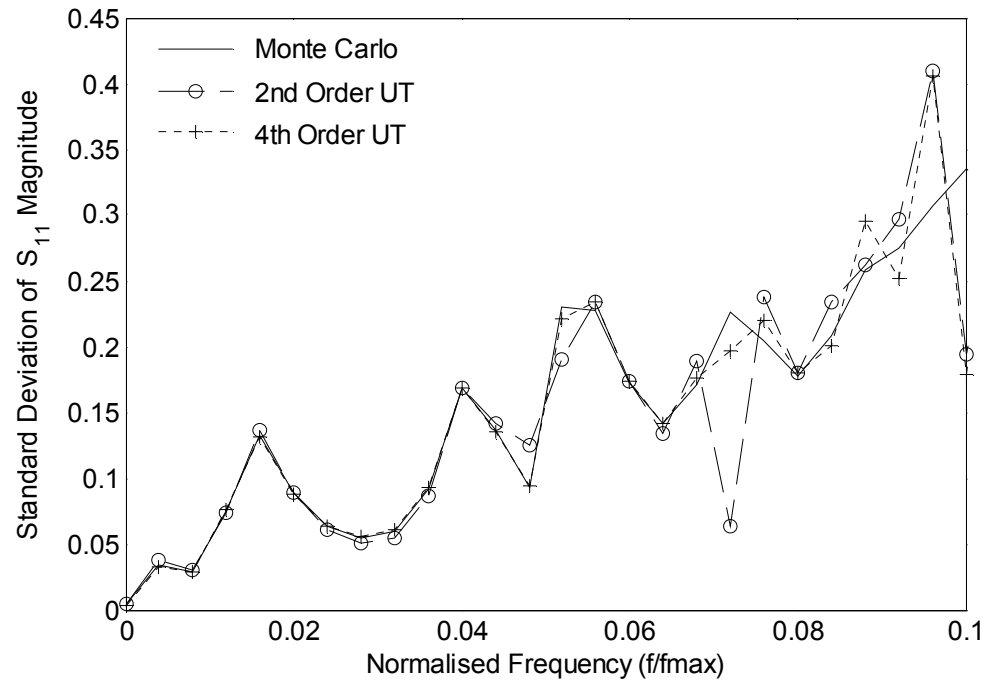
Fig. 9-7A Comparison between the MC and UT approximations of the standard deviation of S_{11} Magnitude
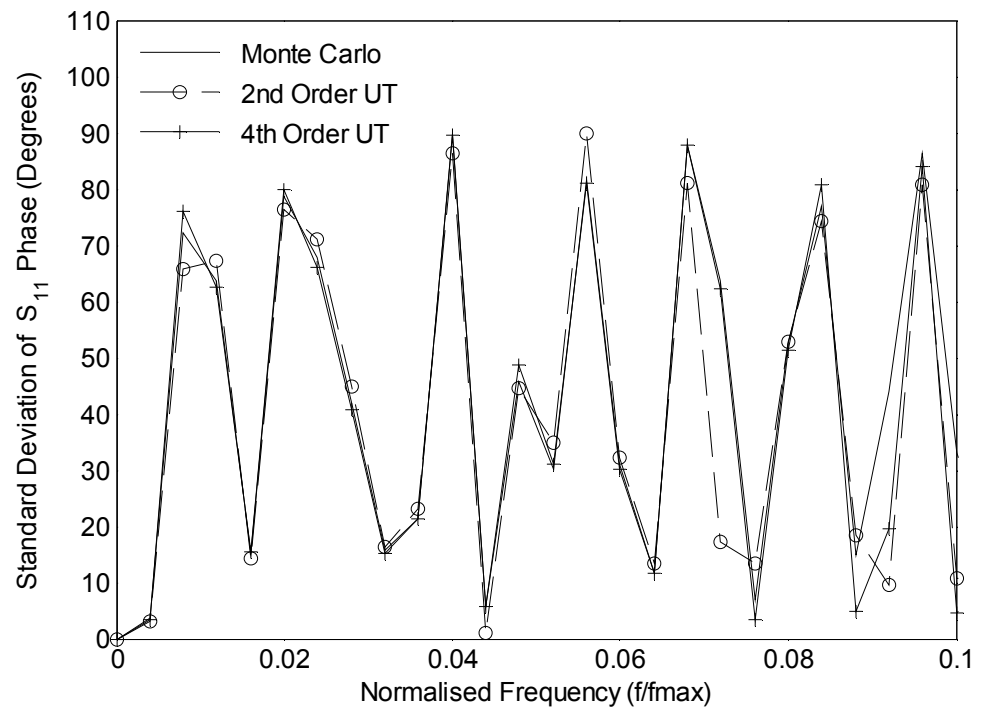
Fig. 9-7B Comparison between the MC and UT approximations of the standard deviation of S_{11} Phase

189

The PDF of the electric field at the output point in Fig. 9-1A can be approximated at a specific frequency from sub-section 8.1.5. The example illustrated in Fig. 9-8 is the electric field PDF when the input frequency is 8.48 GHz. The second and seventh order UT approximations show good agreement with the MC method.
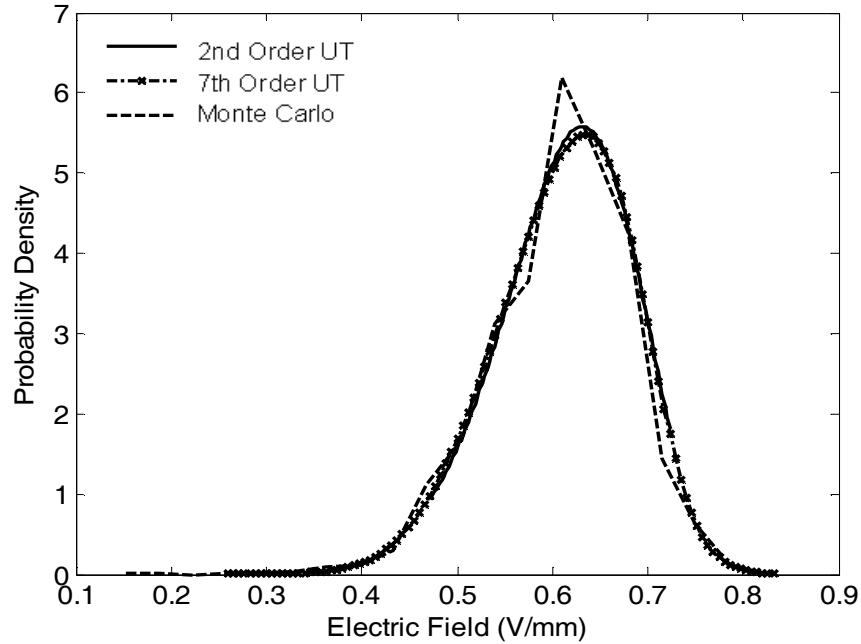
Fig. 9-8 Comparison between the MC and UT approximations of the probability distribution function at a frequency of 8.48GHz

The next problem involves the coupling of two wire monopoles in a metallic box as shown in Fig. 9-9. This detailed description of the theoretical coupling model between the monopoles and waveguide in the frequency domain is found in [9.2 – 9.3]. Uncertainty in the length and position of one wire monopole affects the coupling with the other in the box. The parameter of interest S_{21} is calculated in [9.2]. This is the ratio of the voltage at the receiving monopole to the voltage of the transmitting monopole in the frequency domain. The random variables considered for this problem are normal. These include the length of the receiving wire and its position in *x-z* plane. The MC method runs for a total of 10,000 simulations which lasts about 6 hours on a PC with a AMD Athlon 2.01GHz processor. Using the approach described in sub-section 8.1.3, a total of 15 sigma points are required for a second order UT approximation.

The box used has dimensions used 36 x 12 x 42 cm. Both wire monopoles are perpendicular to the $x - z$ plane. The variations in wire lengths are not long enough to make a significant difference to the box resonances. The transmitting wire has a length of 3.5cm and is placed at co-ordinates $x =$ 18 cm and $z = 6$ cm. The receiving wire has a mean length of 0.5 cm with uncertainty in x and z positions. The mean position of the recieving wire is at $x = 18$ cm, $z = 36$ cm. The position of both monopoles at the centre box in the *x-y* plane implies only odd harmonics are observed. The first and third modes are considered for this problem. The variance of all the random variables is fixed at 0.28868 cm.
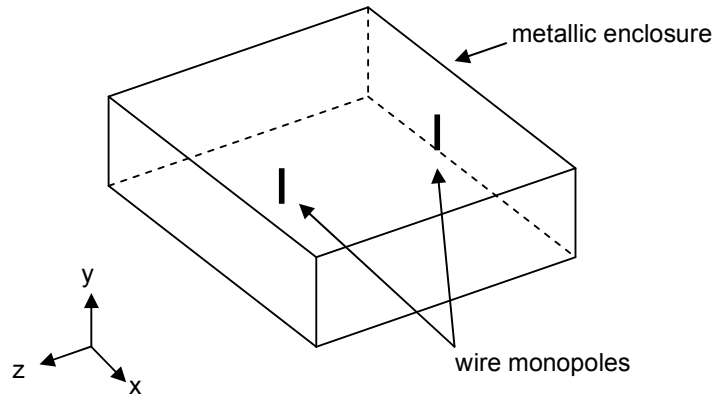
Fig. 9-9 Coupling between two wire monopoles in a metallic enclosure

The sigma points and weights are found from (8.31a) – (8.32b). These are combined to find the UT approximation of the average S_{21} coupling between the fixed and non-deterministic monopoles using (8.6b). Fig. 9-10A shows the comparison between the MC and UT approximations for the average S_{21} coupling over a range of frequencies. The results show good agreement between the two methods. The UT approximation of the standard deviation of S_{21} coupling is calculated using (8.7a). The results for this compared with the MC method and presented in Fig. 9-10B. As the frequency increases, the discrepancy between the methods becomes more evident. The skew and kurtosis of the S_{21} coupling can be approximated with UT using (8.12a) and (8.12b) respectively. The results for the skew using UT are compared with MC in Fig. 9-10C. In general, the skew is positive except at the frequencies corresponding to the box resonance. Both methods appear to be in close proximity over the displayed

frequency range. The same applies to the kurtosis using both methods as shown in Fig. 9-9D. These results support the use of UT as a viable alternative to the conventional MC method in statistical EMC analyses [9.4].
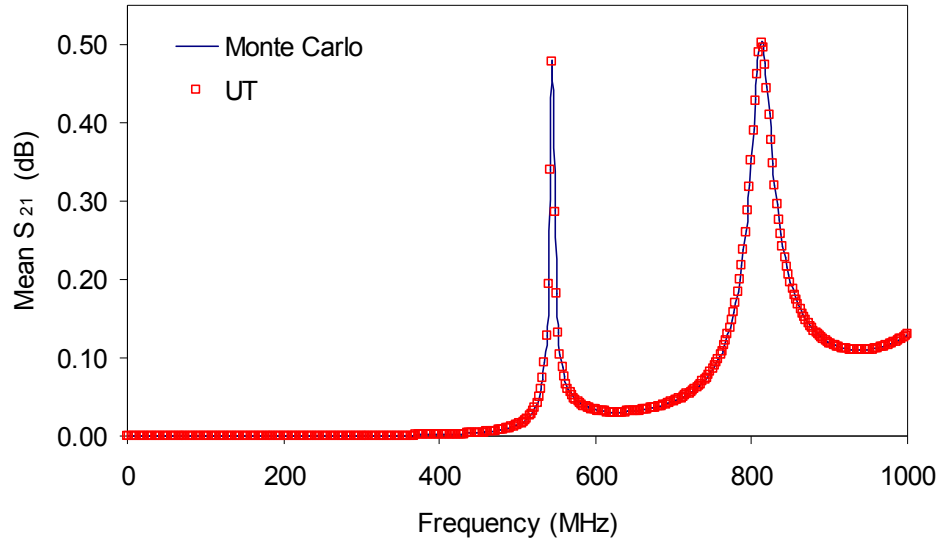
Fig. 9-10A Comparison between the MC and UT approximations of the mean S_{21} coupling between monopoles
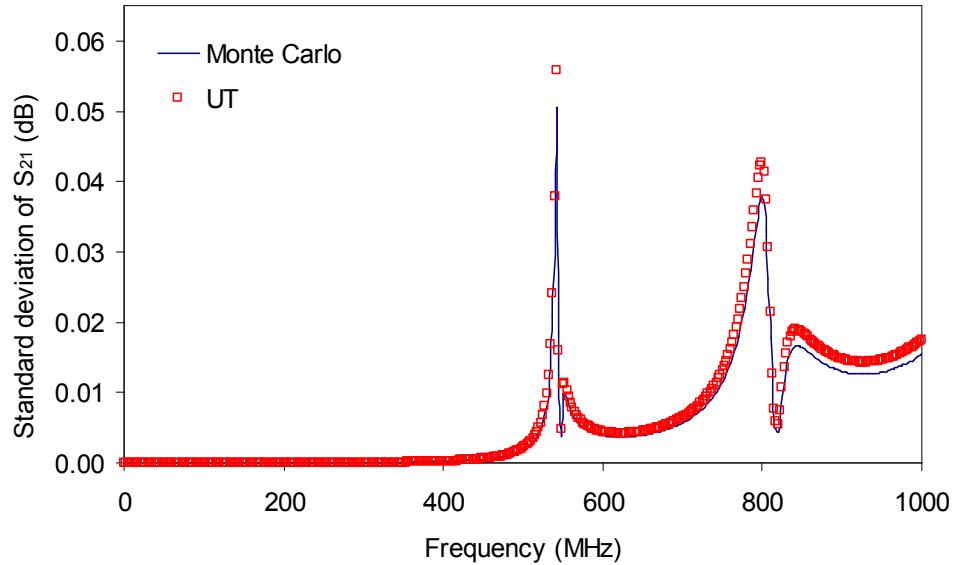
Fig. 9-10B Comparison between the MC and UT approximations of the standard deviation of S_{21} coupling between monopoles
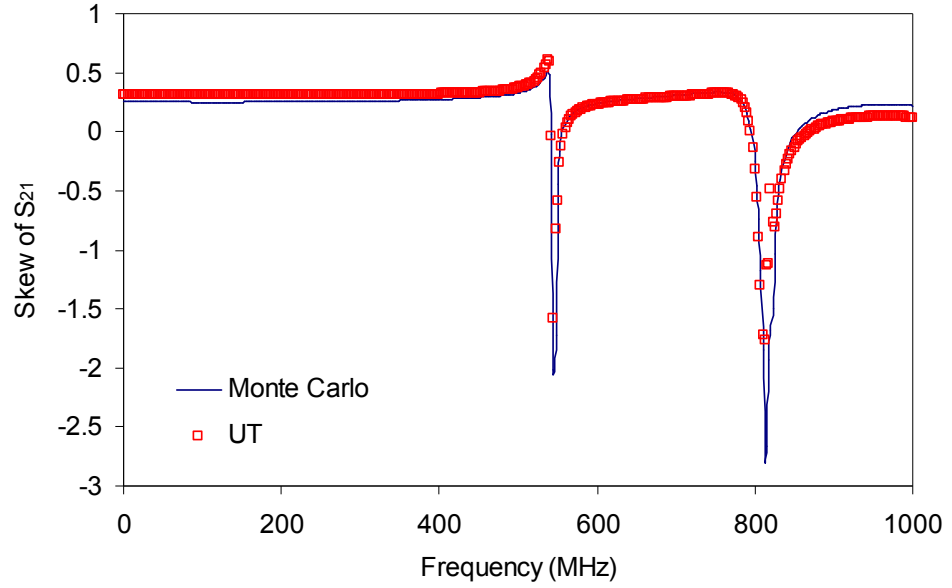
Fig. 9-10C Comparison between the MC and UT approximations of the skew of S$_{21}$ coupling between monopoles.
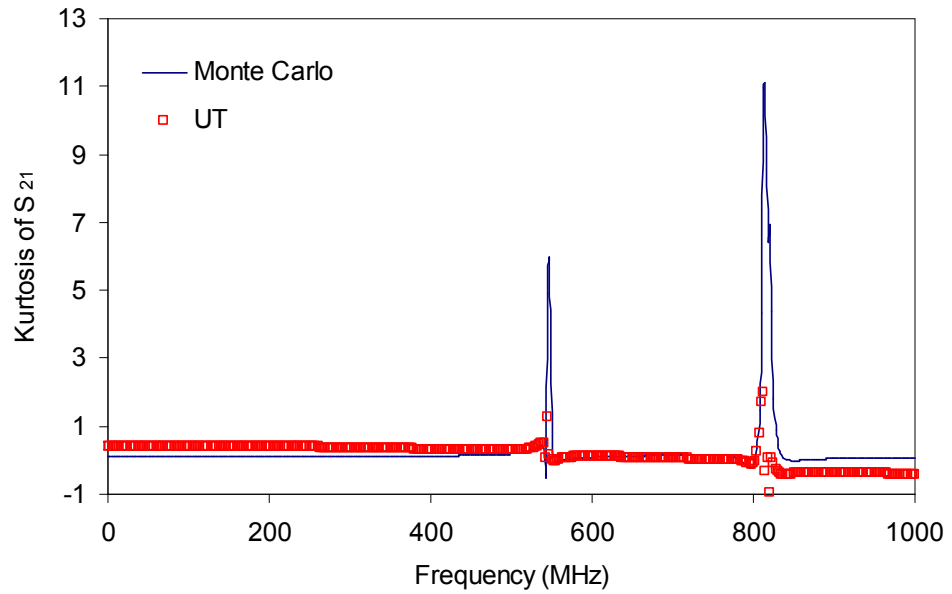
Fig. 9-10D Comparison between the MC and UT approximations of the kurtosis of S$_{21}$ coupling between monopoles

The correlation between the logarithm of voltage at the receiving monopole and each of the input random variables in the *x, y* and *z*-directions for MC and UT

results are shown in Fig. 9-10E and Fig. 9-10F respectively. There is a close relationship between the methods across the displayed frequency range.
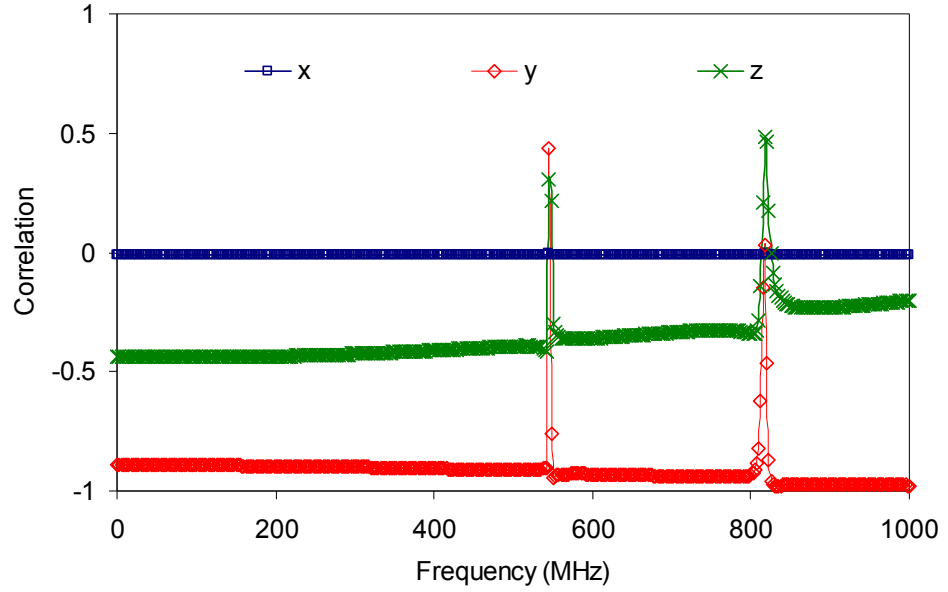
Fig. 9-10E MC results of correlation between x, y and z-directions and logarithm of measured voltage at receiving monopole
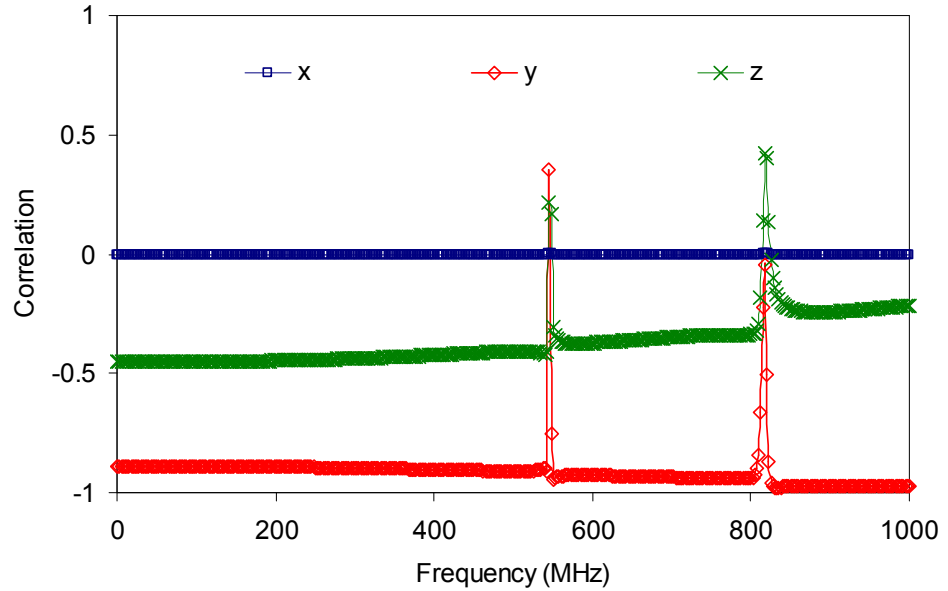
Fig. 9-10F UT results of correlation between x, y and z-directions and logarithm of measured voltage at receiving monopole

The results show that zero correlation occurs in the *x*-direction which means that variation in this direction is insignificant on measured voltage. This is because the monopoles are in the *y-z* plane. This also explains why there is greater correlation in the *y* and *z*-directions. Maximum correlation between *y* and *z*-directions and measured voltage occurs at resonance points.

The effect of correlation between two random variables is considered next. The standard deviation of the fundamental resonant frequency σ_{fr} of a waveguide is assessed in the presence of statistically dependent media as shown in Fig. 9-11A. The two stochastic materials with relative permittivities ε_{r1} and ε_{r3} are separated by a deterministic medium with relative permittivity ε_{r1}. Fig. 9-11A illustrates the relationship between σ_{fr} and the correlation coefficient ρ_{13}. Fig. 9-11B shows the percentage difference between 100,000 converged MC simulations and the second order UT approach as the correlation coefficient between the two discrete dielectric materials in a rectangular waveguide is varied. The UT method for this case study uses the set of equations derived in (8.30) to estimate the variance in (8.7d).   Fig. 9-11B shows the percentage difference between converged MC simulations and the UT approach as the correlation coefficient between the two discrete dielectric materials is varied. From the results, the percentage difference is minimum when both variables are correlated, that is when $\rho_{13} = 1$, and remains acceptably low across the complete range of correlations. The second order UT approximation of standard deviation performs much better than the first order DST method used for the same case study in chapter 6. This is another configuration in which the higher the order of an approximation the more accurate the results.
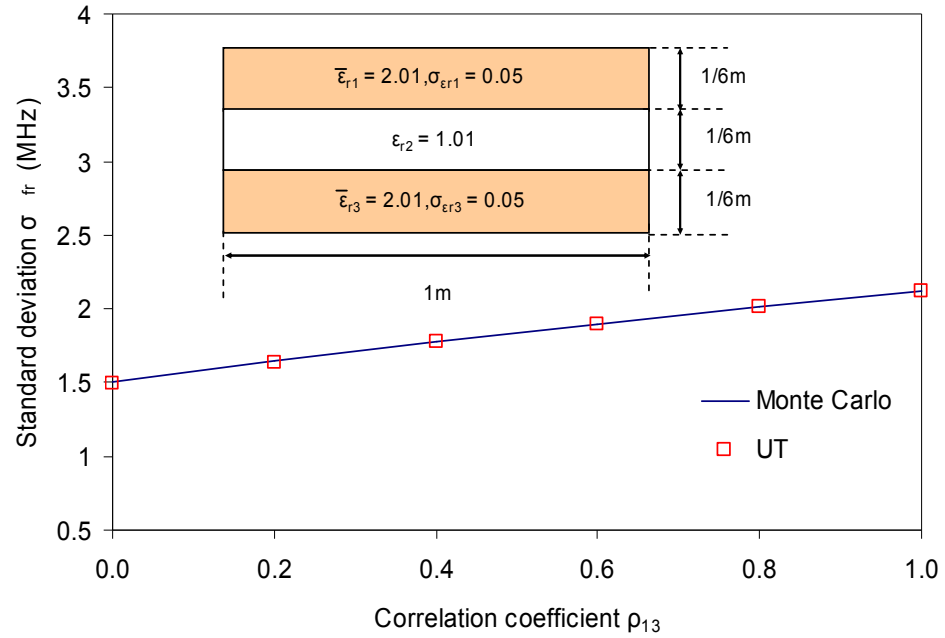
Fig. 9-11A Effect of statistical dependency of two dielectric slabs using the correlation coefficient between them
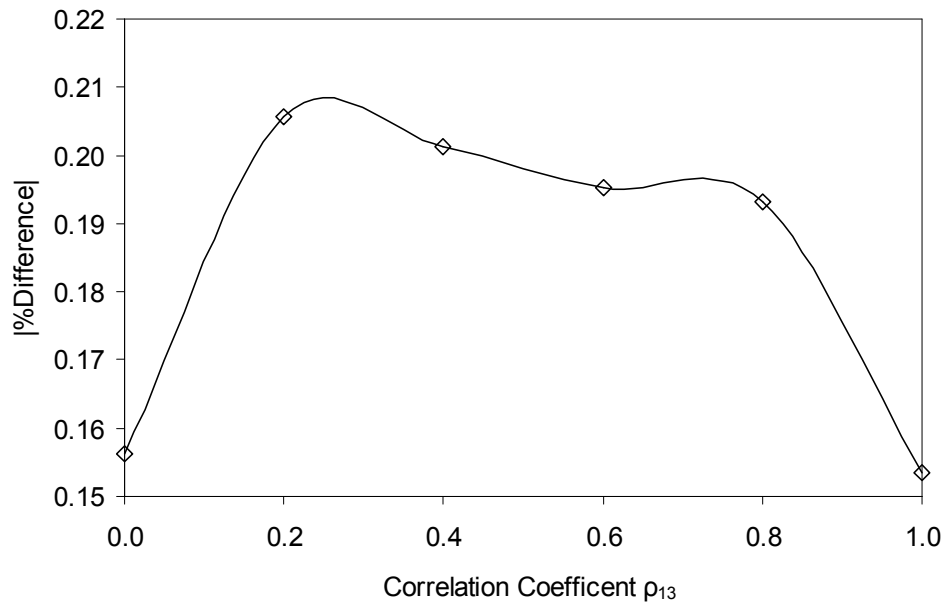
Fig. 9-11B Percentage difference between the converged MC simulations and UT methods for waveguide in Fig. 9-11A

The final case study involves finding the kurtosis of an exponentially distributed relative permittivity of a random variable using UT. The case study is a

stochastic floating dielectric in a waveguide as shown in Fig. 9-12A. This result could not be obtained using DST as explained in Appendix A. The weights and sigma points for the fourth order UT approximation are provided in (8.42). The solutions of the weights and sigma points are used to calculate kurtosis from (8.12b).

The central slab in Fig. 9-11A is stochastic with an exponential distribution of mean relative permittivity of 2.01 and increasing standard deviation values. The surrounding medium is not a random variable and has relative permittivity ε_{r1} of 1.01. The fourth order UT kurtosis approximation is compared with that from 100,000 MC simulations. The results are shown in Fig. 9-12A. The percentage difference between both methods is shown in Fig. 9-12B. Again, the higher the standard deviation of relative permittivity the greater the discrepancy between the two methods.
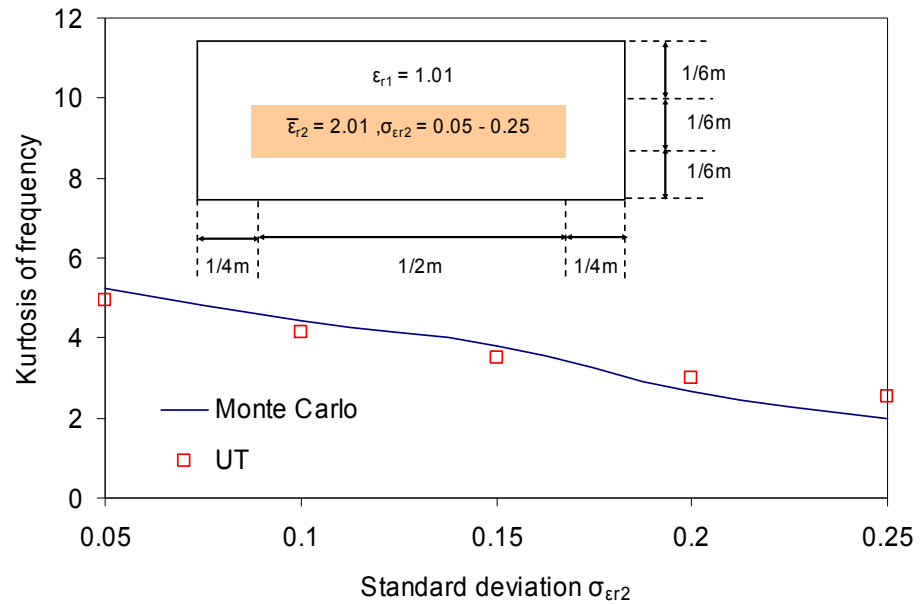
Fig. 9-12A Comparison between the MC and UT approximation of the kurtosis of fundamental resonance for a floating dielectric slab in a waveguide
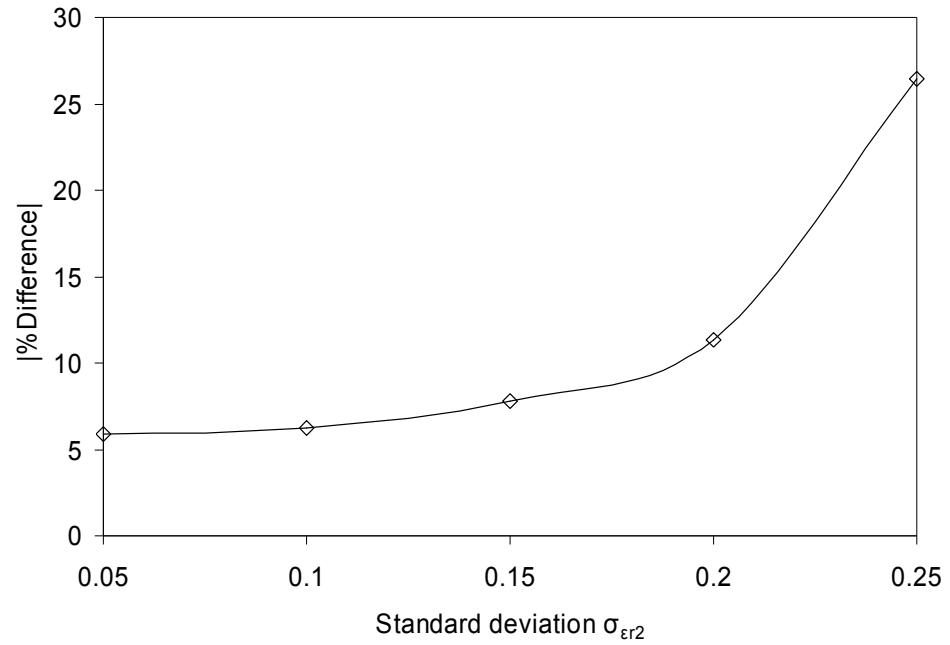
Fig. 9-12B Percentage difference between the converged MC simulations and UT methods for waveguide in Fig. 9-12A

In the next chapter, the conclusions to this thesis are presented. The findings of the research are summarised and suggestions are made for further work.

9.3   References

[9.1]   P.P.M. So and W.J.R. Hoefer, MEFiSTo-2D Classic, April 2007, Available Online: http://www.faustcorp.com/

[9.2]   T. Konefal, J.F. Dawson, A. Denton, T.M. Benson, C. Christopoulos, A.C. Marvin, S.J. Porter and D.W.P. Thomas, "Electromagnetic Coupling Between Wires Inside a Rectangular Cavity Using of Multiple Mode Analogous Transmission Line Circuit Theory" IEEE Trans. on Electromag. Comp., Aug. 2001, vol. 43, pp. 273 – 281.

[9.3]   A. Nanni, D.W.P. Thomas, C. Christopoulos, T. Konefal, J. Paul, L. Sandrolini, U. Reggiani and A. Massarini "Electromagnetic Coupling Between Wires and Loops Inside a Rectangular Cavity Using Multi-Mode Transmission Line Theory" EMC Europe 2004 International Symp. on Electromag. Comp., Eindhoven-Netherlands, pp. 609 – 614, Sep. 2004.

[9.4]   L. R.A.X. de Menezes, D.W.P. Thomas, C. Christopoulos, A. Ajayi and P. Sewell, "The Use of Unscented Transforms for Statistical Analysis in EMC, EMC Europe 2008 International Symp. on Electromag. Comp., Hamburg-Germany, Sep. 2008.

Chapter 10   Conclusions

The main contribution of this research work is to formulate computationally efficient methods for approximating statistical moments in electromagnetic problems. This chapter presents a summary of the findings in this thesis and some general conclusions on the development and use of the proposed methods. Recommendations for future research are also briefly discussed.

10.1   Development of the Direct Solution Technique (DST)

The DST approach for performing electromagnetic simulations in the presence of statistically defined input parameters is introduced in this thesis. Based upon Taylor's series approximations, it was possible to explicitly provide rapid approximate solutions that obviate the need for extremely slowly converging and time consuming MC analysis of multiple simulations. The scope of the DST has been explored and initial observations made upon both the degree of problem complexity and the extent of stochastic variation permitted and the accuracy compared with exhaustive multiple simulations.

Several computational modelling tools are available in electromagnetic research are based on the use of matrix algebra. The TLM was the preferred choice in this thesis due to its widespread use in the laboratory and excellent stability. The challenges of using the MC method in 1-D electromagnetic problems in the time domain were explored in chapter 4. For problems with explicit differentiable parameters, the statistical moments can be approximated from the Taylor series. However, for instances where this is not possible, numerical solving techniques are used. This was the motivation for developing an approximation technique that was compatible with numerical electromagnetic models.

The main advantage of using DST for stochastic problems in TLM is that it was formulated to work on matrices. This was demonstrated in chapter 5. A simple test circuit that represents transmission line models with stochastic impedances was used. The aim was to use DST to approximate the statistical moments of mesh currents. The first and second derivatives of current are found to be related to the voltage vector, impedance and admittance matrices. The accuracy of the DST method was shown to improve when higher order current derivatives and impedance moments were considered. The DST method is shown to work on problems with different probability distribution functions. The normal and exponential distribution types were used in this thesis to emphasise this point. The odd moments of a normal distribution made no contributions to improved accuracy of the mean. The higher order moments included in DST approximations gave better agreement with the MC method. This effect was more pronounced for stochastic variables with exponential distribution than for normal case. With the foundation of DST now in place, the onus was to apply the method to more challenging problems.

10.2 Application of DST to Stochastic Electromagnetic Problems

Following the success of the DST approach on a matrix algebra problem, it was then applied to case studies modelled in 2-D and 3-D frequency domain TLM. Both methods involved the use of connect and scatter matrices combined to reflect the physical scenario being studied. The type of problem defined determines whether either or both these matrices are differentiated to find sensitivity parameters of interest. Once this is established, the relevant statistical moments can be calculated.

In chapter 6, the DST was applied to 2-D waveguides with stochastic dielectrics. As the fundamental resonant frequency f_r was the parameter being measured, the DST involved the approximation of its statistical moments. The validity of the method for approximating the standard deviation of f_r was verified with an analytical approximation approach. The first order second moment

approximation f_r showed favourable comparison with MC method based on repeated use of the deterministic TLM solvers. The percentage difference between both methods was consistently shown to increase with standard deviation of random variables. A wide range of other waveguide problems was studied to further illustrate the efficacy of the DST. These included case studies with material correlation effects and those with irregular and movable boundaries. The general conclusion is that the DST does not require higher order moments for stochastic input variables with small variability.

The effect of statistical dependency between two dielectrics with stochastic relative permittivities on f_r was investigated. The standard deviation of percentage difference between DST and MC methods was highest between a correlation coefficient of zero and one.

The impact of higher order derivatives on approximation of statistical moments was more evident for a dielectric with an exponential distribution of relative permittivity than normal distribution.

The DST was also applied to a 2-D problem with absorbing boundaries. The configuration was a set of four wires with random radii in a rectangular enclosure with absorbing boundaries. The TLM wire node was used to devise the numerical model from which shielding effectiveness of the wire screen was calculated. The mean and standard deviation of the shielding effectiveness approximated from the DST was consistent with that found from the MC method. This demonstrated that the method can also be applied to more general problems with non-reflecting boundary conditions.

In chapter 7, the 3-D SCN was used to model a 2-D cross-section of a waveguide. The idea here was to prove that the DST was not only restricted to 2-D TLM problems. Due to prohibitive computation demands to obtain MC benchmark results more challenging 3-D problems were not dealt with here. The results from case studies investigated showed results consistent with chapter 6. However, because the model efficiency is increased in the 3-D case, there was better agreement between the DST and MC methods than for the 2-D equivalent.

This proves that although the effort to improve a model might be computationally expensive it gives a better platform for statistical analysis. The fact that DST drastically cuts down the computational overhead endorses it as a very attractive option for 3-D statistical analysis.

From the results discussed in this section, the development and application of the DST meets the need of quick and precise approximations of uncertainties associated with model outputs provided input variations are small.

10.3   Development of the Unscented Transform (UT) Method

The theory behind the UT method was explained in chapter 8. The motivation for using this method was because it was adaptable to black-box type models. This implies that the mathematical details of the models it is applied on need not be defined explicitly. The statistical moments are approximated using a power series of standard random variables with unknown coefficients. The distribution of the input random variables are sampled at deterministic sigma points which are assigned with weights. The conventional approach for calculating statistical moments of discrete distribution functions is applied to these UT parameters. Therefore, the accuracy of approximations is directly related to the number of weights and sigma points. A set of equations are obtained that need to be solved to find the UT parameters. These equations increase with the number of input random variables. The identification of the sigma points help point out which model input samples contribute the most to output uncertainties. The weights are needed together with the sigma points to approximate the statistical moments of model outputs. Alternate ways to calculate weights and sigma points from geometric and trigonometric identities were examined. From the later, it was possible to use a transformation technique to incorporate statistical dependency between two random variables.

The Gaussian Quadrature (GQ) method based on orthogonal series expansions was used as another approach for finding UT parameters. The advantage of this

standpoint is the way it copes with the solving a large system of equations. The elegance of the GQ method is such that the sigma points correspond to the roots of a weighting function. This function is a polynomial of has an arbitrary order and is dependent on the distribution of input variables being inspected. The Hermite and Laguerre polynomials are used for normal and exponential distributions respectively. The order of the weighting function corresponds to the number of sigma points. The Rodrigues formula provides the relationship between weights and sigma points.

Finally, the PDF of the output distribution $f_y(y)$ was estimated from the weights and sigma points. The coefficients of the standard series expansion are found from the UT parameters and the approximations of output statistical moments. The coefficients are substituted back into the approximate expressions of $f_y(y)$. The UT theory explained in chapter 8 was applied to the stochastic electromagnetic problems in chapter 9.

10.4   Application of UT to Stochastic Electromagnetic Problems

The UT method was applied to a variety of problems in the time and frequency domains in chapter 9. The first case study involved the time domain simulation of a TEM waveguide with a stochastic dielectric. The UT and MC methods were used to approximate the mean and standard deviation of observed voltage from a TLM algorithm. The agreement between both methods was found to reduce as the number of time steps increases. This effect was mitigated but not eliminated when higher order approximations are used. The reason for this is that the voltage incident at node at a time step k is related to the product of the connect and scatter matrices raised to the power k. Therefore, the more the time steps used the greater the order of approximations needed to maintain accuracy. This is because the effects of correlation in the time domain is not considered as the TLM nodes are treated as independent. The PDF of the observed electric field were approximated using the UT and MC methods at a certain time steps. The agreement between them reduced at higher time steps although a higher order approximation improved this trend. The frequency domain analysis of the

problem yielded some interesting results. The mean and standard deviation of the S_{11} parameter was assessed at different frequency points. The UT and MC methods were closer at lower frequencies and better agreement was attained when higher order expressions were included. The TLM model introduces errors at higher frequencies which contribute to the limitations at a given order.

The second case study was a pair of wire monopoles in a metal box with non-deterministic dimensions. The receiving monopole has a stochastic length. The mean, standard deviation, skew and kurtosis of the S_{21} parameter were shown to be in close proximity for the UT and MC methods. The correlation between the voltage at receiving monopole and the random variables is maximum along the length; and minimum in the direction outside the plane where the monopoles are positioned.

The third case study involves two dielectrics with statistically dependent relative permittivities in a waveguide. The results again show that the percentage difference between the UT and MC methods was highest between correlation coefficients of zero and one.

The last case study involves a dielectric slab with an exponentially distributed relative permittivity. The kurtosis of f_r was found using the UT method. This was an important result as the equivalent could not be attained using the DST as shown in Appendix A. The percentage difference between the UT and MC methods increased with standard deviation of relative permittivity.

10.5   Direction for Future Research

This thesis used the DST and UT methods as mathematical surrogates to the traditional MC technique in stochastic electromagnetic problems. All the case studies in the thesis used either normal or exponential PDFs of stochastic random variables. However, this is not extensive and there should be applications to other distribution functions. For the UT method, this is straightforward as the set of equations to find weights and sigma points is related to the moments of input

distributions. The GQ approach requires modification to the weighting function which is available in literature. The DST on the other hand, requires substitutions of relevant distribution functions and corresponding statistical moments into expressions derived in Appendix A.

The calculation of statistical moments of measured parameters in the time domain remains a formidable challenge. The UT method is satisfactory for a small number of time steps. For larger values, a suggestion is to devise a model that updates the order of the UT parameters with increasing time steps. Another situation for future research is that of random processes where stochastic variables are time dependent.

Appendix A   Approximation of Statistical Moments

This section contains the rigorous mathematical derivation of approximating the statistical moments of the function of a random variable using Taylor series expansion. The normal and exponential distribution functions considered here are consistent with the case studies presented in the thesis.

A.1   Approximating the Expected Value of a Random Variable Function

Let $g(x)$ be the function of a random variable x whose stochastic properties can be defined using its mean $\overline{x}$ and standard deviation σ. The mean of the distribution is given by the expression:

$$E[x] = \int\limits_{-\infty}^{+\infty} x f(x)\, dx \tag{A.1}$$

where $f(x)$ is the probability density is function of the random variable x and satisfies the expression:

$$\int\limits_{-\infty}^{+\infty} f(x)\, dx = 1 \tag{A.2}$$

Similarly, the mean of $g(x)$ is:

$$E[g(x)] = \int\limits_{-\infty}^{+\infty} g(x) f(x)\, dx \tag{A.3}$$

The function $g(x)$ can be expressed as a polynomial from Taylor's series about the mean value $\overline{x}$:

$$g(x) \cong g(\overline{x}) + g'(\overline{x})(x - \overline{x}) + \frac{g''(\overline{x})(x - \overline{x})^2}{2!} + \ldots + \frac{g^{(n)}(\overline{x})(x - \overline{x})^n}{n!} \quad \text{(A.4)}$$

Substituting the approximate expression for $g(x)$ in (A.3):

$$E\{g(x)\} \cong \int_{-\infty}^{+\infty} \left(g(\overline{x}) + g'(\overline{x})(x - \overline{x}) + \frac{g''(\overline{x})(x - \overline{x})^2}{2!} + \ldots + \frac{g^{(n)}(\overline{x})(x - \overline{x})^n}{n!} \right) f(x) dx \quad \text{(A.5)}$$

The derivatives of $g(x)$ are defined about the mean value are:

$$g'(\overline{x}) = g' = \left. \frac{dg}{dx} \right|_{x = \overline{x}} \qquad g''(\overline{x}) = g'' = \left. \frac{d^2 g}{dx^2} \right|_{x = \overline{x}} \qquad g'''(\overline{x}) = g''' = \left. \frac{d^3 g}{dx^3} \right|_{x = \overline{x}}$$

$$g^{iv}(\overline{x}) = g^{iv} = \left. \frac{d^4 g}{dx^4} \right|_{x = \overline{x}} \qquad g^{(n)}(\overline{x}) = g^{(n)} = \left. \frac{d^n g}{dx^n} \right|_{x = \overline{x}}$$

where n is the order of the derivative included to obtain an estimate of $E[g(x)]$.

Let $\mu_n = \int_{-\infty}^{+\infty} (x - \overline{x})^n f(x) dx$ be the nth central moment about the mean. Finding the first four central moments of random variable x about the mean $\overline{x}$ would give a truncated approximation of the expected value of x. This can be found as follows:

First Moment : $\mu_1 = \int_{-\infty}^{+\infty} (x - \overline{x}) f(x) dx = \int_{-\infty}^{+\infty} x f(x) dx - \overline{x} \int_{-\infty}^{+\infty} f(x) dx = 0$

Second Moment : $\mu_2 = \int_{-\infty}^{+\infty} (x - \overline{x})^2 f(x) dx = \int_{-\infty}^{+\infty} \left(x^2 - 2x\overline{x} + \overline{x}^2 \right) f(x) dx$

$$= \int_{-\infty}^{+\infty} x^2 f(x) dx - \overline{x} \int_{-\infty}^{+\infty} 2x f(x) dx + \overline{x}^2 \int_{-\infty}^{+\infty} f(x) dx = \int_{-\infty}^{+\infty} x^2 f(x) dx - 2\overline{x} \int_{-\infty}^{+\infty} x f(x) dx + \overline{x}^2$$

$$= \int_{-\infty}^{+\infty} x^2 f(x) dx - 2(\overline{x})^2 + (\overline{x})^2 = \int_{-\infty}^{+\infty} x^2 f(x) dx - \overline{x}^2 = E[x^2] - (\overline{x})^2 = \sigma^2$$

$$\text{Third Moment}: \mu_3 = \int\limits_{-\infty}^{+\infty} (x-\bar{x})^3 f(x)dx = \int\limits_{-\infty}^{+\infty} \left(x^3 - 3\bar{x}x^2 + 3(\bar{x})^2 x - (\bar{x})^3\right) f(x)dx$$

$$= \int\limits_{-\infty}^{+\infty} x^3 f(x)dx - 3\bar{x}\int\limits_{-\infty}^{+\infty} x^2 f(x)dx + 3(\bar{x})^2 \int\limits_{-\infty}^{+\infty} xf(x)dx - (\bar{x})^3 \int\limits_{-\infty}^{+\infty} f(x)dx$$

$$= E\left[x^3\right] - 3\bar{x}\left(\sigma^2 + (\bar{x})^2\right) + 3\bar{x}(\bar{x})^2 - (\bar{x})^3 = E\left[x^3\right] - 3\bar{x}\left(\sigma^2 + (\bar{x})^2\right) + 2(\bar{x})^3$$

$$\text{Fourth Moment}: \mu_4 = \int\limits_{-\infty}^{+\infty} (x-\bar{x})^4 f(x)dx = \int\limits_{-\infty}^{+\infty} \left(x^4 - 4\bar{x}x^3 + 6(\bar{x})^2 x^2 - 4(\bar{x})^3 x + (\bar{x})^4\right) f(x)dx$$

$$= \int\limits_{-\infty}^{+\infty} x^4 f(x)dx - 4\bar{x}\int\limits_{-\infty}^{+\infty} x^3 f(x)dx + 6(\bar{x})^2\int\limits_{-\infty}^{+\infty} x^2 f(x)dx - 6(\bar{x})^3\int\limits_{-\infty}^{+\infty} xf(x)dx + (\bar{x})^4\int\limits_{-\infty}^{+\infty} f(x)dx$$

$$= E\left[x^4\right] - 4\bar{x}E\{x^3\} + 6(\bar{x})^2\left(\sigma^2 + (\bar{x})^2\right) - 6(\bar{x})^4 + (\bar{x})^4$$

$$= E\left[x^4\right] - 4\bar{x}E\{x^3\} + 6(\bar{x})^2\left(\sigma^2 + (\bar{x})^2\right) - 5(\bar{x})^4 \qquad\qquad \text{(A.6)}$$

The second moment about the mean is called the variance and the ratio of the third moment to the cube of standard deviation (or the product of variance and standard deviation) is termed the skewness of the distribution. The ratio of the fourth moment to that of the square of variance is the kurtosis.

Taking the first few terms from (A.6) and placing it in (A.5) gives:

$$\text{First term}: \int\limits_{-\infty}^{+\infty} g(\bar{x})f(x)dx = g(\bar{x})\int\limits_{-\infty}^{+\infty} f(x)dx = g(\bar{x})$$

$$\text{Second term}: \int\limits_{-\infty}^{+\infty} g'(\bar{x})(x-\bar{x})f(x)dx = g'(\bar{x})(0) = 0$$

$$\text{Third term}: \frac{1}{2!}\int\limits_{-\infty}^{+\infty} g''(\bar{x})(x-\bar{x})^2 f(x)dx = \frac{g''(\bar{x})}{2}\mu_2 = \frac{g''(\bar{x})}{2}\sigma^2$$

$$\text{Fourth term}: \frac{1}{3!}\int\limits_{-\infty}^{+\infty} g'''(\bar{x})(x-\bar{x})^3 f(x)dx = \frac{g'''(\bar{x})}{6}\mu_3$$

$$= \frac{g'''(\bar{x})}{6}\left(E\left[x^3\right] - 3\bar{x}\left(\sigma^2 + (\bar{x})^2\right) + 2(\bar{x})^3\right)$$

Fifth term: $\dfrac{1}{4!}\displaystyle\int_{-\infty}^{+\infty} g^{iv}(\bar{x})(x-\bar{x})^4 f(x)dx = \dfrac{g^{iv}(\bar{x})}{24}\mu_4$

$$= \frac{g^{iv}(\bar{x})}{24}\left(E\left[x^4\right]-4\bar{x}E\left[x^3\right]+6(\bar{x})^2\left(\sigma^2+(\bar{x})^2\right)-5(\bar{x})^4\right) \qquad (A.7)$$

The fourth order expected value of $g(x)$ can be approximated by the expression:

$$E\left[g(\bar{x})\right] \cong g(\bar{x}) + \frac{g''(\bar{x})\sigma^2}{2} + \frac{g^{iv}(\bar{x})\sigma^4}{8} \qquad (A.8)$$

Let the random variable have an exponential distribution defined as:

$$f(x) = \frac{1}{\sigma}e^{\left(-\frac{x}{\sigma}\right)} \qquad (A.9)$$

The fourth order approximation of the expected value from (A.5) of the function of the exponential random variable defined in (A.9) is:

$$E\left[g(x)\right] \cong g + g'\sigma + g''\sigma^2 - g''\sigma\bar{x} - g'''\sigma^2\bar{x} + \frac{1}{2}g'''\sigma\bar{x}^2 + g'''\sigma^3 + g^{iv}\sigma^4 - g^{iv}\sigma^3\bar{x}$$

$$+ \frac{1}{2}g^{iv}\sigma^2\bar{x}^2 - \frac{1}{6}g^{iv}\sigma\bar{x}^3 - g'\bar{x} + \frac{1}{2}g''\sigma\bar{x}^2 - \frac{1}{6}g'''\bar{x}^3 + \frac{1}{24}g^{iv}\bar{x}^4 \qquad (A.10)$$

The distribution of the random variable x will dictate which of the higher order moments will make a contribution to an approximation of the expected value or any higher order moments of $g(x)$.

For a normal distribution of x, μ_3 and other odd central moments is zero whilst $\mu_4 = 3\sigma^4$ which further simplifies the approximation of by eliminating some terms. For other distributions it is possible that this is not the case and in this instance, μ_3 and μ_4 can be evaluated *a priori* from the skew and kurtosis and substituted directly into the above terms.

A.2   Approximating the Expected Value of the Square of a Random Variable Function

The procedure for calculating the moments of the square of the function $g(x)$ is similar to highlighted above. The expression of the mean of $g^2(x)$ in terms of the moments of the independent variable x :

$$E\left[g^2(x)\right] \cong g^2(\bar{x}) + \left(g^2(\bar{x})\right)'' \frac{\sigma^2}{2} + \left(g^2(\bar{x})\right)''' \frac{\mu_3}{3!} + \left(g^2(\bar{x})\right)^{iv} \frac{\mu_4}{4!} + ... + \left(g^2(\bar{x})\right)^{(n)} \frac{\mu_n}{n!} \quad \text{(A.11)}$$

The derivatives of $g^2(x)$ in the above expression are:

$$\left(g^2(\bar{x})\right)'' = \left(2g(\bar{x})g'(\bar{x})\right)' = 2\left[g(\bar{x})g''(\bar{x}) + \left(g'(\bar{x})\right)^2\right] \quad \text{(A.12)}$$

$$\left(g^2(\bar{x})\right)''' = \left[\left(g^2(\bar{x})\right)''\right]' = 2\left[g(\bar{x})g'''(\bar{x}) + 3g'(\bar{x})g''(\bar{x})\right] \quad \text{(A.13)}$$

$$\left(g^2(\bar{x})\right)^{iv} = \left[\left(g'''(\bar{x})\right)^2\right]' = 2\left[g(\bar{x})g^{iv}(\bar{x}) + 4g'(\bar{x})g'''(\bar{x}) + 3g''(\bar{x})g''(\bar{x})\right] \quad \text{(A.14)}$$

The general form for finding the nth derivative of $g^2(x)$ is:

$$\left(g^2(\bar{x})\right)^{(n)} = \left[\left(g^2(\bar{x})\right)^{(n-1)}\right]' \quad \text{(A.15)}$$

A.3   Approximating the Variance of a Random Variable Function

In order to approximate the variance of a distribution, a parameter that defines the rth moment about the mean of a function $g(x)$ is given by the expression:

$$\mu_{gr} = E\left[g(x) - E\left[g(x)\right]\right]^r \tag{A.16}$$

Adopting the binomial series expansion to μ_{gr} above gives:

$$\mu_{gr} = E\left[\begin{array}{l} \left[g(x)\right]^r - \binom{r}{1}\left[g(x)\right]^{r-1} E\left[g(x)\right] + ... + (-1)^m \binom{r}{m}\left[g(x)\right]^{r-m} E\left[g(x)\right]^m \\ + ... + (-1)^{r-1}\binom{r}{r-1}\left[g(x)\right]E\left[g(x)\right]^{r-1} + (-1)^r E\left[g(x)\right]^r \end{array} \right] \tag{A.17}$$

Let an auxiliary term called the raw moment defined as the rth moment about the origin and is given by the expression:

$$\mu'_{gr} = E\left[g(x)\right]^r \tag{A.18}$$

Substituting for $E\left[g(x)\right]^r$ with μ'_{gr} in (A.17) above:

$$\mu_{gr} = \left[\begin{array}{l} \mu'_{gr} - \binom{r}{1}\mu'_{gr-1} E\left[g(x)\right] + ... + (-1)^m \binom{r}{m}\mu'_{gr-m} E\left[g(x)\right]^m \\ + ... + (-1)^{r-1}\binom{r}{r-1}\mu'_{g1} E\left[g(x)\right]^{r-1} + (-1)^r \mu'_{g0} E\left[g(x)\right]^r \end{array} \right] \tag{A.19}$$

From (15) $\mu'_{g1} = E\left[g(x)\right]$ and $\mu'_{g0} = 1$, thus μ_{gr} becomes:

$$\mu_{gr} = \begin{bmatrix} \mu'_{gr} - \binom{r}{1}\mu'_{gr-1} E[g(x)] + ... + (-1)^m \binom{r}{m}\mu'_{gr-m} E[g(x)]^m \\ +...+ (-1)^{r-1}\binom{r}{r-1} E[g(x)]E[g(x)]^{r-1} + (-1)^r E[g(x)]^r \end{bmatrix} \qquad \text{(A.20)}$$

Now, $\binom{r}{r-1} = r$ and $E[g(x)]E[g(x)]^{r-1} = E[g(x)]^r$

Therefore, (A.20) can be further simplified to give:

$$\mu_{gr} = \begin{bmatrix} \mu'_{gr} - \binom{r}{1}\mu'_{gr-1} E[g(x)] + ... + (-1)^m \binom{r}{m}\mu'_{gr-m} E[g(x)]^m \\ +...+ (-1)^{r-1} rE[g(x)]^r + (-1)^r E[g(x)]^r \end{bmatrix} \qquad \text{(A.21)}$$

Now from (A.19), the second moment about the mean or the second central moment is the variance and this gives

$$\mu_{g2} = \left[\mu'_{g2} - E[g(x)]^2\right] = \left[E[g^2(x)] - E[g(x)]^2\right] = \sigma_g^2 \qquad \text{(A.22)}$$

By substituting the approximate expressions derived earlier for $E[g^2(x)]$ and $[E[g(x)]]^2$ into (A.22), the variance for a normally distributed random variable x (that is, $\mu_3 = 0$ and $\mu_4 = 3\sigma^4$) can be estimated as:

$$\mu_{g2} \cong g'^2 \sigma^2 + \left(\frac{1}{2}g''^2 + g'g'''\right)\sigma^4 + \left(\frac{5}{12}g'''^2 + \frac{1}{2}g''g^{iv}\right)\sigma^6 + \left(\frac{1}{6}g^{iv2}\right)\sigma^8 \qquad \text{(A.23)}$$

The corresponding equation of (A.23) for the exponential random variable in (A.9) is:

$$\mu_{g2} \cong \left(\begin{array}{l} \dfrac{1}{3}g''g'''\,\overline{x}^4 + g'g'''\overline{x}^2 + \dfrac{1}{36}g'''^2\,\overline{x}^6 + g'^2 + g''^2\,\overline{x}^2 - \dfrac{1}{6}g'''g'''\,\overline{x}^5 \\[2mm] -g''g'''\overline{x}^3 + \dfrac{1}{4}g'''^2\,g'''\,\overline{x}^4 - 2g'g''\overline{x} - \dfrac{1}{3}g'g'''\overline{x}^3 \end{array} \right)\sigma^2$$

$$+ \left(\begin{array}{l} 4g'g'' - 4g''^2\,\overline{x} + 2g'g'''\overline{x}^2 - 2g'''^2\,\overline{x}^3 - \dfrac{1}{3}g'''^2\,\overline{x}^5 - 4g'g'''\overline{x} \\[2mm] +\dfrac{5}{3}g'''g'''\,\overline{x}^4 + 6g''g'''\overline{x}^2 - \dfrac{8}{3}g''g'''\,x^3 \end{array} \right)\sigma^3$$

$$+ \left(\begin{array}{l} 8g'''^2\,g''\overline{x}^2 - 6g'g'''\overline{x} - 16g''g'''\overline{x} + \dfrac{9}{4}g'''^2\,\overline{x}^4 + 5g''^2 \\[2mm] -9g'''g'''\,\overline{x}^3 + 11g''g'''\,\overline{x}^2 + 6g'g''' \end{array} \right)\sigma^4$$

$$+ \left(\begin{array}{l} -\dfrac{31}{3}g'''\,\overline{x}^3 - 26g''g'''\,\overline{x} + 18g''g''' + 31g'''g'''\,\overline{x}^2 \\[2mm] -18g'''^2\,\overline{x} + 8g'g''' \end{array} \right)\sigma^5$$

$$+ \left(19g'''^2 - 66g'''g'''\,\overline{x} + 28g''g''' + 33g'''^2\,\overline{x}^2 \right)\sigma^6$$

$$+ \left(68g'''g''' - 68g'''^2\,\overline{x} \right)\sigma^7 + 69g'''^2\,\sigma^8 \tag{A.24}$$

A.4 Approximating the Skew of a Random Variable Function

In order to approximate the skew of a distribution, a parameter is defined for the third moment about the mean of a function $g(x)$ given by the expression:

$$\mu_{g3} = \mu'_{g3} - 3\mu'_{g2}\,E\big[g(x)\big] + 2E\big[g(x)\big]^3 \tag{A.25}$$

Substituting the Taylor series expressions about the mean in similar fashion to (A.11) and restricting to fourth order derivatives and normal probability distribution in x:

$$\mu_{g3} \cong \left(3g'^2 g''\right)\sigma^4 + \left(\frac{3}{2}g'^2 g^{iv} + 6g'g''g''' + g''^3\right)\sigma^6 + \left(\frac{9}{4}g''^2 g^{iv} + \frac{15}{4}g''g'''^2 + 4g'g'''g^{iv}\right)\sigma^8$$

$$+ \left(\frac{25}{8}g'''^2 g^{iv} + 2g''g^{iv2}\right)\sigma^{10} + \left(\frac{11}{16}g^{iv3}\right)\sigma^{12} \tag{A.26}$$

The third moment about the mean of a function $g(x)$ of an exponential random variable in (A.9) is:

$$\mu_{g3} \cong \begin{pmatrix} \frac{1}{6}g'g^{iv2}\overline{x}^6 - \frac{3}{2}g''g'''^2\overline{x}^5 + 3g''^2 g'''\overline{x}^4 + 6g'g''^2\overline{x}^2 + g''g'''g^{iv}\overline{x}^6 + 2g'^3 \\[4pt] -g'g'''g^{iv}\overline{x}^5 - g''^2 g^{iv}\overline{x}^5 - \frac{1}{4}g'''^2 g^{iv}\overline{x}^7 + 3g'^2 g'''\overline{x}^2 - 2g''^3\overline{x}^3 \\[4pt] +2g'g''g^{iv}\overline{x}^4 - g'^2 g^{iv}\overline{x}^3 - 6g'^2 g''g'''\overline{x} + \frac{1}{4}g'''^3\overline{x}^6 - 6g'g''g'''\overline{x}^3 \\[4pt] -\frac{1}{6}g''g^{iv2}\overline{x}^7 - \frac{1}{108}g^{iv3}\overline{x}^9 + \frac{3}{2}g'g'''^2\overline{x}^4 + \frac{1}{12}g'''g^{iv2}\overline{x}^8 \end{pmatrix}\sigma^3$$

$$+ \begin{pmatrix} 18g''^3\overline{x}^2 + \frac{45}{2}g''g'''^2\overline{x}^4 + \frac{7}{2}g''g^{iv2}\overline{x}^6 + \frac{1}{4}g^{iv3}\overline{x}^8 - 36g'g''^2\overline{x} + \\[4pt] 54g'g''g'''\overline{x}^2 + 9g'^2 g^{iv}\overline{x}^2 - 2g'''g^{iv2}\overline{x}^7 - \frac{9}{2}g^{iv3}\overline{x}^5 + 15g'g'''g^{iv}\overline{x}^4 \\[4pt] +18g'^2 g'' - 18g''g'''g^{iv}\overline{x}^5 - 3g'g^{iv2}\overline{x}^5 - 18g'g'''^2\overline{x}^3 - 18g'^2 g'''\overline{x} \\[4pt] -24g'g''g^{iv}\overline{x}^3 + 15g''^2 g^{iv}\overline{x}^4 + \frac{21}{4}g'''^2 g^{iv}\overline{x}^6 - 36g''^2 g'''\overline{x}^3 \end{pmatrix}\sigma^4$$

$$+ \begin{pmatrix} -\frac{7}{2}g^{iv3}\overline{x}^7 - 55g'''^2 g^{iv}\overline{x}^5 + 132g'g''g^{iv}\overline{x}^2 + 27g'g^{iv}\overline{x}^4 \\[4pt] +96g'''^2 g'\overline{x}^2 + 39g^{iv3}\overline{x}^4 + 36g'^2 g''' - 192g'g''g'''\overline{x} \\[4pt] +\frac{49}{2}g'''g^{iv2}\overline{x}^6 + 60g'g''^2 - 156g''g'''^2\overline{x}^3 + 186g''^2 g'''\overline{x}^2 \\[4pt] +158g''g'''g^{iv}\overline{x}^4 - 37g''g^{iv2}\overline{x}^5 - 106g''^2 g^{iv}\overline{x}^3 \\[4pt] -108g'g'''g^{iv}\overline{x}^3 - 60g^{iv3}\overline{x} - 36g'^2 g^{iv}\overline{x} \end{pmatrix}\sigma^5$$

$$+ \begin{pmatrix} 270g'g''g''' - 390g'g''g^{iv}\bar{x} - 270g'g'''^2\,\bar{x} + \dfrac{401}{12}g^{iv3}\bar{x}^6 \\[2mm] -867g''g'''g^{iv}\bar{x}^3 - 492g''^2g'''\bar{x} + 465g'g'''g^{iv}\bar{x}^2 - 209g'''^3\,\bar{x}^3 \\[2mm] +\dfrac{511}{2}g''g^{iv2}\bar{x}^4 + \dfrac{747}{2}g'''^2g^{iv}\bar{x}^4 + 60g'^2g^{iv} - 155g'g^{iv2}\bar{x}^3 \\[2mm] +441g''^2g^{iv}\bar{x}^2 - \dfrac{401}{2}g'''g^{iv2}\bar{x}^5 + 74g'''^3 + 627g''g'''^2\,\bar{x}^2 \end{pmatrix}\sigma^6$$

$$+ \begin{pmatrix} \dfrac{2385}{2}g'''g^{iv2}\bar{x}^4 - 1236g''g^{iv2}\bar{x}^3 + 3114g''g'''g^{iv}\bar{x}^2 \\[2mm] -1188g'g'''g^{iv}\bar{x} + 504g'g''g^{iv} - 1458g''g'''^2\,\bar{x} \\[2mm] +729g'''^3\,\bar{x}^2 + 594g'g^{iv2}\bar{x}^2 - \dfrac{477}{2}g^{iv3}\bar{x}^5 + 342g'g'''^2 \\[2mm] -1767g'''^2g^{iv}\bar{x}^3 + 558g''^2g''' - 1062g''^2g^{iv}\bar{x} \end{pmatrix}\sigma^7$$

$$+ \begin{pmatrix} -1428g'g^{iv2}\bar{x} + 1158g''^2g^{iv} + 1566g''g'''^2 + 4152g''g^{iv2}\bar{x}^2 \\[2mm] -1566g'''^3\,\bar{x} + \dfrac{2621}{2}g^{iv3}\bar{x}^4 - 5242g'''g^{iv2}\bar{x}^3 + 1428g'g'''g^{iv} \\[2mm] -6876g''g'''g^{iv}\bar{x} + 5787g'''^2g^{iv}\bar{x}^2 \end{pmatrix}\sigma^8$$

$$+ \begin{pmatrix} 7212g''g'''g^{iv} - 5504g^{iv3}\bar{x}^3 - 12078g'''^2g^{iv}\bar{x} + 1622g'''^3 \\[2mm] +1656g'g^{iv2} + 16512g'''g^{iv2}\bar{x}^2 - 8868g''g^{iv2}\bar{x} \end{pmatrix}\sigma^9$$

$$+ \left(12336g'''^2g^{iv} + 9156g''g^{iv2} + 16914g^{iv3}\bar{x}^2 - 33828g'''g^{iv2}\bar{x}\right)\sigma^{10}$$

$$+ \left(-34236g^{iv3}\bar{x} + 3423g'''g^{iv2}\right)\sigma^{11} + 34442g^{iv3}\sigma^{12} \qquad (A.27)$$

The skew is given by the expression:

$$Skew = \frac{\mu_{g3}}{\left(\mu_{g2}\right)^{\frac{3}{2}}} \qquad (A.28)$$

Using the approximate expressions for μ_{g2} and μ_{g3}, the skew for the function of a random variable with a normal distribution is:

$$Skew \cong \frac{\begin{pmatrix} \left(3g'^2 g''\right)\sigma^4 + \left(\frac{3}{2}g'^2 g^{iv} + 6g'g''g''' + g''^3\right)\sigma^6 \\ + \left(\frac{9}{4}g''^2 g^{iv} + \frac{15}{4}g''g'''^2 + 4g'g'''g^{iv}\right)\sigma^8 \\ + \left(\frac{25}{8}g'''^2 g^{iv} + 2g''g^{iv2}\right)\sigma^{10} + \left(\frac{11}{16}g^{iv3}\right)\sigma^{12} \end{pmatrix}}{\left(g'^2 \sigma^2 + \left(g''^2 + \frac{1}{2}g'g'''\right)\sigma^4 + \left(\frac{5}{12}g'''^2 + \frac{1}{2}g''g^{iv}\right)\sigma^6 + \left(\frac{1}{6}g^{iv2}\right)\sigma^8\right)^{\frac{3}{2}}} \tag{A.29}$$

A.5   Approximating the Kurtosis of a Random Variable Function

In order to approximate the kurtosis of a distribution, a parameter is defined for the fourth moment about the mean of a function $g(x)$ given by the expression:

$$\mu_{g4} = \mu'_{g4} - 4\mu'_{g3} E\left[g(x)\right] + 6\mu'_{g2} E\left[g(x)\right]^2 - 3E\left[g(x)\right]^3 \tag{A.30}$$

This can be approximated, restricting to fourth order derivatives and normal probability distribution in x as:

$$\mu_{g4} \cong \left(3g'^4\right)\sigma^4 + \left(10g'^3 g''' + 15\left(g'g''\right)^2\right)\sigma^6 + \left(\frac{35}{2}\left(g'g'''\right)^2 + \frac{15}{4}g'^4 + 21g'^2 g''g^{iv} + 39g'g''^2 g'''\right)\sigma^8$$

$$+ \left(9\left(g'g^{iv}\right)^2 + \frac{125}{4}\left(g''g'''\right)^2 + \frac{27}{2}g'''^3 g^{iv} + \frac{35}{2}g'g''^3 + 67g'g''g'''g^{iv}\right)\sigma^{10}$$

$$+ \left(34g'g'''g^{iv2} + \frac{255}{4}g''g'''^2 g^{iv} + \frac{85}{4}\left(g''g^{iv}\right)^2 + \frac{385}{48}g'''^4\right)\sigma^{12} + \left(17g''g^{iv3} + \frac{75}{2}\left(g'''g^{iv}\right)^2\right)\sigma^{14}$$

$$+ \left(\frac{23}{4}g^{iv4}\right)\sigma^{16} \tag{A.31}$$

The kurtosis is given by the expression:

$$Kurt = \frac{\mu_{g4}}{\left(\mu_{g2}\right)^2} \qquad (A.32)$$

Using the approximate expressions for μ_{g2} and μ_{g3}, the kurtosis of a random variable with a normal distribution is:

$$Kurt \cong \frac{\begin{pmatrix} \left(3g'^4\right)\sigma^4 + \left(10g'^3 g''' + 15\left(g'g''\right)^2\right)\sigma^6 \\[4pt] + \left(\frac{35}{2}\left(g'g'''\right)^2 + \frac{15}{4}g''^4 + 21g'^2 g''g^{iv} + 39g'g''^2 g'''\right)\sigma^8 \\[4pt] + \left(9\left(g'g^{iv}\right)^2 + \frac{125}{4}\left(g''g'''\right)^2 + \frac{27}{2}g''^3 g^{iv} + \frac{35}{2}g'g'''^3 + 67g'g''g'''g^{iv}\right)\sigma^{10} \\[4pt] + \left(34g'g'''g^{iv2} + \frac{255}{4}g''g'''^2 g^{iv} + \frac{85}{4}\left(g''g^{iv}\right)^2 + \frac{385}{48}g'''^4\right)\sigma^{12} \\[4pt] + \left(17g''g^{iv3} + \frac{75}{2}\left(g''g^{iv}\right)^2\right)\sigma^{14} + \left(\frac{23}{4}g^{iv4}\right)\sigma^{16} \end{pmatrix}}{\left(g'^2\sigma^2 + \left(g''^2 + \frac{1}{2}g'g'''\right)\sigma^4 + \left(\frac{5}{12}g'''^2 + \frac{1}{2}g''g^{iv}\right)\sigma^6 + \left(\frac{1}{6}g^{iv2}\right)\sigma^8\right)^2} \qquad (A.33)$$

The corresponding expression for the exponential random variable could not be derived as the MAPLE software adopted for the more complicated derivations did not deem this tractable enough to profer approximations.

Appendix B Exponential Correlation Function

This section contains the procedure for selecting random samples of relative permittivity from an exponential correlation function.

B.1 Random Inhomogeneities

There can be two distinct random distributions of relative permittivity having the same behaviour. The distributions, for example, can have the same *root mean square* but different *correlation lengths*. The concept of correlation allows for the description of both distributions in order to distinguish the characteristics [B.1]. The correlation function thus defined here stipulates the degree of interdependence between random inhomogeneities.

The ideas of correlation effects can be developed from a simple scenario considered here. Let the relative permittivity at each node ε_n in the TLM model be the smallest size of inhomogeneity. For a transmission line of N nodes, then the series of permittivity in each node is: $\varepsilon_0, \varepsilon_1, \varepsilon_2, ...\varepsilon_{N-1}$. The dependence of each of these permittivity values on one another in the same medium is described by an autocorrelation function [B.1]:

$$R(a) = \lim_{N \to \infty} \left(\frac{1}{N} \sum_{i=-N/2}^{N/2} \varepsilon_i \varepsilon_{i+a} \right) \tag{B.1}$$

where a is fixed integer value.

The deviation of the permittivity value from being uniform is described by a function $\varepsilon(x)$ where x is the direction of propagation. For a very long transmission line, the statistics of $\varepsilon(x)$ is such that provided it is a stationary random function then it is independent of the position x. The average of all the

measurement is determined *a priori* and is designated by the term $\bar{\varepsilon}$. As $\varepsilon(x)$ represents a continuous distribution, integration is used in place of summation in (B.1) and the autocorrelation function $R(a)$ is defined as:

$$R(a) = \langle \varepsilon(x)\varepsilon(x+a) \rangle = \lim_{X \to \infty} \left(\frac{1}{X} \int_{-X/2}^{X/2} \varepsilon(x)\varepsilon(x+a)\,dx \right) \quad \text{(B.2)}$$

The expression above as shown is the summation over various values of a of the average of the product of the deviation at point x with another $x+a$ further down the transmission line. The property of $R(a)$ is such that it is independent on x and depends only on a.

The ensemble average of the sum of squares of $\varepsilon(x)$ gives is the mean square of the distribution and this coincides with when $a = 0$ and is given by:

$$R(0) = \langle \varepsilon^2(x) \rangle = \lim_{X \to \infty} \left(\frac{1}{X} \int_{-X/2}^{X/2} \varepsilon^2(x)\,dx \right) = \varepsilon^2_{RMS} \quad \text{(B.3)}$$

where ε_{RMS} is the root mean square of the relative permittivity values of the function $\varepsilon(x)$.

$\varepsilon(x)$ is a random function although the ensemble averages in (B.2) and (B.3) are not and can be easily measured. Many random processes are described by an exponential autocorrelation function. This would be defined as [B.2]:

$$R(a) = \varepsilon^2_{RMS}\, e^{\left(-|a|/L_c \right)} \quad \text{(B.4)}$$

where L_c is the correlation length and ε_{RMS} is the root mean square of the central permittivity value.

The correlation length is the scale over which is a measure of how $\varepsilon(x)$ is correlated at two different points along the direction of propagation. Points that

lie within the correlation length will have a greater value of $R(a)$ than those that lie further apart.

The power spectral density can be defined as the Fourier transform of the autocorrelation function:

$$\tilde{R}(\omega) = \int_{-\infty}^{\infty} R(a)e^{-j\omega a}da \qquad (B.5)$$

Substituting $R(a)$ in (B.5) from (B.3):

$$\tilde{R}(\omega) = \int_{-\infty}^{\infty} \lim_{X\to\infty} \left(\frac{1}{X} \int_{-X/2}^{X/2} \varepsilon(x)\varepsilon(x+a)dx \right) e^{-j\omega a}da \qquad (B.6)$$

Collecting like terms together gives:

$$\tilde{R}(\omega) = \int_{-\infty}^{\infty} \lim_{X\to\infty} \left(\frac{1}{X} \int_{-X/2}^{X/2} \varepsilon(x)dx \int_{-\infty}^{\infty} \varepsilon(x+a)e^{-j\omega a}da \right) \qquad (B.7)$$

Let $a' = x + a \Rightarrow a = a' - x, da = da'$

$$\tilde{R}(\omega) = \int_{-\infty}^{\infty} \lim_{X\to\infty} \left(\frac{1}{X} \int_{-X/2}^{X/2} \varepsilon(x)dx \int_{-\infty}^{\infty} \varepsilon(a')e^{-j\omega(a'-x)}da' \right) \qquad (B.8)$$

From the second integral let $\tilde{\varepsilon}(\omega)$ be the Fourier transform of $\varepsilon(a')$. From the frequency shifting rule of Fourier transforms the above expression yields:

$$\tilde{R}(\omega) = \int_{-\infty}^{\infty} \lim_{X\to\infty} \left(\frac{1}{X} \int_{-X/2}^{X/2} \tilde{\varepsilon}(\omega)\varepsilon(x)e^{j\omega x}dx \right) \qquad (B.9)$$

Similarly, let $\tilde{\varepsilon}(\omega)$ be the Fourier transform of $\varepsilon(x)$ then:

$$\tilde{R}(\omega) = \int_{-\infty}^{\infty} \lim_{X \to \infty} \left(\frac{1}{X} \tilde{\varepsilon}(-\omega) \tilde{\varepsilon}(\omega) \right) \tag{B.10}$$

Applying the Parseval's theorem in the spatial domain to equation (B.10) [B.1]:

$$\tilde{R}(\omega) = \int_{-\infty}^{\infty} \lim_{X \to \infty} \left(\frac{1}{X} |\tilde{\varepsilon}(\omega)|^2 \right) \tag{B.11}$$

The next objective is to find the Fourier transform of the exponential autocorrelation function:

$$\tilde{R}(\omega) = \int_{-\infty}^{\infty} \varepsilon^2_{RMS} e^{\left(-|a| / L_c \right)} e^{-j\omega a} da \tag{B.12}$$

Solving the above integrand and substituting the definite integral bounds:

$$\tilde{R}(\omega) = \varepsilon^2_{RMS} \left[\frac{L_c e^{\left(a / L_c \right)} e^{-j\omega a}}{j\omega L_c - 1} \right]_0^{\infty} + \varepsilon^2_{RMS} \left[\frac{L_c e^{\left(-a / L_c \right)} e^{-j\omega a}}{j\omega L_c + 1} \right]_{-\infty}^0 = \frac{2 L_c \varepsilon^2_{RMS}}{1 + \omega^2 \left(L_c \right)^2} \tag{B.13}$$

Equating the above expression to (B.11):

$$\tilde{R}(\omega) = \int_{-\infty}^{\infty} \lim_{X \to \infty} \left(\frac{1}{X} |\tilde{\varepsilon}(\omega)|^2 \right) = \frac{2 L_c \varepsilon^2_{RMS}}{1 + \omega^2 \left(L_c \right)^2} \tag{B.14}$$

The next task is that given the correlation function $R(a)$, a sequence that depicts the appropriate behaviour of $\varepsilon(x)$ from a sequence of uniformly distributed random numbers. First, an assumption that the spectral content of $\tilde{R}(\omega)$ is the filtered output of uniformly distributed random data. Thus, its characteristic is given as:

$$\tilde{\varepsilon}(\omega) = \frac{\varepsilon^2_{RMS} \sqrt{2 L_c}}{1 + j\omega L_c} \tag{B.15}$$

The digital implementation of this filter is found from the bilinear transform using the expression [B.3]:

$$j\omega = \frac{2}{\Delta x}\left(\frac{1-z^{-1}}{1+z^{-1}}\right)$$ (B.16)

where Δx is the spacing between the nodes.

$$\tilde{\varepsilon}(z) = \frac{\varepsilon^2_{RMS}\sqrt{2L_c}}{1+\left(\frac{2}{\Delta x}\left(\frac{1-z^{-1}}{1+z^{-1}}\right)\right)L_c}$$ (B.17)

Multiplying the numerator and denominator of (B.17) by $1+z^{-1}$:

$$\tilde{\varepsilon}(z)\left(\left(1+\frac{2}{\Delta x}\right)+\left(1-\frac{2}{\Delta x}\right)z^{-1}\right) = \varepsilon^2_{RMS}\left(1+z^{-1}\right)\sqrt{2L_c}$$ (B.18)

(B.18) can be rearranged to give:

$$\tilde{\varepsilon}(z)\left(\left(1+\frac{2}{\Delta x}\right)+\left(1-\frac{2}{\Delta x}\right)z^{-1}\right) = \varepsilon^2_{RMS}\left(1+z^{-1}\right)\sqrt{2L_c}$$ (B.19)

The above expression is seen to be a system with memory in the z-domain where the term on the left is the input sequence of uniformly distributed random $r(n\Delta x)$ and on the right is the required output correlated sequence $\varepsilon(n\Delta x)$. The inverse z-transform to the spatial domain of the above expression is :

$$\left(1+\frac{2}{\Delta x}\right)\varepsilon_n = \varepsilon^2_{RMS}\sqrt{2L_c}\left(r_n + r_{n-1}\right) - \left(1-\frac{2}{\Delta x}\right)\varepsilon_{n-1}$$ (B.20)

For a uniformly distributed random sequence $r(n\Delta x)$ between $-\sqrt{3}$ to $\sqrt{3}$ gives a mean value of zero and an RMS value of unity [B.4]. This standardised sequence if adopted in (B.20) would also give a mean of ε_n to be zero.

The actual mean permittivity $\bar{\varepsilon}$ can be into account simply by using the expression:

$$\varepsilon_{actual} = \bar{\varepsilon} + \varepsilon_n \tag{B.21}$$

B.2   References

[B.1] D. Brook, R.J. Wynne, "Signal Processing: Principles and Applications," Edward Arnold, London, 1988.

[B.2]   F. Ladouceur, J.D. Love, T.J. Senden, "Effect of Side Wall Roughness in Buried Channel Waveguides," IEE Proceedings, vol. 141, pp. 242 – 248, Aug. 1994.

[B.3]   S.M. Bozic, Digital and Kalman Filtering, Edward Arnold, London, 1971.

[B.4]   A. Papoulis, "Probability, Random Variables and Stochastic Processes," 2nd Edition, New York, NY: McGraw-Hill, 1984.

Appendix C   Connection in Waveguide Problems

This section describes the connection procedure between ports of adjacent nodes in a discretised TLM waveguide problem.

C.1   Connection Matrix

During the process of connection there is a *handshake* between coupled ports away from the metallic walls of the waveguides. The ports linked directly with boundaries have the incident voltage reflected back in conformity with transmission line theory. As materials are modelled here with the use of open circuit stubs, then the coupling in this case occurs internally with the node centre.

The global connection matrix $\underline{\underline{C}}$ is a square matrix of the order (NX x NY x NP) describes how the nodes are connected via their member ports. This matrix is constructed simply by placing 1 in the position of coupled ports and stub positions. For ports connected to short circuit boundaries the negative unity reflection co-efficient is highlighted by placing -1 in the pertinent matrix elements as will be shown in this section. All the nodes with position co-ordinates $(0, y)$, $(NX - 1, y)$, $(x,0)$ and $(x, NY - 1)$. The global connection matrix is defined as follows:

$$\underline{V}^{i}(t+\Delta t) = \underline{\underline{C}}\,\underline{V}^{r}(t)$$

(C.1)

C.2   Connection of Ports at Boundaries

The port numbering system for the top and bottom boundaries are shown in Fig. C-1. The relationship between neighbouring nodes connected to these boundaries is provided here.

The top boundary corresponds to the position co-ordinate $(x, NY - 1)$ and that of the bottom boundary $(x, 0)$. The left boundary corresponds to the position co-ordinate $(0, y)$ and that of the right boundary $(NX - 1, y)$.

The dotted lines in all the diagrams in this section indicate that the intermediate nodes and the corresponding ports have been omitted to direct attention on the pertinent areas of discussion.
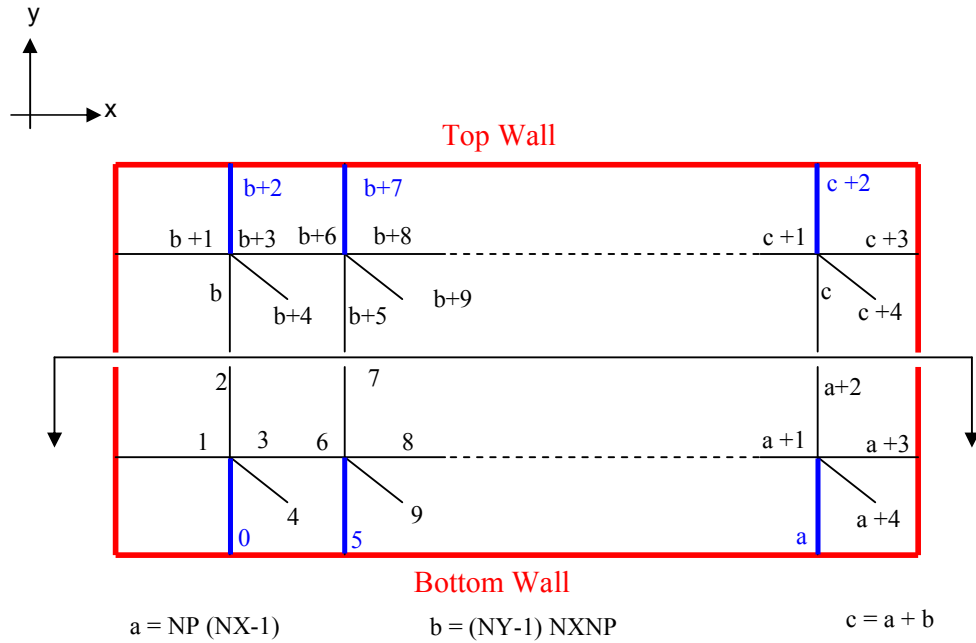
Fig. C-1 Port number configuration for top and bottom walls of dielectric waveguide

d = a + NP   e = d + NP (NX-1)   f = (NY-2) NXNP   g = a + f
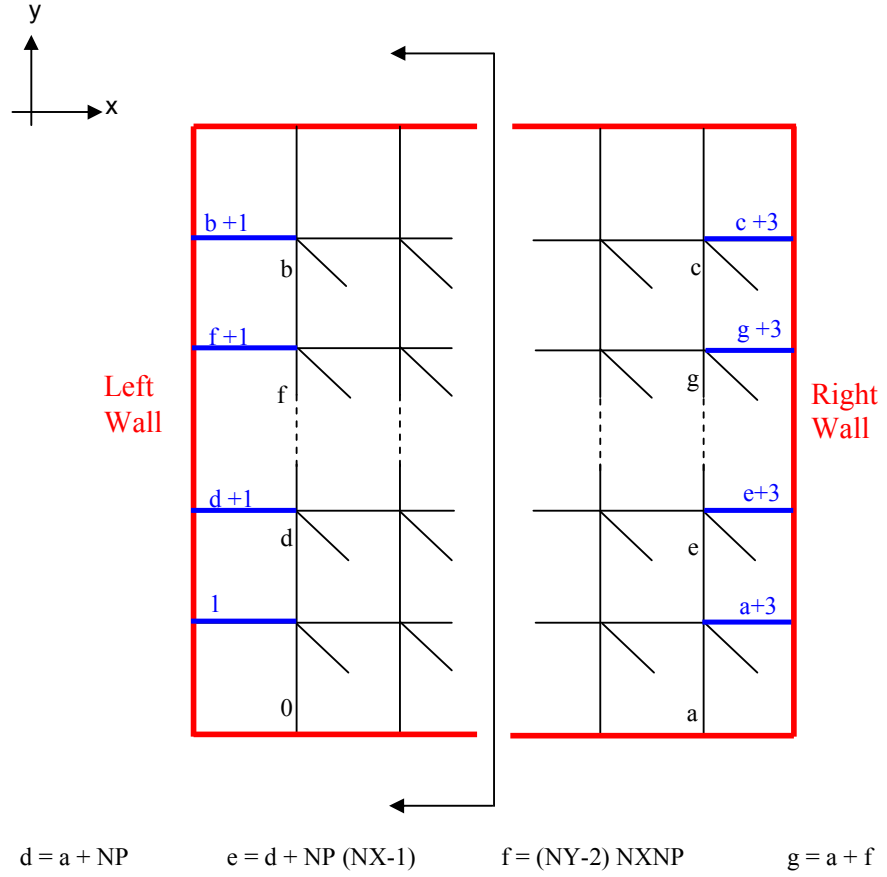
Fig. C-2 Port number configuration for left and right walls of dielectric waveguide

A generic mathematical formula for calculating the port numbers connected at the boundaries of the waveguide along with the corresponding position in the connection matrix can be found from Fig. C-1 and Fig. C-2:

(a) Top Boundary

$$T = \left[(NY-1)\times(NX\times NP)\right] + \left[(2+x)\times NP\right] \qquad 0 \leq x < NX \qquad (C.2)$$

$$\underline{\underline{C}}\left[T\right]\left[T\right] = -1 \qquad (C.3)$$

(b) Bottom Boundary

$$B = x \times NP \qquad\qquad 0 \leq x < NX \qquad (C.4)$$

$$\underline{\underline{C}}\left[B\right]\left[B\right]=-1 \tag{C.5}$$

(c) Left Boundary

$$L = \left[y \times \left(NX \times NP\right)\right] + 1 \qquad 0 \le y < NY \quad \text{(C.6)}$$

$$\underline{\underline{C}}\left[L\right]\left[L\right]=-1 \tag{C.7}$$

(d) Right Boundary

$$R = \left[NP \times \left(\left(NX \times (y+1)\right) - 1\right)\right] + 3 \quad 0 \le y < NY \qquad \text{(C.8)}$$

$$\underline{\underline{C}}\left[R\right]\left[R\right]=-1 \tag{C.9}$$

C.3   Connection of Intermediate Ports

The intermediate ports comprise those that are connected away from waveguide boundaries. A matrix constructed from these port elements alone will possess symmetric characteristics. This is indicative of the exchange between adjacent ports.

C.3.1   Connection Along the X-Direction

Fig. C-3 shows a discretised TLM model of a waveguide with emphasis placed on connecting ports away from the metal walls in the *x*-direction. The definitions of ports a – f are given in Figs. C-1 and C-2 above.
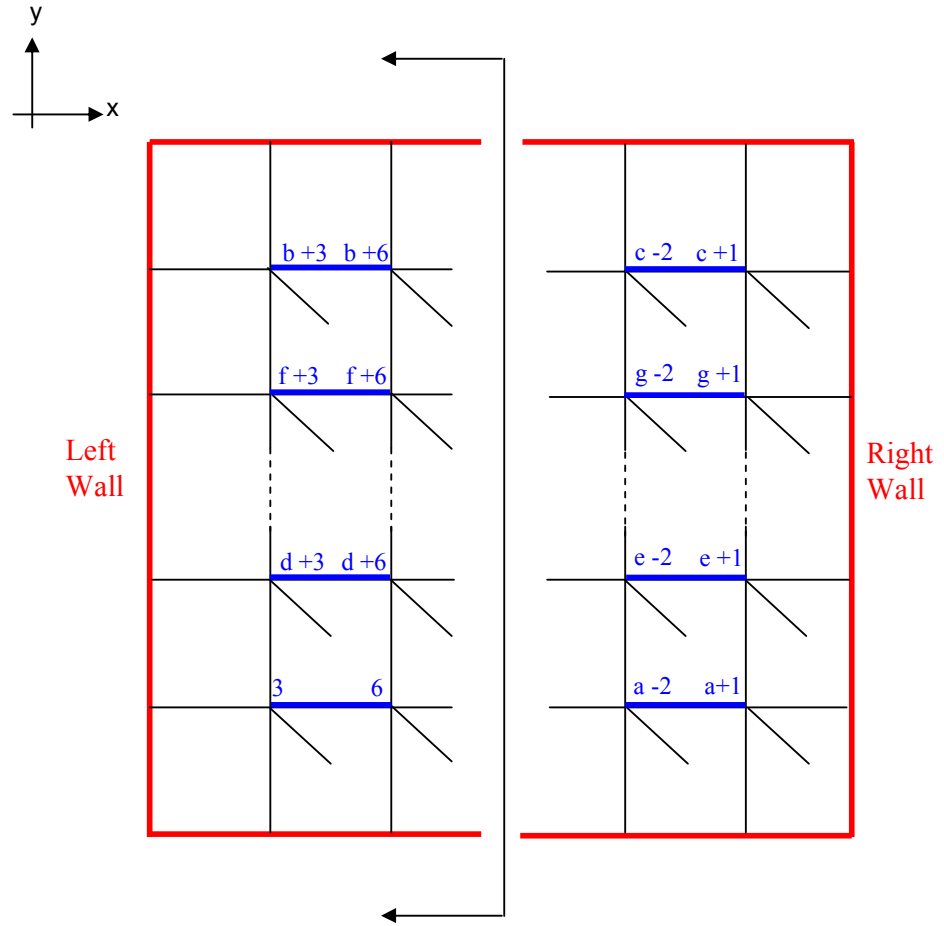
Fig. C-3 Port number configuration of intermediate nodes along *x*-direction of dielectric waveguide

The first and the third port of the nodes in Fig. C-3 are coupled with each other. The exception to this pattern of arrangement is the first port of the nodes with co-ordinate (0, *y*) connected to the left wall and the third port of the nodes with co-ordinate (*NX* – 1, *y*) connected to the right wall.

Using the same principle as for the outer boundaries, a generic mathematical formula for calculating the number assigned to the intermediate coupling ports in the *x*-direction with their position in the connection matrix can be found. The first stage is the connection of the first to the third port and the exchange is complete via the connection of the third to the first port of neighbouring nodes.

(a) Connection of the first and third ports of intermediate nodes

$$r_{y+1} = r_y + \left(y \times NP \times NX\right) \quad r_0 = NP + 1; 0 \leq y < NY \quad \text{(C.10)}$$

$$c_{y+1} = c_y + \left(y \times NP \times NX\right) \quad c_0 = 3; 0 \leq y < NY \quad \text{(C.11)}$$

$$row_{13} = r_y + \left[(x-1) \times NP\right] \quad 1 \leq x < NX; 0 \leq y < NY \quad \text{(C.12)}$$

$$col_{13} = c_y + \left[(x-1) \times NP\right] \quad 1 \leq x < NX; 0 \leq y < NY \quad \text{(C.13)}$$

$$\underline{\underline{C}}\left[row_{13}\right]\left[col_{13}\right] = 1 \quad \text{(C.14)}$$

The $(x - 1)$ term in (C.12) and (C.13) are needed because of the presence of the left boundary and to apply correct conditions to the ports 1 connected to it.

(b) Connection of the third and first ports of intermediate nodes

$$r_{y+1} = r_y + \left(y \times NP \times NX\right) \quad r_0 = 3; 0 \leq y < NY \quad \text{(C.15)}$$

$$c_{y+1} = c_y + \left(y \times NP \times NX\right) \quad c_0 = NP + 1; 0 \leq y < NY \quad \text{(C.16)}$$

$$row_{31} = r_y + \left(x \times NP\right) \quad 0 \leq x < NX - 1; 0 \leq y < NY \quad \text{(C.17)}$$

$$col_{31} = c_y + \left(x \times NP\right) \quad 0 \leq x < NX - 1; 0 \leq y < NY \quad \text{(C.18)}$$

$$\underline{\underline{C}}\left[row_{31}\right]\left[col_{31}\right] = 1 \quad \text{(C.19)}$$

The $NX - 1$ term in (C.17) and (C.18) ensures that the right boundary is avoided. This is because the third ports of the nodes connected to it have a -1 reflection coefficient and are not coupled to any of the ports of the neighbouring nodes.

C.3.2   Connection Along the Y-Direction

Fig. C-4 shows a discretised TLM model of a waveguide with emphasis placed on connecting ports away from the metal walls in the y-direction.
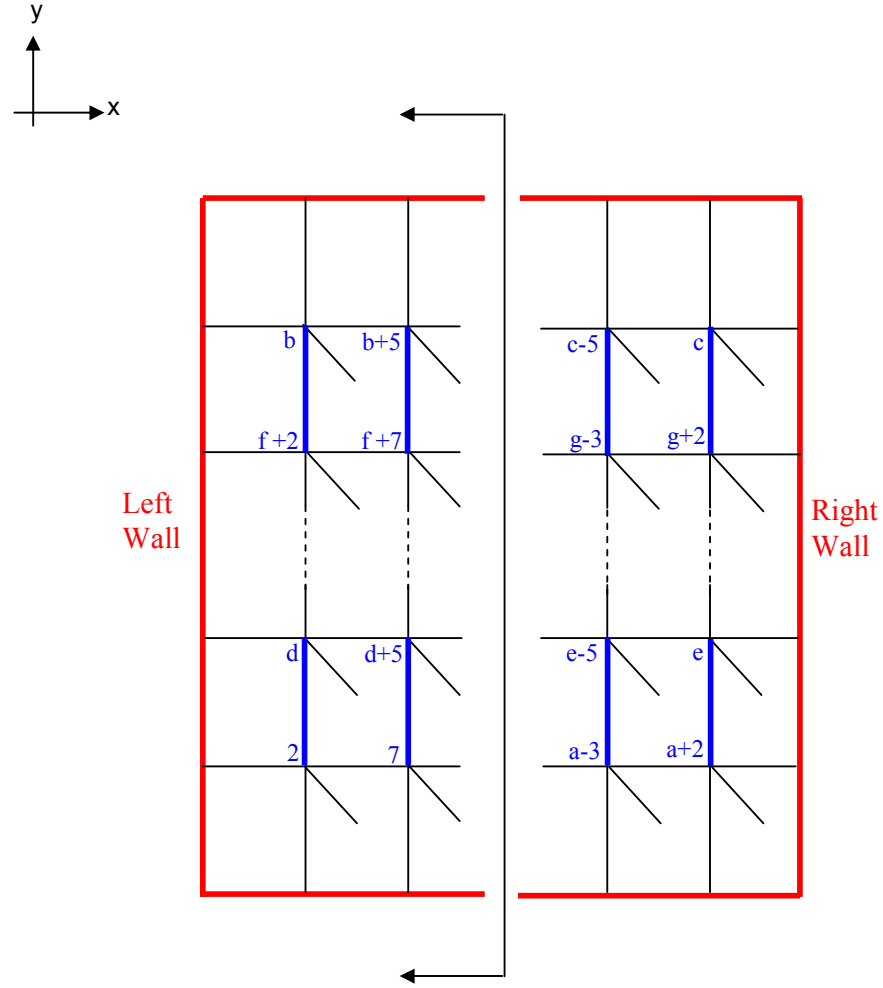
Fig. C-4 Port number configuration of intermediate nodes along the y-direction of dielectric waveguide

The zeroth (this is used due to the ordinate system adopted) and the second port of the nodes in Fig. C-4 are coupled with each other. The exception to this pattern of arrangement is the zeroth port of the nodes with co-ordinate $(x, 0)$ connected to the bottom wall and the second port of the nodes with co-ordinate $(NX - 1, y)$.

The generic mathematical formula for calculating the number assigned to the intermediate coupling ports in the *y*-direction and their position in the connection matrix is similar to the case in the *x*-direction. The only difference here is in the modification to avoid top and bottom boundaries. The first connection is that of the zeroth to the second port. The exchange is complete via the connection of the second to the zeroth port.

(a) Connection of the zeroth and second ports of intermediate nodes

$$r_{y+1} = r_y + \left[(y-1) \times NP \times NX \right] \quad r_0 = NX \times NP; 1 \le y < NY \quad \text{(C.20)}$$

$$c_{y+1} = c_y + \left[(y-1) \times NP \times NX \right] \quad c_0 = 2; 1 \le y < NY \quad \text{(C.21)}$$

$$row_{02} = r_y + (x \times NP) \qquad 0 \le x < NX; 1 \le y < NY \quad \text{(C.22)}$$

$$col_{02} = c_y + (x \times NP) \qquad 0 \le x < NX; 1 \le y < NY \quad \text{(C.23)}$$

$$\underline{\underline{C}} \left[row_{02} \right] \left[col_{02} \right] = 1 \quad \text{(C.24)}$$

The $(y-1)$ term in (C.20) and (C.21) is needed because of the presence of the bottom boundary and to apply correct conditions to the ports 0 connected to it.

(b) Connection of the second and zeroth ports of intermediate nodes

$$r_{y+1} = r_y + \left(y \times NP \times NX \right) \quad r_0 = 2; 0 \le y < NY - 1 \quad \text{(C.25)}$$

$$c_{y+1} = c_y + \left(y \times NP \times NX \right) \quad c_0 = NX \times NP; 0 \le y < NY - 1 \quad \text{(C.26)}$$

$$row_{20} = r_y + (x \times NP) \quad 0 \le x < NX; 0 \le y < NY - 1 \quad \text{(C.27)}$$

$$col_{20} = c_y + (x \times NP) \qquad 0 \le x < NX; 0 \le y < NY - 1 \quad \text{(C.28)}$$

$$\underline{\underline{C}} \left[row_{20} \right] \left[col_{20} \right] = 1 \quad \text{(C.29)}$$

The $NY - 1$ term ensures that the top boundary is avoided as the second ports of the nodes connected to it.

C.4   Connection of Stubs

The stubs are terminated using open circuits to reflect the capacitive properties of modelled materials. The consequence of this is that the coupling is at the node centre where it is redistributed to other ports. This straightforward interpretation of wave propagation is seen calculation of the number assigned to the stub ports and their position in the connection matrix:

$$M = \left(NP \times n \right) + \left(NP - 1 \right) \quad 0 \leq n < N; N = NX \times NY \tag{C.30}$$

$$\underline{\underline{C}}\left[M \right]\left[M \right] = 1 \tag{C.31}$$

It is important to note that this case is only required for materials with permittivity greater than that for air. All the matrix elements of the connection matrix that does not fall into any of the above classifications are assigned a value of zero.

Appendix D   SCN with inductive and capacitive stubs

This section describes the 3-D SCN used to model materials with relative permittivity or permeability that is greater than one.

D.1   The SCN with inductive and capacitive stubs

The SCN without stubs had 12 link lines all with the same characteristic impedance Z_{TL} given by:

$$Z_{TL} = \sqrt{\frac{\mu_0}{\varepsilon_0}} \qquad (D.1)$$

Let all the space dimensions of the SCN be equal to Δl. Then, the velocity of propagation u_{TL} through each link line in free space is [D.1]:

$$u_{TL} = \frac{\Delta l}{\Delta t} = 2\sqrt{\frac{1}{\mu_0 \varepsilon_0}} = 2c \qquad (D.2)$$

where c is the speed of light.

The relationship between link capacitance C and link impedance Z_{TL} in the SCN is [D.1]:

$$C = \frac{\Delta t}{2 Z_{TL}} \qquad (D.3)$$

In free space the total capacitance modelled in the x, y or z-directions of the SCN is $4C$. A lossless material of permittivity ε is modelled by adding a stub

capacitance C_S to the total link capacitance in the x, y and z-directions to give an overall capacitance of:

$$C_{tot} = \varepsilon\Delta l = C_S + 4C \tag{D.4}$$

The characteristic admittance of the capacitive stub using (D.3) and (D.4) in the x, y or z-directions is:

$$Y_{SC} = \frac{2C_S}{\Delta t} = \frac{2(\varepsilon\Delta l - 4C)}{\Delta t} = 2\left(\frac{\varepsilon\Delta l}{\Delta t} - \frac{2}{Z_{TL}}\right) \tag{D.5}$$

Therefore, the normalised stub admittance in the x, y or z-directions using (7.10a), (7.10b) and (D.5) is:

$$\hat{Y}_{SC} = Y_{SC}Z_{TL} = 2\left(\frac{\varepsilon_0\varepsilon_r\Delta l}{\Delta t}\sqrt{\frac{\mu_0}{\varepsilon_0}} - 2\right) = 2\left(\frac{\varepsilon_r\Delta l}{c\Delta t} - 2\right) \tag{D.6}$$

The relationship between link capacitance L and link impedance Z_{TL} in the SCN is [D.1]:

$$L = \frac{Z_{TL}\Delta t}{2} \tag{D.7}$$

Similarly, a lossless material of permittivity μ is modelled by adding a stub inductance L_S to the total link capacitance $4L$ in the x, y and z-directions to give an overall inductance of:

$$L_{tot} = \mu\Delta l = L_S + 4L \tag{D.8}$$

The characteristic impedance of the inductive stub using (D.7) and (D.8) in the x, y or z-directions is:

$$Z_{SL} = \frac{2L_S}{\Delta t} = \frac{2(\mu\Delta l - 4L)}{\Delta t} = 2\left(\frac{\mu\Delta l}{\Delta t} - 2Z_{TL}\right) \tag{D.9}$$

The normalised stub admittance in the *x, y* or *z*-directions using (D.1), (D.2) and (D.9) is:

$$\hat{Z}_{SL} = \frac{Z_{SL}}{Z_{TL}} = 2\left(\frac{\mu_0 \mu_r \Delta l}{\Delta t} \sqrt{\frac{\varepsilon_0}{\mu_0}} - 2 \right) = 2\left(\frac{\mu_r \Delta l}{c \Delta t} - 2 \right) \qquad \text{(D.10)}$$

The capacitive stubs have an open circuit termination while short circuit stubs have a closed circuit termination. Both stubs have pulses incident on them reflected back to the node after round trip propagation in one time step. The inductive stub has the incident voltages at the next time step equal to minus the reflected voltage at the previous time step. On the other hand, the capacitive stub has the incident voltage at the next time step equal to the reflected voltage at the previous time step. The connection process of link lines remains unchanged from the free space SCN model. The global connection matrix contains all the information relating incident voltages at the next time step with reflected voltage at the previous time step of all the ports associated with each SCN in the discretised 3-D problem space.

To incorporate material properties into scattering matrix, the capacitive stubs in the *x, y* and *z*-directions are assigned port numbers 13 to 15, while inductive stubs port numbers 16 to 18 respectively. This augments the scattering sub-matrix to an order 18 *x* 18. A voltage pulse incident on port 1 is scattered into ports 1, 2, 3,9,11 and 12. As E_x and H_z are the associated fields, part of the scattered pulse couples with ports 13 and 18 respectively. This procedure is repeated for all the ports in the SCN stub model and the scattering sub-matrix is [D.1, D.2]:

$\underline{S}_{x,y,z} =$

	1	2	3	4	5	6	7	8	9	10	11	12	13	14	15	16	17	18
1	a	b	d						b		-d	c	g					i
2	b	a			d				c	-d		b	g				-i	
3	d		a	b				b			c	-d		g				-i
4			b	a	d		-d	c			b			g		i		
5				d	a	b	c	-d		b					g	-i		
6		d			b	a	b		-d	c					g		i	
7				-d	c	b	a	d		b					g	i		
8			b	c	-d		d	a			b			g		-i		
9	b	c				-d			a	d		b	g				i	
10		-d			b	c	b		d	a					g		-i	
11	-d		c	b				b			a	d		g				i
12	c	b	-d						b		d	a	g					-i
13	e	e							e			e	h					
14			e	e				e			e			h				
15					e	e	e			e					h			
16				f	-f		f	-f								j		
17		-f			f				f	-f							j	
18	f		-f								f	-f						j

$$(D.11)$$

where

$$a = \frac{-\hat{Y}_{SC}}{2\left(\hat{Y}_{SC}+4\right)} + \frac{\hat{Z}_{SL}}{2\left(\hat{Z}_{SL}+4\right)}$$

$$b = e = \frac{4}{2\left(\hat{Y}_{SC}+4\right)}$$

$$c = \frac{-\hat{Y}_{SC}}{2\left(\hat{Y}_{SC}+4\right)} - \frac{\hat{Z}_{SL}}{2\left(\hat{Z}_{SL}+4\right)}$$

$$d = i = \frac{4}{2\left(\hat{Z}_{SL}+4\right)}$$

$$f = \frac{4\hat{Z}_{SL}}{2\left(\hat{Z}_{SL}+4\right)}$$

$$g = \frac{4\hat{Y}_{SC}}{2\left(\hat{Y}_{SC}+4\right)}$$

$$h = \frac{\hat{Y}_{SC}-4}{\hat{Y}_{SC}+4}$$

$$f = \frac{4\hat{Z}_{SL}}{2\left(4 + \hat{Z}_{SL}\right)}$$

The global scattering matrix of the SCN with material stubs is found by substituting (D.11) into (7.9).

D.2   References

[D.1] C. Christopoulos, "The Transmission-Line Modelling Method," IEEE Press, 1995.

[D.2]   P.B. Johns, "A Symmetrical Condensed Node for the TLM method," IEEE Trans. Microwave Theory Tech., vol. MTT-35, pp. 370-377, April 1987.